High resolution decoding of the tobacco chloroplast translatome and its dynamics during light-intensity acclimation

Maja Schuster

Dissertation

zur Erlangung des akademischen Grades
"doctor rerum naturalium" (Dr. rer. nat.)
in der Wissenschaftsdisziplin "Biochemie und Molekularbiologie"

eingereicht an der
Mathematisch-Naturwissenschaftlichen Fakultät
Institut für Biochemie und Biologie
der Universität Potsdam
und dem
Max-Planck-Institut für Molekulare Pflanzenphysiologie

Disputation erfolgte am 26. April 2021 in Potsdam-Golm

Betreuer

Prof. Dr. Ralph Bock (Max-Planck-Institut für Molekulare Pflanzenphysiologie und Universität Potsdam, Potsdam)

Dr. Reimo Zoschke (Max-Planck-Institut für Molekulare Pflanzenphysiologie, Potsdam)

Gutachter

1. Prof. Dr. Ralph Bock (Max-Planck-Institut für Molekulare Pflanzenphysiologie und Universität Potsdam, Potsdam)

2. Prof. Dr. Kristina Kühn (Martin-Luther-Universität, Halle-Wittenberg)

3. PD Dr. Bettina Bölter (Ludwig-Maximilians-Universität, München)

Published online on the
Publication Server of the University of Potsdam:
https://doi.org/10.25932/publishup-51268
https://nbn-resolving.org/urn:nbn:de:kobv:517-opus4-512680

'But it was the Great Question! The Ultimate Question of Life, the Universe and Everything!' howled Loonquawl.
'Yes,' said Deep Thought with the air of one who suffers fools gladly, 'but what actually *is* it?'

The Hitchhiker's Guide to the Galaxy **by Douglas Adams**

Abstract

Chloroplasts are the photosynthetic organelles in plant and algae cells that enable photoautotrophic growth. Due to their prokaryotic origin, modern-day chloroplast genomes harbor 100 to 200 genes. These genes encode for core components of the photosynthetic complexes and the chloroplast gene expression machinery, making most of them essential for the viability of the organism. The regulation of those genes is predominated by translational adjustments. The powerful technique of ribosome profiling was successfully used to generate highly resolved pictures of the translational landscape of *Arabidopsis thaliana* cytosol, identifying translation of upstream open reading frames and long non-coding transcripts. In addition, differences in plastidial translation and ribosomal pausing sites were addressed with this method. However, a highly resolved picture of the chloroplast translatome is missing. Here, with the use of chloroplast isolation and targeted ribosome affinity purification, I generated highly enriched ribosome profiling datasets of the chloroplasts translatome for *Nicotiana tabacum* in the dark and light. Chloroplast isolation was found unsuitable for the unbiased analysis of translation in the chloroplast but adequate to identify potential co-translational import. Affinity purification was performed for the small and large ribosomal subunit independently. The enriched datasets mirrored the results obtained from whole-cell ribosome profiling. Enhanced translational activity was detected for *psbA* in the light. An alternative translation initiation mechanism was not identified by selective enrichment of small ribosomal subunit footprints. In sum, this is the first study that used enrichment strategies to obtain high-depth ribosome profiling datasets of chloroplasts to study ribosome subunit distribution and chloroplast associated translation.
Ever-changing light intensities are challenging the photosynthetic capacity of photosynthetic organism. Increased light intensities may lead to over-excitation of photosynthetic reaction centers resulting in damage of the photosystem core subunits. Additional to an expensive repair mechanism for the photosystem II core protein D1, photosynthetic organisms developed various features to reduce or prevent photodamage. In the long-term, photosynthetic complex contents are adjusted for the efficient use of experienced irradiation. However, the contribution of chloroplastic gene expression in the acclimation process remained largely unknown. Here, comparative transcriptome and ribosome profiling was performed for the early time points of high-light acclimation in *Nicotiana tabacum* chloroplasts in a genome-wide scale. The time-course data revealed stable transcript level and only minor changes in translational activity of specific chloroplast genes during high-light acclimation. Yet, *psbA* translation was increased by two-fold in the high light from shortly after the shift until the end of the experiment. A stress-inducing shift from low- to high light exhibited increased translation only of *psbA*. This study indicate that acclimation fails to start in the observed time frame and only short-term responses to reduce photoinhibition were observed.

Zusammenfassung

Chloroplasten sind die photosynthetischen Organellen in Pflanzen- und Algenzellen, die photoautotrophes Wachstum ermöglichen. Aufgrund ihrer prokaryotischen Herkunft besitzen moderne Chloroplasten ein Genom mit 100 bis 200 Gene. Diese kodieren für zentrale Komponenten der Photosynthesekomplexe und des Genexpressionsapparates, was sie für die Lebensfähigkeit des gesamten Organismus essenziell macht. Die leistungsstarke Methode *Ribosome Profiling* wurde bereits erfolgreich eingesetzt, um hochaufgelöste Bilder der zytosolischen Translationslandschaft von *Arabidopsis thaliana* zu erstellen, wobei Translation von der Hauptsequenz vorgelagerten, kodierenden Sequenzen und langen, nicht-kodierenden Transkripten identifiziert wurde. Ferner wurden mit dieser Technik Regulationen der Plastidentranslation und spezifische Regionen mit unterschiedlicher Elongationsgeschwindigkeit aufgedeckt. Es fehlen jedoch hochaufgelöste Datensätze des Chloroplasten-Translatoms. Chloroplastenisolation und Affinitätsaufreinigung chloroplastidiärer Ribosomen wurde verwendet, um hochangereicherte *Ribosome Profiling*-Datensätze des Chloroplastentranslatoms für *Nicotiana tabacum* im Dunkeln und unter Licht zu erzeugen. Wenngleich sich die Chloroplastenisolation als ungeeignet für eine unverfälschte Analyse der Translation im Chloroplast erwies, ermöglichte sie die Identifizierung von potentiellem co-translationalen Proteinimport. Die entsprechenden Datensätze spiegelten die Ergebnisse des zellulären *Ribosome Profilings* wider. Für *psbA* wurde im Licht erhöhte Translationsaktivität festgestellt. Alternative Initiationsmechanismen konnten durch spezifische Anreicherung der kleinen ribosomalen Untereinheit nicht verifiziert werden. Zusammenfassend, dies ist die erste Studie, die mittels Anreicherungsstrategien hochaufgelöste *Ribosome Profiling*-Datensätze zur Analyse von Ribosomuntereinheitsverteilungen und Chloroplast-assoziierter Translation nutzte.

Ständig wechselnde Lichtintensitäten stellen die Photosynthesekapazität von photosynthetischen Organismen auf die Probe. Erhöhte Lichtintensitäten können zu einer Überreizung der photosynthetischen Reaktionszentren führen, was Beschädigungen von zentralen Komplexeinheiten der Photosysteme verursacht. Neben einem aufwändigen Reparaturmechanismus für das Photosystem II-Protein D1 entwickelte der photosynthetische Organismus verschiedene Mechanismen um lichtinduzierte Schäden zu reduzieren oder zu verhindern. Langfristig kommt es zu einer Anreicherung spezifischer Photosynthesekomplexen um eine effiziente Ausnutzung der erhöhten Strahlung zu gewährleisten. Der Beitrag der chloroplastidiäeren Genexpressionsregulation zum Akklimatisierungsprozess ist jedoch weitgehend unbekannt. Hier wurde ein vergleichendes Transkript- und *Ribosomen Profiling* für die frühen Zeitpunkte der Akklimatisierung unter Starklicht in Tabakchloroplasten in einem genomweiten Maßstab durchgeführt. Die Zeitverlaufsdaten zeigten ein unverändertes Transkriptniveau und nur geringe Änderungen der translationalen Aktivität von chloroplastidiären Genen im Hochlicht im Vergleich zu Kontrollproben. Die *psbA*-Translation war jedoch unter Hochlicht schon kurz nach Beginn bis zum Ende des Experiments um etwa das Zweifache erhöht. Der stressinduzierende Wechsel von Schwach- zu Hochlicht bewirkte ebenfalls eine auf *psbA*-beschränkt, erhöhte Translation. Die Ergebnisse zeigen, dass die Akklimatisierung im beobachteten Zeitrahmen nicht begonnen hatte und nur kurzfristige Reaktionen zur Verringerung der Photoinhibition wirksam gewesen sein konnten.

Contents

List of Figures

List of Tables

Abbreviations and Units

%	percent
°C	degree Celsius
μmol·s^{-1}·m^{-2}	*micro*mol per second and square meter (light intensity)
AA	amino acid amino acyl
aadA	gene encoding spectinomycin/streptomycin adenylyl transferase
ATP	adenosine triphosphate
a.u.	arbitrary unit
ave	average
CI	chloroplast isolation
conc.	concentration
cp	chloroplastic
CPM	count per million
CTAB	cetrimonium bromide
ctrl	control
cyt	cytosolic
cyt b_6f	cytochrom b_6f complex
d	day
ddH_2O	double distilled water
Dig	predigested (digestion of cytosolic RNA attached to the chloroplast envelope)
DNA	deoxyribonucleic acid
EDTA	2,2′,2″,2‴-(ethane-1,2-diyldinitrilo)tetraacetic acid
EF	elongation factor
e.g.	*exempli gratia*
etc.	*et cetera*
EM	electron microscopy
EON	end of the night
ER	endoplasmic reticulum
ETRII	linear electron transport rate of PSII
FC	fold change
FD	ferrodoxin
FP_{SSU}	footprint of small ribosomal subunit
g	gram
g	standard gravity ($g \sim 9.81$ m·s^{-2})
GB	grinding buffer
GFP	green fluorescent protein
h	hour
HA	human influenza hemagglutinin
HEPES	4-(2-hydroxyethyl)-1-piperazineethanesulfonic acid
HRP	horse radish peroxidase
HS	HEPES sorbitol / high sensitivity (commercial kits)
IAA	isoamyl alcohol (3-methylbutan-1-ol)

i.e.	*id est*
IF	initiation factor
IgG	immunoglobulin G
IR	inverted repeat
J	Joule
kDa	kilo Dalton (unit for protein size)
l	liter
LED	light-emitting diode
LSU	large subunit
m	meter
M	molar (mol*l^{-1})
mg	milligram
min	minute
ml	milliliter
mRNA	messenger RNA
mt	mitochondrial
MNase	micrococcal nuclease
NAD(P)H	reduced nicotinamide adenine dinucleotide (phosphate)
n.d.	not detected
NDH	NADH dehydrogenase-like complex
NEP	nucleus-encoded RNA polymerase
no.	number
noDig	not predigested (see Dig)
NPQ	non-photochemical quenching
nt	nucleotide
OAc	salt of acetic acid (acetate)
ORF	open reading frame
p.adj	corrected *p*-value
PAGE	polyacrylamide gel electrophoresis
PCR	polymerase chain reaction
PEG	polyethylene glycol
PEP	plastid-encoded RNA polymerase
PGS	polysome gradient salt
POE	polyoxyethylene-(10)-tridecyl ether
PPF	Percoll-PEG-Ficoll
PPR	pentatricopeptide repeat
PSI	photosystem I
PSII	photosystem II
RBP	RNA binding protein
rel.	relative
RF	release factor
RFLP	restriction fragment length polymorphism
RFP	ribosomal footprint
Ribo-array	microarray coupled ribosome profiling
Ribo-seq	deep sequencing coupled ribosome profiling
RNA	ribonucleic acid
RNase 1	Ribonuclease I
ROS	reactive oxygen species
RP	ribosome profiling

rpm	round per minute
rRNA	ribosomal RNA
s	second
SC	start codon
SD	standard deviation/Shine-Dalgarno sequence
SDS	sodium dodecyl sulfate
SOD	start of the day
SRP	signal recognition particle
SSC	saline-sodium citrate
SSPS	saline sodium phosphate EDTA
SSU	small subunit
Suppl.	Supplemental
TBE	Tris - boric acid - EDTA
TE	translational efficiency
TESS	Tris - EDTA - saline - SDS
TRAP	translating ribosome affinity purification
Tris	2-amino-2-(hydroxymethyl)propan-1,3-diol
tRNA	transfer RNA
U	unit of enzyme activity
UTR	untranslated region
UV	ultraviolet (light spectrum)
V	Volt
vs.	versus
W	Watt

1 Introduction

1.1 Chloroplast gene expression - New features for old processes

1.1.1 Chloroplast's origin

Chloroplasts are photosynthetically active plastids, semi-autonomous organelles in algae and plants. They arose from an endosymbiotic event around 1 billion years ago by engulfment of a phototrophic cyanobacteria-like prokaryote into an eukaryotic-like host cell (Lewin, 1993; Sato, 2006; Theissen and Martin, 2006). Today's plastids can differentiate not only into chloroplasts but also into other organelles that fulfill diverse functions such as coloring flowers and fruits (chromoplasts) or storing starch and oil (amyloplasts and elioplasts, respectively). To what kind of plastid, the proplastid will differentiate depends on the surrounding tissue (Pyke, 2007).
Due to the process of co-evolution of endosymbiont and host cell to their today's form, the plastid genome (plastome) was reduced significantly. Whereas around 1,300 to 4,200 proteins were detected in the plastid of *Arabidopsis thaliana* (*A. thaliana*) (Sun et al., 2004; Richly and Leister, 2004; Zybailov et al., 2008) only 132 genes reside in the plastome (Sato et al., 1999). Plastidial genes were either integrated into the nuclear genome, from which they are expressed and further imported into the chloroplast, or abandoned because of redundancies with host genes (Gantt et al., 1991).

1.1.2 Genome structure of plastids

Regardless of its considerable reduction, the plastome has kept multiple characteristics of its prokaryotic ancestor.
The plastome of typical phototrophic organism comprises around 100 to 200 genes in a bacterial-like circular mapping double-stranded DNA. Also similar to bacteria, multiple genome copies are packed in nucleoids. A large fragment containing the gene cluster for the ribosomal RNAs occurs duplicated and in inverse direction in many species of the green lineage (inverted repeat, IR, Figure 1.1) (Bohnert et al., 1982; Wakasugi et al., 1998; Bock, 2007).
The genes are densely organized in operon-like clusters and can be categorized into three groups. (1) genes that encode subunits of the photosynthetic complexes. These genes represent around one-third of all plastid-encoded protein-coding genes, while they are only active in the chloroplast. (2) genes involved in the plastidial gene-expression machinery. Those genes include a full set of ribosomal and transfer RNAs (rRNA and tRNA, respectively) next to around 30 % of the ribosomal proteins and a bacterial-type RNA polymerase. (3) genes that are involved in other metabolic processes of the plastid, such as complex assembly (e.g., *ycf3,*

ycf4) or fatty acid synthesis (i.e. *accD*) and RNA maturation (i.e. *matK*) (Wakasugi et al., 1998; Sato et al., 1999; Bock, 2007).

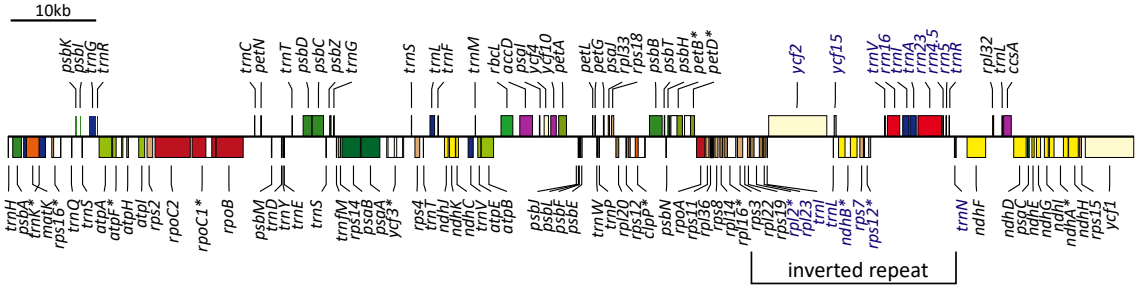

Figure 1.1: Physical map of the chloroplast genome of *Nicotiana tabacum* in a linearized form. Genes on top are transcribed from left to right and genes below *vice versa*. Only one inverted repeat region is shown (region marked by the bracket below) and genes belonging to the repeat and thus occurring in double copy number are highlighted blue. Genes marked with asterisk * contain introns. The map was drawn based on the genomic information from Wakasugi et al. (1998) with the online tool OGDRAW (Lohse et al., 2013; Greiner et al., 2019).

1.1.3 Transcription and transcript processing

The next feature, that links chloroplast to its bacterial progenitor, is a bacterial gene expression machinery for the expression of the plastid-encoded genes. The plastome encoded for all four subunits of a bacterial-type RNA polymerase (plastid-encoded RNA polymerase, PEP). As in bacteria, this polymerase function in association with different σ-factors, six in *A. thaliana* (Schweer et al., 2010; Chi et al., 2015). All of them are nucleus-encoded and have to be imported into the chloroplast. Some of the transcription factors act in the transcription under specific conditions.

But not only transcription factors are imported into the plastid for proper transcription. Next to PEP also nucleus-encoded RNA polymerases (NEP) serve plastidial gene expression. They are single subunit enzymes of the T3/T7-phage type (Lerbs-Mache, 1993; Hess et al., 1993; Liere et al., 2011). In dicotyledons, two NEPs act in the plastid whereas in monocotyledons only one NEP was found (Liere et al., 2011).

Early studies suggested either a functional or developmental separation of NEP and PEP function. Thus, NEP was thought to act early in development to serve the expression of "house-keeping", genes while PEP acts in the expression of photosynthetic genes (Hajdukiewicz et al., 1997; Swiatecka-Hagenbruch et al., 2007; reviewed by Börner et al., 2015). However, apart from *rpoB*, which is exclusively NEP transcribed, most plastidial genes are transcribed by NEP and PEP at least to some extent (Legen et al., 2002).

Produced transcripts are commonly in the first instance polycistronic. Different to bacterial gene expression, plastidial transcripts undergo massive processing by intercistronic cleavage into smaller transcription units, splicing of introns and editing of single nucleotides to restore codons (reviewed by Barkan, 2011; Maier et al., 2008). The complexity of messenger RNA (mRNA) maturation was illustrated extensively for the *psbB*-operon (Tanaka et al., 1987; Westhoff and Herrmann, 1988; Barkan, 1988). However, protein synthesis is not entirely dependent on fully processed transcripts in the plastid. Studies showed translation on oligocistronic and

even unspliced transcripts in the plastid (Friemann and Hachtel, 1988; Barkan, 1988; Zoschke et al., 2013; Zoschke and Barkan, 2015).
Factors involved in transcript processing are also determinants for the high stability of plastidial transcripts (Rapp et al., 1992, and references herein). Many factors involved in processing belong to the group of RNA-binding proteins (RBP) that recognizes defined RNA sequences by helical-repeat motifs (reviewed by Hammani et al., 2014). The binding protects the mRNA from exonuclease degradation and may also promote translation (Barkan et al., 1994; Pfalz et al., 2009; comprehensive review on PPR proteins by Barkan and Small, 2014).

1.1.4 Translation

1.1.4.1 The plastid ribosome

Translation of plastidial transcripts is performed by a 70S bacterial-type ribosome. The plastid ribosome shares high homology with its relative in *Escherichia coli* (*E. coli*). Different to *E. coli*, the plastidial ribosome is composed of four rRNA species which show, however, highly similarity to the bacterial ones. The 16S rRNA of the plastid small ribosomal subunit (SSU) shares more than 70 % sequence identity with 16S rRNA from *E. coli*. It is to highlight that the 3'-terminal region also includes the recognition motif for the Shine-Dalgarno sequence (SD) of mRNA (Schwarz and Kössel, 1980), a *cis*-element recognized in translation initiation in prokaryotes (Shine and Dalgarno, 1974). Further, all *E. coli* ribosomal proteins from SSU have an orthologue in the plastidial ribosome. Additionally, three proteins were identified lacking homologues in *E. coli*, yeast, and mammals (plastid-specific ribosomal protein, PSRP)(Yamaguchi et al., 2000; Yamaguchi and Subramanian, 2003). PSRP1, which was assigned in the first place to this group, was later found to be a functional homologue of pY, a stabilization factor for 70S ribosomes on the mRNA in *E. coli* in translation-unfavorable conditions (Sharma et al., 2010).
The plastidial large ribosomal subunit (LSU) comprises three rRNAs and 33 proteins. Plastidial 23S rRNA is shorter than its bacterial relative and may contain in the mature ribosome two strand breaks, so called "hidden breaks". The 4.5S rRNA is homologous to the 3'-terminus of *E. coli*'s 23S rRNA (Edwards and Kössel, 1981). The 5S rRNA from plastids is highly sequence homologues to bacterial 5S rRNA and exhibits also a similar secondary structure that differs minorly in the length of double-strand stretches (Delihas et al., 1981). Additionally, 31 proteins of LSU have orthologues in *E. coli*, but homologues of the bacterial ribosomal proteins L25 and L30 are missing. Also in LSU, two PSRPs were identified (Yamaguchi and Subramanian, 2000, 2003).
In total, the plastid ribosome is larger than its bacterial relative by approximately 170 kDa, because of N- and C-terminal extensions of the proteins. They probably serve stability demands due to the modified rRNA frame. But, extensions could also be assigned to new interactions with the mRNA and structural changes in the mRNA entry site which could be interaction points for translational regulation (Ahmed et al., 2017; Graf et al., 2016; Bieri et al., 2017).
There are three binding sites for tRNA that span both ribosomal subunits. At the A-site (aminoacyl-site) the aminoacyl-tRNA decodes the mRNA by codon-anticodon interaction. tRNA bound to the nascent peptide chain is translocated to the P-site (peptidyl-site) after chain elongation. Moreover, finally, tRNAs are released from the ribosome at the E-site (exit-site) after deacylation. Depending on the occupations of the binding sites on both subunits by tRNA and on the reactions performed, the ribosome is in different rotation states

(Noller et al., 2017; Wu et al., 2019a).
The chloroplast ribosome is encoded by a chimera of genes residing in the plastid and in the nucleus. Whereas all rRNA components are plastid-encoded, about twelve and 24 proteins for SSU and LSU, respectively, are imported from the cytosol (Yamaguchi et al., 2000; Yamaguchi and Subramanian, 2000). Further, it was shown that equivalent to bacteria, not all proteins are essential for plastid function and thereby also plant viability. However, the essential character of ribosomal proteins does not seem to be conserved between bacteria and plastids (reviewed by Tiller and Bock, 2014).

1.1.4.2 Co-transcriptional translation

Whereas eukaryotic translation is timely and spatial separated from transcription, they are coupled in *E.coli* (Miller Jr et al., 1970). The co-transcriptional translation was proposed to have multiple advantages for the prokaryotic organism. During transcription elongation, RNA polymerase oscillates between active and "backtrack" state. In the backtrack state, RNA polymerase is inactive and slides along the DNA and RNA (Komissarova and Kashlev, 1997; Nudler et al., 1997). Translating ribosomes, however, push the RNA polymerase forward and define thereby also the rate of transcription (Proshkin et al., 2010; Burmann et al., 2010). Furthermore, by preventing backtracking, collisions between RNA polymerase and the DNA replication complex are prevented and DNA integrity is preserved (Dutta et al., 2011).
Co-transcriptional translation was proposed for plastid gene expression as well. This assumption was supported by a study from Rose and Lindbeck (1982) who found translating ribosomes associated with transcripts in the nucleoids. Additionally, proteomic studies identified ribosomal proteins and translation factors in their nucleoid preparations (Pfalz et al., 2006; Majeran et al., 2012). However, chloroplast transcripts have much longer half-lives than known from bacteria (Klaff and Gruissem, 1991; Kim et al., 1993b) and transcriptional regulation was found to be not limiting for the majority of plastid-encoded genes (Deng and Gruissem, 1987; Deng et al., 1987; Bendich, 1987). Additionally, there is clear evidence of mRNA targeting to the thylakoid membrane (Uniacke and Zerges, 2009; Zoschke and Barkan, 2015). Thus, co-transcriptional translation plays probably a minor role in the plastid gene expression.

1.1.4.3 Translation initiation

Three different modes of translation initiation are known in prokaryotes. The *de novo* initiation involves the pre-initiation complex that comprises SSU together with initiation factors (IF) 1, IF2, IF3 and the fMet-tRNA^{fMet} that are bound to the mRNA (Figure 1.2 A). Eubacteria, such as *E. coli*, contain in the 5'-region of their mRNAs the SD, a purine-rich sequence stretch around nine nucleotides upstream of the translation start codon. This sequence is complementary to the pyrimidine-rich sequence at the 3'-terminus of 16S rRNA. The interaction of both sequences facilitates and stabilizes the initiation complex and guides the positioning of the start codon to the P-site of the SSU (Shine and Dalgarno, 1974). Additionally, the C-terminus of ribosomal protein S1 protrudes from the ribosome and associates preferentially with AU-rich sequences which are upstream of the SD. By this, S1 further facilitates and stabilizes

SSU-mRNA interaction and enables also SD-independent initiation (Boni et al., 1991; Tzareva et al., 1994). Upon formation of the initiation complex, LSU joins the complex and through hydrolyzation of IF2-bound GTP, $tRNA^{fMet}$ is positioned in the P-site of SSU and LSU. In this position, all IFs are released and translation elongation starts (Milon et al., 2008). In plastids, orthologues for all three initiation factors were identified (Sijben-Müller et al., 1986; Campos et al., 2001; Zheng et al., 2016) and around two thirds of the protein-coding genes possess a SD in their 5'-UTR. However, positioning to the start codon and composition of the sequence vary within SD containing genes (Ruf and Kössel, 1988; Bonham-Smith and Bourque, 1989; Scharff et al., 2017). Also, ribosomal protein S1 in the plastidial ribosome was found to bind unspecifically to mRNA and thus its involvement in translation initiation in the plastid is under discussion (Shteiman-Kotler and Schuster, 2000). Scharff et al. (2011) found in a bioinformatical approach, where they analyzed nearly 64,000 prokaryotic gene sequences (11,238 where plastidial) for SD and secondary mRNA structures around the start codon, that SD-independent initiation is mostly associated with unstructured mRNA sequences which may enable the start-codon recognition. However, SD-independent initiation was also observed for genes containing SD (Sakamoto et al., 1994; Plader and Sugiura, 2003; Scharff et al., 2017) and different nucleus-encoded factors were already identified that may regulate initiation in the chloroplast (see Section 1.2). Moreover, Burkhardt et al. (2017) found that, in bacteria, the polycistronic mRNA consists of open-reading frame (ORF)-wide modules with different degrees of structure. Especially the translation start sites of all cistrons of a polycistronic mRNA were found rather unstructured.

The second mode of initiation was successfully demonstrated a few years ago. Here, the ribosome will not dissociate after completing the translation of a cistron but instead scans the mRNA for proximal translation initiation sites (Figure 1.2 B), typical for prokaryotic polycistronic transcripts (Yamamoto et al., 2016). There are also genes overlapping, i.e. *atpB/E*,*psbD/C*, *ndhC/K*, or being separated only by few nucleotides ($\leq$ 10 nts), i.e. *rpoB/C1*, *psbE/F*, *ndhH/A*, in the plastome. Ribosome scanning may be the mode of initiation in those cases.

The third and rarest mode describes initiation on mRNAs without a leader sequence (Figure 1.2 C). Thus, the start codon is found within the first bases of the mRNA. Only a few genes are known in *E. coli* that are encoded without 5'-untranslated regions (UTR). Additionally, this kind of mRNA may be formed in stress responses (Vesper et al., 2011; Romero et al., 2014). Experiments showed successful initiation of assembled 70S ribosomes on leaderless mRNA (Moll et al., 2004; Udagawa et al., 2004). So far, no leaderless mRNA was found in plastids and this mode of translation initiation may not be presented in plastids.

Translation initiation in the eukaryotic system differs strongly from the prokaryotic. Already in the 70's of the last century, Marilyn Kozak found that circular RNA could not be translated in eukaryotic systems (Kozak, 1979). This implied that eukaryotic ribosomes need the m^7G CAP at the 5'-end of mRNA for recognition and translation initiation which was different to the prokaryotic system (Bretscher, 1968). She postulated a scanning mechanism of the eukaryotic SSU on the mRNA to find the first start codon in a favorable context (Figure 1.2 D) (Kozak, 1978). Briefly, the 40S ribosomal subunit•initiation factor complex would bind at the CAP of the mRNA and slide in 3'-direction until reaching an AUG codon within a GC-rich sequence motif, the Kozak sequence (Kozak, 1987, eukaryotic translational initiation reviewed by Hinnebusch, 2011). Because eukaryotic ribosomes will initiate at the first AUG and dissociate after reaching a stop codon, the presence of ORFs upstream of the primary ORF function as translational repressor of the later (Kozak, 1995; Calvo et al., 2009; von Arnim et al., 2014).

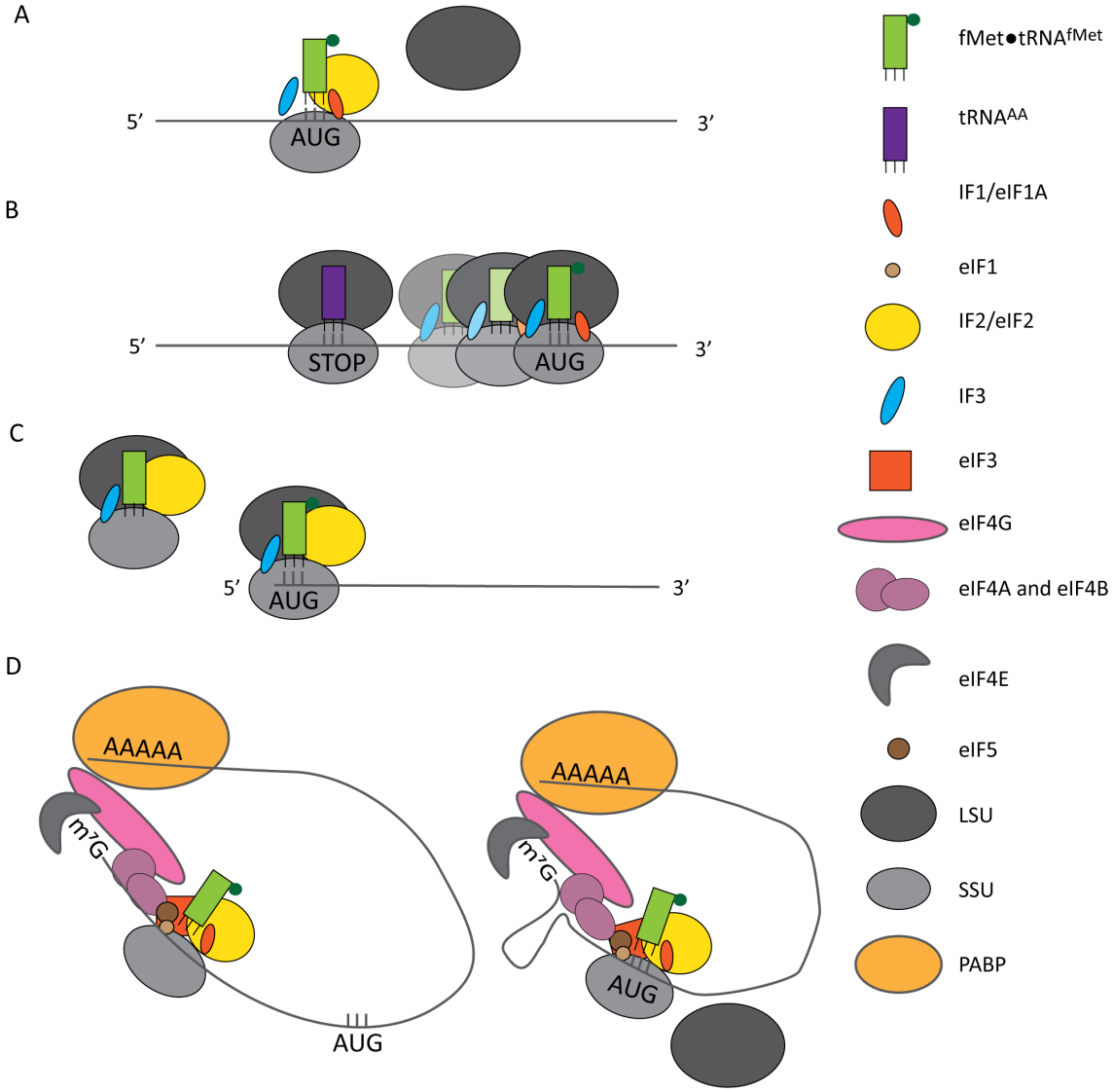

Figure 1.2: Abstract representation of translation initiation modes. (A-C) Observed modes of translation initiation in the eubacterial system. (A) *de novo* translation initiation, (B) 70S ribosome scanning after completion of translation for a proximal start codon, (C) initiation of 70S ribosomes on leaderless transcripts. (D) Scanning mechanism of eukaryotic pre-initiation complex for start codon.

1.1.4.4 Translation elongation

Translation elongation describes the progression of the fully assembled ribosome along the mRNA in a codon-wise manner and extension of the nascent peptide chain. In prokaryotes, the ribosome is thereby assisted by four elongation factors (EF). EF-Tu•GTP delivers and presents the amino-acyl tRNA (AA-tRNA) to the ribosome. In the A-site, codon and anti-codon are matched, and EF-Tu•GDP released after GTP hydrolysis (Loveland et al., 2020, and references herein). EF-Ts helps to recycle EF-Tu by enabling the release of GDP after successful delivery of the AA-tRNA to the ribosome (Kawashima et al., 1996). By this EF-Tu can bind fresh GTP and a new AA-tRNA.
The role of EF-P that binds to the E-site is not fully elucidated. It was proposed to stabilize the alignment of fMet-tRNA^{fMet} in the post-initiation complex and facilitates the first peptide-bond formation (Blaha et al., 2009). Newer studies also showed its importance during translation of poly-proline stretches, which are stiffer because of the proline structure and may introduce frame-shifts of the ribosome (Ude et al., 2013; Doerfel et al., 2013).
Further, the primary amino group of the A-site tRNA starts a nucleophilic attack on the ester bond of the tRNA. This process is catalyzed by structure in the 23S rRNA, the peptidyl transferase center. As a consequence, a peptide bond is formed between the primary amino group of the A-site tRNA and the primary carboxyl group of the P-site tRNA (Pech and Nierhaus, 2012). The ester bond between peptide chain and P-site tRNA is deacylated during this process and the nascent peptide fully transferred to the A-site tRNA (Hiller et al., 2011). After peptide-bond formation, the deacylated tRNA is translocated to the E-site and tRNA with the nascent peptide to the P-site, respectively. Full translocation has high activation energy and is mediated by EF-G•GTP. EF-G•GTP reaches into the decoding center of the ribosome and detaches the $tRNA_2$•mRNA complex (Moazed and Noller, 1989; Ratje et al., 2010; Ermolenko and Noller, 2011). The mRNA, fixed by the codon-anticodon interactions, is moved by one codon with respect to the decoding center of the ribosome. In the post-translocation state, EF-G•GDP dissociates from the ribosome and leaves the A-site free for the next ternary complex of AA-tRNA•EF-Tu•GTP. It is still a matter of discussion whether E-site-tRNA release is spontaneous or coupled to A-site occupation and hydrolysis of the cognate ternary complex (Hausner et al., 1988; Petropoulos and Green, 2012; Nierhaus and Pech, 2012; Chen and Williamson, 2013).
Orthologues for all four EFs were identified in plants and algae and chloroplast translation elongation is assumed to proceed like elongation in *E. coli* (Beligni et al., 2004; Singh et al., 2004; Albrecht et al., 2006; Ruppel and Hangarter, 2007; Aryal et al., 2014).

1.1.4.5 Translation termination

Upon arrival of the ribosome at the stop codon in the A-site, the release factor (RF) 1, serving UAA and UAG, or RF2, serving UAA and UGA, enters the A-site highly codon-specific (Freistroffer et al., 2000) and stimulates the hydrolysis of the ester bond between tRNA at the P-site and the peptide chain (Zavialov et al., 2002; Laurberg et al., 2008). The RF remains stably bound to the ribosome, even after hydrolysis of the peptidyl-ester bond. The removal of RF1/RF2 is assisted by RF3 (Freistroffer et al., 1997). The direct mode of RF1/RF2 release is still under debate. However, the general agreement states a RF3-induced intersubunit and head rotations (comparable to EF-G induced rotations) which disturb the RF1/RF2-ribosome interaction and following the dissociation of the release factor, always under the prerequisite

that the peptide chain was released. RF3 dissociates after hydrolysis of bound GTP (Zavialov et al., 2001, 2002; Koutmou et al., 2014; Peske et al., 2014). Probably, the release functions in the same way in plastids as it does in bacteria (Beligni et al., 2004). Plastidial orthologues for RF1 and RF2, PrfA and PrfB1, respectively, recognize the same stop codons (Meurer et al., 2002; Motohashi et al., 2007). The paralogue of PrfB1, PrfB3, which lacks the stop codon recognition and hydrolytic activity domains, was found to stabilize the transcript of *petB* in the plastid (Stoppel et al., 2011).
In the case the ribosome reaches the last nucleotides of the mRNA without stop codon recognition, the ribosome is unable to recruit RFs and stalls. This may happen because of faulty transcription, cleavage of the mRNA, or frameshifting of the ribosome. In prokaryotes, a process called ribosome rescue starts in those cases and the alternative ribosome-rescue factor A (ArfA) relieves stalled ribosomes using RF2 peptidyl-tRNA hydrolytic capacity (Zeng et al., 2017; Ma et al., 2017; Huter et al., 2017). Recently, an orthologue of ArfB, which has a hydrolytic domain and is therefore independent of RFs, was identified in the genome of *A. thaliana* and was localized in the chloroplast (Gagnon et al., 2012; Nagao et al., 2020).

1.1.4.6 Ribosome recycling

Post-termination disassembling of the ribosome requires ribosome recycling factor (RRF) which binds the A-site and together with EF-G facilitates the dissociation of ribosomal subunits. The structure of RRF was found to be superimposable to tRNA, and a mechanism was proposed that RRF takes the same position as the tRNA in the A-site (Selmer et al., 1999). However, newer structure visualizations of RRF and EF-G bound to the 70S ribosome showed an orthogonal orientation of RRF to the tRNA position (Lancaster et al., 2002; Agrawal et al., 2004). There is a debate about the cascade of actions during ribosome recycling, but groups agree that RRF targets LSU and that EF-G induces molecule rotations. The rotation would lead to breakage of the intersubunit connection and the subunits would dissociate (Hirokawa et al., 2005; Weixlbaumer et al., 2007; Barat et al., 2007; Borovinskaya et al., 2008). A RRF orthologue was also found in plastids which probably has the same function as its bacterial homologue (Rolland et al., 1999; Perez Boerema et al., 2018).

1.1.5 Post- and co-translational protein import

By the development of the endosymbiont to an organelle, plastids became dependent of protein import from the cytosol to fulfill various processes essential for the organism, e.g. photosynthesis, synthesis of amino and fatty acids, hormones and a lot more (reviewed by Wise and Hooper, 2006). The majority of plastid-destined proteins enters the organelle via the "general import pathway" through two large translocation complexes which span the outer and inner envelope of the plastid. Accordingly, they were named Toc and Tic for translocon at the outer/inner envelope of chloroplasts. Proteins passing through the Toc/Tic system feature a N-terminus peptide sequence that is recognized by targeting factors and chaperones. However, in contrast to mitochondrial transit peptides, which share a characteristic secondary structure (Brix et al., 1997; Abe et al., 2000), the transit sequence of plastidial proteins displays high variability and different tools were developed to predict transit peptides (von Heijne et al., 1991; Emanuelsson et al., 1999, 2000). von Heijne et al. (1991) speculated that transit peptides show such variability to enable the interaction with a multitude of chaperons and factors. Additionally,

the variability would add another layer onto regulation of plastidial metabolism by allowing or preventing the translocation under specific conditions of specific proteins according to their transit peptide (comprehensively reviewed by Jarvis, 2008; Li and Chiu, 2010; Shi and Theg, 2013).
In parallel to the general protein import via Toc/Tic, glycoproteins must pass through the endoplasmic reticulum and Golgi before they are imported into the plastid. The import may happen through vesicle fusion with the outer membrane which releases the protein into the intermembrane space from where it passes through some translocon or as a new vesicle into the plastid (Radhamony and Theg, 2006; Nanjo et al., 2006). In addition, a small group of proteins was identified whose import was associated with a very high energy demand but without interaction of the Toc complex (Nada and Soll, 2004; Miras et al., 2007). The components of this pathway are widely unknown.
The protein import into the chloroplast is postulated to be exclusively post-translationally (Weis et al., 2013, and references herein). The protein import of another cell organelle, the mitochondrion, seems to occur also co-translationally, which raises the question if the chloroplastic protein import may also occur co-translationally. Mitochondria arose equally to plastids from an endosymbiosis and lost over the co-evolutionary process most of their genes. Thus, also mitochondria depend on protein import from the cytosol. Mitochondria comprise a translocon import system spanning the outer and inner envelope of the organelle (Tom/Tim) which is the general passage for proteins. However, in electron micrographs, cytosolic ribosomes could be observed associated with the mitochondrial outer membrane (Kellems and Butow, 1972; Kellems et al., 1974, 1975). Later, a study showed that the mRNA of around one-half of the mitochondrially located proteins was enriched in the mitochondrial vicinity (Marc et al., 2002). Obviously, mRNAs of mitochondrion-localized proteins are actively targeted to the mitochondrion by different mechanisms that facilitate the import of the synthesized proteins into the organelle (mRNA localization to mitochondria was reviewed by Weis et al., 2013). Also, mitochondria do not exhibit only post-translational import of proteins, but also co-translational import for a small group of genes was proven (Fujiki and Verner, 1993; Lesnik et al., 2014; Gold et al., 2017; Vincent et al., 2017). Most surprising was the observation by Chang and Clayton (1987). When they analyzed the substrate of the mitochondrially located RNase MRP in mammalian cells, they found a nucleus-encoded tRNA which must have been imported into the mitochondrion. The import of tRNA into mitochondria was later successively shown for yeast and plants which shows its universal need (Small et al., 1992; Tarassov and Entelis, 1992).
In summary, plastids and mitochondria are both cell organelles that have their origin in endosymbiotic events. Due to enormous evolutionary gene loss, both organelles highly depend on the supply of nucleus-encoded genes. Most proteins are imported through a translocon complex system spanning the outer and inner envelop of the respective organelle. However, mechanisms like mRNA targeting to the organelle and co-translational import were observed for mitochondria only. Data supporting a similar mechanism for plastids are absent (Weis et al., 2013).

1.1.6 Membrane insertion and complex assembly

Around 20 % of the estimated plastid proteome consists of integral membrane proteins (Schwacke et al., 2003; van Wijk, 2004). They are located either in the envelope (outer and inner envelope) or the internal thylakoid membrane system. In the next section, the focus will be on the membrane insertion and complex assembly into the thylakoid membrane of

chloroplasts.
The majority of plastid-encoded proteins with transmembrane domains are subunits of the thylakoid complexes involved in the electron transport of photosynthesis. The thylakoid is an intra-organelle membrane compartment unassociated with the inner envelope within the chloroplast stroma. The thylakoid appears either as stacked thylakoid disks (grana) or stroma lamellae which connect the grana. The thylakoid membrane surrounds the lumen (Shimoni et al., 2005; Mustárdy et al., 2008).
The protein complexes of photosynthetic reactions are spatially arranged within the thylakoid network. Studies of the thylakoids revealed photosystem II (PSII) and the cytochrome b_6f complex (cyt-b_6f) as the dominant photosynthetic complexes in grana, whereas PSI and ATP synthase are located in the grana margins and the stroma lamellae (Andersson and Anderson, 1980; Miller, 1980; Johnson et al., 2014). However, complex assembly and maintenance are only feasible at the stroma-accessible thylakoid regions of stroma lamella and grana edges.
The complex assembly happens within the membrane, and the complex subunits must be inserted either post-translationally or co-translationally. Additionally, the thylakoid complexes are bound by a multitude of co-factors. These co-factors play important roles in light-harvesting (chlorophyll), reducing reactions (organometallic clusters), and photoprotection (carotenoids). Studies showed that the binding of the co-factors occurs co-translationally at specific time points in the chloroplast. The time points were identified with toe-printing experiments and referred to as ribosome pausing sites. It was suggested that the early binding enables proper folding and stability of the nascent protein (Kim et al., 1991, 1994a,b).
The transport of complex subunits across or into the thylakoid membrane is supported by four different pathways. The secretory (Sec) and the twin-arginine-translocase (Tat) pathway transfer proteins across the membrane into the lumen, e.g. plastocyanin and PSBO (Hulford et al., 1994; Robinson et al., 1994). Notably, none of the plastid-encoded proteins is lumen-localized. Additionally, proteins can be inserted into the membrane spontaneously or proton gradient (ΔpH) driven (Mant et al., 1994), e.g. PSBW, PSBX, and CF_0-II (Robinson et al., 1996; Kim et al., 1998). Beside, proteins are also inserted into the thylakoid membrane by the signal recognition particle (SRP) pathway which was studied in detail for the membrane insertion of light-harvesting chlorophyll-binding proteins (Schünemann et al., 1998; Bals et al., 2010, reviewd by Ziehe et al., 2018).
The SRP pathway in chloroplasts (cpSRP pathway) is outstanding among SRP pathways known. Thus, in contrast to cytosolic and bacterial SRP pathways, the cpSRP pathway has the ability to process co- and post-translationally proteins (Schünemann et al., 1998; Yuan et al., 2002). Especially, the post-translational membrane insertion is crucial for chloroplasts because multiple components of the thylakoid complexes are imported from the cytosol and have to be inserted post-translationally, e.g. light-harvesting complexes (LHC). Moreover, only in chloroplasts the RNA component of the pathway is missing and an organelle-specific SRP protein was identified (Schünemann et al., 1998). Plastid-encoded proteins are either co-translationally, e.g. PsaA/PsaB and PetA or post-translationally, e.g. AtpA/H and PetD, inserted into the membrane (Friemann and Hachtel, 1988; Zoschke and Barkan, 2015; Zoschke et al., 2017). However, the precise mechanisms of membrane insertion of the plastid-encoded thylakoid proteins are not clarified yet. Nascent PsbA/D1, for example, was found interacting with the chloroplastic SRP protein cpSRP54, but not with cpSRP43 (Nilsson et al., 1999) which builds a heterodimer with cpSRP54 for LHC transfer through the stroma. Additionally, cpSECY was found interacting with ALB3, VIPP1, and cpSRP54 during co-translational membrane insertion of D1 in an *in vitro* reconstructional experiment (Zhang et al., 2001; Walter et al., 2015). But, cpSECY was not found necessary for LHC-membrane insertion (Nilsson et al., 1999). However, mutant experiment with Δ*cpsrp54* in *A. thaliana* showed

only a mild phenotype which indicates potential alternative membrane-insertion modes for D1 (Amin et al., 1999; Tzvetkova-Chevolleau et al., 2007). Additionally, a mutant experiment in *Zea mays* (maize) Δ*cpsecY* revealed a highly disturbed membrane system when *cpsecy* was knocked-out (Roy and Barkan, 1998). Thus, the role of cpSECY is not fully elucidated yet and the complex process of thylakoid membrane insertion remains to be uncovered.
The membrane insertion of plastid-coded proteins but also their assembly into the complex happen partially co-translational. For now, the best studied example of co-translational complex assembly focus on the repair of PSII by the exchange of D1 (Zhang et al., 1999, reviewed by Nickelsen and Rengstl, 2013). In yeast, sophisticated experiments are now established to identify co-translational complex assembly (Shiber et al., 2018; Panasenko et al., 2019) and may be adapted soon also for plastids to uncover and confirm the process of co-translational complex assembly also for other components of the thylakoid membrane complexes.
Furthermore, thylakoid complexes, particularly ATP synthase, are assembled in a specific stoichiometry of the subunits. Studies in *Chlamydomonas reinhardtii* (Chlamydomonas), vascular plants, but also yeast cells and mammalian cells, showed proportional protein synthesis of complex subunits to fit the stoichiometry in the complex (Chotewutmontri and Barkan, 2016; Lukoszek et al., 2016; Trösch et al., 2018; Taggart and Li, 2018). However, the mechanism of regulation seems to be different. Whereas in yeast, the translational output was linked to the gene copy number in the genome (Taggart and Li, 2018), it correlated well with the transcript abundance in Chlamydomonas chloroplasts (only one copy per gene) (Trösch et al., 2018). And, the stoichiometric synthesis of ATP synthase subunits seemed to be defined by translational regulation in *A. thaliana* and *Nicotiana tabacum* (tobacco) chloroplasts (Trösch et al., 2018).

1.2 Light - The driving force of photosynthesis

Chloroplasts are the organelles in plants and algae that can convert light energy into chemical energy that is the fuel for multicellular life on earth. In 1998, the global net primary productivity (the amount of carbon integrated into organic compounds) was estimated as 104.9 pentagrams (Pg = 10^{15} g, of which were 56.4 Pg of terrestrial origin) of carbon per year (Field et al., 1998). This productivity was not only determined by the number of producers but also by the environmental condition they have. Especially, sessile plants are susceptible to changes in the habitat, which is evident from the seasonal and ecosystem related differences in the net primary productivity. Thus, the productivity decreased towards the winter season when days become short, and was generally the highest in regions close to the equator where climate and day length are constant over the year (Field et al., 1998; Geider et al., 2001).

1.2.1 Photosynthesis

Photosynthesis describes the process of the conversion of light energy into chemical energy. Two main processes are defined in the oxygenic photosynthesis. (1) the light reactions that include the oxygen evolution and generation of reducing equivalent (NADPH) and chemical energy (ATP) in the thylakoid membrane by using photons. (2) the dark reactions, or Calvin-Benson-Bassham cycle, that expend NADPH and ATP to assimilate CO_2.

The light reactions of photosynthesis are performed in the thylakoid membrane by the major complexes PSII, cyt b_6f, PSI, and ATP synthase. Both, PSII and PSI are composed of a core complex associated with LHCs, i.e., LHCII with PSII and LHCI and LHCII with PSI. PSII and cyt b_6f are organized as a dimer, whereas PSI ant ATP synthase function as monomers. Photons are captured in the LHCs by chromophores. This process leads to the excitation of electrons and gradual transfer of the excitation energy to the reaction centers of the core complexes of the two photosystems, P_{680} and P_{700}, respectively. Both reaction centers are characterized by two closely arranged chlorophyll-*a* molecules.

Light-harvesting complexes are encoded in the nucleus and imported via the Toc/Tic system into the stroma from where they are inserted into the thylakoid membrane via the SRP pathway (Schünemann et al., 1998). In *A. thaliana*, six LHCI and 15 LHCII genes were identified. Each of them consists of three transmembrane domains and binds up to eight molecules of chlorophyll-*a* (chl-*a*), six molecules of chl-*b* and four xanthophyll molecules (Liu et al., 2004). However, the chlorophyll content and the ratio between chl-*a* and chl-*b* depends on the species and the habitat (Murchie and Horton, 1997).
Isolated chlorophylls in 80 % acetone absorb light of wavelengths in the visible spectrum. chl-*a* has its absorption maxima at around 430 nm and 660 nm and chl-*b* absorbs light preferentially of wavelengths around 450 nm and 640 nm. The embedment of the chlorophyll molecules into large protein complexes enables the gradual decrease of the absorbed energy by energy transfer over the chlorophyll molecules to the reaction centers of PSII and PSI, respectively, and thereby match the excitation energy of the reaction centers. Additionally, through the binding in the LHCs, the absorption spectrum of each chlorophyll molecule is mildly changed to different wavelength, which depends on the chemical surrounding (Rivadossi et al., 2004). Hence, the excitation of the reaction centers can be fulfilled from a broader spectrum of light.

Linear electron transport starts with the excitation of P_{680} in PSII. The excitation leads to the release of an electron of one chlorophyll molecule which is successively transferred to pheophytin and two plastoquinones, of which the later can diffuse through the thylakoid membrane to cyt b_6f. The excitation of P_{680} must happen twice to yield fully reduced plastoquinone (PQH_2). The lack of an electron in PSII is compensated by the oxidation of water at the oxygen-evolving complex (OEC) on the lumenal site of PSII. Here, water is split into protons and molecular oxygen catalyzed by the manganese cluster. The electrons are transferred to $P_{680}{}^{+}$ via Tyr_Z (redox-active amino acid in D1) (Ferreira et al., 2004).
Cyt b_6f performs two consecutive single electron transfers. The first electron of PQH_2 is released to the Rieske protein and transported to cytochrome-*f* where it serves the reduction of plastocyanin, a water soluble metalloprotein in the lumen. The generated semiquinone radical releases a second electron to the stromal plastoquinone binding site. Here, an oxidized plastoquinone from the plastoquinone pool is reduced and takes two protons from the stromal site to the lumenal site of the thylakoid membrane as part of the Q cycle (Hasan and Cramer, 2012, and references herein).
The reaction center of PSI (P_{700}) is composed of two closely located chlorophylls, similar to the reaction center of PSII. It is excited by photons of wavelength 700 nm and the excitation leads to a charge separation resulting in a positively charged chlorophyll radical. The radical is reduced afterwards by an electron delivered by plastocyanin that diffuses in the lumen between cyt-b_6f and PSI. The released electron from the reaction center is probably transferred to a chl-*a* monomer and further to a phylloquinone. Following, the electron is consecutively

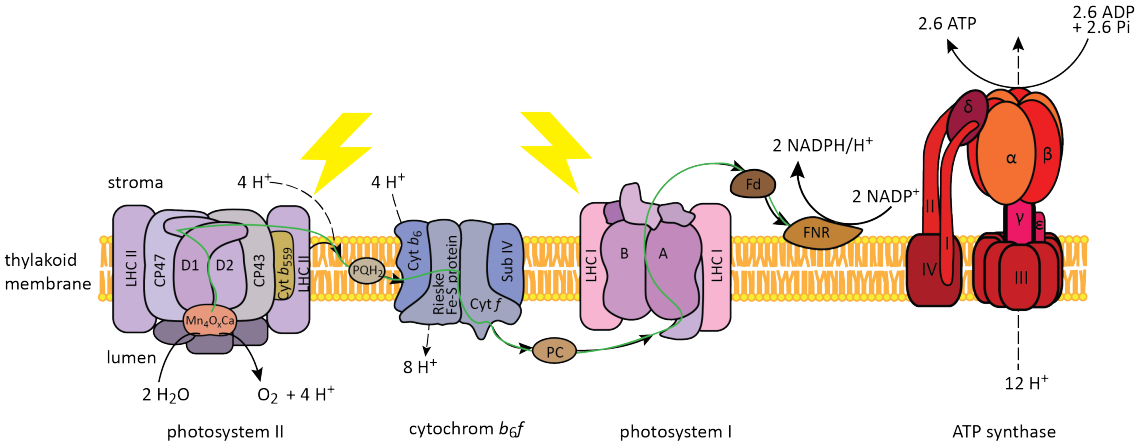

Figure 1.3: Schematic representation of the linear electron transport. Electrons generated in the reaction center of PSII are transported to cyt-b_6f and further to PSI from where they are transferred to ferredoxin. The transport route is represented by the green line. Protons generated by the reduction of water or pumped into the lumen by cyt-b_6f are used to drive ATP synthesis by ATP synthase.

transferred via iron-sulfur clusters to reduce ferredoxin. The reduced ferredoxin diffuses on the stromal site to ferredoxin-$NADP^+$-oxidoreductase, where it serves as co-factor to reduce $NADP^+$ to $NADPH/H^+$ (Amunts et al., 2005, and references herein).
By the action of the linear electron transport of photosynthesis, the lumen is acidified through the water splitting process and the proton pump cyt b_6f. This leads to increased ΔpH at the thylakoid membrane that is the main component of the proton motive force in chloroplasts (Takizawa et al., 2007; Lyu and Lazár, 2017). To balance the proton concentration from lumenal and stromal site, protons are channeled to the stromal site via the ATP synthase and by this providing mechanical power for the phosphorylation of ADP to ATP (Seelert et al., 2000; Junge et al., 2001). Based on measurements in tobacco a transport of 14 protons through the ATP synthase is needed to produce three ATP (Seelert et al., 2000).

1.2.2 Light-induced changes in chloroplast metabolism

Light is a significant environmental signal for plant growth and development and is the ultimate energy source that drives plant metabolism. However, excessive light leads to a significantly reduced photosynthetic efficiency, thus increased photoinhibition which is an unavoidable consequence of the light reaction (Tyystjärvi and Aro, 1996; Anderson and Chow, 2002). The primary target of photodamage is PSII. But as the first complex in the linear electron transport, its function influences the activity of subsequent complexes. Different mechanisms of photodamage were discussed in the last years. Shortly, in the acceptor site mechanism the plastoquinone pool is fully reduced which disables the secondary electron transfer from PSII. However, charge separation still happens in the reaction center and promotes the formation of chlorophyll triplets which further results in the reactive oxygen species (ROS) formation and damage of D1 (Vass et al., 1992). In the donor site mechanism, reduction of the oxidized $P_{680}{}^+$ and $Tyr_Z{}^+$ cannot be performed at sufficient speed or is inhibited by the destruction of the OEC and the manganese cluster. This results in inhibited electron transfer and also a destruction of D1 (Krieger et al., 1998; Hakala et al., 2005). Further, unbound chlorophyll which is immensely photoreactive, leads to a high accumulation of ROS (Santabarbara et al.,

2002).
To summarize, reactions involved in the linear electron transport of photosynthesis result in highly reactive intermediates and also lead to the formation of ROS. Accumulation of ROS and reaction intermediates may act as signal molecules within the cell and/or whole organism (Karpiński et al., 2003; Mateo et al., 2004; Bechtold et al., 2005) but also as a source for enzyme deactivation or destruction.

1.2.2.1 Protection mechanism

The change of thylakoid, cell, and leave morphology is one possibility for plants to temper irradiation effects or even avoid high irradiation. Photonastic movements, for example, are widely described as movements of leaflets to the light. However, if irradiation is too intense, plants hinge down or fold up their leaves to reduce the area exposed to the light source (Saeedi and Roblin, 1986). Additionally, plants may change the location of their chloroplasts in the cells to the lateral cell walls to avoid irradiation (Kasahara et al., 2002; Semer et al., 2018; Howard et al., 2019). Chloroplast movement seems, however, to be an *ad hoc* reaction to high-light intensities and is not used in plants acclimated/adapted to these conditions (Higa and Wada, 2016). Further, the morphology of the thylakoid membrane can be adjusted reversibly. Observation of thylakoid organization in *Spinecea oleracea* (spinach) showed altered stacking of the membrane. Whereas thylakoids of samples harvested in the dark showed a low number of large highly stacked grana, thylakoids of samples harvested in the light had much smaller grana but in higher quantity (Rozak et al., 2002; Wood et al., 2018).

The destructive influence of excessive light on D1 was already described above. To overcome photoinhibition and to reactivate PSII, an energy expensive and complex repair mechanism by which D1 is sacrificed and replaced by newly synthesized protein emerged in photosynthetic organisms.
The half-life of the D1 protein was estimated as $t_{1/2} \sim$ 2 h in *Brassica napus* (rapeseed) seedlings at moderate- (350 μmol·s^{-1}·m^{-2}) and high-light intensities (1,500 μmol·s^{-1}·m^{-2}) and $\sim$ 7 h at low light (20 μmol·s^{-1}·m^{-2}) (Sundby et al., 1993). In *A. thaliana* seedlings, a half-life for D1 of $\sim$ 15 h at a growth irradiation of around 100 μmol · m^{-2} · s^{-1} was measured (Li et al., 2017). D1 is translated from the *psbA* transcript, that shows the highest mRNA transcript level in mature chloroplasts in maize and equally high levels as *rbcL* (encoding the large subunit of ribulose-1,5-bisphosphat-carboxylase/-oxygenase (Rubisco)) in Chlamydomonas, tobacco, and *A. thaliana* (Chotewutmontri and Barkan, 2016, 2018; Trösch et al., 2018). However, under moderate light irradiation, D1 is only translated from a fraction of *psbA* transcript whereas another fraction remains untranslated in the stroma (Minami and Watanabe, 1984; Klein et al., 1988; Minami et al., 1988).
To replace the damaged D1 protein in PSII and enable photosynthesis, the PSII complex has to be moved from grana where it resides in super- or megacomplexes with LHCIIs and PSIIs (organization of PSII in grana reviewed by Dekker and Boekema, 2005) to the accessible region of grana margins and stroma lamellae. This process is initiated by light-dependent phosphorylation of PSII core subunits by STN8 (Tikkanen et al., 2008; Fristedt et al., 2009). When PSII monomer is migrated to grana margins or stroma lamellae, it needs to be partially disassembled to give access to D1. Thus CP43 (encoded by *psbC*) and the OEC are released. Following, D1 is degraded by the membrane-bound exoprotease FtsH, which binds the N-terminus (stromal side) of D1 and degrades it in an ATP-dependent manner. For the action of

FtsH, D1 needs to be dephosphorylated (Rokka et al., 2000; Lindahl et al., 2000). Additionally, DegP-like endoproteases (Deg1, Deg5, and Deg8) cleave loops connecting transmembrane domains of D1 on the lumenal side whereas Deg7 takes this action on the stromal side of the thylakoid membrane (Kapri-Pardes et al., 2007; Sun et al., 2007, 2010). Insertion and assembly of D1 into the CP43- and OEC-lacking complex happens co-translationally. Nascent D1 is targeted by cpSRP54 (probably interacting with the ribosome) to cpFTSY and inserted through cpSecY translocase into the membrane (Walter et al., 2015). However, as described in Section 1.1.6, mutants of cpSRP54 and cpSecY displayed phenotypes which could not finally prove their role in D1 membrane insertion. After successful insertion of D1, CP43 is reinserted. For the proper re-assembling of OEC, the C-terminus of D1 is cleaved to allow the interaction with the manganese cluster (Anbudurai et al., 1994). The repaired PSII is moved back into the grana and inserted into PSII supercomplexes (for comprehensive reviews on PSII repair see Komenda et al., 2012; Nickelsen and Rengstl, 2013; Theis and Schroda, 2016).

It is evident that repair of PSII should be kept at a minimum and that processes, which prevent D1 damage, have to act early. Upon absorption of energy a molecule will be in an excited state, which is in the present case a photon absorbed by a chlorophyll. For relaxation, the excess energy can either be dissipated as heat or light (fluorescence), by transfer to other molecule (energy transfer through the antenna to the reaction center), or chemical changes (release of an electron) (DeEll and Toivonen, 2003; Zhu et al., 2005, and references herein). The non-photochemical quenching of chlorophyll fluorescence (NPQ) describes the decline of fluorescence of antenna chlorophylls in excessed energy accumulation states. NPQ has different components whereas in high light qE is dominating. It was shown that qE is dependent on the proton gradient formed between stroma and lumen. Different components that enhance qE were identified: (1) the zeaxanthin cycle that enables qE at lower ΔpH (Noctor et al., 1991; Rees et al., 1992) and (2) PsbS, a protein in the LHC that does not bind chlorophyll but is sensitive to changes in lumenal pH (Li et al., 2004). Both components enhance the protonation of the LHC and dissipation of excessive energy as heat by conformational changes in the complex (Johnson and Ruban, 2009).

1.2.2.2 Light-modulated gene expression

The above mentioned mechanisms act very fast and are probably meant to protect and adjust the photosynthetic capacity of the system for relatively short exposures to higher light or other stresses that influence photosynthesis, e.g. low temperatures that decrease enzyme activities (Hetherington et al., 1989). However, more extended changes in the environment lead to acclimation responses in the organism to optimize their assimilation and electron transport capacity to the new condition. Plant species use different mechanisms to accomplish this goal. Plants change their leaf morphology by increasing the number of mesophyll cells or leaf veins, the number of chloroplasts per cell which facilitates the adjustment of downstream processes (Lichtenthaler et al., 1981; Amiard et al., 2005; Stewart et al., 2017), and/or the composition of the photosynthetic apparatus (Chow and Anderson, 1987; Evans, 1987; Bailey et al., 2001; Schöttler and Tóth, 2014).
Nevertheless, it must be pointed out that there is a difference in activation and regulation of gene expression in the plant cell due to plastid transition from photosynthetically inactive (etioplast) to active (chloroplast) organelles and due to photosynthesis-mediated triggers.
As described in Section 1.2.1, an increase of irradiation leads to the formation of ROS because of photodamage. ROS and other products of photosynthesis, e.g., redox equivalents, sugars,

amino acids, may act as a signal molecules that traverses the chloroplast membranes and act as a retrograde signal to the nucleus (Pfannschmidt et al., 2001; Fey et al., 2005; Khandelwal et al., 2008). Microarray studies on high-light treated *A. thaliana* revealed transcriptional upregulation of genes involved in antioxidant pathways, e.g., ascorbate peroxidase and glutathione reductase, as well as heat shock proteins and chaperones (Rossel et al., 2002; Kimura et al., 2003). The studies also showed a decrease in transcripts associated with photosynthesis. Moreover, it was shown that the transcription rate of RNA polymerase II (PolII) is increased in the light compared to the dark and that these variations in the transcription speed induce alternative splicing of the genes (Godoy Herz et al., 2019). However, it is not known if PolII activity is further enhanced in high light which would lead possibly to altered transcript stabilities or isoforms. Likewise, no study was published so far following nucleus-gene expression throughout the process of acclimation to find limiting steps in the adaptation of thylakoid complexes to the new light environment.
Also, post-transcriptional processes are regulated by light. Fed-1, for example, is a small protein in PSI encoded by the nucleus. Upon illumination of white tissue, its transcript level increase phytochrome-dependent (Kaufman et al., 1985; Dobres et al., 1987), however in green tissue this gene is regulated on post-transcriptional level by altered transcript stability and translation (Elliott et al., 1989; Dickey et al., 1992; Petracek et al., 1998).
A genome-wide study of polysome-bound mRNA on *A. thaliana* experiencing sudden dark revealed a general downregulation of polysomal loading. Further, a group of genes was identified that showed stable transcript levels in the dark and increased polysomal loading upon re-illumination. This group comprised mainly genes associated with photosynthesis and ribosomal proteins of the chloroplast and cytosol (Juntawong and Bailey-Serres, 2012). Additionally, Eisa et al. (2020) found that chloroplast-located proteins are kept in the cytosol upon high-light treatment because of increased phosphorylation of precursors by STY kinases and a reduction of Toc proteins. However, this study investigated only a few genes that were already shown to be down-regulated in their expression in these conditions, e.g. LHC (Kimura et al., 2003). High-throughput studies would be needed to investigate a potential co-regulation of cytosolic gene expression and import into the chloroplast altered by high light.
In the former section, the repair mechanism of PSII was described and the unique role of D1 highlighted. The regulation of D1 expression was therefore the target of investigation to identify regulators and sequence elements that act in the increased expression upon illumination. Until the 80's of the last century, it was generally believed that the transcript levels of plastid-encoded genes (mainly *psbA* and *rbcL*) were light regulated (Link, 1982; Thompson et al., 1983). However, these studies were based on dark-grown seedlings exposed to light which induced *de novo* assembly of the photosynthetic complexes and did examined the mature chloroplasts. Fromm et al. (1985) found that D1 synthesis is independent of its transcript levels in *Spirodela oligorrhiza* (common duckweed). Multiple experiments followed, confirming the stability of plastidial transcripts and the independence of translation of the transcript levels (Klein and Mullet, 1986; Klaff and Gruissem, 1991; Rapp et al., 1992; Kim et al., 1993b). Especially, experiments with Chlamydomonas identified factors binding on the 5'-UTR of *psbA* which exhibits a stem-loop structure (Danon and Mayfield, 1991; Mayfield et al., 1994; Danon and Mayfield, 1994b). Further experiments suggested potential regulation through redox-potential changes induced by photosynthesis in Chlamydomonas (Danon and Mayfield, 1994a,b; Trebitsh et al., 2000; Trebitsh and Danon, 2001) and also *Hordeum vulgare* (barley) (Pötter and Kloppstech, 1993; Mühlbauer and Eichacker, 1998). So far, multiple factors in Chlamydomonas (Yohn et al., 1998, and references herein) and two factors in *A. thaliana* were identified that were found associated with *psbA* transcript and seem necessary for the translation of D1 (Schult et al., 2007; Link et al., 2012). The two factors in *A. thaliana*

were shown, recently, not to act in a redox-sensitive way (Chotewutmontri and Barkan, 2020). In summary, light induces changes in the chloroplast metabolites that likely act as signaling molecules. Excessive light induces rescue mechanism to protect the cell and its organelles from destructive photosynthetic products. In the long term, plants adjust their morphology to optimize photosynthesis to the available light, either by altered leaf morphology or thylakoid complex accumulation. However, the temporal orchestration of gene expression in the acclimation process was not investigated yet.

1.3 Methods to address translation

Translation is always coupled to the presence of ribosomes on the mRNA and the incorporation of amino acids into a nascent peptide chain. Different methods were established to identify translational features by addressing these characteristics.
Identifying and isolating translating ribosomes would eventually uncover the translated mRNA *in vivo*. Often, the presence of polysomes, mRNAs bound by multiple ribosomes, is associated with active translation. Polysome profiling uses the fact that with an increasing number of bound ribosomes on the mRNA, also the mass of the entire mRNA•ribosome complex increases. Through density gradient centrifugation, ribosomal fractions (mono-, di-, polysomes) can be separated by their mass. Subsequently, mRNA in the different fractions can be isolated and analyzed, either specifically by RNA gel blot (northern blot) (Barkan, 1998) and quantitative polymerase chain reaction (qPCR) (Pal et al., 2013) or by genome-wide approaches using microarrays or deep sequencing (Kawaguchi et al., 2004; Kahlau and Bock, 2008; Yángüez et al., 2013; Bai et al., 2020). Polysome profiling can give a proximation for the ribosomal engagement for specific transcripts and thereby an estimate for its translational strength. However, polysome profiling is more suitable for eukaryotic systems because of the monocistronic character of the mRNA. In prokaryotic systems, like chloroplasts, this method is only limited usable, because of the oligo- and polycistronic character of many transcripts which makes a clear identification of the translated gene nearly impossible. Indeed, polysome profiling was refined to track the exact position of a ribosome on the mRNA by digestion of polysomal mRNAs with nucleases to gain monosomes covering only the small mRNA fragment that was protected from nuclease attack (Ingolia et al., 2009). The obtained mRNA fragments (ribosomal footprints, RFP) can be further analyzed by microarray (Ribo-array) or by deep sequencing (Ribo-seq). For the small plastome, customized microarrays were developed for *A. thaliana*, Chlamydomonas, maize, and tobacco with a ten codon resolution (Zoschke et al., 2013; Trösch et al., 2018). Ribo-seq results in datasets with codon resolution for each translated gene of the organism (Juntawong et al., 2014; Hsu et al., 2016; Chotewutmontri and Barkan, 2016; Wu et al., 2019b). Because each ribosome is associated with one nascent peptide, ribosome profiling (RP) provides an estimate of the translational output of a specific gene and is, therefore, more quantitative as polysome profiling which gives only an estimate for the engaged mRNA.
A related method for polysome and RP is Targeted Ribosome Affinity Purification (TRAP). With TRAP, polysomes or monosomes are immunopurified with specific antibodies that either bind an accessible epitope of the ribosome or an affinity tag introduced to one of the ribosomal proteins. The co-immunoprecipitated mRNA can be analyzed by microarray or deep sequencing (Zanetti et al., 2005; Juntawong and Bailey-Serres, 2012; Juntawong et al., 2014). However, TRAP on cell lysates cannot distinguish between light and heavy polysomal fractions.
Moreover, protein preparations from polysome/RP and TRAP experiments can be used to

analyze the composition of the ribosome as well as to identify associated factors binding the ribosome or the mRNA. This can be done for selected proteins via immuno blot (western) or mass spectrometry analyses (Menschaert et al., 2013; Tadini et al., 2016).
Though, none of these methods can answer the question if the ribosome was translating in the moment of isolation or just sitting on the mRNA waiting for a signal, tRNA, or rescue factor (paused or stalled). Tracing newly translated proteins can be performed by labeling with easily detectable substrates that do not interfere with the translational process. *In vitro* translation systems, cells, tissue, or organism can be fed with radioactive (^{35}S) isotopes incorporated into amino acids or heavy (^{15}N) isotopes provided as nitrogen source, e.g., amino nitrate, that are used as building blocks for the newly synthesized proteins. The readout can either be generated by protein gels for radio-labeled or mass spectrometry for heavy isotope-labeled proteins. Regardless, both methods are challenging for the identification of small proteins or when translational output is dominated by one or two targets, e.g. D1 and Rubisco (Barkan, 1998). Additionally, labeling of whole tissue is limited by the uptake of the substrate. Thus, inhomogeneous distribution and uptake by the system may impair downstream analyses.
In a nutshell, different methods are available to identify translated transcripts and to quantify their output and the proteins that modulate their translation. This being said, none of these methods can address all questions at ones and sophisticated experiments have to be developed which combine features of the different methods in a save and comprehensive way.

1.4 Aim

1.4.1 High-depth chloroplast translatome

In the last decade, multiple studies were published that addressed ongoing translation in plants in high resolution. Using RP, a high-resolution cytosolic translatome of *A. thaliana* was used to confirm annotated and predicted translational sites. Additionally, small ORFs in annotated non-coding RNAs and pseudogenes were identified (Hsu et al., 2016). In maize, the analysis of the translatome along the leaf blade showed developmental changes in the expression of plastidial genes. Further, cell-type specific translation of plastidial genes in bundle sheath and mesophyll cells was elucidated in this study (Chotewutmontri and Barkan, 2016). The separation of membranous and soluble fractions of cell lysates from maize and subsequent RP of the fractions were used to identify membrane engagements of nascent peptides in the chloroplast (Zoschke and Barkan, 2015; Zoschke et al., 2017). Comparison of plastidial translation in *A. thaliana*, Chlamydomonas, and tobacco revealed conservation of translational output between the three organisms (Trösch et al., 2018). And, data obtained from *A. thaliana* were used to identify ribosome pausing sites in the chloroplast by interfering the relative ribosome occupation around specific transcript sites based on secondary structure estimates (Gawroński et al., 2018). Moreover, RP studies were used to identify translational alteration during exposure of plants to various stress condition, such as hypoxia (Juntawong et al., 2014) and high temperature (Lukoszek et al., 2016) as well as sudden light-dark transitions (Chotewutmontri and Barkan, 2018; Chotewutmontri et al., 2020; Gawroński et al., 2020b). Besides, also various mutants displaying disturbed photosynthetic phenotypes were analyzed by ribosome profiling to understand the contribution of the gene in plastidial gene expression processes, i.e. translation regulation (Zoschke et al., 2013, 2017; Trösch et al., 2018; Chotewutmontri et al., 2020).

However, all published studies using RP for plants and algae did tissue enrichment by focusing on roots)(Wu et al., 2019b), enriched for cytosolic ribosomes prior footprint isolation by immunoprecipitation (Juntawong and Bailey-Serres, 2012; Bazin et al., 2017), or did *in silico* enrichment for chloroplastic reads or by hybridizing whole-cell RFP to microarray selective for plastidial genes (Zoschke et al., 2013; Chotewutmontri and Barkan, 2016; Trösch et al., 2018).
Thus, the goal of this project was the establishment of two experimental strategies for the selective enrichment of chloroplastic ribosomal footprints prior library preparation to obtain Ribo-seq datasets of high depth and resolution for the chloroplast. The first strategy was based on previous experiments for the selective enrichment of cytosolic ribosomal footprints (Juntawong et al., 2014) and was adapted for chloroplasts. Two tobacco lines expressing tagged ribosomal proteins in the chloroplast were subjected TRAP experiments and resulting datasets were used to analyze the differential mRNA occupation by the SSU and LSU. Differential expression analysis of the two lines revealed altered translational output for PEP and NDH genes, pointing to potential regulation of the two complexes, but stoichiometric occupation of chloroplastic transcripts by SSU and LSU. In the second strategy, chloroplasts of tobacco seedlings were isolated prior to Ribo-seq experiments either in dark or in light. Analysis of the data revealed selective enrichment of cytosolic ribosomal footprints for chloroplast-targeted genes in chloroplast samples obtained in light hinting to co-translational targeting and/or import of nucleus-encoded proteins into the chloroplast.

1.4.2 Chloroplast translational dynamics during light acclimation

Plants are sessile organisms that are exposed to the environmental conditions. Increased light intensity features photoprotective mechanisms to overcome photoinhibition and destruction of sensitive components that are essential for plant viability. Due to the fact that fluctuating light intensities are typical in nature, e.g., shading by clouds or leaf motions, many mechanisms act fast and can be regulated on multiple levels to fine-tune the effect on the actual situation. However, long-lasting changes in light intensity need an adaptation of the photosynthetic system to optimally use the provided energy. This acclimation of the system takes days to weeks (Schöttler and Tóth, 2014; Grebe, 2015).
By shifting tobacco seedlings from moderate light intensities to high irradiation, I aimed to monitor changes in the chloroplast gene expression pattern in a genome-wide manner to identify modulators of high-light acclimation. Following chloroplast translation using Ribo-array over two days of high-light acclimation revealed a constant upregulation of *psbA* translation which was in line with minor photoinhibition, and constant electron transfer measured for the investigated time frame. However, no other pronounced differences in the plastidial gene expression pattern over two days was observed. These observations suggest an inferior contribution of chloroplastic gene expression regulation, which was limited to the expression of D1, and a predominance of other regulatory mechanisms to high-light acclimation in the analyzed time frame and under the experienced light intensities.

2 Materials and methods

2.1 Materials

2.1.1 Plant lines

Nicotiana tabacum cv. 'Petit Havana' (tobacco) was used for chloroplast isolation (CI) and light-shift experiments.
Plant lines for TRAP were already generated and kindly provided. All used lines were homoplastomic and contain the *aadA* cassette as selection marker for spectinomycin resistance. The endogenous version of the genes was replaced by homologous recombination with the tagged gene version.
A N-terminal 3x human influenza hemagglutinin (HA) tagged Rps15 expressing line was used as tagged version of the SSU of chloroplast ribosomes, hereinafter called HA-Rps15. As control served the line lacking the genomic information for the 3x HA-tag, further referred to as Rps15ctrl. Both lines were generated by Sabrina Finster in the laboratory of Prof. Dr. Christian Schmitz-Linneweber, Humboldt University, Berlin (Finster, 2014).
The line used to tag explicitly the LSU of the chloroplastic ribosome expressed Rpl32 with a C-terminal green fluorescent protein (GFP) tag, in the following called Rpl32-GFP. This line was generated by Sibah Alkalib in in the laboratory of Prof. Dr. Ralph Bock, Max Planck Institute of Molecular Plant Physiology (MPI-MP), Potsdam (unpublished). As control served a line expressing GFP in the chloroplast as a soluble protein (Ruf et al., 2007), further called freeGFP.
Homoplasmy was confirmed for all transplastomic lines by restriction fragment length polymorphism (RFLP) and seed segregation tests by the providing lab.

2.1.2 Antibodies

Table 2.1: List of antibodies used. Information includes the name, target, working dilution used for western blots, and the provider.
(ATP - adenosine triphosphate, GFP - green fluorescent protein, HRP - horse radish peroxidase, IgG - immunoglobulin G)

Antibody name	target molecule	working dilution	order no.	provider
α-Actin	plant actin	1:5,000	A0480	Sigma-Aldrich Corporation (St. Louis, MO, USA)
α-AtpA	ATP synthase subunit alpha, plastidic	1:3,000	AS08304	Agisera (Vännäs, Sweden)
α-GFP	GFP (HRP linked)	1:5,000	GTX26663	GeneTex, Inc. (Irvine, CA, USA)
α-HA	human influenza hemagglutinin	1:5,000	H3663	Sigma-Aldrich Corporation (St. Louis, MO, USA)
α-mouse	mouse IgG (HRP linked)	1:40,000	A9044	sigma
α-NdhH	NADH dehydrogenase-like complex subunit H, plastidic	1:2,000	customized	Peter Westhoff (Kubicki et al., 1996; Kofer et al., 1998)
α-PetB	cyt-b_6 protein of cyt-b_6f complex	1:5,000	AS184169	Agisera (Vännäs, Sweden)
α-PSAD	Photosystem I reaction center subunit II	1:1,000	AS09461	Agisera (Vännäs, Sweden)
α-PsbD	Photosystem II D2 protein	1:1,000	AS06146	Agisera (Vännäs, Sweden)
α-rabbit	rabbit IgG (HRP linked)	1:40,000	170-6515	Bio-rad

2.1.3 Buffers and stock solutions

Table 2.2: List of buffers. Buffers are ordered for the specific experiment. The final volume was adjusted with ddH_2O if not stated otherwise. The buffers used for RNA experiments were filtered through 0.22 μm sterile nitrocellulose filters.

buffer name	composition
Chloroplast isolation	
10x Grinding buffer (10x GB)	500 mM HEPES-KOH - 3.3 M sorbitol - 20 mM EGTA (pH 8.0) - 10 mM $MgCl_2$ - 10 mM $MnCl_2$
1x Grinding buffer (1x GB)	50 mM HEPES-KOH - 330 mM sorbitol - 2 mM EGTA (pH 8.0) - 1 mM $MgCl_2$ - 1 mM $MnCl_2$ - 1 g/l ascorbic acid - 1 g/l PVP-40 - 100 mg/l chloramphenicol - 100 mg/l cycloheximide

List of buffer continued ...

buffer name	composition
HEPES-sorbitol (HS) buffer	50 mM HEPES-KOH - 330 mM sorbitol - 100 mg/l chloramphenicol - 100 mg/l cycloheximide
PPF	3.75 mM PEG 8,000 - 25 μM Ficoll - in Percoll
PPF gradients	10 % (v/v) 10x GB - 40 % (v/v) or 80 % (v/v) PPF
DNA analysis	
CTAB-extraction buffer	2 % (w/v) CTAB - 1.4 mM NaCl - 20 mM EDTA - 100 mM β-mercaptoethanol
TAE buffer	40 mM tris - 40 mM acetic acid - 1 mM EDTA
RNA analysis	
10x MOPS buffer	200 mM MOPS - 80 mM NaOAc - 10 mM EDTA - pH adjusted with NaOH (pH 8.0 for the gel or pH 7.0 for the reservoir buffer)
20x SSC buffer	3 M NaCl - 0.3 M Na-citrate - pH 7.0 with HCl
5x SSC buffer	25 % (v/v) 20x SCC buffer
Northern gel	10 % (v/v) 10x MOPS buffer (pH 8.0) - 3.7 % (w/v) formaldehyde - 1.3 % (w/v) agarose
Methylene blue solution	0.03 % (w/v) methylene blue - 0.3 M NaOAc
Northern sample buffer	3 M deionized formamide - 1 M formaldehyde - 13 % (v/v) 10x MOPS buffer (pH 8.0) - 0.02 % (v/v) bromophenol blue - 0.02% (v/v) xylene cyanole
Reservoir buffer	10 % (v/v) 10x MOPS buffer (pH 7.0) - 3.7 % (v/v) formaldehyde
Polysome analysis	
10x Polysome gradient salts (PGS)	0.4 M tris-HCl (pH 8.0) - 0.2 M KCl - 0.1 M $MgCl_2$
Chase solution	65 % (w/v) sucrose - bromophenol blue for light coloring of chase solution
Sucrose gradients	10 % (v/v) 10x PGS - 0.1 mg/ml chloramphenicol - 25 μg/ml cycloheximide - 15 % / 30 % / 45 % / 60 % (w/v) sucrose
Protein analysis	
1x Transfer buffer	20 % (v/v) 5x transfer buffer - 20 % (v/v) ethanol
2x SDS protein sample buffer	125 mM tris-HCl (pH 6.8) - 4 % (w/v) SDS - 2.7 M glycerol - 25 mM EDTA - 0.02 % (v/v) bromophenol blue - 286 mM β-mercaptoethanol
5x Transfer buffer	124 mM tris - 430 mM glycine
Antibody solution	2 % (w/v) dry milk - 15 mM EDTA - in TBST - antibody stock solution
Blocking solution	4 % (w/v) dry milk - 15 mM EDTA - in TBST
Ponceau S solution	0.1 % (w/v) Ponceau S - 5 % (v/v) acetic acid

List of buffer continued ...

buffer name	composition
Protein isolation buffer	100 mM tris-HCl (pH 7.2) - 40 mM β-mercaptoethanol - 10 % (w/v) sucrose - 5 mM EDTA - 5 mM EGTA - EDTA-free protease inhibitor cocktail (1 tablet/50 ml buffer)
Running buffer	25 mM tris - 86 mM glycine - 3.5 mM SDS
TBST	20 mM tris - 150 mM NaCl - 0.1 % (v/v) Tween 20
Ribosome profiling	
12 % Denaturing polyacrylamide gel	8 M urea - 37.5 % (v/v) acrylamide:bis-acrylamide 19:1 (40 % solution) - in TBE buffer
20x SSPE	3 M NaCl - 20 mM EDTA - 118.2 mM NaH_2PO_4 - 81.8 mM Na_2HPO_4
Polysome extraction buffer	200 Mm sucrose - 40 mM tris-OAc (pH 8.0) - 200 mM KCl - 10 mM $MgCl_2$ - 1 % (v/v) Triton X-100 - 2 % (v/v) polyoxyethylene-(10)-tridecyl ether (POE) - 100 mg/l chloramphenicol - 100 mg/l cycloheximide - 10 mM β-mercaptoethanol
Hybridization buffer	30 % (v/v) 20x SSPE - 10 % (v/v) deionized formamide - 0.01 mg/ml BSA - 0.01 % (v/v) Tween 20
Loading buffer (FDM)	90 % (v/v) deionized formamide - 20 mM tris-HCl (pH 7.5) - 20 mM EDTA - 0.02 % (w/v) bromophenol blue - 0.02 % (w/v) xylene cyanole
RNA fragmentation buffer	400 mM tris-OAc (pH 8.3) - 1,000 mM KOAc - 300 mM $Mg(OAc)_2$
RNA isolation buffer	10 mM tris-HCl (pH 8.0) - 1 mM EDTA - 100 mM NaCl - 1 % (w/v) SDS - 100 mM EGTA
Sucrose cushion	880 mM sucrose ($\sim$ 30 % (w/v)) - 40 mM tris-OAc (pH 8.0) - 100 mM KCl - 15 mM $MgCl_2$ - 100 mg/l chloramphenicol - 100 mg/l cycloheximide - 5 mM β-mercaptoethanol
TBE buffer	89 mM tris - 89 mM boric acid - 2 mM EDTA
TESS	10 mM tris-HCl (pH 8.0) - 1 mM EDTA - 100 mM NaCl - 0.2 % (w/v) SDS
Targeted ribosome affinity purification - TRAP	
Suspension buffer	40 mM tris-HCl (pH 8.3) - 150 mM KCl - 15 mM $MgCl_2$ - 1 mM EGTA - 10 % (v/v) glycerol - 0.1 % (v/v) IGEPAL - 100 mg/l chloramphenicol - 100 mg/l cycloheximide - 300 mg/l heparin - 160 U/ml RNasin® Ribonuclease Inhibitor - EDTA-free protease inhibitor cocktail (1 tablet/50 ml buffer)
Wash buffer	40 mM tris-HCl (pH 8.3) - 150 mM KCl - 15 mM $MgCl_2$ - 1 mM EGTA - 10 % (v/v) glycerol - 0.1 % (v/v) IGEPAL - EDTA-free protease inhibitor cocktail (1 tablet/50 ml buffer)

Table 2.3: List of stock solutions. Stock solutions were prepared in ddH_2O, if not stated otherwise, and filtered through 0.22 μm sterile nitrocellulose filters.

1 % (w/v) Bromophenol blue solution
10 mg/ml Chloramphenicol in ethanol
10 mg/ml Cycloheximide
0.5 M EDTA, pH adjusted with sodium hydroxide to 8.0
0.5 M EGTA, pH adjusted with sodium hydroxide to 8.0
50 % (v/v) Glycerol solution
1 M HEPES-KOH, pH adjusted with KOH to 8.0
10 % (v/v) IGEPAL solution
5 M KOAc
3 M KCl
1 M $Mg(OAc)_2$
1 M $MgCl_2$
1 M $MnCl_2$
1 M NaOAc, pH adjusted with acetic acid to 5.2
3 M NaCl
1 M NH_4OAc in methanol
20 % (v/v) POE solution
10 % (w/v) SDS solution
1 M Tris-OAc, pH adjusted with acetic acid to 8.0 or 8.3, respectively
1 M Tris-HCl, pH adjusted with hydrogen chloride solution to 6.8, 7.2, 7.5, 8.0, or 8.3, respectively
10 % (v/v) Triton X-100
1 % (w/v) Xylene cyanole solution

2.1.4 Chemicals

Table 2.4: List of chemicals. Given are the names used in the laboratory and protocols, the order number, and the supplier at the moment of purchase.

Name	order No.	supplier
β-Mercaptoethanol	63689-100ML-F	Sigma-Aldrich Corporation (St. Louis, MO, USA)
APS	V3131	Promega Corporation (Fitchburg, WI, USA)
Ascorbate	11140-250g	Sigma-Aldrich Corporation (St. Louis, MO, USA)
ATP (100 mM)	GE27-2056-01	Sigma-Aldrich Corporation (St. Louis, MO, USA)
Bis-acrylamide 19:1, 40 % solution	1300-500ML	Merck Chemicals GmbH (Darmstadt, Germany)
Bromophenol blue	17-1329-01	GE Healthcare (Chicago, IL, USA)
BSA	A7906-500G	Sigma-Aldrich Corporation (St. Louis, MO, USA)
Certified™M Molecular Biology Agarose	1613101EDU	Bio-Rad Laboratories, Inc. (Hercules, CA, USA)

List of chemicals continue ...

Name	order No.	the supplier
Chloramphenicol	C0378-5G	Sigma-Aldrich Corporation (St. Louis, MO, USA)
Chloroform/Isoamyl alcohol mixture 24:1	25666-100ML	Sigma-Aldrich Corporation (St. Louis, MO, USA)
cOmplete™, EDTA-free Protease Inhibitor Cocktail	5056489001	Sigma-Aldrich Corporation (St. Louis, MO, USA)
CTAB	9161.2	Carl Roth GmbH (Karlsruhe, Germany)
Cycloheximide	C1988-5G	Sigma-Aldrich Corporation (St. Louis, MO, USA)
Cycloheximide (100 mg/ml in DMSO)	C4859-1ML	Sigma-Aldrich Corporation (St. Louis, MO, USA)
EGTA Titriplex®VI	1.08435.0100	VWR International GmbH (Darmstadt, Germany)
Ficoll PM400 (Typ 400)	F4375-500G	Sigma-Aldrich Corporation (St. Louis, MO, USA)
Formamide deionized	P040.1	Carl Roth GmbH (Karlsruhe, Germany)
GlycoBlue™Coprecipitant	AM9516	Thermo Fisher Scientific, Inc. (Waltham, MA, USA)
Heparin	7692.2	Carl Roth GmbH (Karlsruhe, Germany)
IGEPAL® CA-630	I8896-100ML	Sigma-Aldrich Corporation (St. Louis, MO, USA)
Methylene blue	M9140-25G	Sigma-Aldrich Corporation (St. Louis, MO, USA)
Milk powder	T145.3	Carl Roth GmbH (Karlsruhe, Germany)
PEG 8,000	0263.2	Carl Roth GmbH (Karlsruhe, Germany)
Percoll	17-0891-01	GE Healthcare (Chicago, IL, USA)
POE	P2293-500G	Sigma-Aldrich Corporation (St. Louis, MO, USA)
Ponceau S	5938.1	Carl Roth GmbH (Karlsruhe, Germany)
PVP40	PVP40-100G	Sigma-Aldrich Corporation (St. Louis, MO, USA)
Quartz wool	9208.2	Carl Roth GmbH (Karlsruhe, Germany)
Restore™Western Blot Stripping Buffer	21059	Thermo Fisher Scientific, Inc. (Waltham, MA, USA)
Roti®-phenol	38.1	Carl Roth GmbH (Karlsruhe, Germany)

List of chemicals continue ...

Name	order No.	the supplier
Roti®-phenol/chloroform/ isoamyl alcohol mixture 25:24:1	A156.2	Carl Roth GmbH (Karlsruhe, Germany)
TEMED	T7024-25ML	Sigma-Aldrich Corporation (St. Louis, MO, USA)
Triton X-100	3051.2	Carl Roth GmbH (Karlsruhe, Germany)
TRIzol Reagent	15596018	Thermo Fisher Scientific, Inc. (Waltham, MA, USA)
Tween 20	P9416-50ML	Sigma-Aldrich Corporation (St. Louis, MO, USA)
Xylen cyanole	33919	Riedel - de Haën AG (Seelze, Germany)

Please mark that general lab chemicals, e.g., salts, alcohols, etc., are not listed. Further, Sigma-Aldrich Cooperation is now part of Merck KGaA (Darmstadt, Germany). Riedel - de Haën AG is now a brand of Thermo Fisher Scientific Inc. (Waltham, MA, USA).

2.1.5 Enzymes

Table 2.5: List of enzymes. Enzymes are given with the name, the order number, and the provider.

Enzyme name	order no.	supplier
[.1ex] Ambion™RNase I	AM2295	Thermo Fisher Scientific, Inc. (Waltham, MA, USA)
DreamTaq polymerase	EP0701	Thermo Fisher Scientific, Inc. (Waltham, MA, USA)
Nuclease S7 (micrococcal nuclease, MNase)	10107921001	Sigma-Aldrich Corporation (St. Louis, MO, USA)
Phusion™High-Fidelity DNA Polymerase	F-530L	Thermo Fisher Scientific, Inc. (Waltham, MA, USA)
RNasin® Ribonuclease Inhibitor	N2511	Promega Corporation (Madison, WI, USA)
T4 Polynucleotide Kinase	EK0031	Thermo Fisher Scientific, Inc. (Waltham, MA, USA)

2.1.6 Equipment

Table 2.6: List of equipment. Not listed are consumables, e.g. tubes, sterile filters, and pipette tips.

Equipment name	provider
2100 Bioanalyzer Instruments	Agilent Technologies, Inc. (Santa Clara, CA, USA)
μMACS® Column	Miltenyi Biotec B.V. & Co. KG (Bergisch Gladbach, Germany)
μMACS® Separator	Miltenyi Biotec B.V. & Co. KG (Bergisch Gladbach, Germany)
AllegraTM 25R Centrifuge	Beckman Coulter (Brea, CA, USA)
Amersham™Hybond™-N membrane	GE Healthcare (Chicago, IL, USA)
Amersham™Protran™0.2μm NC	GE Healthcare (Chicago, IL, USA)
Conviron Model BDR16	Conviron Germany GmbH (Berlin, Germany)
Density Gradient Fractionation System	Brandel (Gaithersburg, MD, USA)
DynaMag™Spin Magnet	Thermo Fisher Scientific, Inc. (Waltham, MA, USA)
Eppendorf Centrifuge 5417R	Eppendorf (Hamburg, Germany)
Eppendorf Centrifuge 5804	Eppendorf (Hamburg, Germany)
Eppendorf Centrifuge MiniSpin®	Eppendorf (Hamburg, Germany)
Eppendorf Concentrator Plus	Eppendorf (Hamburg, Germany)
F-6500 fluorometer	JASCO Inc (Easton, MD, USA)
GenePix 4000B Microarray-Scanner	Molecular Devices, LLC (San Jose, CA, USA)
HOBO Pendant® data logger	Onset Computer Corporation (Bourne, MA, USA)
Imaging-PAM M-series, MAXI version	Heinz Walz GmbH (Effeltrich, Germany)
Laboratory Blender	Waring Commercial (Torrington, CT, USA)
Labor-pH-Meter Lab 850	Carl Roth GmbH (Karlsruhe, Germany)
LightCycler® 480 Instrument	Carl Roth GmbH (Karlsruhe, Germany)
Mini centrifuge with slide rotor	Carl Roth GmbH (Karlsruhe, Germany)
Mini Trans-Blot® Electrophoretic Transfer Cell	Bio-Rad Laboratories, Inc. (Hercules, CA, USA)
Mini-Multi-Rotator	Kisker Biotech GmbH (Steinfurt, Germany)
Mini-PROTEAN® Vertical Electrophoresis Cell	Bio-Rad Laboratories, Inc. (Hercules, CA, USA)
Mini-PROTEAN® TGX™gels, 4 - 20 %	Bio-Rad Laboratories, Inc. (Hercules, CA, USA)
NanoDrop™One	Thermo Fisher Scientific, Inc. (Waltham, MA, USA)
OptimaTM L-80 XP Ultracentrifuge	Beckman Coulter (Brea, CA, USA)
OptimaTM L-100K Ultracentrifuge	Beckman Coulter (Brea, CA, USA)
Peqlab Horizontal Gel Electrophoresis System	Peqlab Biotechnologie GmbH (Erlangen, Germany)
PerfectBlue™ Doppel-Gelsystem Twin M	Peqlab Biotechnologie GmbH (Erlangen, Germany)
PerfectBlue™ Doppel-Gelsystem Twin L	Peqlab Biotechnologie GmbH (Erlangen, Germany)
Power Supply EV233	Carl Roth GmbH (Karlsruhe, Germany)
Quantum CX5 Gel Documentation System	Vilber Lourmat (Marne La Vallee, France)

List of technical equipment continued ...

Equipment name	provider
Qubit™4 Fluorometer	Thermo Fisher Scientific, Inc. (Waltham, MA, USA)
Sorvall™RC6 Centrifuge	Thermo Fisher Scientific, Inc. (Waltham, MA, USA)
SW55-Ti Rotor	Beckman Coulter (Brea, CA, USA)
SW41-Ti Rotor	Beckman Coulter (Brea, CA, USA)
Syngene G:BOX Chemi XT4	SynOptics (Santa Clara, CA, USA)
T100™Thermal Cycler	Bio-Rad Laboratories, Inc. (Hercules, CA, USA)
Thermomixer comfort	Eppendorf (Hamburg, Germany)
Tobacco Microarray	Arbor Biosciences (Ann Arbor, MI, USA)
UV-crosslinker BLX-254	Vilber Lourmat (Marne La Vallee, France)
V650	JASCO Inc (Easton, MD, USA)
Vortex-Genie2	VWR International (Darmstadt, Germany)
VWR Thermal Shake lite	VWR International (Darmstadt, Germany)

2.1.7 Kits

Table 2.7: List of commercial kits. Kits are given with the name, the order number, and the provider.

Kit name	order no.	supplier
μMACS HA Isolation Kit	130-091-122	Miltenyi Biotec B.V. & Co. KG (Bergisch Gladbach, Germany)
μMACS GFP Isolation Kit	130-091-125	Miltenyi Biotec B.V. & Co. KG (Bergisch Gladbach, Germany)
Agilent High Sensitivity DNA kit	5067-4626	Agilent Technologies, Inc. (Santa Clara, CA, USA)
Agilent RNA 6000 Nano Kit	5067-1511	Agilent Technologies, Inc. (Santa Clara, CA, USA)
Agilent Small RNA Kit	5067-1548	Agilent Technologies, Inc. (Santa Clara, CA, USA)
ECL Plus Western Blotting Detection	RPN2133	GE Healthcare (Chicago, IL, USA)
NEXTflex® Small RNA-Seq Kit v3	NOVA-5132-06	PerkinElmer, Inc. (Waltham, MA, USA)
Pierce™BCA Protein Assay Kit	23227	Thermo Fisher Scientific, Inc. (Waltham, MA, USA)
Qubit™dsDNA HS Assay Kit	Q32851	Thermo Fisher Scientific, Inc. (Waltham, MA, USA)
Qubit™microRNA Assay Kit	Q32880	Thermo Fisher Scientific, Inc. (Waltham, MA, USA)
Qubit™RNA HS Assay Kit	Q32852	Thermo Fisher Scientific, Inc. (Waltham, MA, USA)
ULS aRNA Labeling Kit	EA-006	Kreatech Biotechnology B.V. (Amsterdam, Netherlands)

2.1.8 Markers

Table 2.8: List of molecular weight markers. Markers are sorted by the type of target molecule. They are listed with the name, the order number, and the supplier

Marker name	order no.	supplier
DNA markers		
GeneRuler 100 bp DNA Ladder	SM0241	Thermo Fisher Scientific, Inc. (Waltham, MA, USA)
GeneRuler 1 kb DNA Ladder	SM0311	Thermo Fisher Scientific, Inc. (Waltham, MA, USA)
Protein markers		
Precision Plus Protein™Dual Xtra Prestained Protein Standards	1610377	Bio-Rad Laboratories, Inc. (Hercules, CA, USA)
RNA markers		
Century™-Plus RNA Markers	AM7145	Thermo Fisher Scientific, Inc. (Waltham, MA, USA)
DynaMarker® Prestain Marker for Small RNA Plus	DM253	Biodynamics Laboratory, Inc. (Tokyo, Japan)
Millennium™RNA Markers	AM7150	Thermo Fisher Scientific, Inc. (Waltham, MA, USA)

2.1.9 Oligo nucleotides

Table 2.9: List of oligo nucleotides. Oligo nucleotides were used as primers for genotyping of transplastomic tobacco lines. Abbr.: f - forward, r - reverse

running no.	name	sequence
1	f-HA-rps15	GTA CCT ACC ATC TTT TTG GAT TCC
2	r-HA-rps15	ACA AAT AAG CTA GGA GTC GTT GAC
3	f-rps15-ctrl	TCA ACG ACT CCT AGC TTA TTT GTC
4	r-rps15-ctrl	TGT TCG GTT TTC CGC AAT TTT CTC
5	f-rpl32-GFP	CAG TTC CAA AAA AAC GCA CTT CG
6	r-rpl32-GFP	ACA GGT AGT TTT CCA GTA GTG C
7	f-GFP	CAT GGT CCT TCT TGA GTT CGT AAC AGC
8	r-GFP	AAC TTG ATG AGT CGA TCC ACC TAC ACG

2.1.10 Software

Table 2.10: List of software. Software is given with version number and reference.

Software	version	reference
Bedtools	2.29.2	Quinlan and Hall (2010)
cutadapt	2.8	Martin (2013)
DESeq2	1.26.0	Love et al. (2014)
GenePix®Pro 7		Molecular Devices, LLC, USA
Image Lab	6.0	Bio-Rad Laboratories, Inc., USA
Plastid	0.4.8	Dunn and Weissman (2016)
R	3.6.3	R Core Team (2019)
Samtools	1.9	Li et al. (2009)
STAR	2.7.3a	Dobin et al. (2013)
UMI-tools	1.0.0	Smith et al. (2017)

2.2 Methods

2.2.1 Plant growth on soil

Seeds were sown on P-Erde (lowly fertilized potting soil, Kausek Gartenbau & Floristenbedarf) and germinated under a transparent plastic cover. For germination, a day - night regime with 16 hours light (130 μmol·s^{-1}·m^{-2} of photons) and 8 hours dark (0 μmol·s^{-1}·m^{-2} of photons) was used. Temperature and relative humidity were kept constant with 22 °C and 70 %, respectively.

2.2.1.1 Plant growth for CI and TRAP

Eight days after sowing, seedlings were transplanted into trays filled with "tobacco soil" (two parts of Einheitserde® Typ T with 1/3 quartz sand, Kausek Gartenbau & Floristenbedarf, Mittenwalde, and one part vermiculite, Floragard, Oldenbrg). Seedlings were kept under germination condition (see above) for another two days before transferring to the green house. The green house had a set day - night regime of 16 h light (350 μmol·s^{-1}·m^{-2} of photons) and 8 h dark with temperatures of 25 °C and 20 °C, respectively. The humidity was kept at 55 % for day and night. Real light hours and intensities were further influenced by the sun light (representative recordings see Supplemental (Suppl.) Figure S1).
Aerial parts (except cotyledons) of the plants were harvested 21 days after sowing either in the dark (30 min before the light was switched on, EON) or in the light (30 min after the light was switched on, SOD). Plants for TRAP were snap-frozen in liquid nitrogen and kept in -80 °C until usage. Plants for CI were immediately processed (see Section 2.2.2).

2.2.1.2 Plant growth for light shift experiment

Eight days after sowing, seedlings were transplanted individually into pots (diameter of 6 cm) filled with P-Erde and kept in germination condition for additional two days. Ten days after sowing, the plants were transferred to their respective standard growth conditions (see Table 2.11).

The shift experiment was performed 21 days after sowing as described by us previously

Table 2.11: Standard growth conditions for the light shift experiments. Plants were acclimated to standard growth conditions prior to the shift experiment for 11 days in low, medium or high light, respectively.

	Light intensity	temperature [°C]		humidity [%]	
	day [μmol·s^{-1}·m^{-2}]	day	night	day	night
Low light	50	24	20	60	55
Medium light	350	24	20	60	55
High light	1,000	24	20	60	55

(Schuster et al., 2020). Shortly, the shift experiment was performed in the light period of day 21, 5 h after SOD. Prior to the shift, "0 min" samples were harvested and snap-frozen in liquid nitrogen. The shift was performed with two identical growth chambers. All plants were removed from standard growth conditions and placed either back to standard (control) or to high-light condition within 1 min. Tissue samples of control and shifted plants were harvested in parallel at defined time points (see Figure 3.11) and snap-frozen in liquid nitrogen. Samples were stored at -80 °C until usage.

2.2.2 Chloroplast isolation - CI

Chloroplasts were isolated from tobacco leaves as described by Fish and Jagendorf (1982) with modifications. To inhibit plastidial and cytosolic translation immediately, each solution and buffer was supplemented with 100 mg/l chloramphenicol and 100 mg/l cycloheximide. Leaves were cut into smaller pieces and blended with 1x GB in a laboratory blender (Waring Commercial, USA) by two intervals with 18,000 rpm and one interval with 22,000 rpm. Each interval lasted five seconds. The homogenate was filtered through four layers of cheese cloth and centrifuged for 4 min at 4 °C with 3,000 *g*. The pellet was resuspended in 1x GB and intact chloroplasts were separated from broken membranes and nuclei in a 40/80 % Percoll step gradient. Intact chloroplasts were located in the interface of 40 % and 80 % Percoll solutions. Chloroplasts were washed three times with HS buffer to remove the Percoll. Chloroplast RNA content was estimated from chlorophyll content in the samples.

For chloroplasts from dark harvested plants, each step of isolation was performed in the dark. Light intensity during the isolation was monitored with HOBO Pendant® data logger (Onset Computer Corporation, USA).

For removal of loosely attached cytosolic RNA on the outer envelope of the chloroplast, separated aliquots of chloroplast suspension were spiked with 250 U/ml of MNase and incubated for 20 min at 4 °C. Chloroplasts were washed twice with HS buffer.

Chloroplasts were pelleted and snap-frozen in liquid nitrogen. They were stored at -80 °C until usage.

2.2.3 Measurement of photosynthetic parameters

Chlorophyll content in leaf discs of defined area or in chloroplast suspension of defined volume was measured in 80 % acetone based on the protocol of Porra et al. (1989). Chlorophyll-*a* 77K fluorescence emission spectra and *in vivo* measurements of chlorophyll-*a* fluorescence parameters were performed on shifted and control plants using a F-6500 fluorometer (JASCO Inc, USA) and the MAXI Version of the Imaging-PAM M-series (Heinz Walz GmbH, Germany), respectively, as described in Schuster et al. (2020), in collaboration with AG Schöttler (MPI-MP).

2.2.4 Nucleic acid analysis

2.2.4.1 DNA isolation from leaf tissue

Genomic DNA was extracted according to the CTAB-based method of Doyle and Doyle (1990). 20-50 mg of leaf tissue were ground in liquid nitrogen to a fine powder and subjected with 500 μl CTAB-extraction buffer. The suspension was incubated for 30 min at 60 °C. While incubation, the mixtures was roughly mixed twice by vortexing. Following, the suspension was washed with 200 μl chloroform and phase separation was done for 10 min at 4 °C with 10,000 *g*. The aqueous phase was rewashed with chloroform. An equivalent volume of iso-propanol was added to the aqueous phase, mixed, and the DNA was precipitated for 30 min on ice. The DNA was pelleted for 30 min at 4 °C with 20,000 *g*, washed with 70 % ethanol and air-dried. Finally, the DNA was resolved in 50 μl ddH_2O supplemented with RNase I and incubated for 30 min at 37 °C. The DNA samples were stored at -20 °C until usage.

2.2.4.2 Polymerase chain reaction - PCR

DNA fragments were amplified by PCR using gene-specific oligonucleotides in a T100™Thermal Cycler (Bio-Rad Laboratories Inc., USA). The DreamTaq DNA polymerase (Thermo Fisher Scientific Inc., USA) was used for the amplification of DNA fragments up to 700 bp and the Phusion™High-Fidelity DNA polymerase (Thermo Fisher Scientific Inc., USA) was used for the amplification of larger DNA fragments. PCR reactions were prepared following the manufacturer's instructions.

2.2.4.3 Agarose gel electrophoresis for DNA separation

Depending on the expected DNA fragment size obtained by PCR amplification, DNA was separated using a 1 or 2 % (w/v) agarose gel in TAE buffer, supplemented with ethidium bromide for DNA detection under UV light. 100-bp and 1-kb Gene Ruler DNA Ladder (Thermo Fisher Scientific, Inc., USA) were loaded in parallel and the gel was run at 5 V/cm in TAE buffer using the Peqlab Horizontal Gel Electrophoresis System (Peqlab Biotechnologie GmbH, Germany). Quantum CX5 Gel Documentation System (Vilber Lourmat, France) was used to record the gel.

2.2.4.4 Northern blot analysis

Northern blot analysis of RNA was performed as described by Barkan (1998) with some minor modifications. Equal volumes of RNA isolated from polysome fractions were concentrated by vacuum centrifugation and resolved in 5 μl northern sample buffer and denatured for 5 min at 70 °C. RNA electrophoresis was performed in the Peqlab Horizontal Gel Electrophoresis System (Peqlab Biotechnologie GmbH, Germany). RNA was loaded on the RNA gel in parallel to Century™-Plus RNA Markers and Millennium™RNA Markers (both Thermo Fisher Scientific, Inc., USA) and electrophoresed for 10 min with low voltage (2 V/cm) to allow samples to enter the gel. The voltage was increased to 4 V/cm for 2 h. During electrophoresis, the reservoir buffer was circulated and chilled from the exterior with ice.
The RNA was transferred to an Amersham™Hybond™-N membrane (GE Healthcare, USA) by capillary blot. Thus, the gel was laid onto the membrane and 5x SSC buffer was supplied from the top. RNA blotting was performed overnight. Subsequent, RNA was crosslinked to the membrane using UV light (120 mJ/cm^2).
rRNA bands were visualized through methylene blue staining of the membrane.

2.2.5 Polysome analysis

Analytical polysome fractionation was performed as previously reported for maize by Barkan (1993) with minor modifications. Briefly, deep-frozen leaf tissue was ground in liquid nitrogen and suspended in 1 ml per 100 mg fresh tissue of polysome extraction buffer supplemented with 0.5 mg/ml heparin and cOmplete, EDTA-free Protease Inhibitor (final concentration according to manufacturer's instruction). The suspension was filtered through glass wool and centrifuged for 10 min at 4 °C with 15,000 *g*. 2 ml of supernatant were gently laid onto 9 ml continuous sucrose gradient (15 to 60 % sucrose) and polysome fractions were size separated by ultracentrifugation in a SW41 Ti rotor (Beckman Coulter, USA) for 4 h at 4 °C with 37,000 rpm ($\sim$ 235,000 *g*). 1 ml fractions were obtained for further analysis using a Density Gradient Fractionation System (Brandel, USA). Fractions were split into aliquots of 300 μl.
RNA was isolated following the procedure described by Barkan (1998). Proteins were isolated from fraction aliquots using methanol chloroform-based method for quantitative protein extraction described by Wessel and Flügge (1984).

2.2.6 Protein analysis

2.2.6.1 Protein isolation from leaf tissue

Proteins from leaf tissue were isolated according to the protocol from Cahoon et al. (1992) with some adaptations. Shortly, 200-400 mg plant tissue were ground in liquid nitrogen to a fine powder and resuspended in 250 μl of protein isolation buffer per 100 mg fresh tissue. The suspension was extracted with 500 μl of Roti®-phenol. Phase separation was performed by centrifugation for 10 min with 10,000 *g*. 200 μl of the aqueous phase were transferred to 1 ml of 0.1 M NH_4OAc in methanol. Proteins were precipitated at -20 °C overnight. Proteins were pelleted for 1 h at 4 °C with 20,000 *g*. The pellet was washed with 500 μl of 0.1 M NH_4OAc in methanol, air-dried and resolved in 100 μl of 1 % (w/v) SDS.

2.2.6.2 Protein quantification

Proteins were quantified using Pierce™BCA Protein Assay Kit (Thermo Fisher Scientific, Inc., USA) according to manufacturer's instructions.

2.2.6.3 Western blot analysis

For qualitative and quantitative detection of specific proteins, proteins were denatured in one volume equivalent of 2x SDS loading buffer for 10 min at 65 °C. Proteins were loaded, either by the same amount (quantitative) or the same volume (qualitative), on a 4-20 % Mini-PROTEAN® TGX™Precast Protein Gel (Bio-Rad Laboratories, Inc., USA) in parallel to Precision Plus Protein™Dual Xtra Prestained Protein Standards (Bio-Rad Laboratories, Inc., USA). The gel was run for 1 h at 4 °C with 120 V in running buffer. Proteins were transferred electrophoretically onto an Amersham™Protran™NC membrane with a pore size of 0.2 μm (GE Healthcare, USA) with the Mini Trans-Blot® Electrophoretic Transfer Cell (Bio-Rad Laboratories, Inc., USA) in 1x transfer buffer for 4 h at 4 °C with 26 V.
Abundant proteins were stained with Ponceau S solution on the membrane according to manufacturer's instructions. Further, the membrane was sequentially incubated with blocking solution, primary antibody solution, and secondary antibody solution for 1 h each. In between, the membrane was washed three times with TBST for 10 min. Detection was performed with ECL Plus Western Blotting Detection Reagents (GE Healthcare, USA) according to manufacturer's instruction and Syngene G:BOX Chemi XT4 (SynOptics, USA).
Quantification of chemiluminescent signals was done using Image Lab software (version 6.0, Bio-Rad Laboratories, Inc., USA).

2.2.7 Microarray-based RP - Ribo-array

2.2.7.1 Ribosome footprint isolation

RFPs from leaf tissue were prepared as described by Schuster et al. (2020). In brief, tissue was ground in liquid nitrogen to a fine powder and suspended in 1 ml polysome extraction buffer per 100 mg fresh tissue (sampling of 500 μl suspension for RNA fragmentation, see Section 2.2.7.2). The suspension was filtered through glass wool and insoluble components were pelleted for 10 min at 4 °C with 15,000 g. The solution was spiked with $CaCl_2$ solution (final conc. 5 μM) and MNase (final activity 150 U/ml) and incubated for 1 h at room temperature (between 23 and 25 °C). Monosomes were purified via ultracentrifugation through 1 ml sucrose cushion in a SW55 Ti rotor (Beckman Coulter, USA) for 1.5 h at 4 °C with 55,000 rpm ($\sim$ 300,000 g).
The monosome pellet was resuspended in 500 μl RNA isolation buffer. RNA was isolated with TRIzol™Reagent (Thermo Fisher Scientific, Inc. USA) according to manufacturer's instructions. An additional washing step of the aqueous phase with chloroform/isoamyl alcohol (IAA) was introduced before RNA precipitation. The RNA pellet was solved in 50 μl ddH_2O and RNA concentration was determined with NanoDrop™One (Thermo Fisher Scientific, Inc., USA).

RFPs were purified on a customized 12 % denaturing polyacrylamide gel (19:1 acrylamide:bisacrylamide, PAGE). RNA was concentrated to dryness with a Concentrator Plus (Eppendorf, Germany) and resolved in 1 μl RFP loading buffer per 1 μg RNA. The sample was mixed for 10 min at 45 °C. Further, the RNA was denatured for 10 min at 70 °C and loaded on the gel (35 μl per lane). The gel was run in TBE buffer at 10 °C and with 30 W for 2 h. According to DynaMarker® Prestain Marker for Small RNA Plus (Biodynamics Laboratory, Inc., Japan), the segment between 20 and 50 nt was excised and the RNA was eluted in 4 ml TESS buffer per gel slice at 4 °C over night with gentle rotation.
The solution was extracted with an equivalent volume of Roti®-phenol/chloroform/IAA spiked with 2.5 μl GlycoBlue™Coprecipitant (Thermo Fisher Scientific, Inc., USA) per gel slice. The aqueous phase was mixed with 2.5 volume equivalents of ethanol and precipitated over night at -20 °C. The RNA was pelleted for 1 h with 15,000 *g* at 4 °C. For further purification and concentration, the RNA was resolved in 500 μl 0.1 M NaCl solution and mixed with an equal volume of Roti®-phenol/chloroform/IAA. The resulting upper aqueous phase was washed with 200 μl chloroform/IAA 24:1 to remove traces of phenol. The aqueous phase was mixed with 2.5 volume equivalents of ethanol and the RNA was precipitated over night at -20 °C. RNA was pelleted for 1 h at 4 °C with 20,000 *g* and following it was washed with chilled 70 % ethanol and air-dried. The RNA pellet was resolved in 20 μl ddH_2O and the final concentration was determined with NanoDrop™One.

2.2.7.2 RNA fragmentation

RNA from 500 μl tissue-polysome extraction buffer suspension was immediately isolated with TRIzol™Reagent according to manufacturer's instruction. The RNA was solved in 50 μl ddH_2O and RNA concentration was determined with NanoDrop™One.
10 μg RNA were diluted in a of 22.5 μl ddH_2O and mixed with 2.5 μl RNA fragmentation buffer. The mixture was incubated for 12.5 min at 85 °C. The fragmentation reaction was stopped by adding 225 μl chilled TESS buffer and was mixed with an equal volume of Roti®-phenol/chloroform/IAA. The resulting upper aqueous phase was washed with 200 μl chloroform/IAA 24:1 to remove last traces of phenol. Fragmented RNA was mixed with 2.5 volume equivalents of ethanol and precipitated over night at -20 °C. RNA was finally pelleted for 1 h at 4 °C with 20,000 *g*. The resulting RNA pellet was washed with chilled 70 % ethanol and air-dried. The RNA pellet was resolved in 20 μl ddH_2O and the final concentration was determined with NanoDrop™One.

2.2.7.3 RNA labeling and array hybridization

RNA labeling was performed as described by Schuster et al. (2020). Summarized, 4 μg of RFP or 3.5 μg of fragmented total RNA isolated from shifted and control samples were differentially chemically labeled with Cy5 and Cy3 using the ULS aRNA Labeling Kit (Kreatech Biotechnology B.V., Netherlands), respectively, according to manufacturer's instructions. Labeled RNA was concentrated by vacuum centrifugation. Cy5- and Cy3-labeled RFP or fragmented total RNA, respectively, were suspended together in 110 μl hybridization buffer and denatured for 10 min at 70 °C. The denatured sample mixture was hybridized to a custom tiling microarray (Arbor Biosciences, USA) which was designed for the tobacco plastome (Scharff et al., 2017).

The hybridization and microarray scanning were performed as described by Schuster et al. (2020).

2.2.7.4 Data analysis from microarray

Data processing and analysis were performed as described by Schuster et al. (2020). Shortly, primary analysis of the array was done with GenePix®Pro 7 software (Molecular Devices, LLC, USA). Saturated spots were excluded from further analysis, and from the remaining spot signals their respective local background signal was subtracted.
Further analysis was performed with Excel 2016 (Microsoft, USA). Signal intensities below 100 a.u. were considered as background and accordingly set to zero to reduce the noise in the analysis. Each probe signal was normalized to the average probe signal of all protein coding regions and over all analyzed samples. Average ORF signals were $\log_2$-transformed and normalized by the zero-control average ORF signal of three biological replicates. The relative abundance of each ORF signal was calculated to the average ORF signal of the sample. The $\log_2$-fold change was calculated between shifted and control samples for translational output (RFP signals) and transcript accumulation (transcript signals). Translational efficiency was calculated as the ratio of translational output to transcript accumulation. Considering the physiological condition of the shift experiment, moderate changes in gene expression were considered to occur rather than strong alteration in transcript abundance or translational output, respectively, and a $\log_2$-fold change of $\pm$ 1.3 for three or more consecutive time points was considered as biologically relevant.
For pausing analysis, the signal fraction of each position in the ORF was calculated as described by Chotewutmontri and Barkan (2018) and fold changes of two for two or more consecutive time points between shifted and control samples were considered as possible biologically relevant light-responsive changes in ribosomal-pausing.
The microarray data were summarized in an excel-sheet which can be downloaded from `http://www.plantphysiol.org/content/182/1/424/tab-figures-data#fig-data-additional-files`.

2.2.8 Sequencing-based RP - Ribo-seq

2.2.8.1 RFP isolation from isolated chloroplast

RFPs from isolated chloroplasts were isolated as described in Section 2.2.7.1 with some modifications. Briefly, deep-frozen chloroplasts ($\sim$ 1000 μg chlorophyll) were lysed in 1 ml polysome extraction buffer. The lysate was further diluted with 1 ml polysome extraction buffer. Insoluble particles were pelleted via centrifugation for 10 min at 4 °C with 15,000 *g*. Because chloroplasts aliquots contained much less RNA than samples obtained from leaf tissue, monosomes were prepared by adding only 250 U/ml RNase I. Samples were incubated for 1 h at room temperature (between 23 and 25 °C). Further steps of isolation followed the method described in Section 2.2.7.1 with two exceptions. (1) Concentrations were determined using Qubit™microRNA Assay Kit (Thermo Fisher Scientific, Inc., USA). (2) RNA was resolved in 30 μl RFP loading buffer for PAGE purification and gel segments between 20 and 45 nt were cut out.

2.2.8.2 TRAP

Monosomes for TRAP were isolated as described in Section 2.2.7.1 with modifications. Shortly, plant material was ground in liquid nitrogen to a fine powder and suspended in 1 ml polysome extraction buffer supplemented with cOmplete, EDTA-free Protease Inhibitor per 100 mg fresh weight leave tissue. The suspension was filtered through glass wool and centrifuged for 10 min at 4 °C and at 15,000 *g*. Monosomes were prepared by adding 600 U/ml RNase I to the solution and incubation for 1 h at room temperature. The solution was split into two aliquots for monosome purification via ultracentrifuation. The aliquot for immunoprecipitation (IP) was laid onto a 1 ml sucrose cushion and the aliquot representing the input sample was laid onto a 2 ml sucrose cushion. The samples were centrifuged for 1.5 h at 4 °C and at 55,000 rpm ($\sim$ 300,000 *g*) in a SW55 Ti rotor.
The input sample was further processed as described in Section 2.2.7.1, except that the final concentration determination was performed with the Qubit™microRNA Assay Kit.
The monosome pellet for IP was suspended with 1 ml suspension buffer and incubated with mild shaking on ice for 10 min. Following, the pellet was resuspended by pipetting. Insoluble components were pelleted via centrifugation for 10 min at 4 °C with 10,000 *g*. The supernatant, following manufacturer's instructions, was spiked with 150 μl of antibody-bound super-paramagnetic μMACS MicroBeads (Miltenyi Biotec B.V. & Co. KG, Germany). The sample was carefully mixed and incubated for 1 h on ice in the dark. The suspension was added to the M column of the μMACS separation system. The column was washed four times with wash buffer and removed from the magnetic stand. The MicroBeads were eluted with 500 μl RNA isolation buffer. The sample was further processed as described in Section 2.2.7.1, while RNA concentrations were measured with Qubit™microRNA Assay Kit.

2.2.8.3 Library preparation for deep sequencing

For 5'- and 3'-phosphorylation of RFPs, up to 60 ng RFPs (depending on the yield from RFP isolation) were diluted in 4.9 μl ddH_2O and incubated for 5 min at 65 °C. 1.4 μl PNK master mix (0.7 μl 10x T4 PNK buffer, 0.35 μl T4 PNK, 0.35 μl RNasin) were added to the sample and mixed carefully. The mixture was incubated for 10 min at 37 °C before adding 0.7 μl 10 mM ATP. The reaction was incubated for 30 min at 37 °C, followed by incubation for 20 min at 65 °C.
Phosphorylated RFPs were diluted with ddH_2O to 10.5 μl and the cDNA library was generated with the NEXTflex® Small RNA-Seq Kit v3 (PerkinElmer, Inc., USA) according to manufacturer's instruction. Concentration and quality of cDNA library were assessed with Qubit™dsDNA HS Assay Kit (Thermo Fisher Scientific, Inc., USA) and Agilent High Sensitivity DNA kit (Agilent Technologies, Inc., USA), respectively.
Single-end 75-bp sequencing of barcoded and multiplexed samples was done on Illumina NextSeq 500 platform at the Max Planck Institute for Molecular Genetics, Berlin.

2.2.8.4 Reference Genomes

The sequence information and gene annotation for the mitochondrion and the plastid genome from tobacco were downloaded from NCBI nucleotide database (NC_006581.1 and

NC_001879.2, respectively) (Shinozaki et al., 1986; Yagura, 2005; Yukawa et al., 2005). The nuclear genome sequence information from tobacco was obtained from the Sol Genomic Network (Fernandez-Pozo et al., 2014; Edwards et al., 2017). Since the reference genome for tobacco lacks the information for rRNA and tRNA, the sequences were extracted separately. The references for nucleus- encoded rRNA were also obtained from NCBI nucleotide database (AJ300215.1 (5.8S rRNA), AJ222659.1 (5S rRNA), AJ236016.1 (18S rRNA), AF479172.1 (26S rRNA)). The information for tRNA sequences was extracted from the reference genome of *Nicotiana sylvestris* (Sierro et al., 2013).

2.2.8.5 Sequencing data processing and analysis

Software for data processing and analysis was installed and performed under Ubuntu 18.04.2. Detailed program calls with parameter description are documented in the Supplemental Section A.1.
De-multiplexed .fastq-formated reads were 3'-adapter removed using `cutadapt` (version 2.8) (Martin, 2013). Reads smaller than 25 bases and larger than 45 after adapter removal were excluded from further analysis. Reads were mapped sequentially with `STAR` (version 2.7.3a) (Dobin et al., 2013) to the plastidial, mitochondria, and nuclear reference genomes from tobacco. Mapped reads were deduplicated with UMI-tools (version 1.0.0) (Smith et al., 2017) to remove PCR duplicates. Downstream processing and analysis of mapped reads were performed with `Bedtools` (version 2.29.2) (Quinlan and Hall, 2010), `Samtools` (version 1.9) (Li et al., 2009), `Plastid` (version 0.4.8) (Dunn and Weissman, 2016), and R (version 3.6.3) (R Core Team, 2019). For analysis, only uniquely mapped reads were considered.
The sequencing statistics and read coverage for the samples were summarized in an excel sheet. The excel sheet and the raw sequencing data can be obtained from Dr. Reimo Zoschke (Max Planck Institute of Molecular Plant Physiology, zoschke@mpimp-golm.mpg.de) upon request.

3 Results

3.1 Zoom-in into chloroplast translation

The preparation of RFP from cell lysate is coupled with drawbacks for the analysis of chloroplast translation in high resolution. It was already well documented that reads obtained with the RP protocol are highly enriched for rRNA fragments. Today, laboratories use rRNA depletion with commercial or customized kits to reduce the number of rRNA fragments. Additionally, RFP reads obtained from whole cells have their origin mainly in the cytosol. The fraction of organelle derived RFPs that were not rRNA or tRNA was estimated as less than 10 % from data generated from tobacco by the protocol at hand (Yang Gao, personal communication) and from data published for maize (Chotewutmontri and Barkan, 2016, S2 table), in case of non-green tissue the amount would be negligible. To enrich the samples for chloroplastic RFPs (cpRFPs), two strategies were followed. First, to enrich for cpRFPs isolated chloroplasts were used for the RFP preparation. The second approach followed the co-immunoprecipitation of translating ribosomes (TRAP). This method was already shown to be suitable for the analysis of translated mRNA populations in the plant cytosol (Zanetti et al., 2005; Juntawong et al., 2014).

3.1.1 Chloroplast isolation followed by ribosome profiling as a tool for the investigation of chloroplast and chloroplast-associated translation

3.1.1.1 High amounts of starch accumulated in artificial light conditions hampering high quality chloroplast isolation

A critical component for plant growth, but also for chloroplast isolation is starch accumulated as granules in the chloroplast over the light cycle. The starch is, under physiological conditions, used as carbon source in the night when photosynthesis is inactive (Pal et al., 2013; Strenkert et al., 2019). During the isolation process, those granules disrupt the double membrane of chloroplasts because of their higher density and faster movement in the centrifugal field (Stitt and Heldt, 1981), leaving either empty chloroplast envelopes or thylakoid remnants.
To get high yield of intact chloroplasts from the isolation process, it was critical to find a growth condition that minimized the starch content in tobacco at the harvesting time points. Because it was already shown that in long-day condition the accumulated starch in tobacco chloroplasts is not completely remobilized overnight (Matt et al., 1998), different growth conditions were tested for minimized starch accumulation. Light intensities and light sources were chosen according to established growth conditions for tobacco in the house (see Table 3.1).

Table 3.1: Growth conditions for minimal starch accumulation and high chloroplast yield at SOD from tobacco leaves. Plants were cultivated in trays à 40 plants on soil for 11 days. Light intensities are given in μmol·s^{-1}·m^{-2} if not stated otherwise. Starch accumulation was estimated by the visible starch pellet; – states for very small pellet and ++ for very big pellet. Each condition was represented by one tray. The experiment was performed in May 2017. Abbr.: LED - light-emitting diode; SOD - the start of the day

running no.	light source	light/dark in h	temperature in °C	light intensity given	light intensity measured	fresh weight in g	starch accumulation
1	sun & Na-vapor	>16/<8	20-31	-	350 - 1100	50.8	-
2	LED	16/8	22/18	130	100	9.5	±
3	Fluorescence	12/12	24/20	80 %	220	25.8	-
4	LED	16/8	22/18	100 %	140	8.3	±
5	LED	16/8	26/20	700	340	5.4	++
6	Metal-halide	16/8	24/20	350	290	22.4	++
7	Fluorescence	16/8	24/20	350	270	21.3	+

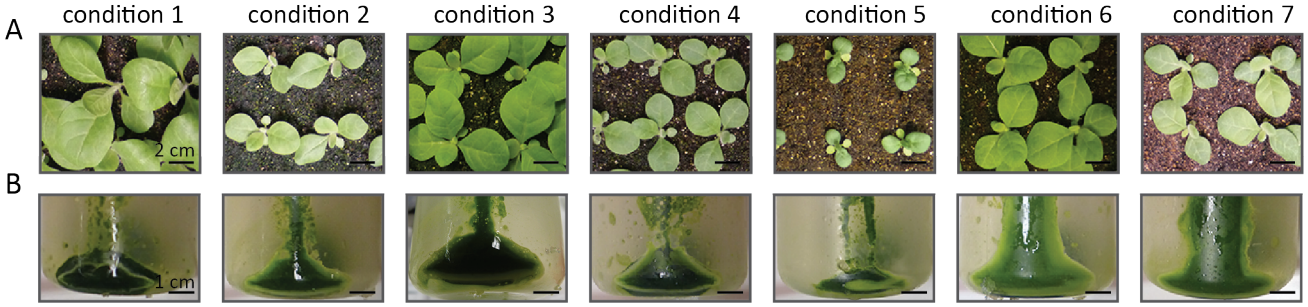

Figure 3.1: Tobacco seedlings grown in different climate conditions displayed distinct growth phenotype and starch accumulation. Seedlings were grown for 10 days together in condition 4 and further grown for 11 days in selected experimental growth conditions (see Table 3.1). (A) Phenotype of plants after 11 days in experimental conditions 1 to 7 (bar = 2 cm). (B) Chloroplast pellets after first pelleting according to CI protocol showed different amounts of free starch (white pellets, bar = 1 cm). Because of the high leaf amount obtained from condition 1, the sample had to be split for the isolation process. Thus, the chloroplast pellet of condition 1 represented only half of the final chloroplast yield.

Additionally, my goal was to make growth conditions for the different experiments (see Sections 3.1.1.3,3.1.2.3, and 3.2) as similar as possible. Thus, seeds were germinated for 10 days in pre-growth condition (condition 4) and subsequently transferred to experimental conditions, where condition 6 corresponded to standard growth condition of the light shift experiment.
After 11 days in the experimental environments, a correlation between growth phenotypes of plants and the experienced light intensities was observed. As expected, the higher the light intensity, the more fresh weight was gained (see Table 3.1 and Figure 3.1 A). The highest fresh weight yield was obtained from the culture grown under greenhouse condition (condition 1), whereas the smallest plants were obtained in condition 5. Condition 5 was considered as inconvenient for further experiments. Here, plants experienced high day temperature and low relative humidity. Even though tobacco is a high-light and high-temperature adapted plant, the shift from pre-growth to the experimental condition 5 was probably too harsh and stressful. Even, the water supply was tightly controlled, seedlings displayed a mild drought-stress phenotype.
To determine the starch accumulation roughly, plants were harvested 30 min after SOD and processed to the first pelleting step of the CI protocol. Starch accumulation was estimated from the visible starch pellet. Chloroplast pellets from plants grown in conditions 1 and 3 showed only a very thin ring of starch, whereas chloroplast pellets obtained from conditions 5, 6, and 7 were completely embedded in starch (Figure 3.1 B). The starch amount could not be estimated from the growth phenotype. In condition 3 and 5, plants showed the same phenotype but contained significantly different amounts of starch. Considering that the growth condition differed in many parameters, it was impossible to determine the specific factor(s) responsible for the starch accumulation from a single experiment. Greenhouse condition led to the highest fresh weight of plants (double amount compared to condition 3 and 6) and lowest starch accumulation at harvesting. These plants also experienced the longest day (because of the natural sun cycle, the harvest was end of April) with most substantial fluctuations in light intensity over the photoperiod (Suppl. Figure S1). From all strictly controlled conditions, however, plants grew optimal for chloroplast isolation in condition 3.
Condition 6 corresponded to the environment used for the light shift experiment. The plants showed high tissue yield but also the highest starch accumulation. Thus, condition 6 was not suitable to grow plants for CI followed by RP. Further, for this project, there was no primary interest in specific responses to selected treatments and associated regulators to make growth conditions as controlled and reproducible as possible.
Consequently, greenhouse condition was chosen as a compromise between reproducibility of growth condition and optimal yield and quality of obtained samples, not only for CI but also for TRAP. This, at least, should ensure better comparability between deep-sequencing data.

3.1.1.2 Chlorophyll content as estimate of RNA concentration in isolated chloroplasts

Important for the quality of RFPs is the adequate digestion of mRNA by nucleases. Here the concentration, activity, and incubation time are the parameters to adjust for optimal results by preventing over- or underdigestion of the RNA samples. The performed experiments relied on the usage of RNase I with a specified incubation time of one hour. The parameter left for adjustment of the digestion protocol was the RNase I concentration. In the RP literature, the RNase I concentration is often adjusted to the RNA concentration of the sample (Juntawong et al., 2014; Lei et al., 2015; Hsu et al., 2016). For the estimation of the RNA concentration in isolated chloroplasts samples, RNA was isolated using TRIzol® and the chloroplast concentra-

tion was adjusted by chlorophyll content that was measured according to Porra et al. (1989) from 100 μl aliquots (Suppl. Figure S2). Chlorophyll content measurements can be done fast and easily from multiple technical and biological replicates without dilution steps which would be necessary for the counting of chloroplasts with a Neubauer chamber or a particle counter. The RNA concentration to chlorophyll content for isolated chloroplasts was, based on these measurements, estimated as 1 μg RNA per approximately 20 μg chlorophyll.
Chloroplast aliquots were lysed in 2 ml extraction buffer, and the digestion was performed with 250 U/ml RNase I which was less concentrated than for the TRAP experiment but 4 times the RNase I proportion used by Wu et al. (2019b) for root tissue. The high concentration of RNase I should compensate for the high dilution of RNA in the solution.

3.1.1.3 Highly enriched chloroplastic reads in CI Ribo-seq data sets

Three different chloroplast samples were generated to obtain highly enriched cpRFPs. They differed in the light condition of harvesting and isolation, i.e. dark and light, and the way of pre-processing, i.e. digestion of chloroplast-attached RNA by MNase, further called "Dig" and "noDig" for digested and not digested, respectively. The obtained mRNA fragments were processed into sequencing libraries, in which Dig:dark and noDig:light samples were multiplexed together and Dig:light was sequenced separately on an Illumina Nextseq 500 platform.
Sequencing resulted in nearly 610 million and 169 million reads for Dig:dark/noDig:light and Dig:light samples, respectively. Individually, the biological replicates counted from 27 to 44 million reads for the first and 49 to 61 million reads for the second sequencing set. After adapter trimming, the number of reads were reduced to around 85 % of the raw input, which was a result of adapter dimer removal, an artifact from PCR amplification (Suppl. Dataset 2). Following, the reads were aligned sequentially to the three genomes of tobacco, i.e., plastidial, mitochondrial, and nuclear, to minimize misalignment of chloroplastic reads to promiscuous sequences of the nuclear and mitochondrial genome, respectively.
The most considerable fraction of reads aligned to the plastome with more than 82 % for the light samples and with up to 75 % for the dark sample. As for the light samples, nuclear reads were reduced to less than 10 %. Here, the pre-processing of chloroplasts reduced the fraction even more (Figure 3.2 A and Suppl. Dataset 2). The Dig:dark sample, however, mainly varied in the portion of organelle reads but had a relative reproducible portion of nuclear reads from around 21 % between the replicates. Mitochondrial reads made up to 1 % of all reads. That was comparable between the samples, though Dig:light had less mitochondrial-derived reads. Interestingly, samples from pre-processed chloroplasts had a high fraction of unmappable reads of 5 to 11 %. In the case of Dig:dark3 even 19 % of reads were not assigned to one of the three genomes (Figure 3.2 A (gray bar) and Suppl. Dataset 2).
Further, mapped reads were categorized into reads mapping to rRNA/tRNA and the remaining genomic regions. rRNA and tRNA made between 65 to 70 % of reads in the noDig:light sample and 71 to 80 % in the Dig:light sample. Equivalent to the high variability within the Dig:dark sample for organelle read contribution, the resulting fractions of rRNA and tRNA were also divers (Suppl. Dataset 2).
As the next step, reads were deduplicated to remove PCR duplicates and multi-mapping reads were filtered out. Both kinds of reads bias results by increasing the coverage of specific genomic regions artificially. Also, rRNA and tRNA related reads were removed from the data because they are not informative.
Further, the read length distribution of all uniquely mapped reads was determined for the

three samples (Figure 3.2 B). All three samples showed a similar read length distribution for the three compartments. The cytosolic reads (average: blue lines, SD: light blue area) were majorly 34 to 35 nt long. This is much longer than the published lengths for cytosolic reads in plants (28 to 31 nt in *A. thaliana* (Juntawong et al., 2014; Hsu et al., 2016), 28 nt in *Solanum lycopersicum* (tomato) (Hsu et al., 2016; Wu et al., 2019b)), and 30 to 31 nt in maize (Chotewutmontri and Barkan, 2016) respectively. Mitochondrial read-size distribution had two local maxima. The dominant read size was 29 to 30 nt which correspond to the reported read size of maize mitochondria (Chotewutmontri and Barkan, 2016), but which is a bit larger than the footprint size of 27-28 nt reported for *A. thaliana* (Planchard et al., 2018). The second maximum was detected with a read size of 43 nt in Dig:dark and noDig:light samples, but was missing in Dig:light. However, no study was published so far that reported a second, not that abundant, but longer read size of around 43 nt. Chloroplast read lengths displayed a multimodal distribution with a significant peak at 30 nt and two minor peaks at 27 nt and 37 nt, respectively. The peak at 37 nt was not pronounced in the Dig:light samples (Figure 3.2 B, right panel). Nevertheless, read sizes are identical to the published data from maize chloroplasts (Chotewutmontri and Barkan, 2016, 2018), yet the maize footprint sizes were uniformly distributed over the read size spectrum. The overall larger read sizes compared to the published data, especially for cytosolic and mitochondrial reads, indicates insufficient digestion of RNA fragments.

Next, the read quality *per se* was analyzed. A criterion of RFPs is the three-nucleotide periodicity, resulting from codon-based progression of the ribosome. Uniquely mapped reads of most abundant read sizes for the three cellular compartments (Figure 3.2 B) were aligned to a region comprising the annotated ORF's translational start sites/start codon (SC, $\pm$ 50 nt around SC) and the 5'-end of the reads were assigned to the corresponding frame. The most abundant frame was defined as frame 0 and the following defined as frame 1 and frame 2, respectively. For all three compartments and all three samples, a major frame was assigned (Figure 3.2 C). However, the contribution of reads to frame 0 was low in this experiment with 40 to 50 % for chloroplastic and cytosolic reads, respectively. Already published data obtained frame 0 abundance of more than 60 % in maize for chloroplast reads (Chotewutmontri and Barkan, 2016) to up to 96 % in *A. thaliana* for cytosolic reads (Hsu et al., 2016). However, the herein observed frame abundances for cytosolic reads are in range of the published abundance for cytosolic reads in maize (Chotewutmontri and Barkan, 2016, 2018). A frame 0 abundance of more than 60 % for mitochondrial reads was obtained but was based on a very low read number which is not considered representative (less than 1,500 reads; Suppl. Dataset 2). Both, read-length distribution and frame abundances point to incomplete digestion by RNase I.

In summary, CI prior RP enriched the deep sequencing data sets to more than 75 % for chloroplastic reads. This was an increase of more than threefold to the expected 30 % chloroplastic reads from the general RP protocol.

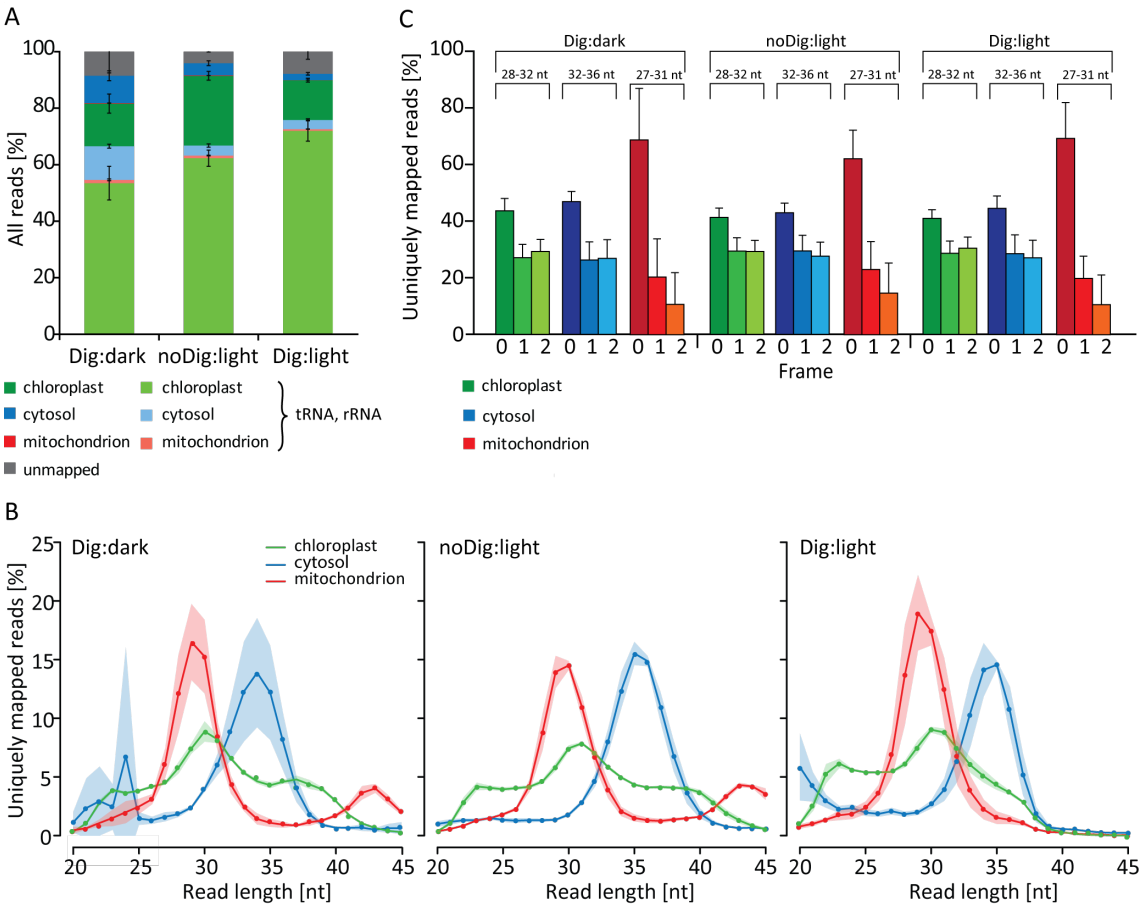

Figure 3.2: RFP characteristics from CI samples for all three subcellular compartments. (A) Bar plots showing the fraction of read origin for all reads of the CI samples, as indicated at the bottom. The values are split into reads originating from rRNA and tRNA (lower part, light colors) or from any other genomic region (upper part, dark colors) as stated by the legend below the graph. Unmappable reads are colored gray. (B) Read length distribution for all uniquely mapped reads as mean values are represented as scatter plot with connective lines. The x-axis shows the read length in nt and the y-axis shows the percentage of reads of the specific size to all reads mapped to the coding sequences of the specific subcellular compartment. (C) The in-frame affiliation of uniquely mapped reads around the translational start site ($\pm$ 50 nt) of annotated ORFs. In-frame fraction is represented for most abundant read sizes as indicated on top.
Represented values are based on three (Dig:dark, noDig:light) or four (Dig:light) biological replicates (Suppl. Dataset 2), respectively. Compartments are color-coded: chloroplast - green, cytosol - blue, mitochondrion - red. Black error bars (A and C) and light-colored areas (B) represent the SD.

3.1.1.4 A distinct fraction of cytosolic reads is enriched in CI samples

One goal of the CI was to find potential co-translational import into the chloroplast which was already observed for mitochondria (Fujiki and Verner, 1993; Weis et al., 2013) and the endoplasmic reticulum (ER, reviewed by Weis et al., 2013). Nevertheless, this process was never observed for chloroplasts and an exclusively post-translational import is postulated.
From the general mapping statistics, a clear enrichment for chloroplastic reads was observed. However, a distinct fraction of cytosolic reads was detected in each sample. To address

corresponding genes, the coverage for each annotated ORF in each subcellular compartment was assessed (total of 69723 annotated ORFs). The counts for all three compartments were combined and the CPM value (counts per million) for each gene in each replicate was calculated.
Because most genes, especially mitochondrion- and nucleus-encoded, were represented by very few reads and could therefore not assigned confidentially as "translated", only genes were further considered that had at least a coverage of 50 reads. Correlation analysis of biological replicates showed a high correlation within the samples (Suppl. Figure S3) for all genes. Comparing light and dark samples, coverage differences of plastidial (green dots) and nuclear (black dots) genes were observed as separation of both populations (dots did not lay on the same diagonal). That separation indicates the activated translation of plastidial genes in light environment and shows that chloroplast isolation in the dark resulted in less cpRFPs. Surprising was the lack of evident read enrichment for *psbA* in the light samples compared to the dark sample, which was expected. In maize, the transition from dark to light led to an increase of six-fold of ribosome abundance on the *psbA* mRNA (Chotewutmontri and Barkan, 2018). Comparisons of the single replicates, however, showed enrichment for *psbA*-derived reads of only up to 2.5-fold, but the enrichment was not specific for *psbA*. Thus, also other plastid-encoded genes displayed high read enrichment in the light (Suppl. Figure S3, *psbA* marked by an arrow). Replicate Dig:dark3 correlated less well with the other dark replicates. Additionally, there was one plastidial gene more enriched compared to all other replicates (Suppl. Figure S3, single green dot above and below scatter plot diagonals compared to dark and light replicates, respectively). This gene was identified as *cp078* (also *orf75*), a hypothetical protein-coding gene.
To see, if cytosolic reads were selectively enriched by chloroplast isolation, Dig:light was compared to the whole tissue light sample and Dig:dark was compared to the whole tissue dark sample (input:light and input:dark, respectively, input samples from TRAP experiment, Sections 2.2.8.2 and 3.1.2.3).

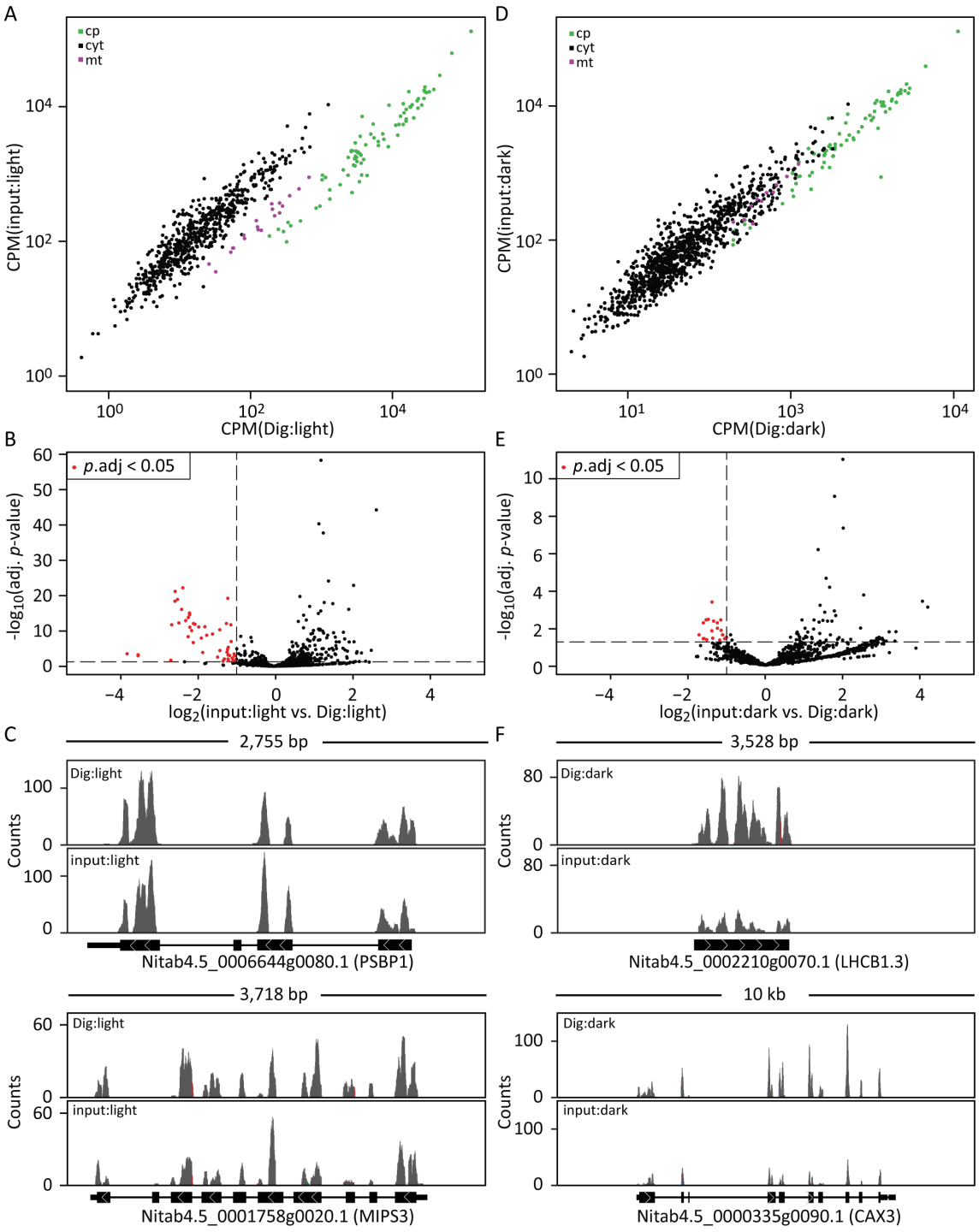

Figure 3.3: Specific cytosolic reads were enriched in isolated chloroplast samples. (A) Scatter plots of CPM values for light samples. The x-axis represents the CPM values of the CI sample, and the y-axis represents the CPM values of the input sample. x-axis and y-axis are in logarithmic scale. The genes are color-coded according to the origin of the reads (magenta - mitochondrion, black - nucleus, green - plastid, representation of mean values from 4 biological replicates). (B) Volcano plots of differentially enriched nucleus-encoded genes in CI light samples. Differentially enriched genes were selected by adjusted p-value < 0.05 and $\log_2$(fold change) $<$ -1 obtained by DESeq2 analysis (thresholds marked by the dashed horizontal and vertical line, respectively). Significantly enriched genes in the CI samples are highlighted as red dots. (C) Gene coverage plots of two representatives of significantly enriched genes for light samples. Shown are the coverage of the gene in the CI sample (upper panel) and input sample (lower panel). Gene models are shown below. Gene coverage plots were generated with IGV (Robinson et al., 2011). (D-F) Equivalent to A-C, but for dark samples. Values in D are averages over three and four biological replicates for Dig:dark and input:dark, respectively.

Dig:light and input:light replicates displayed a differential enrichment for plastidial genes. However, there was also a cluster of nucleus-encoded genes enriched in Dig:light (Figure 3.3 A). To investigate the potential enrichment of specific nucleus-encoded genes in the Dig:light sample, differential expression analysis was performed using the R-package DESeq2 (Love et al., 2014). To be more stringent for this analysis, only genes were considered with read counts in at least three replicates and present in Dig:light (Dig:light - 849 genes, input:light - 3134 genes, overlap - 818 genes). Of those, 131 genes were significantly enriched in the CI sample by, at least, two-fold. However, most of these genes were plastid-encoded, as it would be expected. But 28 genes were encoded by the nuclear genome (Suppl. Table S1 and Figure 3.3 B). Half of the nucleus-encoded and significantly enriched genes in the CI sample are associated with chloroplast function, e.g. chlorophyll-binding and photosystem subunit. If co-translational import occurs and depends on the nascent peptide, an enrichment of reads toward the 3'-terminal of the gene was expected because the nascent peptide chain must have emerged from the ribosome to be exposed to some import system of the chloroplast. The peptide-exit tunnel can cover, depending on the folding of the nascent peptide (α helix is denser), 30 to 60 AA. Thus, enrichment of reads is expected earliest after 90 bp from the start codon. However, no enrichment towards the 3'-end of the genes in the CI sample was observed (Figure 3.3 C).
The comparison of Dig:dark and input:dark was performed accordingly. The enrichment of chloroplastic reads was not that strong in the Dig:dark sample indicating the general downregulation of chloroplastic translation in the dark (Figure 3.3 D). However, some nucleus-encoded genes showed an equal enrichment as plastidial genes and to characterize the enrichment, dark samples were also subjected to differential expression analysis. Because Dig:dark consisted only of three biological replicates and replicate 3 was shown to be less comparable to the other replicates, genes were selected for Dig:dark with read counts in at least two replicates (Dig:dark - 3170, input:dark - 2616, overlap - 2304 genes). DESeq2 analysis resulted in 46 genes that were significantly enriched in Dig:dark by, at least, two-fold. The low number of enriched genes in Dig:dark, which was lower than the number of plastid-encoded proteinogenic genes, confirmed the low translational activity in the chloroplast during the absence of light. Of the enriched genes, 20 genes were nucleus-encoded (Figure 3.3 E and Suppl. Table S1). Enriched nuclear genes encoded mainly for secretory and membrane-bound proteins which were not localized in the chloroplast (exception LHC proteins). Dig:light and Dig:dark overlapped in the enrichment of two genes, an unknown protein (ID: Nitab4.5_0000980g0290.1) and a myo-inositol-1-phosphate synthase (MIPS2, ID: Nitab4.5_0000715g0160.1). Remarkably, the coverage of genes identified in the dark samples was much higher in the CI sample compared to the input sample. The coverage of the light samples was reasonably equal in most cases so that the two-fold enrichment was not apparent from the gene coverage displayed (Figure 3.3 C, F, Suppl. Table S1).
To summarize, chloroplast isolation was an excellent method to enrich for cpRFPs. Additionally, significantly enriched reads of nucleus-encoded genes which products function in the chloroplast were observed in the Dig:light sample. The Dig:dark sample was mostly enriched for membrane-bound and secretory proteins and showed reduced translation of plastid-encoded genes. However, CI would be disadvantageous for the analysis of translation from specific environmental conditions and time series (as shown in Section 3.2), because of the time consuming and harsh procedure of chloroplast isolation that can influence gene expression.

3.1.2 Immunopurification of translating ribosomes from the chloroplast

3.1.2.1 Tagged chloroplast ribosomal proteins are found in actively translating ribosomes

The chloroplast ribosome consists of proteins encoded in the chloroplast itself and proteins imported from the cytosol. To ensure that tagged ribosomal proteins are located in translating chloroplast ribosomes, and do not to compete with endogenous ribosomal protein gene products, homoplastomic tobacco lines in which *rps15* and *rpl32* were replaced with N-terminally and C-terminally of tagged gene copies (Figures 3.4 A, C and 3.5 A, C), in the following named HA-Rps15 and Rpl32-GFP, respectively, were used for TRAP experiments.
For TRAP, young tobacco plants provided the tissue for experiments. HA-Rps15 and Rpl32-GFP showed a wild-type phenotype in the seedling stage of 21 days, as used for the experiment. Also in the generative stage, plants were wild type-like (Figures 3.4 B and 3.5 B). To ensure that the tagged proteins are found in translating ribosomes, polysome analyses were performed (Figures 3.4 D and 3.5 D).
Incorporation of Rpl32-GFP into functional ribosomes was expected because of the essentiality of the protein for chloroplast viability and the wild-type phenotype of the line. Indeed, the tagged protein was detected in the high-density fractions of the polysome gradient demonstrating that Rpl32-GFP-tagged ribosomes can perform translation. Additionally, a second band of smaller molecule size was detected in the low-density fractions, which likely corresponded to soluble, unbound GFP (Figure 3.5 D and Suppl. Figure S4 B). This hinted towards cleavage of the tag from Rpl32 or degradation of the protein to some extent. For the TRAP experiment, fractions of soluble free GFP were uncritical, because it could not penetrate the sucrose cushion for monosome purification (30 % (w/v) sucrose) in the RP protocol and, hence, did not competed with Rpl32-GFP for antibody binding in the immunoprecipitation (IP) step.
For HA-Rps15, one of the non-essential ribosomal proteins in the chloroplast (Fleischmann et al., 2011), the localization of the protein in actively translating ribosomes was in question, because the Rps15-knockout mutant has no visible phenotype under standard growth condition (Fleischmann et al., 2011). Hence, if the HA-tag would cause inactivation of the protein function, the wild-type phenotype of the line was unaffected. However, HA-Rps15 was found in high-density fractions of the polysome gradient (Figure 3.4 D), confirming its assembly into actively translating ribosomes.
Taken together, the selected transplastomic lines for TRAP had wild-type phenotypes under controlled, and greenhouse growth conditions and the tagged ribosomal proteins were found in polysomes. Thus, they were usable for TRAP experiments to enrich cpRFPs for library preparation and sequencing.

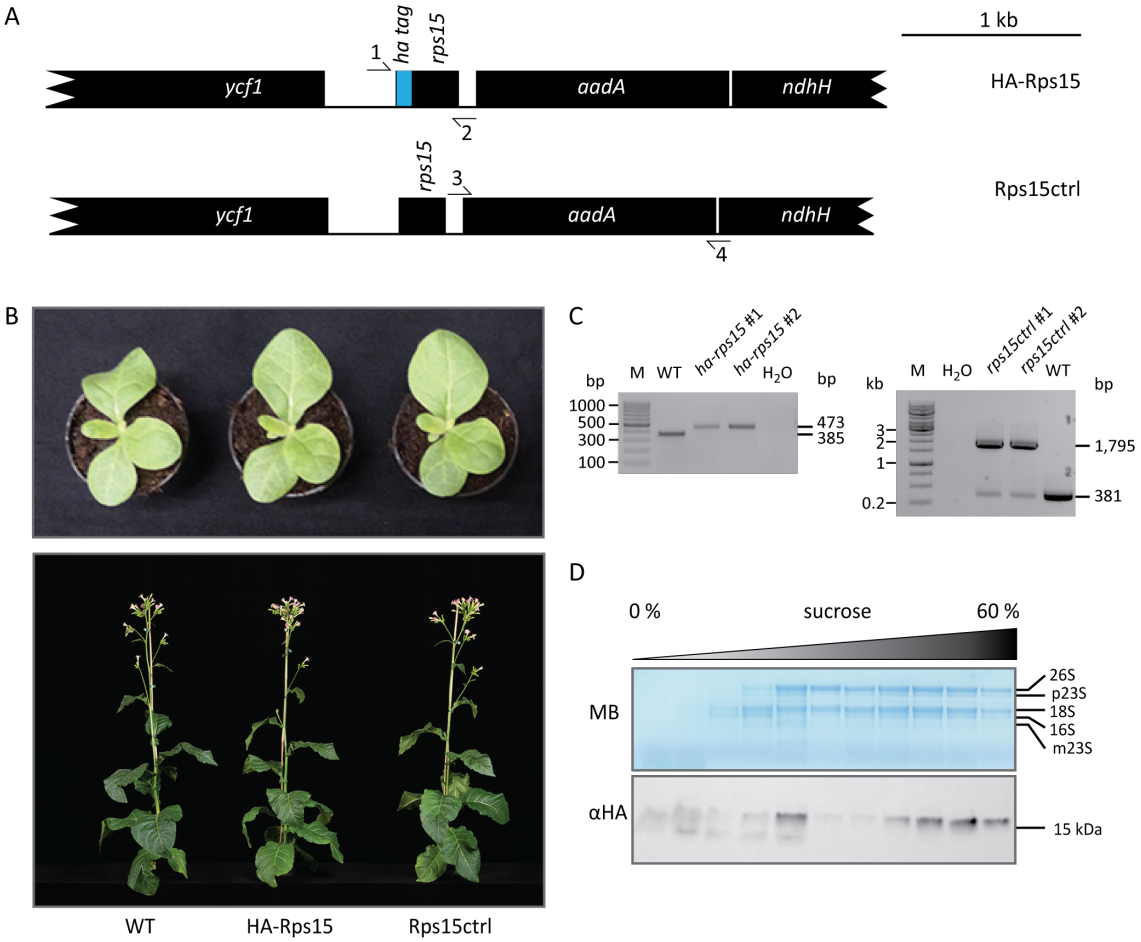

Figure 3.4: HA-tagged Rps15 takes part in translating ribosomes and does not interfere with ribosomal function. (A - D) Characterization of HA-Rps15 and Rps15ctrl (untagged control) provided by Prof. Dr. C. Schmitz-Linneweber (HU Berlin). (A) Physical map of the *rps15* locus in the plastid genome. HA-tag (turquoise) was inserted directly behind the start codon of *rps15* and the *aadA*-cassette as selection marker was inserted between *rps15* and *ndhH*. Small black arrows define the primer binding positions for PCR amplification and are numbered according to Table 2.9. (B) Phenotypes of HA-Rps15 and Rps15ctrl lines at the age of 21 days (top panel: the age for TRAP experiment) and 56 days (bottom panel: flowering) were wild type-like. (C) DNA gel with HA- or *aadA*-spanning PCR amplicons of *ha-rps15* (left) and *rps15ctrl/aadA* (right), respectively. PCR product for *ha-rps15* had a size of 473 bp (wild type: 385 bp). PCR of control samples shows an amplicon with 1.8 kb referring to *aadA*-cassette and a smaller, less abundant, amplicon of wild-type size with 381 bp which may be an artifact of PCR procedure. PCR confirmation of tag and marker insertion was performed with two independent replicates. Homoplasmy of the lines was previously demonstrated by RFLP and seed segregation test. (D) RNA gel blot and immuno blot analysis of polysome fractions of HA-Rps15 shows incorporation of tagged protein into translating ribosomes. Low sucrose density to high sucrose density fractions were loaded on the gels from left to right. rRNA on the RNA gel blot was labeled with methylene blue (MB) and HA-Rps15 was detected on the immuno blot with an α-HA antibody (H3663, Sigma-Aldrich) at the molecular weight of $\sim$ 15 kDa (expected size 14.2 kDa).

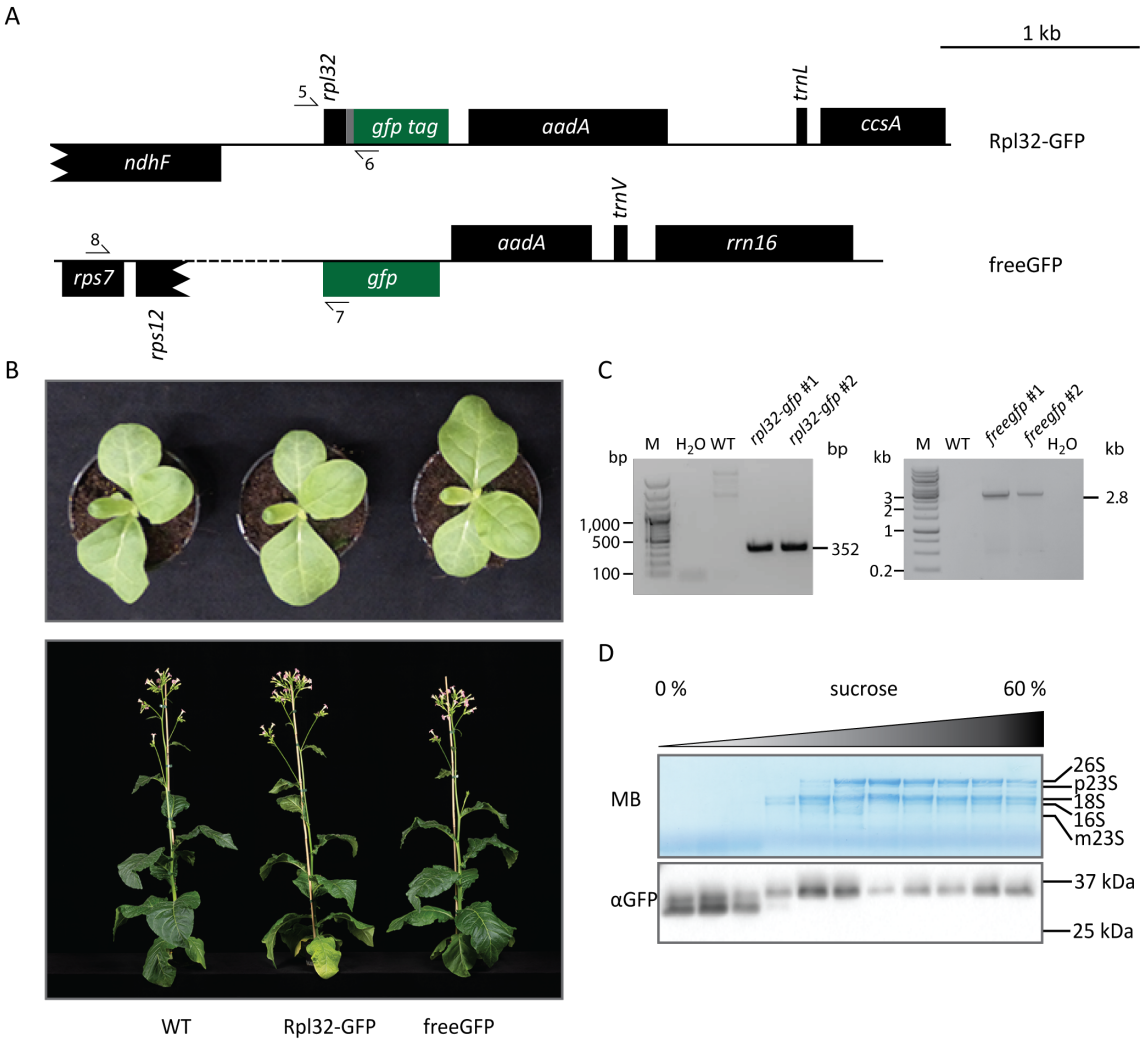

Figure 3.5: GFP-tag of Rpl32 does not interfere with ribosomal function. (A - D) Characterization of Rpl32-GFP and freeGFP (control line for Rpl32-GFP) provided by Prof. Dr. R. Bock (MPI-MP). (A) Physical map of the *rpl32* locus in the plastid genome on top and *gfp* insertion site close to the *rrn16* locus below. GFP-tag (green) was inserted behind the *rpl32* with a linker of 30 nt (grey) and the *aadA*-cassette as selection marker was inserted between *rpl32* and *trnL*. *freegfp* was inserted into the 16S operon as described by Ruf et al. (2007). Small black arrows define the primer binding positions for PCR amplification and are numbered according to Table 2.9. (B) Phenotypes of Rpl32-GFP and freeGFP compared to wild type at the age of 21 days (top panel: the age for TRAP experiment) and 56 days (bottom panel: flowering) were wild-type like. (C) DNA gel of PCR amplicons of *rpl32-gfp* (left) and *freegfp* (right) with primers 6 and 7 binding within the *gfp* locus, respectively. PCR product for *rpl32-gfp* had the expected size of 352 bp. PCR of *freegfp* shows an amplicon with 2.8 kb, which confirms the described insertion site. PCR confirmation of tag and trans-gene insertion was performed with two independent replicates. Homoplasmy of the lines was previously demonstrated by RFLP and seed segregation test. (D) RNA gel blot and immuno blot analysis of polysome fractions of Rpl32-GFP shows incorporation of tagged protein into polysomes. Low sucrose density to high sucrose density fractions were loaded on the gels from left to right. rRNA on the RNA gel blot was detected with methylene blue (MB) and Rpl32-GFP on the immuno blot was confirmed with an α-GFP antibody (GTX26663, GeneTex) at a molecular weight of $\sim$ 35 kDa (expected size 33.5 kDa). The band at lower molecular mass in low-density fraction likely belongs to free GFP (Suppl. Figure S4).

3.1.2.2 Establishment of TRAP

Isolation of ribosome footprints depends highly on the integrity of the translating ribosome. In the standard protocol, ribosomes need to be stable on the mRNA fragments until monosome purification is finished. For TRAP experiments, ribosomes must be stabilized on the mRNA fragment also for the process of IP. The IP system must therefore be adaptable for the needs of stable ribosomes, and yield in a high enrichment of the target.
However, regardless which detergent for monosome resolution after RNAse I treatment in the suspension buffer was used, a high fraction of tagged ribosomal protein was detected in the insoluble fraction (Figure 3.6 A, B). HA-Rps15 stayed mostly in the insoluble fraction (Figure 3.6 A), whereas Rpl32-GFP was better resolvable (Figure 3.6 B). However, other conditions to increase the solubility, e.g., by increasing the temperature or the usage of ultrasonic waves, would lead to ribosome disintegration. Thus, suspension buffer was supplemented with 0.1 % IGEPAL as recommended by protocols for IP experiments.
For excluding differences in the obtained data that originated in the immunoprecipitation method additionally the μMACS system (Miltenyi Biotec B.V. & Co. KG, Germany) was applied for both tagged proteins. The μMACS system was already shown to work on lysates from cyanobacteria (Ossenbühl et al., 2006) and plants (Cole et al., 2006; Sullivan et al., 2008; Smaczniak et al., 2012) for HA- and GFP-tagged proteins with high affinity. The system was adapted for the ribosome profiling approach by using customized (RP-compatible) buffers for incubation with the magnetic beads and washing of the columns. For both lines, it was possible to obtain IP pellets that were positive for the tag in the immuno blot (Figure 3.6 C, D, left panels) and RNA for further analysis. co-IP with the HA- and GFP-specific systems yielded in the same amounts of raw and purified RNAs, respectively. In contrast, control samples did not result in RNA or tag-positive pellets (Figure 3.6 C, D, right panels).
In summary, the μMACS system was suitable for the successful immunoprecipitation of HA- and GFP-tagged proteins, respectively. Furthermore, the implemented protocol resulted in the co-precipitation of RNA which suggest integrity of the ribosomes throughout the immunoprecipitation process.

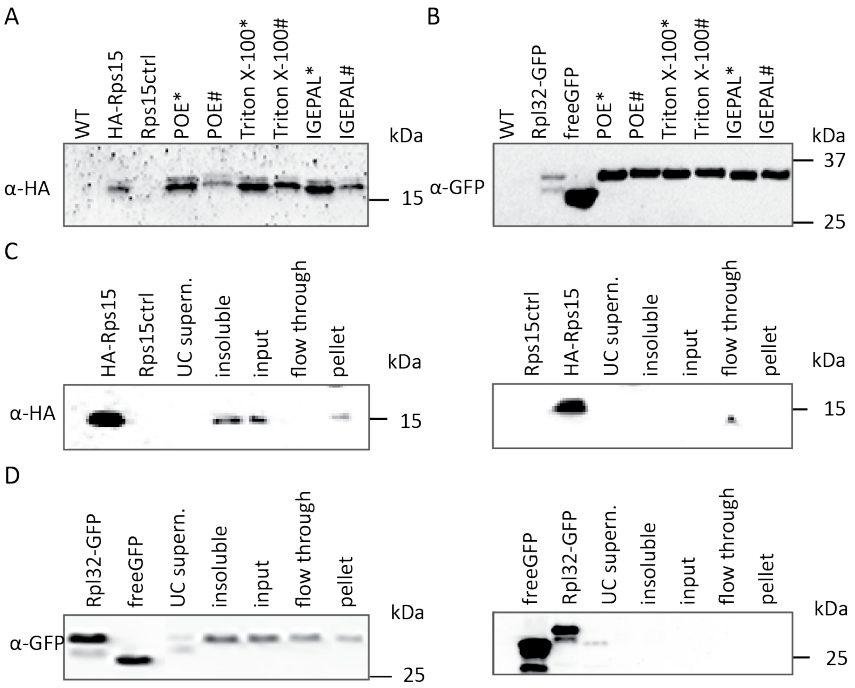

Figure 3.6: Adaptation of IP-system for ribosome profiling. (A) Immuno blot against HA-tag for total proteins of wild type (WT), HA-Rps15, and Rps15ctrl followed by soluble and insoluble fractions of resolved monosome pellets of HA-Rps15 with suspension buffer supplemented with 2 % POE, 1 %Triton X-100, and 0.1 % IGEPAL. (B) The same as in A but for Rpl32-GFP, freeGFP, and monosome pellets of RPL32-GFP. * depicts the insoluble fraction and # depicts the soluble fraction of the monosome pellet. (C) Immuno blot of IP fractions obtained with the μMACS system for HA-Rps15 (left) and Rps15ctrl (right). Note that the reduced intensity of the HA-signal in the pellet fraction in the immuno blot is probably an artifact of the detection method and reflects not the efficiency of the co-IP of RNA. (D) Immuno blot of IP fractions obtained with the μMACS system for Rpl32-GFP (left) and freeGFP (right).
Abbr. UC supern. - upper phase from ultracentrifuge monosome purification with a sucrose cushion

3.1.2.3 Immunoprecipitation of tagged ribosomal proteins strongly enriched cpRFPs

For the IP experiments, samples were split after RNase I digestion into a part dedicated for IP and another part defined as input reference that was processed according to the general RP protocol. Isolated and purified footprints from IP and input samples were further transferred into sequencing libraries, multiplexed, and sequenced on Illumina Nextseq 500 platform.
Sequencing yielded in around 230 million reads. Each replicate contributed with 12 to 20 million reads, except for IP:HA-Rps15-light2 for which only two million reads were obtained despite equivalent RNA concentration in the sequencing library. Adapter trimming reduced the datasets to approximately 83 % of the raw input. The IP:Rps15-light sample was reduced to 55 and 73 % of raw input for replicate 1 and replicate 2, respectively (Suppl. Dataset 2). Equivalent to the sequencing data from CI experiments, trimmed reads were further sequentially aligned to the three tobacco genomes.
Reads from the input samples map, with 70 to 77 % mainly to the nuclear genome, followed by 18 to 26 % mapped reads to the plastome and around 1 % mapping to the mitochondrial

genome. The fraction of reads mapping to the plastome in the HA-Rps15 sample is around 6 % higher than the fraction in the Rpl32-GFP sample. The fraction of reads that align to rRNA or tRNA is from 56 to 64 % for Rpl32-GFP sample and 61 to 66 % for the HA-Rps15 sample (Figure 3.7 A). HA-Rps15-dark2 maps with more than 75 % reads to rRNA/tRNA (Suppl. Dataset 2).
IP experiments result in an enrichment of chloroplastic reads of around three-fold for HA-Rps15 samples and nearly four-fold for Rpl32-GFP samples compared to the input samples (Figure 3.7 A). Despite the precise concentration of chloroplast reads of more than 70 %, IP did not lead generally to the same yield of more than 85 % as did CI (compared to Section 3.1.1.3). Also, IP was weaker in cytosolic-read reduction. IP of HA-Rps15 and Rpl32-GFP retained 15 % and 23 % of cytosolic reads, respectively. An exception is IP:Rps15-light2 which data set is very small (see above) but that comprises 89 % chloroplastic and only 8 % cytosolic reads. For all samples, the fraction of unmappable reads is below 5 % (Figure 3.7 A and Suppl. Dataset 2).
In parallel to the CI samples, also input and IP samples were deduplicated and filtered for uniquely mapping reads not aligning to rRNA/tRNA. For the three subcellular compartments, the read length distribution for the four samples was assessed. All four samples show the same read length distributions for the three subcellular compartments. Different to reads obtained from isolated chloroplasts, chloroplast-originated reads from IP and input samples show a bimodal distribution. The third major read size of 37 nt is only recognizable as small shoulder. Also, the other two peaks are, in this experiment, more distinct with a dominant peak at 29 nt and a smaller peak at 25 nt (Figure 3.7 B; green line). The size distribution of cytosolic reads is shifted to smaller read sizes as well. While the cytosolic reads from the CI experiment are larger with 35 nt, they correspond in the IP and input samples to the published size of ribosomal footprints of around 29 nt (Hsu et al., 2016; Wu et al., 2019b) (Figure 3.7 B; blue line). Mitochondrial reads still show a bimodal read length distribution, yet the dominant sizes are shifted to shorter lengths of 27 nt and 38 nt, respectively (Figure 3.7 B; red line). The most abundant size matches the published read size for mitochondrial ribosome footprints by Planchard et al. (2018).
Overall, the digestion of RNA by RNase I was completer and more efficient than in the CI experiment. Further, it shows that the second and longer read population of mitochondrial reads is not an artifact of incomplete RNA digestion but meaningful.
Next to an improvement of footprint sizes to published reference sizes, also an increase in frame 0 fraction was obtained, for chloroplastic reads to up to 60 % and for cytosolic reads to up to 55 % (Figure 3.7 C). This is an increase of 15 and 10 %, respectively, compared to reads obtained from the CI experiment. Mitochondrial reads are mostly in frame 0 which is again a consequence of extremely low read numbers used for the phase determination (Suppl. Dataset 2, compared to Section 3.1.1.3).

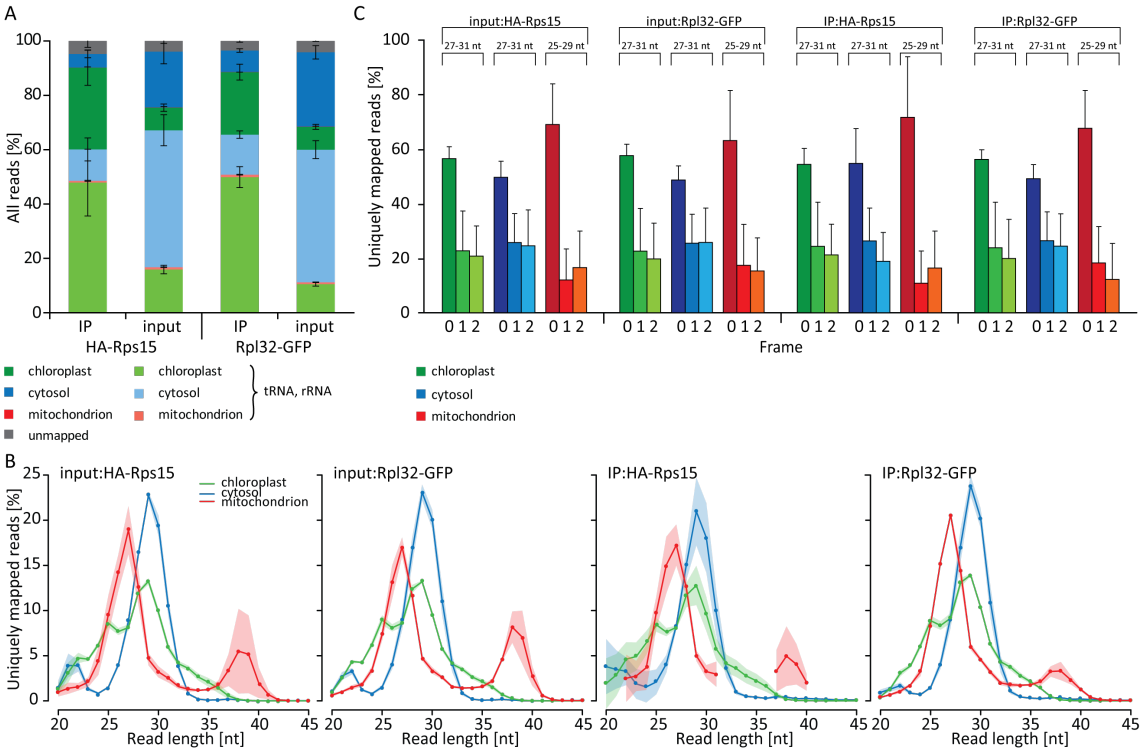

Figure 3.7: Ribosome footprint characteristics from IP and input samples for all three subcellular compartments. (A) Bar plots showing the fraction of read origin for all reads of the two lines HA-Rps15 and Rpl32-GFP, separated in IP and input samples, as indicated on the bottom. The values are split into reads originating from rRNA and tRNA (lower part, light colors) or from any other genomic region (upper part, dark colors) as stated by the legend below the graph. Unmappable reads are colored gray. (B) Read length distribution for all uniquely mapped reads are represented as scatter plot with connective lines. The x-axis shows the read length in nt and the y-axis shows the percentage of reads of the specific size to all reads mapped to the CDS of the specific subcellular compartment. (C) Frame affiliation of uniquely mapped reads around the translational start site ($\pm$ 50 nt) of annotated ORFs. In-frame fraction is represented for most abundant read sizes as indicated on top.
Represented values are based on four biological replicates (2 x light, 2 x dark, Suppl. Dataset 2). Compartments are color-coded: chloroplast - green, cytosol - blue, mitochondrion - red. Black error bars (A and C) and light-colored areas (B) represent the SD.

3.1.2.4 Increased translational output for subsets of plastidial genes

The analysis of the TRAP samples, i.e., IP and input, has in the current setup many advantages. The IP samples can give a high depth insight into the chloroplastic translation. In contrast, the input sample gives information about the translation in the other cellular compartments of the very same tissue. However, the focus will be on the chloroplastic translation. To analyze the dataset from TRAP experiments, counts were normalized as described above (Section 3.1.1.3) and samples from IP and input were further filtered for genes represented by at least 50 counts. Especially in the IP samples, the number of nuclear and mitochondrial genes were reduced because of low coverage. The replicates of the samples correlate well and a clear separation of plastidial and nuclear genes into two clusters is observed in the

comparisons of input and IP samples (Suppl. Figures S5 and S6).

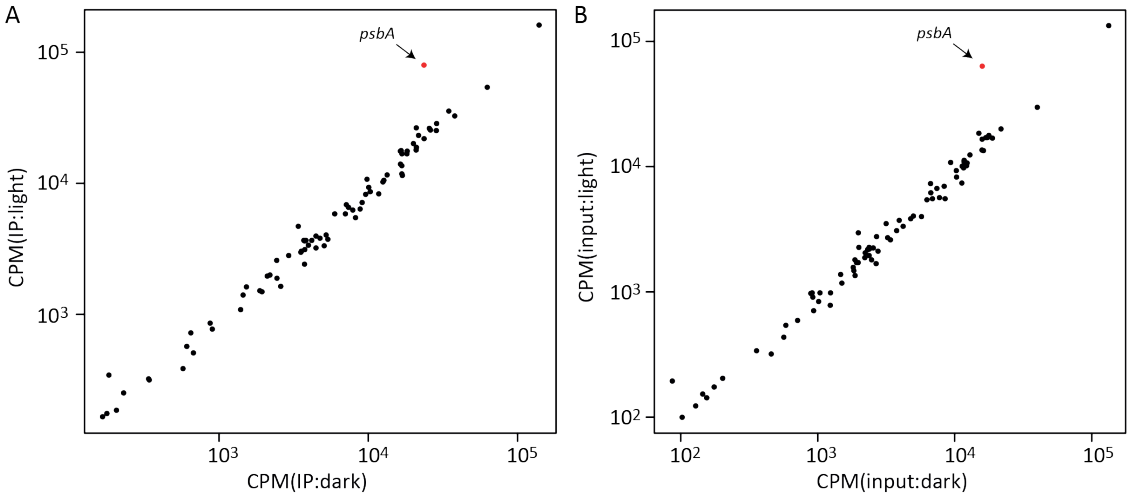

Figure 3.8: Comparisons of light and dark samples from IP and input show upregulation of *psbA* expression in the light. Scatter plots of CPM values for plastid-encoded genes from IP samples (A) and input samples (B) show similar expression for nearly all genes in dark (represented by the x-axis) and light (represented by the y-axis). *psbA* reads were more than three-fold enriched in the light samples, resulting in a higher CPM value. *psbA* is highlighted as reed dot and emphasized by an arrow. Values represent the average of four biological replicates (2 x HA-Rps15, 2 x Rpl32-GFP for IP and input, respectively, Suppl. Dataset 2).

To see, if the IP was successful in means of qualitative enrichment of chloroplastic RFPs, samples from dark and light harvested tissue were compared. Based on the data from Chotewutmontri and Barkan (2018), an increased read density for *psbA* is expected in the light compared to dark samples. In the comparison of the replicates, one plastidial gene was enriched in the light samples, regardless of the used line and the experimental RFP isolation. The enrichment analysis confirmed that, indeed, *psbA* CPM values are significantly increased in the light samples compared to the dark samples, i.e., 3.3-fold in the IP sample and four-fold in the input sample (Figure 3.8). Additionally, the very lowly expressed gene *ycf10* is enriched in light by 1.9 and 2.2-fold in the IP and input sample, respectively. Also, Chotewutmontri and Barkan (2018) saw higher levels of *ycf10*, but rather in relation to the day time than to light *per se* which hints to circadian regulation of the gene. However, only *psbA* enrichment was tested significantly.

Further, two different plant lines were used for TRAP experiments, (1) HA-Rps15 which expresses a tagged non-essential ribosomal protein of the SSU and (2) Rpl32-GFP which expresses an essential ribosomal protein of the LSU. Thus, both lines enabled an analysis of RFPs associated with SSU or LSU independently and the influence of non-essential ribosomal proteins on the translational behavior in the plastid. For cytosolic ribosomes, populations with different protein composition that may be involved in the translation of functionally or developmentally related genes were observed in different species and cell types (Daftuar et al., 2013; Shi et al., 2017; Ferretti et al., 2017; Sapkota et al., 2019). Different populations of ribosomes in the chloroplast could imply another kind of translational regulation, e.g., binding of *trans*-factors and/or recognition of *cis*-elements. Additionally, Rps15 is known in bacteria to bind its own mRNA to negatively regulate its expression (Slinger et al., 2015). Thus, Rps15

may also be a good candidate for targeted mRNA binding of the ribosome by recognition of distinct *cis*-elements.

In the first step, the general coverage of plastidial genes in the IP samples was assessed. Differential expression analysis was performed comparing the IP sample obtained from HA-Rps15 with the IP sample from Rpl32-GFP. Genes were selected if they showed a significant two-fold enrichment in one of the two samples (Figure 3.9 A, left panel). And in fact, eight genes were found deferentially enriched in one of the two IP samples. HA-Rps15 is enriched for two genes and Rpl32-GFP shows enrichment for six genes. However, comparison of the input samples leads to the same observation (Figure 3.9 A, middle panel). Here, no selection based on ribosomal proteins was performed which leads to the conclusion that no enrichment of diverse ribosome pools (pools with or without Rps15) was obtained.

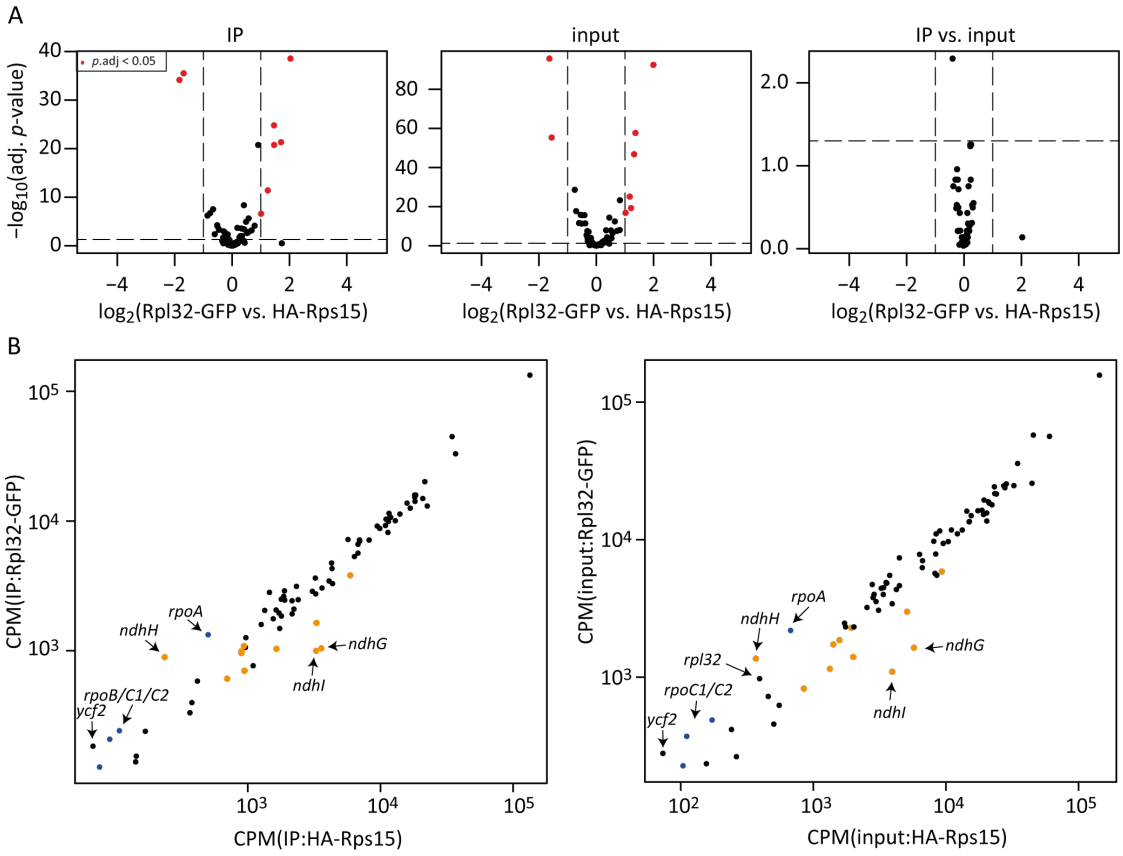

Figure 3.9: Differential enrichment of plastidial genes by IP was the result of differential expression within the lines. (A) Volcano plots for plastid-encoded genes from values obtained by differential expression analysis for IP samples, input samples and IP samples normalized to the input (from left to right as indicated on top). The x-axes show the $\log_2$-fold change between Rpl32-GFP and HA-Rps15 and the y-axes show the -$\log_{10}$-value of the adjusted *p*-value (*p*.adj). Thresholds for $\log_2$-fold change and *p*.adj are marked with dashed lines and genes passing the thresholds are highlighted in red. (B) Scatter plots of CPM values of plastid-encoded genes from IP samples (left panel) and input samples (right panel). x-axes represent the CPM values of HA-Rps15 samples and y-axes show the CPM values of Rpl32-GFP samples. Genes coding for subunits of the NADH dehydrogenase-like complex (NDH) are highlighted in orange and PEP genes are colored in blue. Significantly enriched genes are further emphasized by arrows. x and y-axes are displayed in $\log_{10}$-scale.

Interested in the type of deferentially enriched genes, the eight genes were selected. Rpl32-GFP shows increased coverage of all four PEP genes, *ycf2*, and *ndhH* with the highest enrichment by four-fold. Interestingly, *ndhH* is in the same operon as *rps15* and the two genes enriched in HA-Rps15, i.e., *ndhG* and *ndhI* (Figure 3.9 B and Figure 1.1). Thus, the clear depletion of *ndhH* reads in HA-Rps15 was unexpected. As shown in Figure 3.4 A, the *aadA*-cassette was inserted directly in front of the *ndhH* gene. The *aadA*-cassette is driven by a strong promoter to ensure high transcript levels and antibiotic resistance. As a consequence and because of unspecific transcriptional termination in the chloroplast (Pfalz et al., 2009; Zhelyazkova et al., 2012; Castandet et al., 2019), downstream genes are also transcribed to higher levels (Schöttler et al., 2017; Fu et al., 2020). Higher transcript level would suggest higher translational output if the translation depended on the template. This is observed for all other genes in this operon (more or less potent, Suppl. Figure S7 and Suppl. Table S2), except for *ndhH* which is clearly translationally down-regulated. Potential reasons for this regulation are discussed in Section 4.3.2.

3.1.2.5 No indication for alternative mRNA coverage by SSU and LSU

So far, translation initiation in chloroplasts was described either as SD-sequence dependent or secondary-structure related (Scharff et al., 2011, 2017; Gawroński et al., 2020b). But in both scenarios, the SSU will find the SC immediately and the LSU will join to form the initiation complex. In bacteria, a re-initiation at proximal SC on a polycistrons was described in which the fully assembled ribosome scans the mRNA after termination of translation for the next SC (Yamamoto et al., 2016). In the cytosol, however, the pre-initiation complex follows the 5'-untranslated region (5'-UTR) from the CAP-region until finding an appropriate start codon. While plastids were originating from prokaryotes and many processes act alike the ancestor's, also new characteristics had to be developed to conform with the needs of a dependent organelle. So, the dataset was used to find translational initiation based on differential occupation of 5'-UTRs by SSU and LSU, e.g., scanning-like mechanism.
To determine a potential scanning mechanism of SSU, genomic regions of 100 nt upstream to 30 nt downstream of the annotated plastidial SC were extracted. Reads from input and IP samples mapping to these regions were counted and normalized. Counts were subjected to differential expression analysis to identify genes with 5'-UTRs exhibiting differential coverage by SSU and LSU. Differential coverage was determined for input and IP samples independently. Input samples should not show any differential coverage between the samples, because no selection for SSU or LSU was done, and served thus as control. Only the 5'-UTR of *orf74* is specifically enriched in the IP:HA-Rps15 sample (Suppl. Table S3). However, the coverage depth of this specific region is very low and if the signal derives from proper SSU binding without LSU association or from the binding of a RBP that bound to the anti-HA beads has to be determined with mass-spectrometry of IP samples.
Because the defined region for UTRs also included the SC, initiation may cover the SSU scanning. To complicate the search for alternative initiation modes, plastidial genes occur in polycistrons or are often separated by few nucleotides. Thus, three genes were selected for visual inspection of the SC region. (1) *psbA* was selected because of its monocistronic transcript, SD-independent translation initiation, and its known *cis*-elements in the 5'-UTR. (2) *atpA* was chosen, because its SC is only separated by 53 nucleotides from the stop codon of *atpF*. Thus, potential reinitiation of the ribosome without prior disassembling could be a potential initiation mechanism. And (3) *rbcL* was picked as representative of SD-dependent

translation initiation.
The zoom-in to the 5'-region of the two genes, however, confirms the results from the differential expression analysis of the 5-UTRs. No increased footprint coverage is observed neither in HA-Rps15, hinting to SSU scanning, nor in HA-rps15 and Rpl32-GFP IP samples, indicating ribosome scanning for proximal start codons after completing the translation of one cistron. Eye-catching is a drop in footprint coverage of the *psbA* reading frame around 60 to 65 codons behind the start codon. This region was assigned by Kim et al. (1991) as pause site A and correlates with the emergence of the first transmembrane domain (Figure 3.10). Gawroński et al. (2018) identified also a primary pausing site at around 70 nt downstream of the SC of *psbA*. The sharp spike in the present figure upstream of the transmembrane region (light-gray background) may correspond to the described pausing site. It was suggested that it corresponds to SRP-binding and mRNA translocation to the thylakoid membrane (Pechmann et al., 2014; Gawroński et al., 2018).

To summarize, the TRAP dataset can be used to analyze the ribosome occupancy of transcripts in each subcellular compartment. With additional transcript data, the expression of the *ndh* operon and its regulation can be an attractive target for further inquiries. Moreover, translational features like pausing sites can be inferred. However, the dataset is not suitable to investigate SSU scanning and potential reasons are discussed in Section 4.3.1.

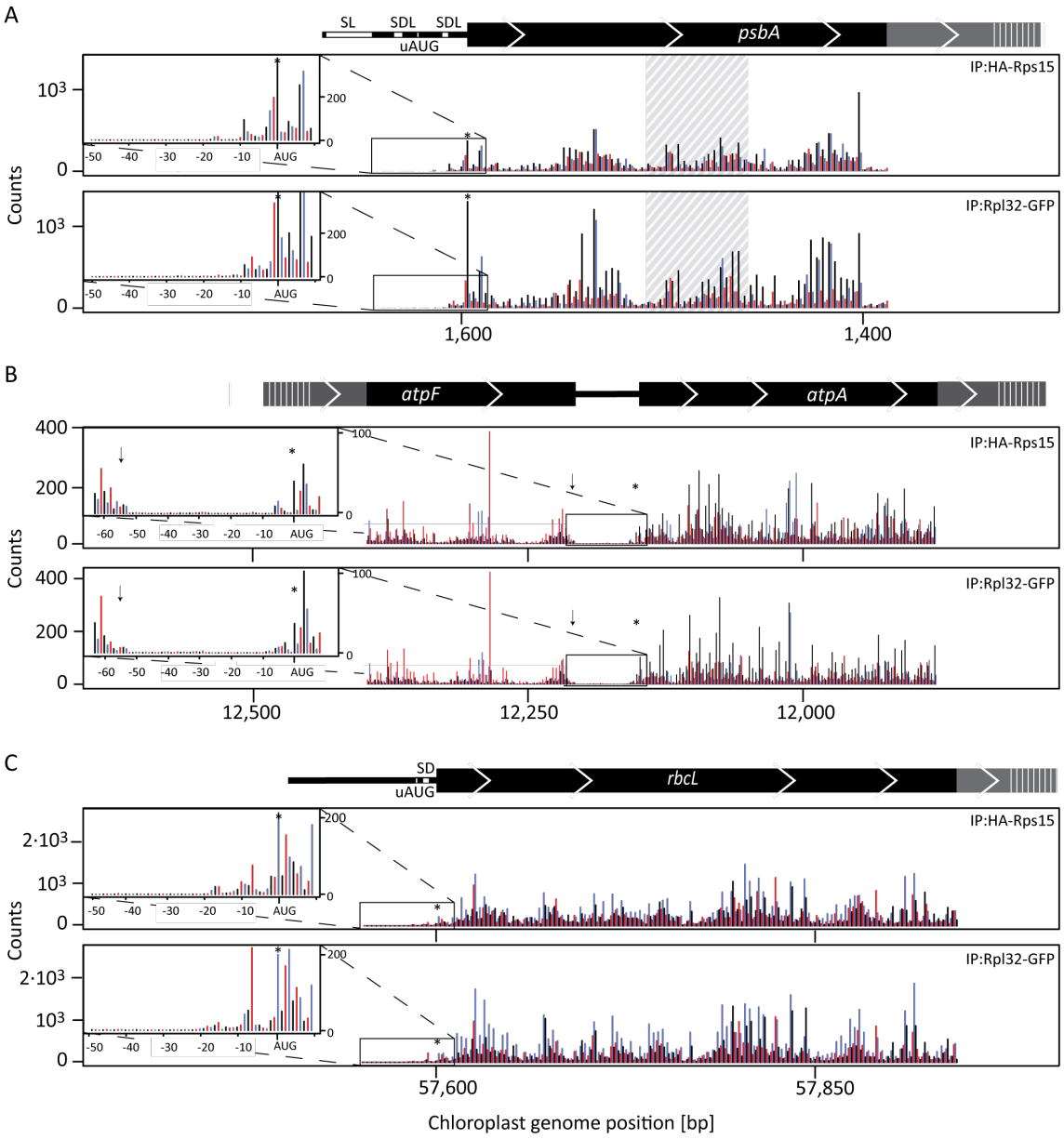

Figure 3.10: Genome coverage plots for *psbA*, *atpF/A*, and *rbcL*. (A) Mapping of reads by their first nucleotide in the P-site to the *psbA* 5'-region including the 5'-UTR and 280 nt of the ORF for HA-Rps15 (upper panel) and Rpl32-GFP (lower panel) IP samples. Positions are color-coded according to the reading frame. The SC is marked by an asterisk (*). The coverage is given in counts as an average of four biological replicates. The reduced gene model is shown above where the gray area describes the gene region for which no coverage is further displayed. Thin white bars at the end of the gray area depict that not the full-length gene model is represented. White blocks in the 5'-UTR indicate identified *cis*-elements: SDL - SD-like motif, uAUG - upstream-AUG, SL - stem-loop structure (Hirose and Sugiura, 1996). The first transmembrane domain is highlighted with a striped background. (B) Equivalent to A but for *atpA* 5'-region including the 3' coding region of the *atpF*-ORF (230 nt), 53 nt intercistronic region, and 350 nt of the *atpA* 5'-coding region. The stop codon of *atpF* is marked by an arrow. No *cis*-element is known in the intercistronic region. (C) 5'-region of the *rbcL* transcript displayed as described for A and B. White blocks in the 5'-UTR of the gene model indicate the position of identified *cis*-elements: SD - SD-motif, uAUG - upstream-AUG.
All panels display a zoom-in into the region of interest (5'-UTR for *psbA* and *rbcL*, intergenic region between *atpA* and *atpF*) in the upper left corner and a small frame indicating the exact position of the selection in the gene-coverage plot.

3.2 Results - Chloroplast gene expression contributed only little to high-light acclimation

The following results were published in 2020 in *Plant Physiology* (Schuster et al., 2020). Presented figures from this publication were mildly modified in the color theme and arrangement for this thesis.

3.2.1 Experimental setup induced mild phenotypic alterations

For studying the effects of increased light irradiation on chloroplast gene expression as part of acclimation processes, an experimental setup was designed that should mimic natural condition for plants. Thus, not de-etiolated seedlings nor sudden dark-light transitions or destructive irradiation were used for the experiment. In short, young tobacco plants in the four-leaves stage, grown under moderate light intensity of 350 μmol·m^{-2}·s^{-1}, were shifted during the light period of the day 21 after sowing (5 h after SOD) to an approximately three-fold higher light intensity of 1,000 μmol·m^{-2}·s^{-1} (Figure 3.11A). From the moment of shift, the aerial parts of the plants (excluding cotyledons) were collected from shifted plants. To exclude circadian responses and development-driven differences compared to starting condition, leaf tissue from seedlings kept under moderate light intensity was collected in parallel. The harvesting time points were chosen over a two-day period to cover early, medium, and late responses in gene expression (Figure 3.11B). Sampling of tissue beyond two days after high-light exposure would have resulted in strong developmental differences of shifted and control plants (Grebe, 2015). Thus, observed effects would have been impossible to disentangle for acclimation responses and developmental effects.
Because higher light is often associated with higher temperature, leaf and soil surface temperatures were recorded for shifted plants to ensure that observed effects originate solely from light intensity increase rather than higher temperature. Due to separation of the bulbs from the interior of the experimental chambers by Plexiglas, leaf and soil temperatures did not increase less than 1 ° and 2 °C in a recorded time frame of five hours, respectively (Suppl. Figure S8). Another potential confounder when changing light intensity is a change in the emission spectrum of the light. Specific wavelengths may change their contribution to the total emitted light and trigger wavelength-specific responses, e.g., due to the different excitation spectra of PSI and PSII. Thus, emission spectra at the used light intensities were recorded as well (Suppl. Figure S9), and indeed differences in the amplitudes were observed. However, no differences of wavelength at the border of the spectra were present. More energy-rich light (towards UV light) can lead to activate transcription of plastid-encoded genes (Chun et al., 2001) or damage the acceptor and donor sides of PSII (van Rensen et al., 2007). An increase in the red to far-red wavelengths regulates phytochrome (Barnes et al., 1996; Rossel et al., 2002), which acts as transcriptional regulator in the nucleus and influences thereby through anterograde signaling the gene expression in the chloroplast (Oh and Montgomery, 2013). Both, UV- and far-red light would ultimately bias observations of translational regulation induced by light intensity alterations.
Plants that were shifted to higher light intensity displayed an unaltered phenotype compared to the control plants for the first five hours of the experiment. However, after 24 hours in the high-light regime, plants were slightly retarded in growth compared to their siblings in the control condition and started to display a very mild fading in leaf color that was not recovered

after additional 24 hours (Figure 3.11C).

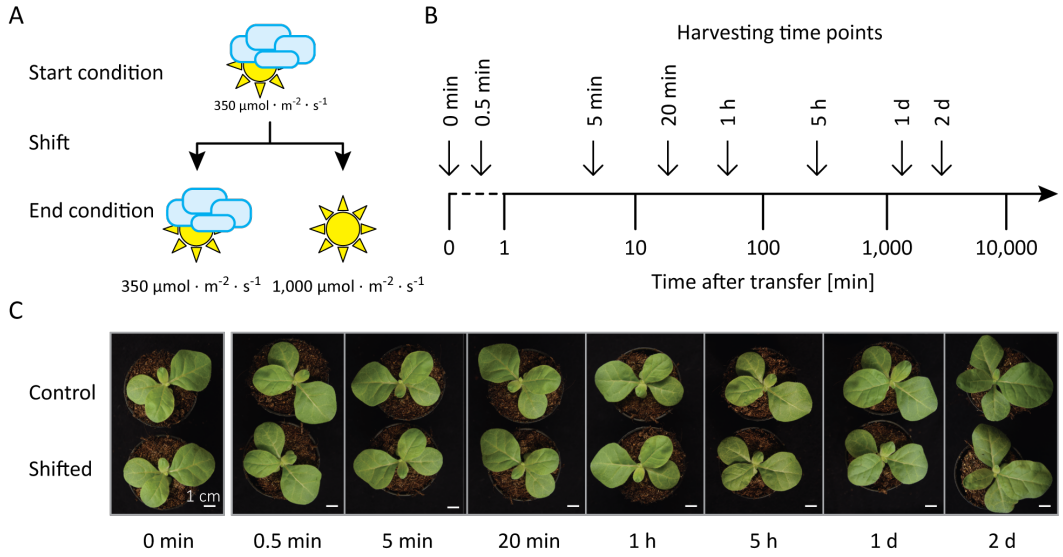

Figure 3.11: Experimental setup of light shift and plant phenotypes. (A) The procedure of shift experiment with tobacco seedlings, adapted to moderate-light conditions. The shift was conducted 5 h within the light period to high-light intensity, while some seedlings were kept as control samples in moderate-light intensities. (B) Chosen time points of tissue sampling after the shift to high-light condition for shifted and control plants, respectively. "0 min" time point was harvested immediately before the shift as an untreated control. (C) Phenotypes of control (upper part of the picture) and shifted (lower part of the picture) seedlings at the individual harvesting time points. Note that the phenotypes started to differ very mildly in size and leaf color at time point "1 d". (bar = 1 cm)

3.2.2 Photosynthetic parameters supported non-stressful high-light condition for the shift experiment

Considering the mild phenotypic difference between shifted and control plants in the later time points, i.e., one and two days after the shift, the question arose if the phenotype of shifted plants was a consequence of disturbed photosynthetic activity. For excluding a stress response in the shifted plants that might also be the reason for potential gene expression regulation as well instead of acclimation processes, different photosynthetic parameters and markers were assessed.

Therefore, plants grown in low light conditions of 50 μmol·m^{-2}·s^{-1} and also shifted to high light, equivalent to the experiment described above, were analyzed for changes in photosynthetic parameters as "stress" control (Suppl. Figure S10). Due to their low-light growth, these plants were very small and had delicate leaves with long petioles at the time point of shift. Starting from the earliest time points of the shift, the displayed fading of the green leaf color. In contrast to the paler leaf color in the shift from moderate to high light (physiological experiment), which was likely a consequence of physiological antenna reduction, the fading phenotype in this stress experiment was potentially caused by the direct destruction of chlorophyll through a sudden high-light stress.

First, the chlorophyll content was determined for a selection of time points. This seemed to be the most reasonable measurement because of the slightly paler phenotype of shifted plants at later time points in the physiological experiment and a strong bleaching phenotype in the stress experiment. Indeed, the chlorophyll content per leaf area was reduced two days after the shift and the chlorophyll *a/b* ratio was increased in the physiological experiment (Figure 3.12A, first and second box). This observation hints to reduction of LHCII which contains the majority of chlorophyll-*b* (Kitajima and Hogan, 2003). The relative reduction in chlorophyll content was indeed higher in the stress experiment and the chlorophyll *a/b* ratio was just mildly increased, indicating that chlorophyll-*a* and chlorophyll-*b* were reduced in the same manner.

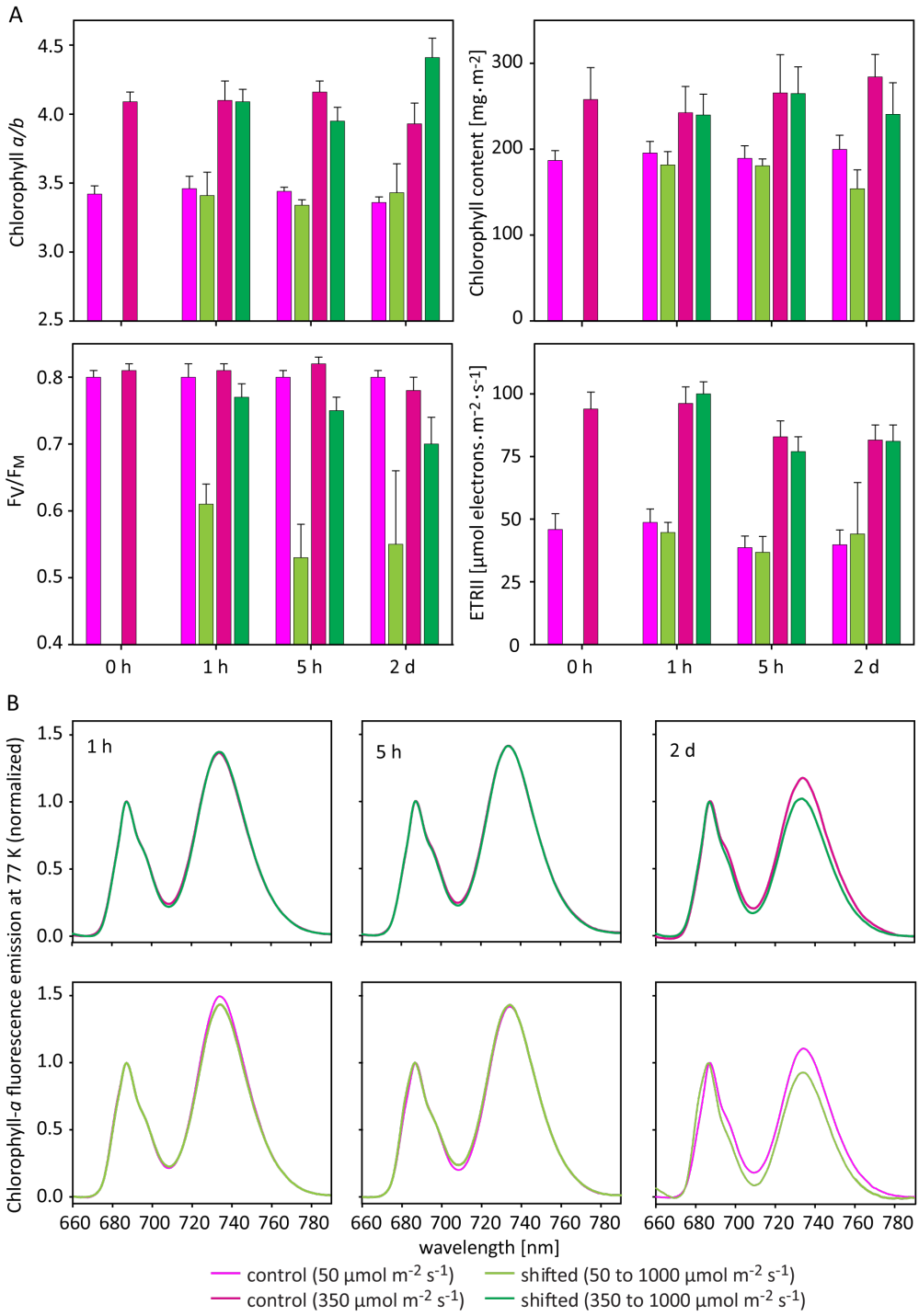

Figure 3.12: Photosynthetic parameters from control plants grown at moderate and low light, and respective high-light shifted plants. (A) Chlorophyll a/b, chlorophyll content, F_V/F_M, and ETRII for shifted and control plants for selected time points of the shift experiment. (B) Chlorophyll-a emission spectra at 77 K for moderate-light to high-light shift (upper panel) and low-light to high-light shift (lower panel).
Values were averaged over nine biological replicates (except for the "2 d" time point that is based on five replicates). Error bars depict SD. Color legend below subfigure B applies for A and B.

To see if there was an effect on the antenna molecules distribution, 77K fluorescence emission measurements were performed. This measurement enabled the detection of rearrangements or destruction of antenna molecules through differentiation of chlorophyll-*a* fluorescence in dependence of photosystem association. These measurements showed a small reduction in the chlorophyll-*a* fluorescence of the second local maximum at 735 nm in the "2 d" high-light sample, indicating relative reduction of chlorophyll content around PSI. However, no sign of unbound chlorophyll (shift of amplitudes to smaller wavelength; Figure 3.12B, left panel) in the physiological experiment was observed. Chlorophyll fluorescence at 77 K of stressed leaf tissue showed no difference to the control sample after 1 and 5 hours. But the spectrum from the "2 d" stress sample was strongly reduced in fluorescence emission for the maximum at 735 nm and the local minimum in between the maxima. Additionally, both maxima were shifted to shorter wavelengths which was a sign of unbound chlorophyll (Figure 3.12B, right panel).
From the measurement of maximum quantum efficiency of PSII (F_V/F_M) a gradual but minor reduction in the shifted plants could be observed throughout the time course of the experiment (Figure 3.12A, third box). This mild photoinhibition of PSII was expected due to the high light and consequently higher excitation pressure on PSII. The unchanged linear electron transport rate of PSII (ETRII) indicated unchanged relative complex contents of PSI and PSII. Plants grown under low-light condition showed strong photoinhibition after the shift to high light. However, also during the stress experiment, ETRII did not change. Thus, the described upregulated formation of cyt-b_6f and ATP synthase in response to high light (Schöttler and Tóth, 2014, and references herein) might not have started until the end of the experiment.
The obtained data supported the assumption that, indeed, the shift from moderate to high light was physiological and potential changes in chloroplast gene expression would be rather results of acclimation processes than stress reactions to destructive irradiation.

3.2.3 Plants exhibited constant transcript level of plastid-encoded genes during the shift experiment

After elucidating that the shift from moderate to high light could be considered as physiological and was not introducing major stresses to the plants, ribosome profiling (RP) in parallel to transcript profiling was performed. Information about changes in the transcript abundance are important to interpret changes in RFP abundance. Thus, if more RNA is generated more ribosomes can bind, or fewer ribosome footprints (RPF) may be obtained by degradation of RNA, if the relative translation of the mRNA (translational efficiency, TE) was unchanged. However, changes in translational output (RFP levels) without changes of transcript abundance in the same direction (increase or decrease in levels, respectively)are indicative of targeted translational regulation.
Obtained total transcript from shifted, and control samples were differentially labeled with fluorescent dyes and competitively hybridized on customized microarrays that covered all annotated ORFs of the tobacco plastome (Scharff et al., 2011). Fluorescence signals were normalized to the average signal over all samples. Biological replicates exhibited similar transcript signals for the individual plastid-encoded genes (Suppl. Figure S11). But also samples from different time points or condition correlated well (Suppl. Figure S12). Taken the high similarity between the transcript levels of all samples, the minimal differences in transcript abundance between shifted and corresponding control samples were not surprising (Figure 3.13). Fold changes were below 1.5 and passed the selected threshold of 1.3 only for two genes for only one time point (*matK* at "1 h" and *psbN* at "1 d"; Figure 3.13A). Both genes displayed high variation among the

biological replicates (Suppl. Dataset 1). Consequently, the fold changes from *matK* and *psbN* above the threshold were not considered robust.
Hence, no shift-induced changes in transcript accumulation were observed. In conclusion, no gene expression regulation in high-light acclimation happened on the level of transcript accumulation in the observed time frame.

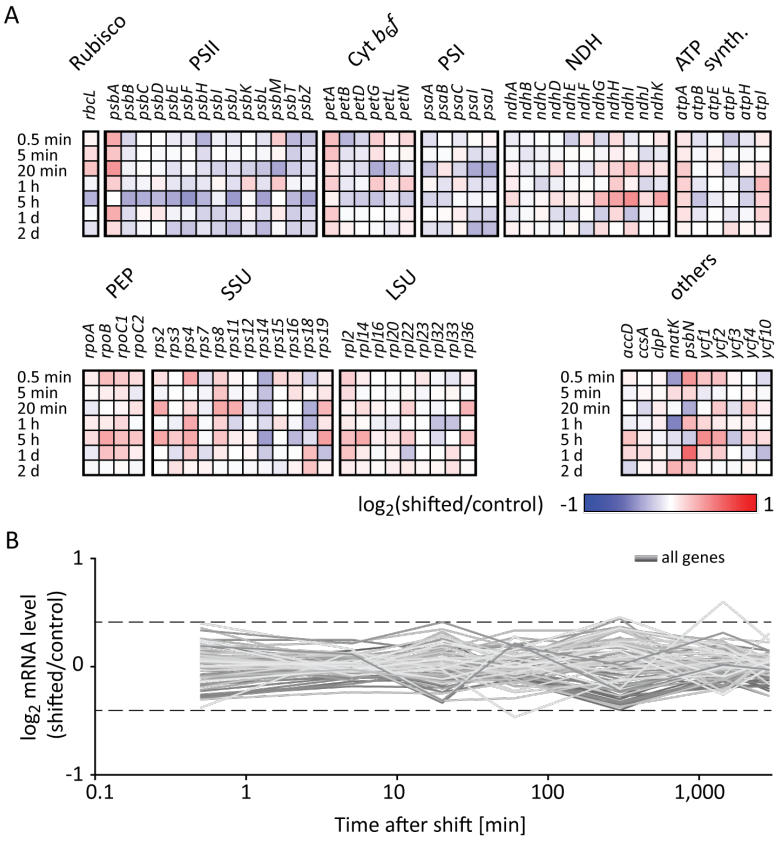

Figure 3.13: Constant transcript accumulation in the high-light acclimation process of chloroplast. (A) Heatmap representing the $\log_2$-fold change ($\log_2$FC) of transcript levels of protein-coding genes between shifted and control samples. Genes are grouped (1) by gene category (photosynthesis, gene expression, other), and (2) by complex. Time points are ordered from early time points on top to late time points on the bottom. Due to the very mild changes, the $\log_2$-fold change scale is limited from -1 (blue) to 1 (red). (B) Line plot representation of $\log_2$-fold changes shown in A. Horizontal dashed lines at $\log_2$ values -0.4 and 0.4 represent the threshold of 1.3-fold change in transcript accumulation between shifted and control samples. None of the protein-coding genes displayed a constant above threshold fold change in transcript accumulation for more than one time point. All data points were calculated as the average of three biological replicates.

3.2.4 Only *psbA* translation was mildly upregulated after shifting to higher light intensity

Given the observation of stable transcript levels during the shift experiment, potential gene expression regulation during acclimation could happen at downstream processes, e.g., transla-

tion. To test this hypothesis, RP were further processed and analyzed as described above for transcript levels.
To estimate the translational regulation in the acclimation process, fold changes between shifted and control samples for the individual time points were calculated. As represented in the heatmap and line plot in Figure 3.14 (A and B, respectively), chloroplast translation seems to respond only mildly to the higher light intensity. The given results do not exclude a general up- or down-regulation of chloroplast translation, because of the microarray design which exclude housekeeping genes with consecutive translational output for normalization. Thus, if all plastid-encoded genes were transcriptionally/translationally up- or down-regulated was impossible to determine from the array data. However, specifically, *psbA* translation is up-regulated after the shift from moderate to high light. The increase in the fold change was detectable after 20 min in high light and stayed above the set threshold of 1.3-fold until the end of the shift experiment (Figure 3.14B, red line). No other gene, even if their fold change passed the threshold (see below), showed a constant and reproducible up-regulation. The increased *psbA* translation upon the shift to high light is expected because of the PSII repair mechanism to counteract photoinhibition and serves in this study as an internal positive control for gene expression regulation.

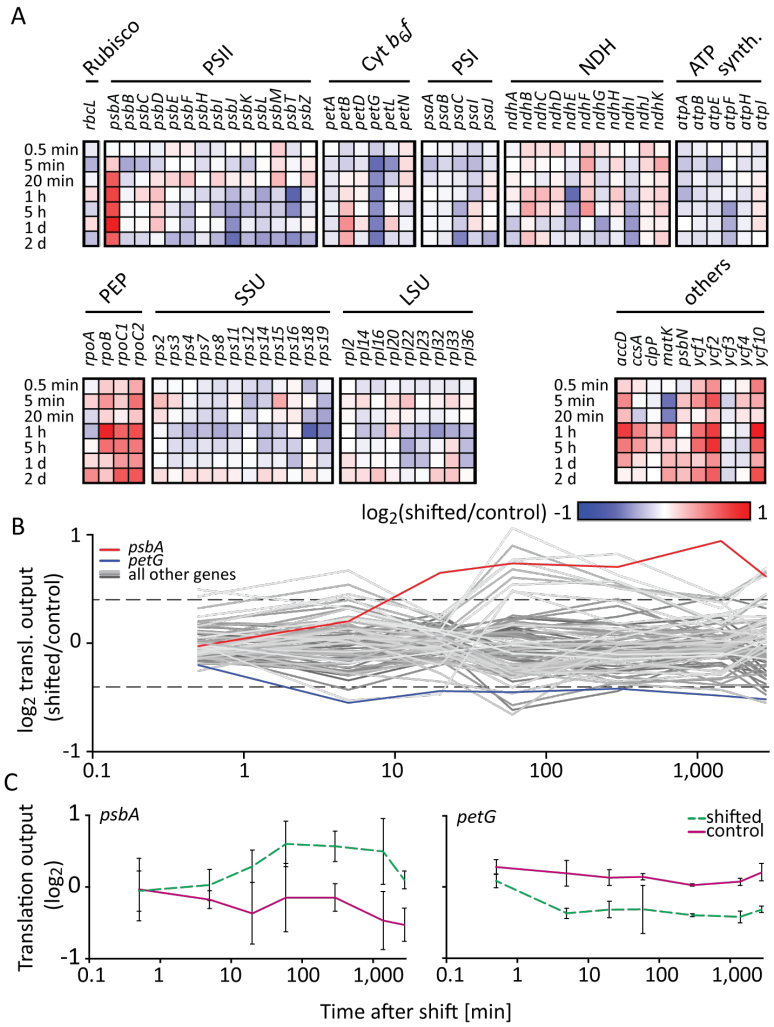

Figure 3.14: Mild differences in translational output between shifted and control samples over the time course of high-light acclimation. (A) Heatmap representing the $\log_2$-fold change ($\log_2$FC) of translational output of protein-coding genes between shifted and control samples. Genes are grouped (1) by gene category (photosynthesis, gene expression, other), and (2) by complex. Time points are ordered from early time points on top to late time points on the bottom. Due to the very mild changes, the $\log_2$-fold change scale is limited from -1 (blue) to 1 (red). (B) Line plot representation of $\log_2$FC. *psbA* and *petG* translational output fold change is highlighted red and blue, respectively, for passing the $\log_2$FC threshold of $\pm$ 0.4 in more than three consecutive time points. (C) Detailed view of *psbA* and *petG* translational output. Normalized $\log_2$-transformed relative abundances from shifted and control samples are represented as green dashed and solid magenta lines, respectively. All data points were calculated as the average of three biological replicates. Error bars depict the SD.

To confirm that the increased *psbA*-translational output mirrored increased D1 exchange in PSII rather than increased *de novo* PSII complex assembly, immuno blots for core components of the thylakoid membrane complexes were produced to address complex accumulation during the light shift experiment. The D2 protein, encoded by the plastid-encoded gene *psbD*, was chosen as representative for PSII accumulation. It forms a heterodimer with D1 in the reaction center of PSII, but it has a much higher protein half-life than D1 (Li et al., 2017) and is therefore more suitable for the estimation of PSII accumulation based on immuno blots. Figure

3.15 shows the protein abundance of core proteins of the thylakoid membrane complexes for the harvesting time points in control and shifted plants. The D2 accumulation was constant throughout the shift experiments, in both, control and shifted plants, respectively. Equally, the accumulation of the representative proteins from the other complexes was stable for the investigated time points and between the experimental conditions. Thus, it can be assumed that neither *de novo* assembly nor complex degradation was increased during the light-shift experiment, and the increase in D1 synthesis serves PSII repair.
Another reproducible and constantly regulated gene was *petG*. Down-regulation of *petG* translation started within the first five minutes of the experiment (Figure 3.14B, blue line). The translational output in shifted plants stayed stably below the output of control samples for the remaining experiment. *petG* is an essential subunit of cyt-b_6f and it was suggested to function in the complex assembly (Schwenkert et al., 2007). However, the reduction in translational output was very mild and did not have any detectable consequence for the accumulation of the complex (represented by PetB, Figure 3.15.)
Apart from *psbA* and *petG*, only few genes showed an above-threshold regulation in translational output in high light, especially at medium and late time points. Those genes, i.e., genes coding for PEP core subunits (excl. *rpoA*) and *ycf1/2/10*, have extremely low expression levels (Suppl. Dataset 1), which quickly results in increased fold changes up to two-fold, and show high variations within the biological replicates (Suppl. Dataset 1). Their apparent translational regulation is therefore considered less robust.
Taken together, apart from *psbA*, translational regulation appears unlikely to play a major role in the acclimation process to three-fold increased light intensity in the time frame of this analysis.

3.2.5 No substantial changes in ribosome distribution within chloroplast reading frames by a shift to high light

Since the levels of RFPs were similar between shifted and control samples, it was concluded that the number of ribosomes on the mRNAs were alike. If the rate of translational elongation were constant throughout the experiment, increased or decreased translational-output values would result from different initiation activities between the conditions. So, my analysis showed that translational initiation, apart from *psbA*, was unchanged by the shift (see above). However, this result could not tell anything about potential sub-ORF changes of ribosome occupancies on the RNA, because of altered secondary structures or different binding of regulatory factors. To address the possibility of altered ribosome distributions within ORFs, the contribution of each probe to the summarized signal of the respective ORF (relative ribosome occupancy) was calculated. Differences of more than two-fold between shifted and control samples for two or more consecutive time points in the signal fraction were considered as potential changes in elongation regulation.
The distribution of ribosomes along the ORFs were similar between time points and light conditions. Lowly expressed genes, i.e., PEP genes and *ycf1/2*, showed more dynamics in relative ribosome occupancy, but differences did not pass the threshold of two-fold (Figure 3.16A). Two sites were detected where the differences in ribosome occupancy between shifted and control samples passed the threshold for two or more consecutive time points (Figure 3.16A, red dashed lines). One position is in the first third of the *psbA* reading frame and shows a decrease in relative ribosome occupancy at this position in the shifted samples (Figure 3.16B, left panel). The other positions in the ORF are unaltered. The second potential pausing site is found in the *psaC* ORF, ~100 nt downstream of the translational start site

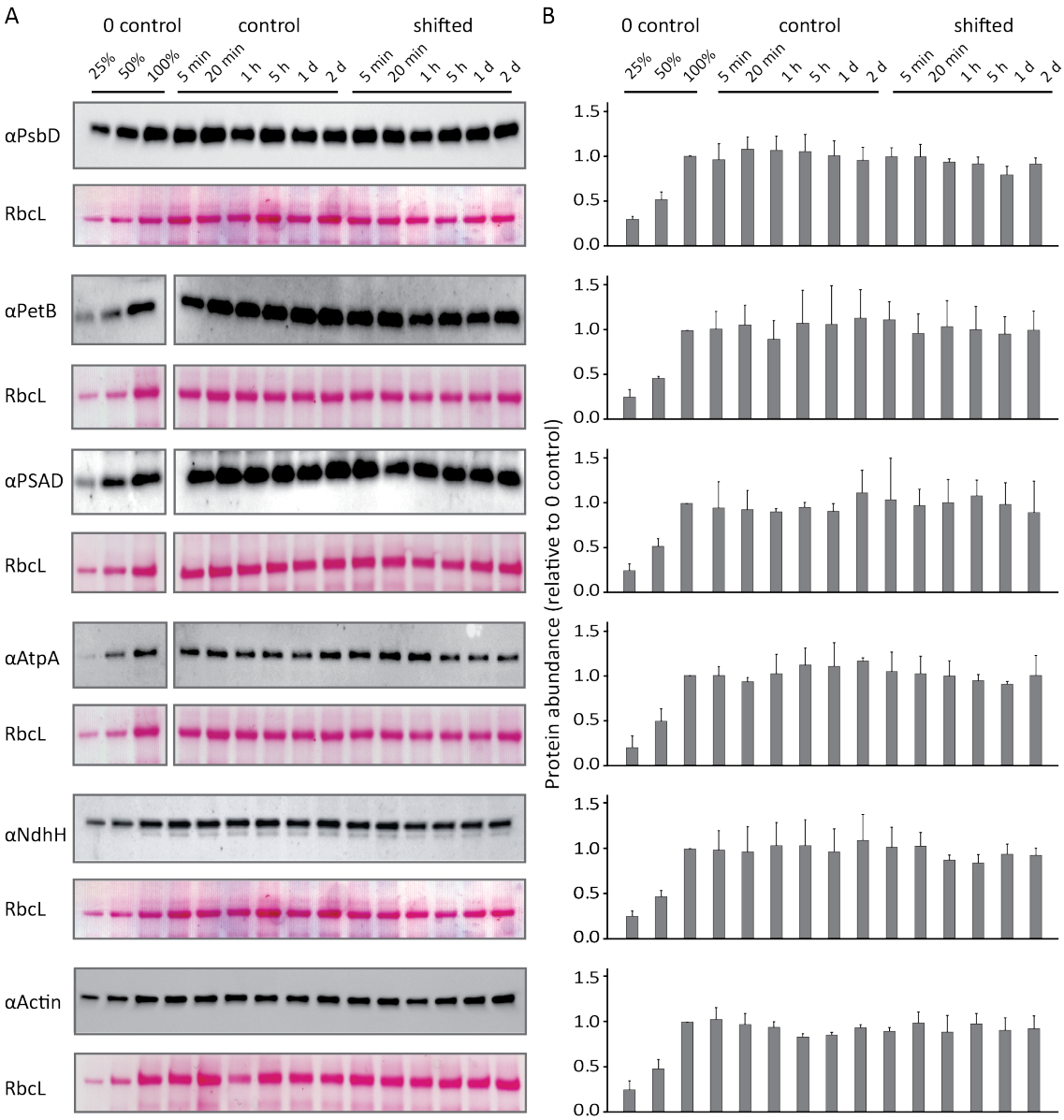

Figure 3.15: Immuno blot analyses of photosynthetic complex contents in shifted and control plants show constant protein accumulation. (A) Core proteins of PSII, cyt-b_6f, PSI, NDH, and cpATP synthase, were analyzed via immuno blots for all time points (excl. 0.5 min) for shifted and control plants. The Ponceau staining of RbcL serves as loading control. The dilution series for PetB, PSAD, and AtpA were initially on the right side of each blot but are displayed on the left side for better comparison. Actin is the representative of cytosolic proteins and serves as additional loading control. (B) Quantification of protein abundance by the luminescence signal was performed with Image Lab (version 6.0, Bio-Rad Laboratories, Inc., USA). Values were normalized to the 100 % "0 control" signal. All data points were calculated as the average of three biological replicates, each represented by two technical replicates. Error bars depict SD.

(Figure 3.16B, middle panel). However, it should be noted that this region generally emits low ribosome occupancy. Interestingly, the shifted samples show higher relative occupancies until this position, and after this region lower occupancies than the control samples. Nevertheless,

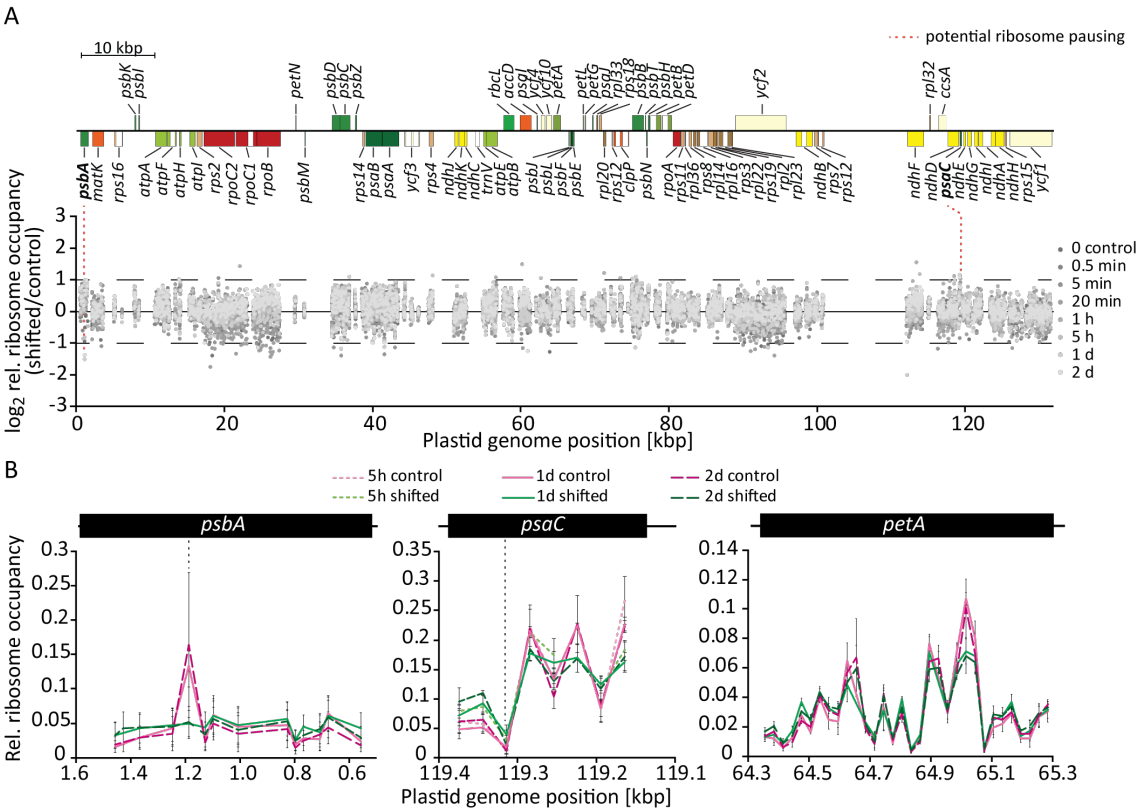

Figure 3.16: Shift from moderate to high lightdid not substantially affect ribosome distribution along ORFs. (A) Quantitative analysis of differences in ribosome distribution along the protein coding regions of the plastome of tobacco between shifted and control samples for selected time points. The signal fraction of each probe to the ORF signal was calculated from three biological replicates (positions with missing signal (n.d. or saturated signal) or signal values below 100 were excluded from the time point and analysis), and the differences between shifted and control samples were plotted against their positions in the genome (dots in different gray shades as depicted in the legend, right side). The representation of the genome displays only one IR. Fold changes over two-fold (horizontal dashed line) for two or more consecutive time points were considered as potentially altered ribosome distribution. Two positions displaying potentially altered ribosome occupancy are highlighted with dashed red lines to the gene map above. The corresponding genes *psbA* and *psaC* are shown in bold. (B) Detailed representation of relative ribosome occupancies along the genes where altered relative ribosome distribution is detected for respective time points. Samples are represented in shades of magenta and green for control and shifted samples, as well as different types of dashed lines for the time points, respectively, as represented by the legend on top. *petA* is plotted similarly as a representative for unaltered relative ribosome occupancy between control and shifted samples. Shown data points are average values of three biological replicates. Error bars depict the SD.

the observed differences are very mild.

In summary, no considerable differences in ribosome distribution along the tobacco plastome, indicating altered elongation regulation, between shifted and control samples were detected. The shift from moderate to high light had little effect on plastidial gene expression. Thus, plastidial gene expression did not seem to contribute to the acclimating process to high light in the investigated condition and time frame.

3.2.6 Solely *psbA* translation was upregulated after the shift from low light to high light at 20 min

To test, if the stress experiment had different effects on chloroplast gene expression, samples harvested 20 min after high-light exposure and corresponding control samples were subjected to transcript profiling and RP. Based on the bleached leaf phenotype at "20 min" (Figure 3.17A) and photosynthetic parameters at "1 h" (Figure 3.12) of high-light stressed plants, damage, not only of PSII, but also of the other complexes involved in electron transport may have occurred. Thus, it was astounding to detect no differences in transcript abundance nor translation output in the high-light stressed sample (Figure 3.17B,C). Again, only *psbA* translation was increased. However, *psbA* translation was only mildly increased by up to two-fold when shifting from moderate to high light. In contrast, after shifting to 20-fold higher light intensity, *psbA* translation was more than five-fold upregulated (Figure 3.17B and Suppl. Dataset 1). The increased translational activity could be partially reversed by a shift from high light to low light (> two-fold, Figure 3.17D-F).

Different to translation output data from the physiological shift, in the group of lowly expressed

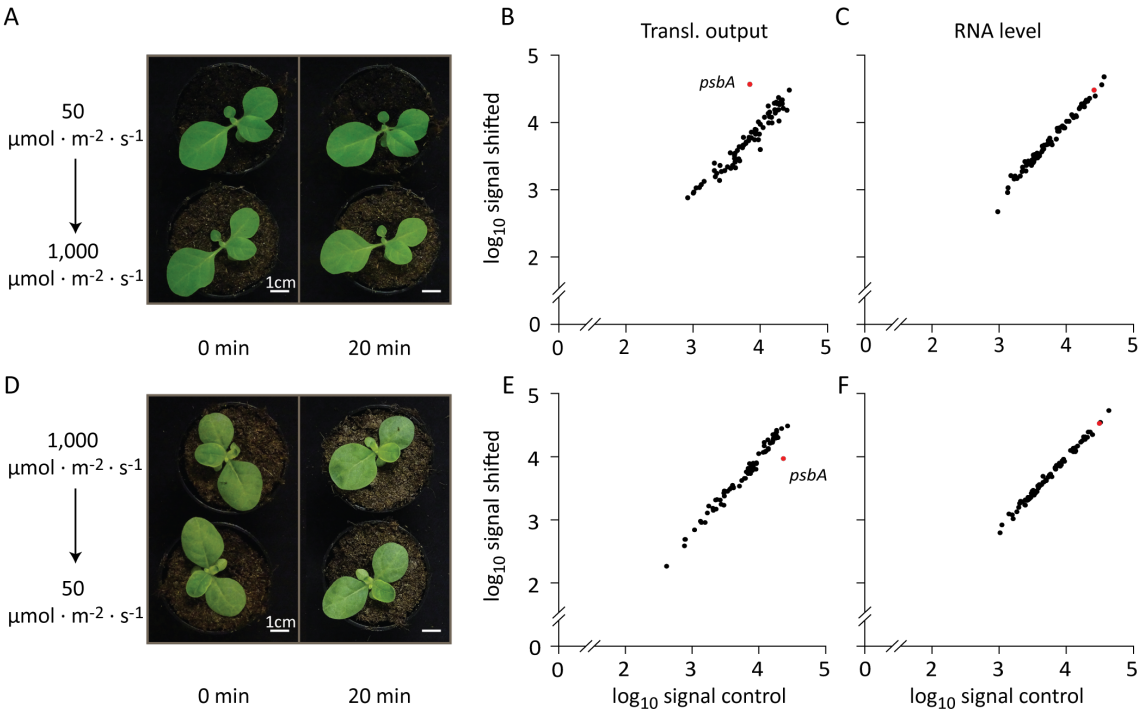

Figure 3.17: High-light stress leads to a bleached leaf phenotype and induces *psbA* translation at 20 min. (A) Phenotype of shifted and control plants at "0 min" and "20 min" of the stress experiment (phenotypes for all time points, see Suppl. Figure S10). (B & C) Scatter plots of expression signals from microarray analysis of one biological replicate for (B) translational output and (C) transcript levels. x-axes represent the signal from the control sample and the y-axes represent the values for the shifted sample. *psbA* is highlighted in red. (D-F) The same as in A-C but for the reciprocal shift from high light (1,000 μmol·m^{-2}·s^{-1}) to low light (50 μmol·m^{-2}·s^{-1}).

genes, some genes were less translated in high light. This group comprises most genes of the NDH, but also of small components of PSII and two ribosomal proteins from the SSU (Suppl. Dataset 1). The reduction of translational output may be a consequence of ribosome titration

by *psbA* mRNA. However, if the group of *ndh* genes was selectively regulated has to be confirmed by biological replicates and samples of more time points.

3.2.7 Promotion of *psbA* translation was already activated at low light intensities

An increase in light intensity resulted in an increased translational output of *psbA*, in both, the physiological and the stress experiment, respectively. Additionally, the magnitude of increased translational output seemed to correlate with the magnitude of increased light intensity. However, from the previous analyses, no conclusion could be drawn of the basal translational output of *psbA* and its relationship to the experienced light intensity from the previous analyses. Thus, the translational activities of *psbA* in the different light conditions were analyzed for a better understanding of this relationship. In addition to the translational output data from the physiological and the stress experiment, data from high-light adapted, thus grown continuously at high light, tobacco plants were included.
For comparison, the "20 min" time point was chosen. Referring to the translational output signals of *psbA* at standard growth conditions (Figure 3.18, first panel, magenta bars), D1 synthesis is the lowest at low light and increases with increased light intensity. However, the difference in translational output between low and moderate light (seven-fold increased light intensity) is 2.8-fold whereas the difference from moderate to high light ($\sim$ three-fold increased light intensity) is 1.2-fold. The translational output for *psbA* was nearly as high in moderate standard light condition than in high standard light condition at a signal intensity of approximately 20,000 to 23,000 a.u. (Figure 3.18, first panel). Also, the difference from low to high light (20-fold increased light intensity) is with 3.3-fold unexpectedly low. Translation activity of *psbA* in standard growth was not in a linear relationship to experienced irradiation. Furthermore, the translational activity of *psbA* was probably not exhausted in the standard high light. From the RFP signal intensities from shifted samples (Figure 3.18, first panel, green bars), it can be estimated that D1 synthesis was not limited by transcript abundance or the translation machinery in the conducted experiments but could have been increased even further by increased stimulus.

Comparisons of other plastidial genes show similar translation levels regardless of the light intensity and the experiment (Figure 3.18) which indicates that the expression of those genes was not reduced due to a high demand of energy and translational factors for D1 synthesis.
psbA translation and its regulation is outstanding in the conducted experiments and resources for the expression of *psbA* may be separated from the resources for the basal gene expression. Therefore, the expression of *psbA* and its regulation seem to be critical for chloroplasts in the light acclimation process.

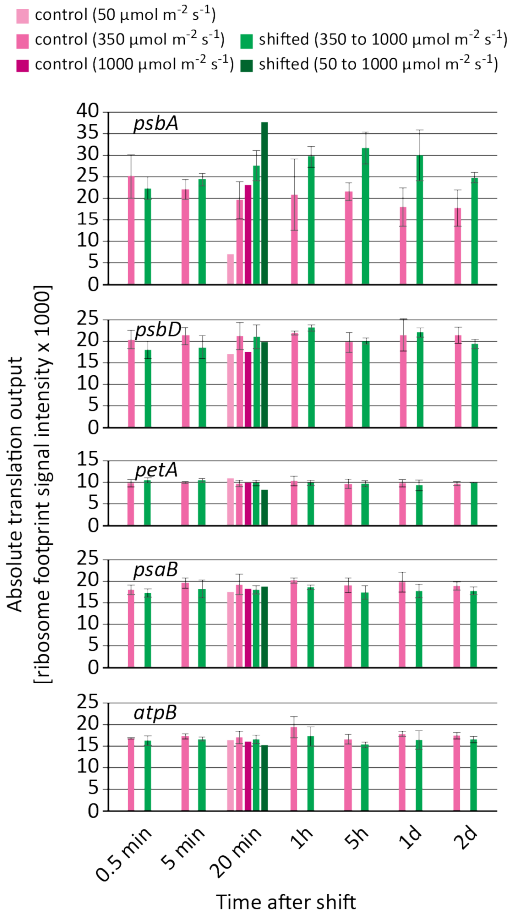

Figure 3.18: Comparison of the translational output of plastidial genes in different light regimes revealed a unique response for *psbA* translation. Absolute translational output in selected ORFs inferred from RFP signal intensities for low, moderate, and high growth light in magenta and after shift in green, as shown in the legend above. Harvesting time points of samples are specified below. Values from control (350 μmol·m^{-2}·s^{-1}) and shifted (350 to 1,000 μmol·m^{-2}·s^{-1}) samples were averaged over three biological replicates. Error bars depict the SD.

4 Discussion

The present thesis was designed to deepen the understanding of translational processes in the chloroplast of higher plants and to identify regulatory targets of organelle gene expression that are affected in acclimation to different light intensities.

4.1 Why not using the "gold standard" of plant research?

For the research of higher plants, *A. thaliana* is the plant model system *par excellence*. Sophisticated genomic tools were developed to study nuclear gene function and the generation of mutants can be performed easily by dipping of flowers into Agrobacteria solution which results in homozygous mutants in the F_1 generation. Nevertheless, no stable plastid transformation was established until 2019 to manipulate plastidial gene expression in a targeted way (Ruf et al., 2019; Yu et al., 2019).
For tobacco, however, the transformation of the plastome is a standard tool to study organelle biology and to engineer the chloroplast for biotechnological use (Svab et al., 1990; Krech et al., 2012; Ruf et al., 2007; Maliga and Bock, 2011). Certainly, tobacco is not an ideal organism to study nuclear-gene expression and organelle-nucleus interaction. Tobacco is an allotetraploid organism that kept the nuclear genomes of the mother plant *Nicotiana sylvestris* and the potential father plant *Nicotiana tomentosiformis* (Yukawa et al., 2006; Leitch et al., 2008). Due to the allopolyploid character of the genome and the lack of well annotated genomic information for targeted nuclear-genome mutagenesis, manipulations of the tobacco nuclear genome were rather unspecific and the generation of homozygous mutant plants were labor intensive. Only recently, CRISPR/Cas9 technology was successfully used to generate targeted knock-out mutants of tobacco (Schachtsiek and Stehle, 2019; Hayashi et al., 2020). Altogether, when the project was initiated, tobacco was the ideal model organism to identify targets of chloroplastic gene-expression regulation which could be further addressed by plastid transformation. However, for the analysis of nuclear factors involved in the regulation, a switch to orthologous genes in *A. thaliana* was planned.

4.2 Successful establishment of high-depth ribosome profiling for the chloroplast

Nonetheless, before plastid-encoded genes or nucleus-encoded factors that are either regulated or are involved in regulation, respectively, I aimed to generate high-depth profiles of the chloroplast translatome to enable the identification of potential targets.

RP was chosen as useful tool to study the distribution of ribosomes on mRNA and thereby get a prediction for putative *cis*-elements. Because the identity of the obtained RFP can be inferred by deep sequencing or microarray hybridization, the translatome can be analyzed in a genome-wide manner. However, depending on the organism and starting material used, the output is highly heterogeneous. Plants, for instance, have next to the genomic compartments, nucleus and mitochondrion, which are found in each eukaryotic cell, a third genomic compartment, the plastid. In green tissue, the gene expression in the chloroplast is highly active to produce components of the photosynthetic apparatus for new assembly and maintenance of the complexes. Still, transcriptomic and translatomic datasets are dominated by products of nucleus-encoded genes (Dyer et al., 1971; Piques et al., 2009) and methods had to be established for highly cytosolic-reduced RFP datasets.

4.2.1 Isolated chloroplasts as source for RFPs

One approach to minimize the content of cytosolic RNA and to enrich highly for plastidial RFPs is chloroplast isolation. Chloroplast isolation is a well-established method to obtain intact plastids to study components of the import system (Nada and Soll, 2004; Qbadou et al., 2006; Eisa et al., 2020), but also the gene expression (Fish and Jagendorf, 1982; Trebitsh and Danon, 2001; Majeran et al., 2012).

4.2.1.1 Low-carb chloroplasts

Most published protocols used either *A. thaliana* after prolonged night or super-market spinach kept in the fridge for some hours. Both types of tissue have the advantage of a highly reduced starch content in the plastid when it comes to the isolation procedure. Starch, with its high density disrupts the chloroplast envelope in the centripetal field (Stitt and Heldt, 1981) and is, therefore, an issue for isolation of intact chloroplasts. Tobacco, different to *A. thaliana*, contains still high amounts of starch at the end of the night.
Since, the fridge was no option to reduce starch to the minimum, different growth condition for tobacco, that were established in the institute, were tested for optimal starch reduction at EON. The tested environments varied in the intensity and quality of the used light, as well as in temperature, humidity, and day length. Light characteristics were found to be the dominating parameter for the visible phenotype of the cultivated plants. The plant size correlated very well with the experienced light intensity and day length (Table 3.1). Studies on soybeans did also observe a light dependent biomass accumulation (Yang et al., 2014; Feng et al., 2019). Thus, soybean planted as monoculture or at high light intensity had higher biomass than plants grown in the shadow of maize or at lower light intensity. The experiments from Feng et al. (2019) did also observe a correlation of light intensity and enzyme activity for carbohydrate metabolism, including increased accumulation of sucrose and starch. However, in the present study, the light intensity could not give any estimate about the starch accumulation within the leaves, neither could the light quality. The optimal condition for tobacco growth used for CI was the green house which led to high tissue and low starch accumulation at SON and EON. Nevertheless, it has to be noted that also an extended night reduced the starch content in the leaves and is an alternative when highly controlled conditions for mutant experiments or acclimation experiments are needed.

The greenhouse was chosen as growth condition for plants used for CI and, to increase comparability of Ribo-seq datasets, for TRAP.

4.2.1.2 High yield of chloroplastic RFPs from isolated chloroplasts

The isolated chloroplasts were subjected to RP that resulted in low yield of RNA. Still the obtained RNA amount was sufficient for library preparation, but too low for prior rRNA depletion which resulted in high fractions of RNA contaminants, i.e., rRNA and minorly tRNA. The primary analysis of the subcellular origin of obtained sequencing reads showed enrichment of chloroplastic reads of more than 80 and nearly 90 % for the samples generated in light. The sample generated in the dark ranged from 58 % to 73 %. The low amount of cpRFPs from dark-isolated chloroplasts was probably the result of hindered visual control in the isolation process. Disruption the chloroplasts in the resuspension step and selection of broken chloroplast membranes from the percoll gradient are likely to reduce the RNA content in the samples. Unfortunately, also the usage of night-vision devices was of little help after plant harvest. Potential automation of critical steps, e.g., resuspension and chloroplast collection from the percoll gradient, may improve the quality. Another explanation for reduced RFP recovery from dark-isolated chloroplasts is the reduced translational activity in chloroplasts in the dark. Studies on *A. thaliana* showed reduced polysome loading of plastidial RNA in the dark compared to light treated samples (Juntawong and Bailey-Serres, 2012; Pal et al., 2013). Thus, samples with the same chlorophyll and RNA concentration differ probably in the fraction of generated RFPs.
Still, all three samples (Dig:dark, noDig:light, Dig:light) had much higher fractions of chloroplastic reads than the samples obtained from whole leaves (input samples, see below) which ranged from 18 to 26 %. In summary, CI is a useful tool to enrich sequencing libraries selectively for chloroplastidic reads. This enables high depth datasets for the chloroplast and potential determination of translational features that were overlooked because of low coverage.

4.2.1.3 CI is stressful for the sample and biases the results

Chloroplast isolation is a long-known tool to study different aspects of this organelle. However, the process includes many stressful steps that influence chloroplast metabolism. First, each isolation is a cold-stress treatment for the chloroplast, which is independent of the prior treatment of the plant. Further, the cold stress is long-lasting, and the cold does not completely stop molecular processes as snap freezing in liquid nitrogen does. Enzymatic reactions in the chloroplast are decelerated which may increase the excitation pressure on the photosystems, because chlorophyll excitation is independent of the temperature, and increase the accumulation of toxic photosynthetic byproducts. Comparisons with RFP data from cold-treated plant tissue will be helpful to determine the degree of cold-induced translational alterations in the CI sample. The relatively low similarity between Dig:light and input:light samples of cpCPM values (Figure 3.3A) and the minor increase of *psbA* CPM values observed in light compared to dark samples (Suppl. Figure S3) indicates such cold-induced alteration in the translational output of the chloroplast samples. Observations by Yang Gao (Gao et al., 2016) revealed dynamic translation in tobacco chloroplasts in low-temperature acclimation. In the acclimation process, the translation of *psbA* was up-regulated by almost four-fold after one hour in

the cold. The cold-induced translation activation of *psbA* in the chloroplast isolation process, which was the same for light and dark samples, probably affected the extent of differential translation activity. Hence, the expected fold change of six to eight of *psbA* translational output, which was described by Chotewutmontri and Barkan (2018) from dark-light transition data, was only two-fold between the chloroplast samples. Further, also Lukoszek et al. (2016) described differential expression of plastid-encoded genes upon thermal stress that resulted in non-stoichiometric synthesis of complex subunits.
Furthermore, translation is an enzymatic reaction and will thus be slowed down in the cold environment. Of course, translation elongation inhibitors were supplemented to the isolation buffers, but how fast they enter the cellular compartments and stall ribosomes was not tested. From Ribo-seq datasets of elongation inhibitor-treated cell cultures, it is known that the coverage is artificially increased at the start-codon region due to unaffected translation initiation. Additionally, it is known for the 80S translation inhibitor cycloheximide that pre-treatment of cells induced disrupted dynamics of elongation and resulted in codon biases (Hussmann et al., 2015). Recent studies in *E. coli* suggest also for translation inhibition by chloramphenicol a sequence-specific bias (Orelle et al., 2013; Mohammad et al., 2016; Marks et al., 2016).
Chloroplast isolation may introduce many biases to ribosome density which makes its use for detailed analysis of chloroplast translation less informative, especially if pausing and/or *cis*-elements are in focus. However, depending on the scientific question and the information drawn from Ribo-seq datasets from CI experiments, such as chloroplast-associated cytosolic translation and protein-import mechanism (see next section), CI is a use- and powerful tool.

4.2.1.4 Cytosolic RFPs found attached to isolated chloroplasts

For eukaryotic systems, the co-translational import into the secretory system of ER and Golgi are known for decades. Also, co-translational import and mRNA targeting for mitochondria were observed. However, such mechanisms are ultimately rejected for chloroplast protein homeostasis (reviewed by Weis et al., 2013) due to missing electron microscopy evidence of cytosolic ribosomes attached to the chloroplast.
Nevertheless, and mainly since a distinct small fraction of cytosolic reads were obtained from CI samples, co-translational import or at least enrichment of mRNA of chloroplast-localized proteins at the outer membrane was rudimentary analyzed by inspection of the cytosolic read fraction in the CI samples. Cytosolic reads were much longer (35 nt) than reported read sizes for cytosolic RFPs in plants (Juntawong et al., 2014; Hsu et al., 2016; Chotewutmontri and Barkan, 2018; Wu et al., 2019b) and also read sizes obtained in the TRAP experiment (see Section 4.3.2). It was speculated that RNase I digestion of the RNA was insufficient and resulted therefore in longer RFPs. However, the cytosolic read size is nicely distinct which contrasts with the chloroplastic read size (Figure 3.2 B). In addition, the reads showed a convincing frame affiliation as would be expected from moving ribosomes (Figure 3.2 C) and an absence in introns (Figure 3.3). These observations contradict insufficient digestion of cytosolic mRNA by RNase I. Potentially, the longer read size is correct for a subset of cytosolic genes and was just overlooked in whole tissue datasets because of the sheer abundance of 29 nt reads. Zooming-in into the read-length distribution of the TRAP samples suspects a minor population of larger reads between 35 and 40 nt (Figure 3.7 B). However, the fraction of long cytosolic reads obtained by TRAP was too low to compare the identity of their origin with the reads of the CI samples (see Suppl. Dataset 2).
To see if cytosolic reads obtained by CI are also related to chloroplast function or just an accidental contamination of the samples, differential gene expression analysis was performed

to define enrichment in the CI samples compared to the input samples. Probably, plant lysate from the chloroplast isolation would have been a better reference because of identical buffer and antibiotic usage. Further, input samples were obtained from transplastomic plants that displayed a wild-type phenotype but which plastidial gene expression was mildly altered (Sections 3.1.2.3 and 4.3.2) and thus could influence the nuclear gene expression through retrograde signals (Leister et al., 2014). Differential expression analysis detected 28 and 20 nucleus-encoded genes with significantly enriched read number in CI samples from light and dark, respectively. For 14 genes in the light sample and 4 genes in the dark sample, a function in the plastid is predicted. The higher number of genes in the light sample was expected given the enhanced translation in the chloroplast and in the cytosol in light (Juntawong and Bailey-Serres, 2012; Pal et al., 2013; Chotewutmontri and Barkan, 2018, this study). Genes detected enriched in the dark sample are mostly associated with cellular membranes and the secretory system which hints to enrichment of non-chloroplast membranes in the CI samples by either imprecise chloroplast fraction selection in the dark from percoll gradients or increased association of the cytosolic membranes with chloroplasts in dark.
Next to genes directly involved in photosynthesis, e.g., LHCA/B and PSAO, σ-factor 5 (SIG5) could be detected significantly enriched in Dig:light. SIG5 is a transcription factor of PEP that is specifically associated with the activation of the Blue Light-Responsive Promoter of *psbD* (Nagashima et al., 2004). Transcription of *sig5* is activated by blue light which makes SIG5 to a morning gene but also to a marker of high energy-light stress (Kimura et al., 2003; Noordally et al., 2013; Belbin et al., 2017). Thus, the enrichment of *sig5* footprints in the CI sample is potentially related to the time point of CI (SOD) and can be used for validation of the experiments. Further, SIG5 is not a very abundant protein (Noordally et al., 2013) which makes its footprint accumulation in the CI sample even more interesting.
However, investigation of the nucleus-encoded genes found depleted in the CI sample obtained in light also revealed a high fraction of genes whose products function in the chloroplast (72 genes depleted in CI, 46 with function in the chloroplast). Neither group, enriched or depleted, enclosed genes of specific function, e.g., only photosynthetic or carbohydrate metabolism, nor did they differ in gene product length, e.g., genes with short products in depleted group, or the product association with membranes, e.g., transmembrane proteins are synthesized close to the chloroplast import system for the smooth import and fast association with import-related chaperons.
Further experiments are needed to co confirm the specific association of mRNAs from identified nucleus-encoded genes with the outer membrane of the chloroplast. Next, reisolation of tobacco chloroplasts at SOD with subsequent RP by other experimentators is needed. If the enriched set of genes found in this study can be confirmed, an unspecific enrichment can be excluded, and follow-up analyses and experiments can be initiated. From the obtained data, regression analyses or machine learning approaches can be used to disentangle the characteristic responsible for the enrichment or depletion of nucleus-encoded genes functioning in the chloroplast, respectively, e.g., short with transmembrane domain versus long with transmembrane domain. Moreover, the transit peptide is an excellent target for potential import control. If the genes enriched in the CI sample at SOD encode for a defined pattern in the transit peptide this could give a new starting point for the analysis and prediction of the peptides and the related regulation. Thus, CI experiments can be performed in time series or under different light condition to extend the analysis for subsets of genes functioning timely controlled or as response of external triggers. For example, de-etiolation experiments with tobacco showed a distinct pattern of transcript accumulation of plastid-localized nucleus-encoded genes that was recently time-resolved (Armarego-Marriott et al., 2019).
Apart from studies based on RP of isolated chloroplasts, imaging methods can be applied.

Targeting the genes identified by CI-RP can be done by fluorescence *in situ* hybridization (FISH) (Gall and Pardue, 1969; DeLong et al., 1989). Specific mRNAs and DNA fragments were already accessed in root cells with the FISH method (Duncan et al., 2016; Fujimoto et al., 2016). However, leaf tissue has the disadvantage of a high auto-fluorescent signal from chlorophyll that makes the detection and analysis, especially for probes expected in the chloroplast proximity, difficult but feasible as shown for FISH in Chlamydomonas chloroplasts (Uniacke and Zerges, 2009). Additionally, FISH experiments could be performed with etiolated tissue. Besides, imaging methods can be used to determine the association of chloroplasts with the cytosolic membrane system in the dark. Products of genes found enriched in the CI sample obtained in dark are either associated with membranes or secreted (18 of 20 genes). Thus, co-enrichment of cytosolic membrane systems with chloroplasts in the dark is possible. Direct evidence for chloroplast-associated translation can be obtained by proximity studies using the biotin-acceptor peptide (Avi) and the biotin ligase BirA. By tagging soluble proteins, such as ribosomal proteins, with Avi and proteins of the import system, e.g., Toc64, with BirA can give information of potential spatial interaction. A short pulse of biotin leads to the biotinylation of Avi by BirA and the biotinylated ribosomes can be enriched by IP (Jan et al., 2014). This method was successfully used in yeast and mammalian cells to enrich specifically ER and mitochondrion associated RFPs (Jan et al., 2014; Williams et al., 2014). But also specific enrichment of ribosomes associated with guiding proteins, that are known to engage plastid-localized proteins in the cytosol and direct them to the import system of chloroplasts, e.g. ARK2 (Bae et al., 2008) or potentially Toc159 (Smith et al., 2004; Ivanova et al., 2004), offer the possibility to study potential mRNA targeting and co-translational import.
Albeit the analysis of cpRFPs from isolated chloroplasts is restricted by biases originating in the isolation method, CI is a powerful tool to study translation on the outside of chloroplasts.

4.2.2 TRAPing chloroplastic ribosomes

Although, CI led to a remarkable enrichment of cpRFPs, the obtained results were probably influenced by gene expression responses induced by cold and pattern in the ribosome occupancy due to inhibitor usage in the isolation buffer. Thus, another approach to increase chloroplastic RFP concentration in the samples was implemented that took advantage of the well-established transformation of tobacco plastids. Two lines, both homoplastomic for a tagged ribosomal protein were used for IP experiments to selectively enrich ribosomes from the chloroplast and thereby the protected mRNA fragment. TRAP was already successfully used to study translation in the cytosol of various species (Zanetti et al., 2005; Juntawong et al., 2014; Daftuar et al., 2013; Archer et al., 2016; Ferretti et al., 2017).

4.2.2.1 Monosome pellets were highly aggregated

Prior to IP, monosomes were prepared by nuclease digestion and purification through a sucrose cushion. This resulted in a monosome pellet that needed to be resolved for the IP. However, monosome pellets were hard to re-solve despite their high solubility needed to fulfill translation in the cytosol. Different mild detergents were tested as a supplement for the suspension buffer to increase the fraction of solved monosomes. However, the fraction of aggregated and solubilized monosomes stayed constant (Figure 3.6A,B). Also, the substitution of the buffer with

glycol, which should repress molecular movements for efficient antibody binding, was tested. The presence of glycol in the buffer did not influence the aggregation state of the monosomes (data not shown).
Nevertheless, a difference of solubility of the monosomes was observed between HA-Rps15 and Rpl32-GFP. Whereas most HA-Rps15-containing ribosomes stayed mainly in the aggregated fraction, ribosomes carrying the Rpl32-GFP were found at equal amounts in soluble and aggregated fraction, respectively. Unfortunately, no data is available to compare the aggregation behavior of HA-Rps15- and Rpl32-GFP-containing ribosomes in TRAP and RP experiments, respectively. In the general RP protocol, the monosomes are destroyed after purification to isolate the RNA; hence no resolution is needed. Further, publications, where TRAP was used, gave no information about the dissolubility of their preparations. Consequently, comparisons and extrapolations of the solubility of tagged monosomes, and untagged, could not be made. However, the higher solubility of Rpl32-GFP monosome may be based on the GFP-tag which is much larger than the HA-tag and a highly hydrophilic protein (Shimomura et al., 1962). Therefore, it may increase the hydrophilic character of the ribosome. Admittedly, the small size of GFP in comparison to the ribosome may have little influence on the solubility *per se*, but the tags, HA and GFP, respectively, can have an influence on the binding of other protein factors that impact the aggregation strength of the monosome.
Nonetheless, the amount of resolubilized monosomes was, in the case of both lines, sufficient for successful precipitation of the tagged ribosomal protein, including ribosome and protected footprint (Figure 3.7A and Suppl. Dataset 2). Adjustments of the protocol, e.g., cross-linking of proteins and RNA with formaldehyde to increase the stability of the translational complex, but specifically the stability of the pre-initiation complex, may decrease the solubility further, because larger covalently bound RNP complexes would result. However, also the buffer system would need to be adapted which could, on the other hand, improve the solubility.

4.2.2.2 TRAP enriched cpRFPs selectively

IP of tagged ribosomes resulted in low yield of RFPs which was still sufficient for library preparation. Next to the IP samples, input samples of the very same tissue were processed. Separation of IP and input sample happened after nuclease treatment. IP resulted in a three to four-fold enrichment of chloroplastic reads compared to the general RP protocol. The dataset from IP:HA-Rps15 thus contained around 80 % chloroplastic reads (exception HA-Rps15:light2) and IP:Rpl32-GFP up to 75 %. The high fraction of chloroplastic reads in IP:HA-Rps15 was probably not the result of a more efficient IP but of a higher cpRFP content already in the tissue. Also, the input sample from HA-Rps15 had around 25 % chloroplastic reads whereas the input sample from Rpl32-GFP comprised less than 20 % of chloroplastic reads. However, it would be pure speculation to interpret the difference between the two lines regarding the fraction of reads originating from the three subcellular compartments. Because no detailed analysis of the morphology of both lines in respect of chloroplast number, size, and general appearance was done, it is not possible to tell if the higher fraction resulted from a larger number of chloroplasts, higher transcript levels per chloroplast, or higher ribosome occupancy of the transcript.
The content of RNA contaminants was comparable between the IP samples and input of HA-Rps15 with approximately 65 %. Chloroplastic reads from the input sample of Rpl32-GFP did only contain 55 % contaminants. The rRNA contamination of the TRAP samples was much lower as the contamination in the CI samples (70 to 85 %, Section 3.1.1.3 and Suppl. Dataset 2). Analysis of rRNA contaminants in the samples for their fragment length and

genomic origin, and thus position in the mature ribosome could reveal cleavage sites of the nuclease and potential determinants for the different RNA contaminant fractions. This information may be useful for the generation of customized rRNA depletion probes for TRAP experiments. A similar approach is already established for the general Ribo-seq protocol in the Zoschke lab. However, this information was not in focus of this thesis and higher yields of immuno precipitated RFPs are needed for successful rRNA depletion.

4.2.3 Low RNase I concentration is sufficient for successful monosome preparation

Comparing the fraction of rRNA and tRNA contaminants of CI and TRAP led assume that high RNA contamination may be a result of highly fragmented ribosomes due to over-digestion by nucleases that co-purified with the small RFPs in the acryl-amid gel. Yet, the read length distribution and frame affiliation from the CI samples hinted instead into the direction of insufficient digestion of RNA. In comparison to the established maize protocol by Chotewutmontri et al. (2018), much lower concentrated lysates for the nuclease treatment and also only 18 % of the nuclease activity were used to generate RFPs from CI. Thus, lower concentrations of RNA and nuclease may have led to incomplete digestion.
Different to the CI samples, RNA contamination in TRAP samples was lower despite highly elevated RNase I and sample concentration. Digestion of the TRAP sample was done with 40 % of the recommended RNase I activity for maize by Chotewutmontri et al. (2018) and 80 % activity of that used for yeast by Ingolia et al. (2009). The read size distribution for all three compartments was improved regarding the CI samples. Higher RNase I concentration led to more defined abundant read lengths. Also the major read size for cytosolic reads was consistent with the published read sizes found in various eukaryotes (Ingolia et al., 2009, 2011; Hsu et al., 2016). Thus, RNA digestion by RNase I seemed much improved. But still, the fraction of in-frame reads was only mildly increased to 55 % from previously 50 % for cytosolic reads in CI samples. Ingolia et al. (2009) and Hsu et al. (2016) found 75 % and more than 90 % of reads in frame, respectively. However, the read filter applied by those studies for frame affiliation determination was much more stringent than in the present study. Thus, I used all uniquely mapped reads of major read sizes to determine the frame affiliation. Previous studies presented only read sizes showing the highest frame 0 fraction (Ingolia et al., 2009, 2012; Hsu et al., 2016; Chotewutmontri and Barkan, 2016, 2018) or used only reads mapping to defined genes (Ingolia et al., 2009). Thus, there is still potential to manipulate the data to potentially match published data, e.g., by the selection of confirmed coding sequences of the tobacco genome to calculate the fraction of in-frame reads (Sierro et al., 2013; Edwards et al., 2017). But, this would not give a realistic picture of the present datasets and the obtained results.
For chloroplastic reads, published read information, e.g., read length and frame affiliation, are available for maize (Chotewutmontri and Barkan, 2016, 2018) and Chlamydomonas (Chung et al., 2015; Cavaiuolo et al., 2017). As for maize chloroplasts, a more uniform read length distribution from 25 to 38 nt was determined and the frame affiliation was calculated for the longest read sizes. At the same time, footprint preparations of Chlamydomonas yielded more distinct read lengths of 25 to 30 nt with a maximum at 27 nt which showed a very high in-frame contribution (Chung et al., 2015). A small RNA (sRNA) preparation detected RFPs with a read size of 30 to 32 nt and an in-frame fraction of approximately 55 to 60 % (Cavaiuolo et al., 2017). So far, the present read quality for the chloroplast is in good

agreement with already published information for this organelle and with Ribo-seq data from *E. coli* (Mohammad et al., 2019).

Still, when interpreting the quality of cpRFPs, it has to be emphasized that chloroplasts are prokaryotic-like systems and that the RP protocol was mainly established to analyze eukaryotic translation (Ingolia et al., 2009, 2011; Hsu et al., 2016). The use of RNase I as nuclease for the generation of well-defined RFPs was shown to be efficient for plant cytosolic RFPs (Hsu et al., 2016; Chotewutmontri and Barkan, 2018; Wu et al., 2019b). However, read size distribution and frame affiliation of chloroplastic reads from maize and also in this study which were equally or even less defined than naturally occurring small RNA fragments (Cavaiuolo et al., 2017) raise the question of usefulness of RNase I to generate cpRFPs.
RNase I is an *E. coli* enzyme shown to be inhibited by the *E. coli* ribosome (Kitahara and Miyazaki, 2011). Thus, RP protocols for prokaryotes uses MNase or other nucleases for the preparation of monosomes (Oh et al., 2011; Li et al., 2012, 2014; Latif et al., 2015) which was also used in the present Ribo-array protocol (section 2.2.7.1). Read length distribution of bacterial RFPs were of 25 to 35 nt (depending on the experiment) and showed good 3-periodicity (Mohammad et al., 2016, and references therein). Additionally, the use of MNase was shown to reduce rRNA contaminants (Reid et al., 2015) which may be more appropriate for small input sizes where rRNA depletion would likely deplete the whole sample. However, MNase was found to have a clear sequence bias towards [AT] stretches (Dingwall et al., 1981). But if this would compromise the information resulting for chloroplasts have to be tested, given that the plastome of vascular plants is rather AT-rich (Daniell et al., 2016, and references therein). Further, nuclease mixtures may be tested to process the mRNA of each compartment optimally.

4.2.4 Ribosome population of different sizes in the organelles

Conspicuously, in all replicates obtained by CI and TRAP, organelle reads displayed a bi- to trimodal distribution. So far, a bimodal distribution for mitochondrial RFPs was observed in human cell lines (Rooijers et al., 2013) and murine muscle cells (Rudler et al., 2019). However, no observation of multimodal read length distributions for plants and algae were published so far.
RP that focus on mitochondrial translation was only performed once for plants (Planchard et al., 2018). Based on the results from Rooijers et al. (2013), they selectively excised the bands corresponding to the human mitochondrial RFP at 27 and 33 nt from the PAGE. Further analysis showed that the 27 nt reads mapped dominantly to coding sequences and showed clear frame affiliation, whereas the 33 nt read fraction mapped to UTR regions and displayed a random frame distribution. Consequently, they assumed that plant mitochondria RFPs have only a monomodal size distribution. However, a structural study of the plants mitochondrial ribosome revealed that mitochondrial SSU is much larger as its relative in bacteria, plastids, cytosol, and other eukaryotic mitochondria (Waltz et al., 2019). In the present study, the mitochondrial major read size is in good agreement with the size obtained by Planchard et al. (2018). But the second larger read size was potentially overlooked in their approach because of the limited size selection of RNA fragments. Further studies are needed combining the protocol from Planchard et al. (2018) with a more relaxed size selection of RFPs, to also obtain the large RNA fragments, to investigate potential differential functions or targets of the two ribosomal populations. The present datasets are unfortunately to lowly enriched for mitochondrial reads to answer this question (< 0.1 %).

In the case of chloroplasts, a trimodal distribution was observed in the CI samples, whereas the TRAP samples displayed only a bimodal distribution (Figures 3.2C and 3.7C, green line). The higher nuclease concentration for monosome preparation and the clear improvement of the read size distribution to distinct read size majorities raises the assumption that the third peak in the CI samples at the larger read size was an artifact from insufficient digestion and that those read sizes may correspond to combined footprints of ribosomes and tightly binding RBPs. Sequence comparison of longer cpRFPs from the CI datasets with known binding sites of RBPs could confirm this hypothesis and also give the potential identities of the RBPs. Studies in *E. coli* likewise showed a bimodal distribution with reads of around 25 nt and 35 nt, respectively. The different sizes were associated with initiating and elongating ribosomes. Longer reads resulted from SD - antiSD interaction (Li et al., 2012; Mohammad et al., 2016). Re-analysis of CI samples in regard of the three read-length distributions and associated sequence motifs will show if longer cpRFPs do also show a bias toward SD or RBP binding sites in chloroplasts. However, inspection of read distribution in IGV with selected for read sizes larger than 34 nt revealed a distribution equivalent to the distribution of all read sizes (Figure 4.1). To note, the smaller primary footprint size was similar between the CI samples and the TRAP samples at 23 to 25 nt. Based on the observation from Cavaiuolo et al. (2017), biases in the read length result from the usage of different antibiotics. Lincomycin, that inhibits translation shortly after initiation, but does not affect progressed elongation, or the disuse of antibiotics results in smaller RFP sizes. Chloramphenicol, which was used in the present experiments, results apparently in longer RFPs.

RFPs display depending on the cellular department of origin, divergent read length distri-

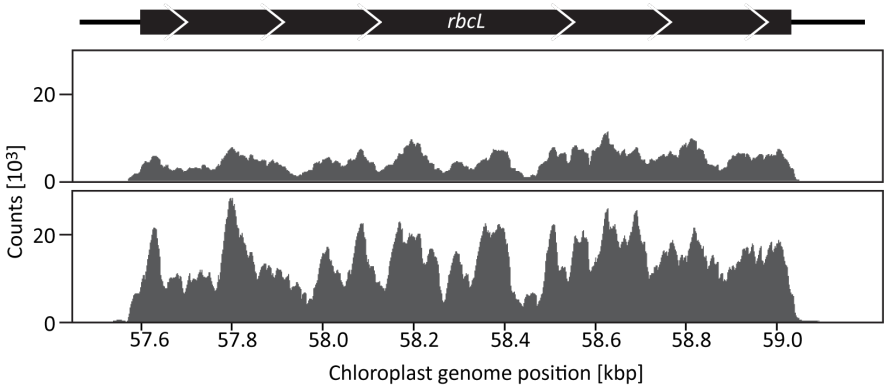

Figure 4.1: Long RFP distribution on chloroplastidic ORFs. *rbcL*-ORF coverage by long RFPs ($>$ 34 nt, upper panel) and all RFPs (20 to 45 nt, lower panel) in the Dig:dark sample. Gene coverage plots were generated with IGV.

butions. It seems likely that mitochondrial RFPs have a bimodal read length distribution in plants but also in other organisms. Thus, biological needs may potentially be served by the two populations. High depth mitochondrial Ribo-seq datasets are needed to investigate this hypothesis. Also, the multimodal distribution of cpRFPs seems likely. Yet, the exact number of modals must be determined, also in regard of the nuclease treatment and antibiotics usage. For chloroplasts, also a species dependent difference in the modality may exist. Hence, maize chloroplast reads showed a broad monomodal distribution that was rather uniform

4.3 Deep insight into the chloroplast translatome by TRAP

TRAP experiments are better reproducible and may have less biases when enriching for chloroplast RFPs than CI. For the isolation process neither pretreatment with translation inhibitors nor chilling stress is applied. Hence, TRAP is a suitable method to explore the translational landscape of chloroplasts from different condition (e.g., temperature, drought) and genotypes (mutants or accessions), or to analyze specific binding sites and target genes.
In the present study, two questions were in focus when designing the TRAP experiment. (1), did co-evolution of chloroplast and host cell led to new modes of translation initiation, that were not observed in prokaryotic systems so far and that could resemble the eukaryotic translation initiation? And (2), do ribosomal subpopulation exist in the chloroplast, and if yes, do they serve different targets?

4.3.1 Independent analysis of RFPs from SSU

Fully assembled ribosomes are highly stable and need specific factors for disassembling, e.g., RRF and Arfs. This stability is used to full capacity by RP. In the present study, two lines were used expressing ribosome with an affinity tag either at SSU or LSU. It should therefore be possible to enrich selectively for the footprint of SSU (FP_{SSU}), if SSU scanning prior translation initiation occurs. Whereas enrichment based on LSU affinity purification should always give full RFPs.
Footprints of SSU only occurs in eukaryotic translation initiation when the pre-initiation complex scan the 5'-UTR from the CAP-region until finding the start codon (Figure 1.2). The enrichment of FP_{SSU} distinct from RFPs in the chloroplast would give first evidence for a SSU scanning mechanism not observed in bacteria or organelles, yet. So far, only 70S ribosomal scanning was observed in bacteria (Figure 1.2 B) (Moll et al., 2004; Udagawa et al., 2004; Yamamoto et al., 2016).

To address scanning of SSU in the chloroplast, TRAP experiments were performed with two independent lines expressing a ribosomal protein with an affinity tag. One line carries the tag on its SSU, whereas the other line had the tag on LSU. If scanning of SSU occurs in the chloroplast, the position of the scanning SSU should be possible to address by TRAP (Figure 4.2 A). Immunopurification of the tagged SSU, however, addresses the position of the assembled ribosome. Hence, RFP profiles of SSU specific TRAP should show coverage of upstream regions of the start codon and LSU specific TRAP profiles cover only the ORF (Figure 4.2 A, B, coverage plots).
The present data, however, does not support such a hypothesis. Two central problems were encountered which may mask potential SSU scanning. The TRAP protocol was not optimized to study independent SSU binding to the mRNA. Even though, the fully assembled ribosome and mRNA build a very stable complex, SSU, and mRNA may not. Initiation is associated with the interaction of SSU-RNA elements with *cis*-elements of the mRNA, e.g., SD - antiSD interaction, and fMet-$tRNA^{fMet}$ hybridization to the start codon. Additionally, ribosomal proteins and regulatory factors enforce the interaction at the specific side (Boni et al., 1991; Tzareva et al., 1994; Danon and Mayfield, 1994b; Yohn et al., 1998; Link et al., 2012). If interactions are missing the affinity towards the mRNA should be relatively low and enable fast dissociation of SSU. Thus, also RP studies in eukaryotic systems used cross-linking methods to stabilize SSU on the mRNA (Martin et al., 2016; Archer et al., 2016; Shirokikh et al., 2017; Wagner et al., 2020). Following, scanning SSU may be lost in the isolation and IP

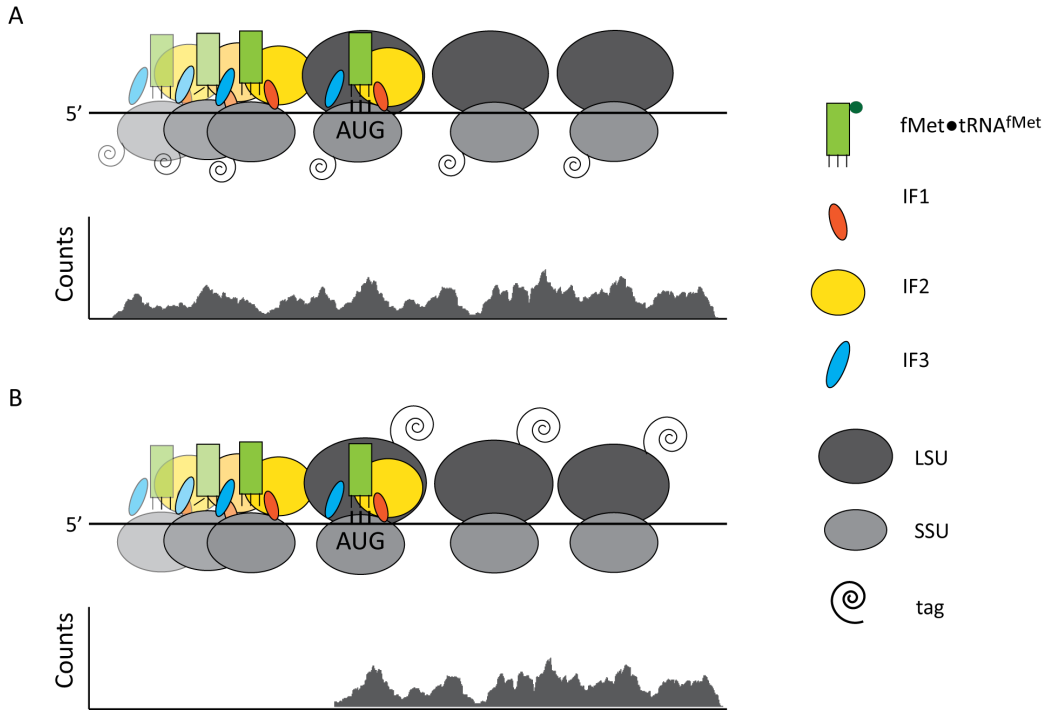

Figure 4.2: Estimation of RFP coverage profiles by TRAP. (A) Potential scanning mode of SSU in the chloroplast and respective coverage plot from TRAP data obtained from immunoprecipitation of the tagged SSU. (B) As for A, but TRAP results from immunoprecipitation of the tagged LSU.

in the present study because of low interactions between SSU and mRNA that were easily disturbed. Future attempts to catch scanning cpSSU should be related to published protocols for eukaryotic cells and use cross linking strategies.
Established protocols for the eukaryotic system also introduced an additional step to separate SSU scanning complex from 80S ribosomes by density gradients. This step enriched highly for SSU and associated RFPs (Archer et al., 2016; Shirokikh et al., 2017; Wagner et al., 2020) and may be adapted for the enrichment of potentially low fractions of scanning SSUs in the chloroplast.
The other problem arises from the structure of the plastome. Plastidial genes are densely packed on the genome (reviewed by Bock, 2007). Some cistrons even overlap, e.g. *psbD/C*, *ndhC/K*, and *atpB/E*, or are only separated by few nucleotides, e.g. *rpoB/C1* and *psbE/F/L*. Determination of 5'-UTR of the downstream cistron may include the 3'-terminal coding region of the upstream cistron. Thus, differential enrichment of FP_{SSU} may be masked by RFPs of the proceeding ORF, as it might have been the case for the differential expression analysis of 5'-UTR coverage in the present study. Sophisticated statistical tools may be able to detect the signal behind the "noise".

4.3.2 Expression of affinity tags altered chloroplastidic translational output

The construction of transplastomic plants depends on the insertion of a marker gene. In most cases, antibiotic resistance genes are included in the transformation vector that enables the

selection of transgenic lines from the initial line. To ensure antibiotic resistance, the selection cassette is driven by a consecutive promoter obtained from some house-keeping genes. Also, other elements of the cassette, e.g., transcript-end site and translation-start site, are selected to ensure optimal resistance without exhaustion of the gene expression system.
In case of the transplastomic lines used for TRAP, the resistance cassette was inserted downstream of the gene of interest, i.e., the gene encoding the tagged ribosomal protein. *rps15* is directly upstream of the *ndhH*-operon, whereas *rpl32* has no proximal neighbor gene (Figure 1.1). Because transcription termination is inefficient in plastids (Stern and Gruissem, 1987; Castandet et al., 2019), the transcription of the resistance cassette leads inevitably to increased transcript accumulation of the downstream cistrons (Schöttler et al., 2017; Fu et al., 2020). Accordingly, higher transcript level for the *ndhH*-operon were expected in the HA-Rps15 line compared to wild type tobacco but also to Rpl32-GFP, which has the resistance cassette on the other strand. It would even be possible that expression of the *ndhH*-operon is further reduced in Rpl32-GFP because read-through transcription could produce anti-sense RNA to the operon and promote its degradation or translation inhibition (Legen et al., 2002; Rott et al., 2011). Thus, more RFPs were expected to map to the *ndhH*-operon in HA-Rps15 than in Rpl32-GFP. Hence, the more than fourfold depletion of *ndhH*-mapping RFPs in HA-Rps15 was surprising (Figure 3.9, Suppl. Figure S7, and Suppl. Table S2). Further, *ndhH* was the only gene in this operon showing this behavior whereas the other genes displayed the expected higher engagement with ribosomes. However, compared to *ndhI* and *ndhG* which are downstream in the operon, *ndhA* which is subsequent to *ndhH*, was relatively low enriched for RFPs (less than two-fold, Suppl. Figure S7).
This observation can be explained by three hypotheses (Figure 4.3). (1), the sequence of the resistance gene and of *ndhH* hybridize to form a secondary structure that blocks start-codon recognition by the ribosome and thereby suppress translation or leads to transcript degradation. Moreover (2), a negative-feedback mechanism which was also observed for RbcL, the large subunit of RuBisCo, that inhibits its own translation in lack of its assembly partner (Wostrikoff and Stern, 2007) actions for NdhH. In both cases, the relatively low occupancy of *ndhA* could imply translational coupling since two nucleotides just separate both genes. The determination of transcript termini of the *ndhH*-operon further showed that in young tissue, the operon is only mildly processed and *ndhH* and *ndhA* majorly appear as dicistronic transcript (del Campo et al., 2006). And lastly (3), the insertion of the *aadA*-cassette may have destroyed the 5' processing element or promoter of *ndhH*.
However, all hypotheses must be tested, and transcript abundances must be determined. In case of induced secondary structure that prevents translation, *in silico* models of potential secondary structures can further be verified by DMS-seq (Gawroński et al., 2020a,b).
To analyze *ndhH* translation for potential feedback-regulation, two strategies can be followed. Negative-feedback regulation is best described for Chlamydomonas and was called "controlled by epistatic synthesis" (CES) (reviewed by Choquet and Wollman, 2009). In higher plants, only RbcL was identified so far to auto-regulate its own translation (Wostrikoff and Stern, 2007). However, CES cascades were identified in Chlamydomonas and each photosynthetic complex harbors at least one CES subunit (Monde et al., 2000; Wostrikoff et al., 2004; Minai et al., 2006; Drapier et al., 2007). But, Chlamydomonas and other algae do not possess the NDH complex in the chloroplast and thus also the genomic information was lost (Martín and Sabater, 2010). Following, inferences about potential CES in the assembly of the NDH complex cannot be made. Still, analysis of tobacco *ndh*-mutants can be done. For nearly all plastid-encoded *ndh* genes, tobacco mutants were generated (Kofer et al., 1998; Burrows et al., 1998; Shikanai et al., 1998; Martín et al., 2004). Mutants show wild type-like phenotypes under standard-growth condition, yet they have disturbed cyclic electron flow around PSI

(Burrows et al., 1998; Shikanai et al., 1998) which is an essential component of photoprotection (reviewed by Shikanai, 2014). CES-like regulation of *ndhH* should also result in decreased ribosome occupancy of the transcript, thus lower RFP abundance. On the other hand, titration experiments with NdhH protein to *in vitro* translation systems can be performed, and the level of newly synthesized NdhH assessed. However, this experiment will only lead to conclusive results if NdhH acts directly on its mRNA or the required factors are present.

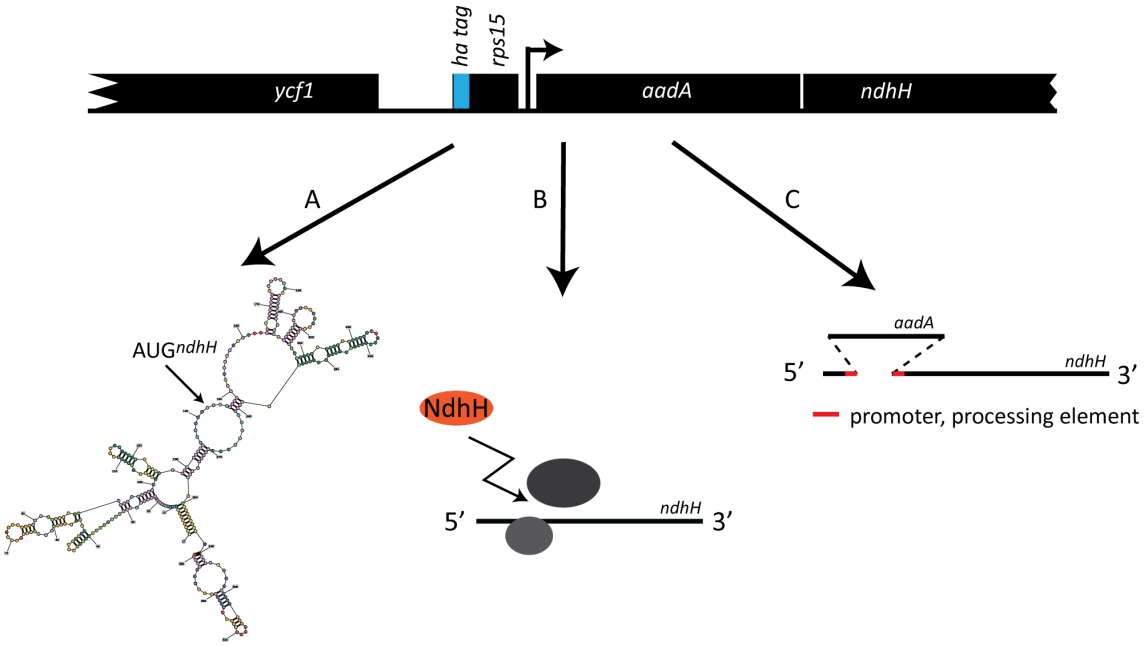

Figure 4.3: Influence of *aadA* insertion on *ndhH* expression. Insertion of *aadA* cassette directly upstream of the *ndhH* operon in HA-Rps15 may influence the expression of *ndhH* in different ways. (A) Potential secondary structure formed between *aadA* and *ndhH* cistron (ΔG = -78.3 kJ/mol) was generated with `RNAstructures` (Reuter and Mathews, 2010). (B) Potential negative feed-back regulation of unassembled NdhH on *ndhH* translation. (C) Potential disruption of regulatory elements of the *ndhH* gene for transcription or transcript processing.

The present datasets of highly enriched cpRFPs were used to address different question regarding chloroplastic translation and protein homeostasis. However, validations of the experiments and data are needed. Further, candidates for further analysis were identified and possibilities to extend and to expand the research on protein import or translational regulation were discussed.

4.4 Role of chloroplastic gene expression to high-light acclimation

The light environment is probably the most unpredictable parameter in plants' life. Apart from the predictable diurnal changes during dusk and dawn, the light intensity may change within seconds to very low or very high irradiation (Kaiser et al., 2018). Mechanisms evolved in plants to scope with these changes to maintain their photosynthetic capacity and homeostasis.
To understand the contribution of chloroplast gene expression to the high-light acclimation

process, a comprehensive and systematic analysis of transcript abundance and protein synthesis of plastid-encoded genes was performed on young tobacco plants exposed to sudden high light for a time frame of two days. The obtained data revealed a minor contribution of chloroplastic gene expression in this time frame of acclimation. My results show that transcript levels and ribosome occupancies of plastid-encoded genes as well as their distribution of ribosomes on the mRNAs were unaltered throughout the experiment. However, a specific increase in translational output and translational efficiency of *psbA* was observed early in the experiment, which was maintained for the remaining time frame of the experiment.
Short-term responses to sudden high light were identified in the expression of nucleus-encoded genes related to stress, e.g., ROS scavengers (Suzuki et al., 2015). Further, chloroplasts harbor multiple sophisticated mechanism to scope with increased light intensity and thereby excitation pressure on PSII to prevent photodamage of PSII and minimize photoinhibition, e.g. dissipation of excess energy as heat or thylakoid rearrangements (Lichtenthaler et al., 1981; Miyake et al., 2005; Hideg et al., 2008; Ware et al., 2015; Wood et al., 2018). The level of photoinhibition is defined by the degree of photodamage and the ability of the system to repair PSII by increased D1 synthesis. However, inhibition of translation was observed as result of ROS accumulation in cyanobacteria under high-light stress (Kojima et al., 2007, 2009) and also in *E. coli* and mammalian cells exposed to H_2O_2 (Ayala et al., 1996; Tamarit et al., 1998). EF-G and EF-2 (EF-G/2) were found oxidized by ROS, respectively, which inhibited the GTP hydrolase activity of the enzyme. Also, Chlamydomonas showed reduced synthesis of RbcL in sudden high light whereas D1 synthesis was increased (Shapira et al., 1997). EF-G/2 were identified as targets for ferredoxin and it was suggested that reduction of EF-G/2 by ferredoxin restores translation elongation. Also, ferredoxin transcription was found increased within 60 s of high-light exposure in *A. thaliana* (Suzuki et al., 2015). Thus, the function of EF-G in the chloroplast may depend on the integrity of the linear electron transport and the pool size of ferredoxin which is reduced at PSI. However, observation of potential elongation inhibition in the early time points of high-light exposure of the present study would have needed supplementation of lincomycin for run-off RP or protein pulse-labeling experiments (Trösch et al., 2018; Chotewutmontri and Barkan, 2018). Run-off RP and pulse-labeling experiments in light and dark on maize tissue, revealed enhanced elongation in the light for nearly all plastid-encoded genes (Chotewutmontri and Barkan, 2018). Yet, maize seedlings were acclimated to the experience light intensity, and lincomycin treatment was performed more than eight hours after SOD (RbcL synthesis was recovered after six hours in Chlamydomonas (Shapira et al., 1997)), which let us suggest that no high ROS accumulation was experienced and elongation inhibition could be prevented by ROS scavengers and a large ferredoxin pool at this time point. Thus, data is still missing to clarify elongation regulation upon the light shift of plastid-encoded genes in vascular plants.
Initiation was found as the rate-limiting step of translation in eukaryotic systems (Shah et al., 2013; Riba et al., 2019). Thus, initiation would predominantly define the level of translational output. For plastidial genes, factors involved in the initiation of D1 synthesis were identified in Chlamydomonas (Danon and Mayfield, 1991), *A. thaliana* (Schult et al., 2007; Link et al., 2012), and also in maize (Chotewutmontri and Barkan, 2020; Chotewutmontri et al., 2020). The regulation of *psbA* expression was described as redox/light-dependent in Chlamydomonas *Danon1991*, barley (Pötter and Kloppstech, 1993; Edhofer et al., 1998; Mühlbauer and Eichacker, 1998), and spinach (Klaff and Gruissem, 1995). Yet, it is unknown, which factors are involved, and if their expression and/or their activity is redox/light-dependent. In the present study, a specific increase in translation initiation was observed only for *psbA* upon a shift from low or moderate light to high light. Similar results were obtained for maize transferred from dark to light (Chotewutmontri and Barkan, 2018). This specific increase in translational activity of *psbA* was reversible by the reciprocal shift (Figure 3.18, Chotewut-

montri and Barkan, 2018). Together with the observation from Chotewutmontri and Barkan (2020) who linked the light-induced synthesis of D1 to the light-induced damage of the same, the present results point to PSII repair and maintenance reactions as early steps in the acclimation processes. Yet, Chotewutmontri and Barkan (2020) defined damaged D1 to be the photosynthetic product driving *de novo*-synthesis of D1. They also found that the enhanced genome-wide elongation was triggered by products of the electron transfer supporting results obtained from barley (Mühlbauer and Eichacker, 1998). Chotewutmontri and Barkan (2020) found this connection by uncoupling linear electron transport from photodamage by the usage of different light qualities, photosynthetic mutants, and inhibitors. A model was then proposed - assembled D1 in PSII inactivates HCF244, OHP1, and OHP2. While D1 is intact in PSII, HCF244, OHP1 and OHP2 build a complex with unassembled D1. Upon the release of damaged D1 from PSII, unassembled D1 is released from the complex with HCF244, OHP1, and OHP2. The three proteins become active and somehow initiates D1 synthesis via the known *psbA* translation activator HCF173 (Link et al., 2012; Chotewutmontri et al., 2020). Further, determination of secondary structure changes identified unstructured *psbA* 5'-UTR and an accessible start codon in high-light treated *A. thaliana* and the footprint of a putative regulatory protein for translation initiation of *psbA* (Gawroński et al., 2020a). Nevertheless, it needs elucidation if the footprint belongs to HCF173 and what drives the reduced secondary structure of *psbA* 5'-UTR in high light. Moreover, the model of proposed by Chotewutmontri and Barkan (2020) cannot explain the whole process and experiments are needed to elucidate each step of the regulation of *psbA* translation.

Strikingly, evaluation of ribosome occupancy of *psbA* transcript in plants acclimated to different light intensities revealed already high translational activity at the moderate light intensity in the present study. In agreement with previous studies, this implies nearly maximal translational activity for *psbA* already in acclimated plants without inducing photodamage by increasing light intensity or other stresses (Sundby et al., 1993; Park et al., 1996; Nishiyama and Murata, 2014). Different expression levels of *psbA* may be explained by the different amounts of PSII under the various light intensities. Under low light, the amount of PSII was found low, whereas PSII amount in medium and high-light treated plants was around four times higher (Schöttler and Tóth, 2014). The measured PSII content thus correlated well with the observed translational activity of *psbA* (Figure 3.18, $\sim$ 2.8-fold and three-fold increase between low light and moderate light or high light, respectively). Synthesis of D1 probably follows the possible amount of damaged PSII in the given environment. This highlights the assumption that photodamage of PSII is an inevitable consequence of photosynthesis and happens in a linear manner at rather low light intensities (Anderson and Chow, 2002, and references herein).

Still, photodamage will be enhanced by changes in the system that cannot be buffered by present mechanisms. In the shift from moderate to high light, the change in the system led only to minor photoinhibition which was slightly increased towards the end of the experiment (Figure 3.12A), but which is generally accepted as part of the lag phase in acclimation (Baker, 2008). However, plants adapted to low light and transferred to sudden high light experienced vast photodamage that could not be compensated by *de novo* D1 synthesis. Further, uncoupling of antenna molecules from PSII was observed in the 77K fluorescent emission spectrum of the "2 d" sample by the shift of emission wavelength from 686 nm to 681 nm. In low light, the antenna cross-section around PSII is large to increase the excitation rate of P_{680} and thereby enable the complete reduction of the mobile plastoquinone which prevents low-light photoinhibition (Keren et al., 1995; Ohad et al., 2011; Vass, 2011). However, shifts to high light increases the excitation pressure on PSII that cannot be drained off by the linear electron transport. this is due to the pools of acceptors ($NADP^+$ and ADP) that are exhausted and thereby limiting downstream processes as phloem loading and carbon assimilation (Adams

et al., 2007; Hideg et al., 2008; Rott et al., 2011; Lyu and Lazár, 2017). Resulting acidification of the lumen inactivates the OEC and enhance photoinhibition (Kramer et al., 1999, and references herein). Thus, uncoupling of LHCII from PSII but also PSI is a protection mechanism to reduce excitation of PSs and the linear electron transport. This assumption is supported by the observation of decreased photoinhibition and recovered ETRII at the "2 d" time point (Figure 3.12A).
In summary, light acclimation is an essential process for plants to efficiently use provided light energy by optimized photosynthesis and related processes to reduce photoinhibition. The light acclimation is accompanied by elevated levels of PSII, plastocyanin, and cyt-b_6f and takes several days to weeks to be accomplished (Chow and Anderson, 1987; Kim et al., 1993a). Yet, the transcript levels and translational output of plastid-encoded genes within the first two days do not correlate with these long-term changes in complex content adjustment but seem only to comply with PSII repair. This was further supported by the determination of the ETRII and the complex content in the samples using immuno blots, which showed virtually constant levels (Figure 3.12A and Figure 3.15). Thus, in the observed time frame of two days, no indication of started acclimation at the level of complex assembly or chloroplast gene expression was observed. At these levels, acclimation to high light of young tobacco plants adapted to moderate light seemed to start later than within two days of high-light exposure.

4.5 Outlook

The present work tried to deepen the understanding of chloroplastic translation and protein homeostasis by highly enriched Ribo-seq datasets. Because light is the primary factor driving chloroplast metabolism, samples for enriched datasets were collected in the dark and the light. Cold-induced translational alterations probably biased the analysis of chloroplastic RFPs from isolated chloroplasts. Validation of the obtained data with samples from cold-treated tissue may disentangle some of the observation, e.g., comparable translational activity of *psbA* between dark and light. Nevertheless, the enrichment of cytosolic RFPs for plastid-localized proteins was detected in the chloroplast sample obtained in light. These candidates for co-translational import or mRNA targeting to the chloroplast must be validated by optical methods, and biochemically by import studies and *in vitro* translation systems, or proximity-labeling. The isolation of chloroplasts in the dark, however, needs significant adjustments of the method to reduce contamination by non-chloroplast membranes.
Chloroplastic RFPs by TRAP were enriched to a lower extent by TRAP. Still, the quality of RFPs was higher, and analysis indicated the absence of biases related to the enrichment method. Yet, to investigate specific translational characteristics in the plastid, i.e., scanning of SSU, the method must be extended by a cross-linking step to fix SSU to the mRNA and subsequent enrichment of SSU by TRAP or by density centrifugation. Hence, the present data can be the starting point for further analysis and to challenge other paradigms of chloroplast gene expression, e.g. suggested RNA import (Nicolaï et al., 2007; Gómez and Pallás, 2010).
Further, the contribution of chloroplastic gene expression was analyzed in the process of acclimation to increased light intensity. The analysis of acclimation in young tobacco plants was limited to a two-day time period by divergent growth phenotypes in the latest time point of the experiment between shifted and control plants. Thus, the experiment was performed for two days and only contributions to PSII maintenance and repair were observed. Under the assumption of acclimation processes taking days to weeks, monitoring gene expression in fully expended leaves for a more extended time period may provide information about the cascade in

which nucleus- and plastid-encoded genes function to adjust photosynthetic complex content. Further, (phospho-) proteomics may extent the knowledge of how, when, and which proteins are imported into the chloroplast in the acclimation process and thereby providing information of potential regulators and regulatory cascades that function in photosynthetic complex adjustments.

A Supplemental information

A.1 Program calls for sequencing-data analysis

For better understanding, text behind # are comments to the program call and \\ show a line break which is not present in the program call

Read pre-processing Adapter trimming of reads was performed with `cutadapt` and reads of size 28 nt to 53 nt were filtered. Following UMIs were removed from the 5'- and 3'-end of the read and the information was written into the read name by a customized `python`-script, kindly provided by Michael Ting, Max Planck Institute of Molecular Plant Physiology, Potsdam.

```
cutadapt -a TGGAATTCTCGGGTGCCAAGG \\
--minimum-length 28 --maximum-length 53 \\ # eight nucleotides
     form the UMIs
-o $trimmed.reads.fastq \\
$raw.reads.fastq

UMI_tagger_dual3.py $trimmed.reads.fastq
```

Mapping to the tobacco genomes Trimmed and UMI removed reads were aligned to the tobacco genomes using STAR aligner. Beforehand, the chloroplast reference genome was reduced by the second inverted repeat region and for the nuclear genome an additional rRNA/tRNA-reference was build.

```
#mapping:
STAR --genomeDir annotation/STARreference \\ #reference build once with STAR
--readFilesIn $trimmed.reads.umi.fastq \\
--alignEndsType EndToEnd \\
--outFilterMismatchNoverReadLmax 0.1 \\ # to allow 10 % mismatches per read
--alignIntronMax 1 \\ # to suppress read-splitting for intron-spanning
--outFileNamePrefix $mappedReads --outSAMtype BAM SortedByCoordinate \\
--outFilterScoreMinOverLread 0 --outFilterMatchNminOverLread 0 \\ # to force
     STAR to align short reads
--outReadsUnmapped Fastx # output of unaligned reads in new .fastq file
     for next mapping

#deduplication:
```

```
umi_tools dedup --stdin=$mappedReads.bam --log=$log --output-stats=$stats \\
> $mappedReads.dedup.bam

#selection of uniquely mapped reads
samtools view -h -q 255 $mappedReads.dedup.bam | \\
samtools view -b -o $mappedReads.uniq.bam
samtools index mappedReads.uniq.bam # indexed files are needed by other
     programs, e.g., IGV, plastid
```

Quantification and quality assessment Plastome and mitochondrial genome annotations are missing information about UTRs. However, the program `plastid` needs this information for p-site and phase definition. Joshua Dunn provides a script to add this information (`https://github.com/joshuagryphon/plastid/issues/3`).

```
#quantification of mapped reads
samtools view -h -F 256 $mappedReads.dedup.bam |wc -l # total number of
     mapped reads
samtools view -h -q 255 $mappedReads.dedup.bam |wc -l # number of uniquely
     mapped reads

#read length distribution
samtools view $mappedReads.uniq.bam | awk '{print length($10)}' | \\
sort | uniq -c > $read_length.txt

#phase affiliation
phase_by_size genome_orfs_rois.txt $phase --count_files $mappedReads.uniq.bam \\
--fiveprime --codon_buffer 5 --min_length 20 --max_length 45

#quantification of gene coverage
bedtools coverage -a $annotationFile -b $mappedReads.uniq.bam -s \\
> $genome.counts # for multiple .bam files "bedtools multicov" can be used
```

The total number of matching reads was counted and transformed to the **R**eads **P**er **K**ilo base per **M**illion reads (RPKM) value and further to the **C**overage **P**er **M**illion (CPM) value (eq. (A.2)).

$$\mathrm{RPKM}_g = \frac{\#\text{ of reads mapped to gene region} * 10^9}{\#\text{ of nucleotides in mappable gene region} * \text{total }\#\text{ of reads}} \tag{A.1}$$

$$\mathrm{CPM}_g = \frac{\mathrm{RPKM}_g * 10^6}{\sum_g \mathrm{RPKM}_g} \tag{A.2}$$

p-site definition Corresponding p-sites of the reads were determined with the python-based software `plastid` (Dunn and Weissman, 2016) and reads were reduced to the first p-site base by a customized R script for the representation of gene coverage (figure 3.10).

```
# p-site call
psite chloro_orfs_rois.txt $psite.offset --min_length 20 --max_length 45 \\
--require_upstream --count_files $mappedReads.uniq.bam --aggregate

# reduction of the mapped reads to p-site position by custom R-function
psiteReduction <- function(bedFile,pOffset) {
     bedFile <- data.frame(read.table(bedFile,header = F,sep = " ", \\
          stringsAsFactors = F))
     bedFile$V7 <- factor(bedFile$V7) # read length
     bedFilePos <- bedFile[which(bedFile$V6 == "+"),]
     bedFileNeg <- bedFile[which(bedFile$V6 == "-"),]
     pOffset <- read.table(pOffset,header = T, \\
          comment.char = "#")[c(1:26),]
     pOffset[,1] <- factor(pOffset[,1]) # read length
     pOffset[,2] <- as.numeric(pOffset[,2]) # p-offset
     for(i in levels(bedFilePos$V7)){
          j <- pOffset[which(pOffset[,1]==i),2]
          bedFilePos$V2[which(bedFilePos$V7==i)] \\
             <- bedFilePos$V2[which(bedFilePos$V7==i)] + j
          bedFilePos$V3[which(bedFilePos$V7==i)] \\
             <- bedFilePos$V2[which(bedFilePos$V7==i)] + 1
     }
     for(i in levels(bedFileNeg$V7)){
          j <- pOffset[which(pOffset[,1]==i),2]
          bedFileNeg$V3[which(bedFileNeg$V7==i)] \\
             <- bedFileNeg$V3[which(bedFileNeg$V7==i)] - j
          bedFileNeg$V2[which(bedFileNeg$V7==i)] \\
             <- bedFileNeg$V3[which(bedFileNeg$V7==i)] - 1
     }
     bedFile <- rbind(bedFilePos,bedFileNeg)
     bedFile <- bedFile[order(bedFile$V2),]
     return(bedFile)
}

# base-wise coverage of the genes
bedtools coverage -a $annotationFile -b $bedFile.bed -s -d\\
> $genome.baseWise.counts # bedFile.bed is the product of psiteReduction
```

A.2 Supplemental figures

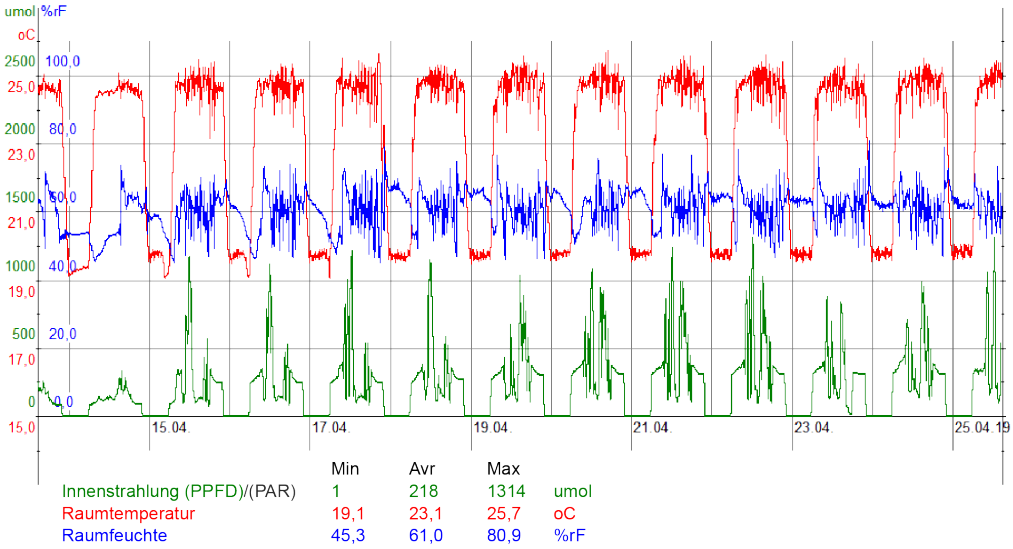

Figure S1: Climate parameters in green house for tobacco growth. The record of climate parameters for the green house cabin in a eleven days interval from April, 14th to April, 25th 2019 shows exemplary the variation of irradiation, temperature, and relative humidity plants experienced. Irradiation, temperature, and humidity are shown in green, red, and blue, respectively. Tobacco seedlings grown under those conditions were used for chloroplast isolation in the dark.

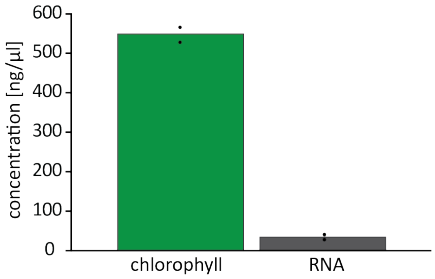

Figure S2: Relationship of chlorophyll content and RNA concentration in isolated chloroplasts. Chlorophyll and RNA concentration were determined for 100 μl aliquots of isolated chloroplasts (two biological replicates, black dots).

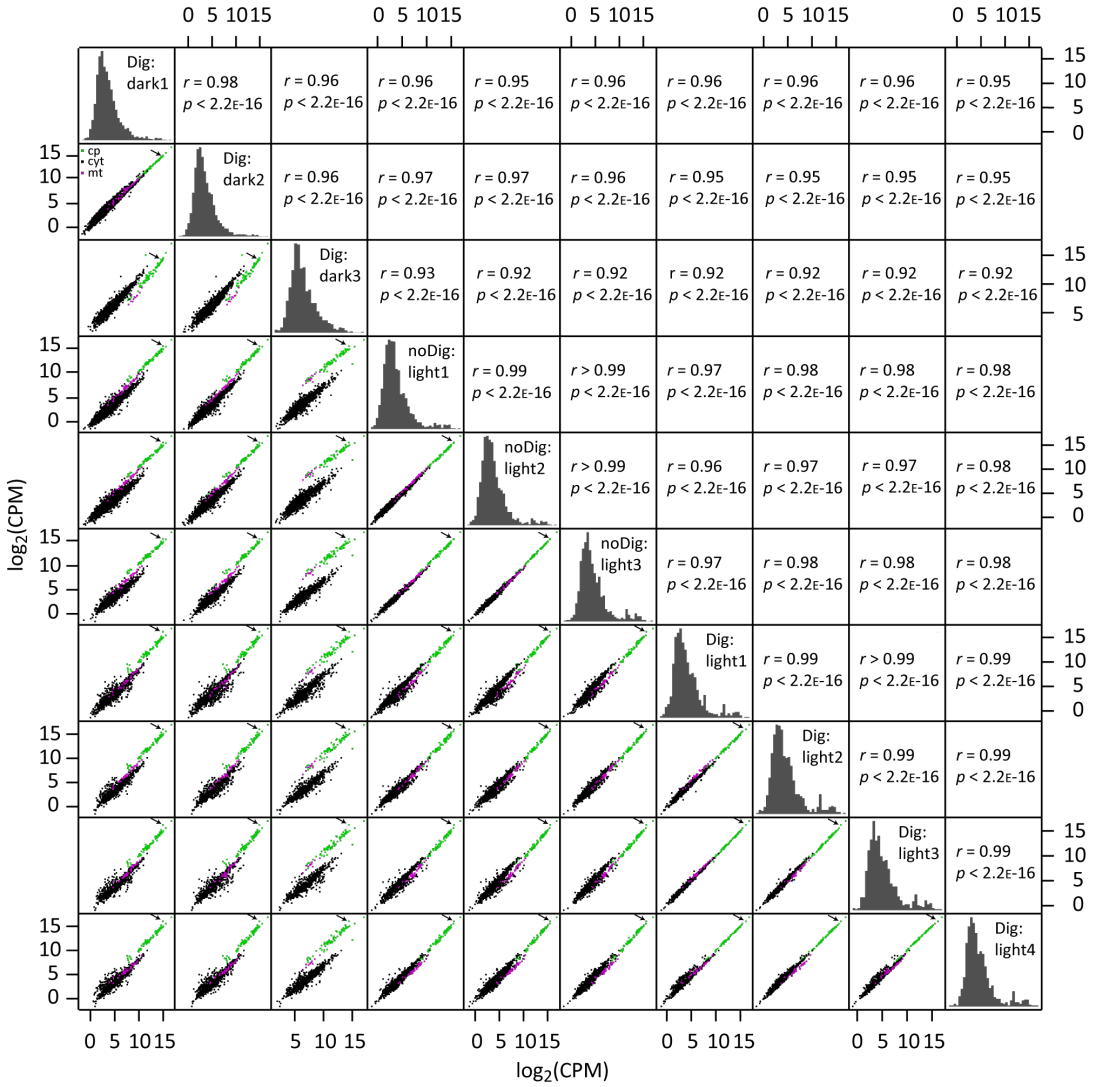

Figure S3: Correlation analysis of CI samples display data agreement. Correlation analysis of replicates from CI samples displayed as matrix. Histograms of CPM values are shown in the diagonal. Above the diagonal, the Pearson correlation coefficient and the significance level of the regression analysis for the pair of replicates are marked. Below the diagonal, scatter plots for the pair of replicates are shown. The x-axis shows the CPM value for the replicate represented in the same column and the y-axis displays the CPM value for the replicate represented in the same row. Plastidial, mitochondrial, and nuclear genes are colored green, magenta, and black, respectively, in the scatter plots. *psbA* is marked by an arrow.

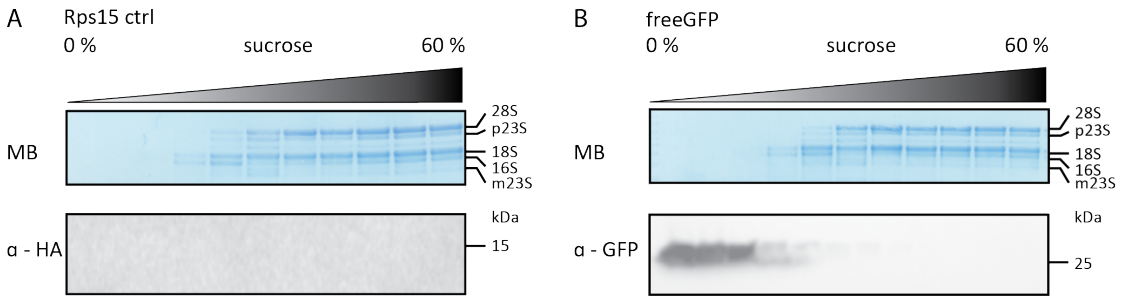

Figure S4: Polysome analysis of control lines did not show signals in polysome fractions. (A) RNA blot and immuno blot analysis of fractions from Rps15ctrl polysome analysis show chloroplast rRNA in high molecular weight fractions but no signal in immuno detection. (B) RNA blot and immuno blot analysis of fractions from freeGFP polysome analysis show chloroplast rRNA in high molecular weight fractions and immuno detection for GFP in soluble and low molecular weight fractions.

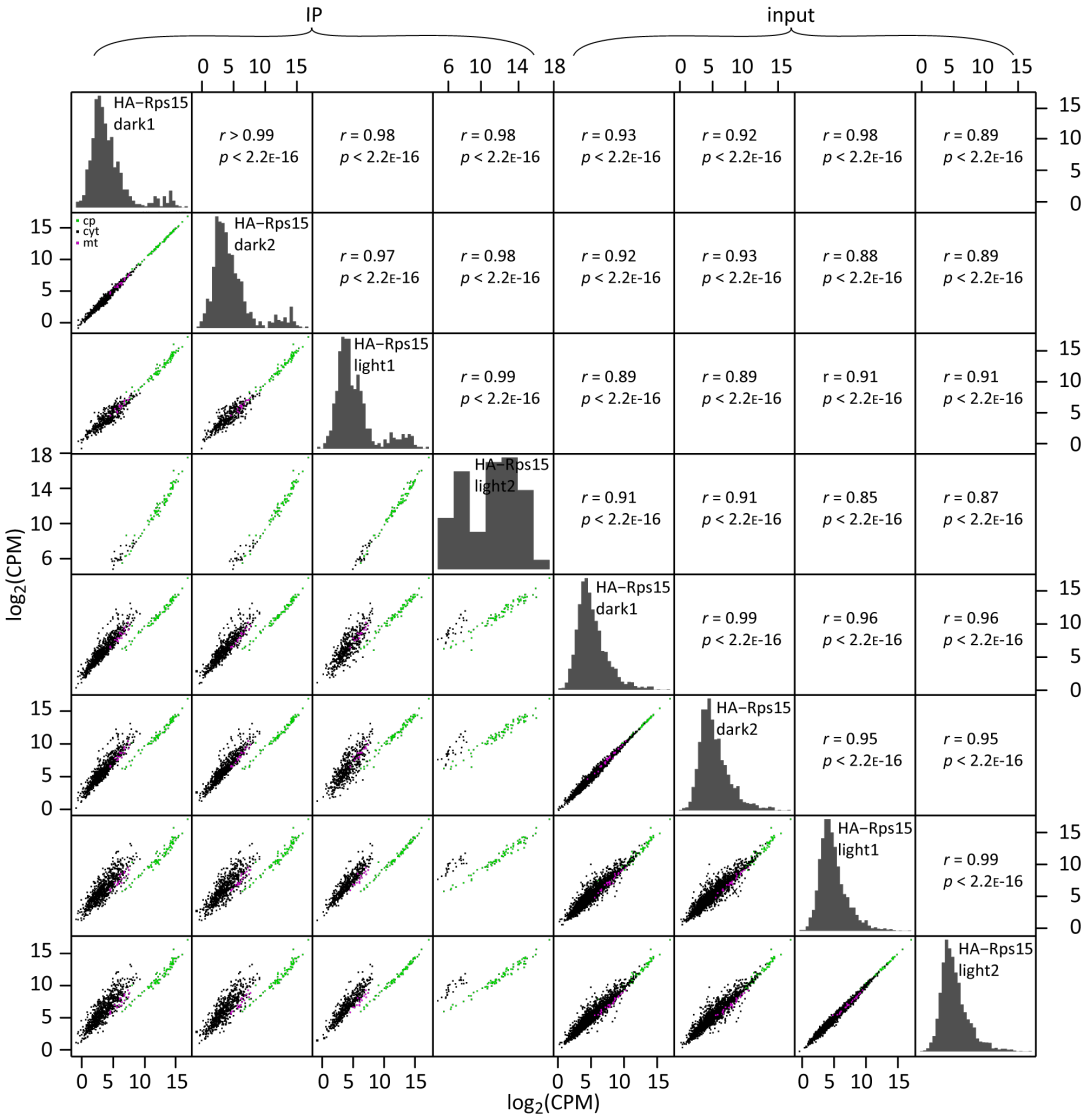

Figure S5: Correlation analysis of biological replicates from HA-TRAP experiment. Correlation analysis of all replicates from HA-TRAP experiment displayed as matrix. Histograms of CPM values are shown in the diagonal. Above the diagonal, Pearson correlation coefficient and the significance level of the regression analysis for the pair of replicates are marked. Below the diagonal, scatter plots for the pair of replicates are shown. The x-axis shows the CPM value for the replicate represented in the same column and the y-axis displays the CPM value for the replicate represented in the same row. Plastidial, mitochondrial, and nuclear genes are colored green, magenta, and black, respectively, in the scatter plots.

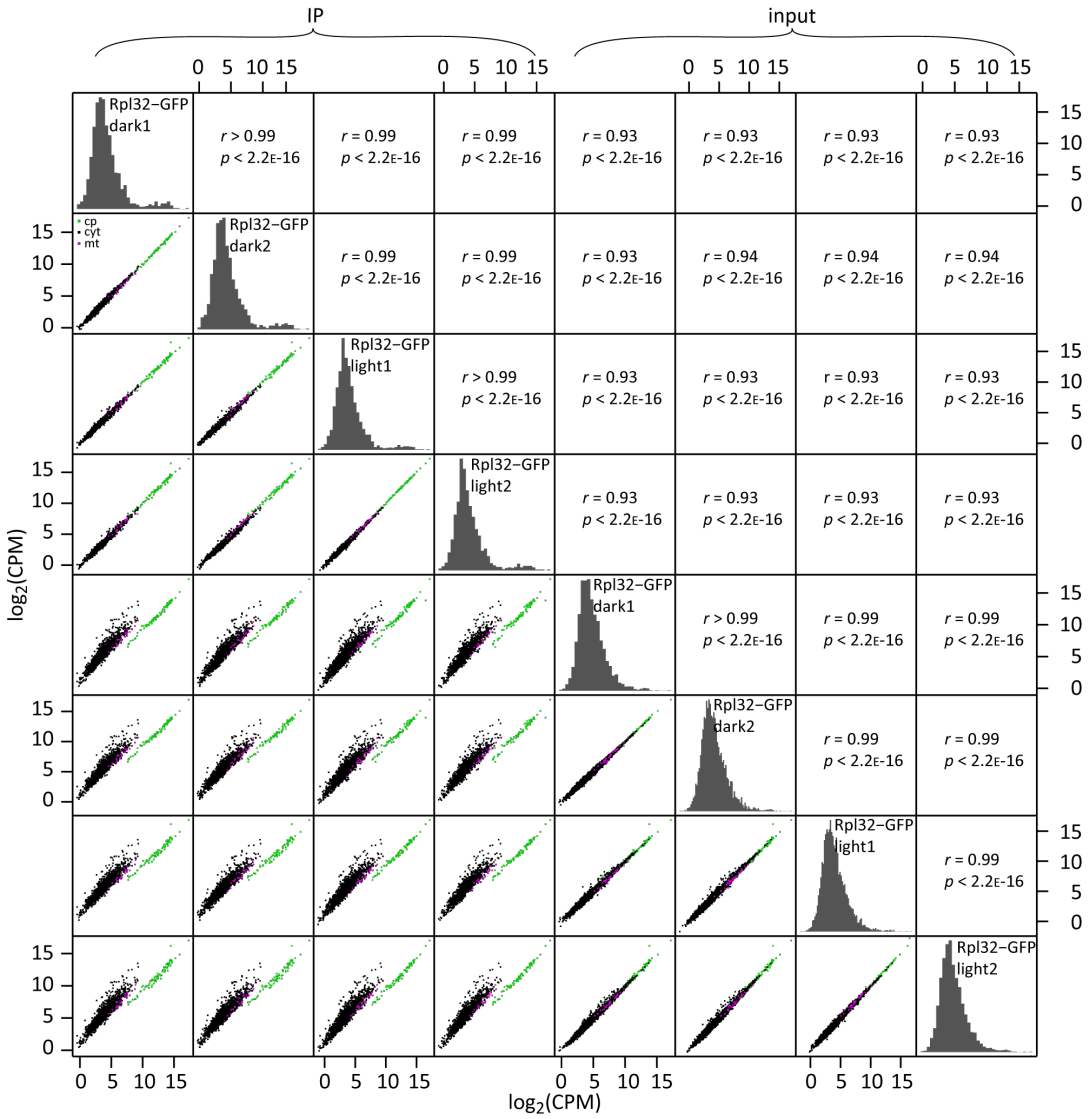

Figure S6: Correlation analysis of biological replicates from GFP-TRAP experiment. Correlation analysis of all replicates from GFP-TRAP experiment displayed as matrix. Histograms of CPM values are shown in the diagonal. Above the diagonal, Pearson correlation coefficient and the significance level of the regression analysis for the pair of replicates are marked. Below the diagonal, scatter plots for the pair of replicates are shown. The x-axis shows the CPM value for the replicate represented in the same column and the y-axis displays the CPM value for the replicate represented in the same row. Plastidial, mitochondrial, and nuclear genes are colored green, magenta, and black, respectively, in the scatter plots.

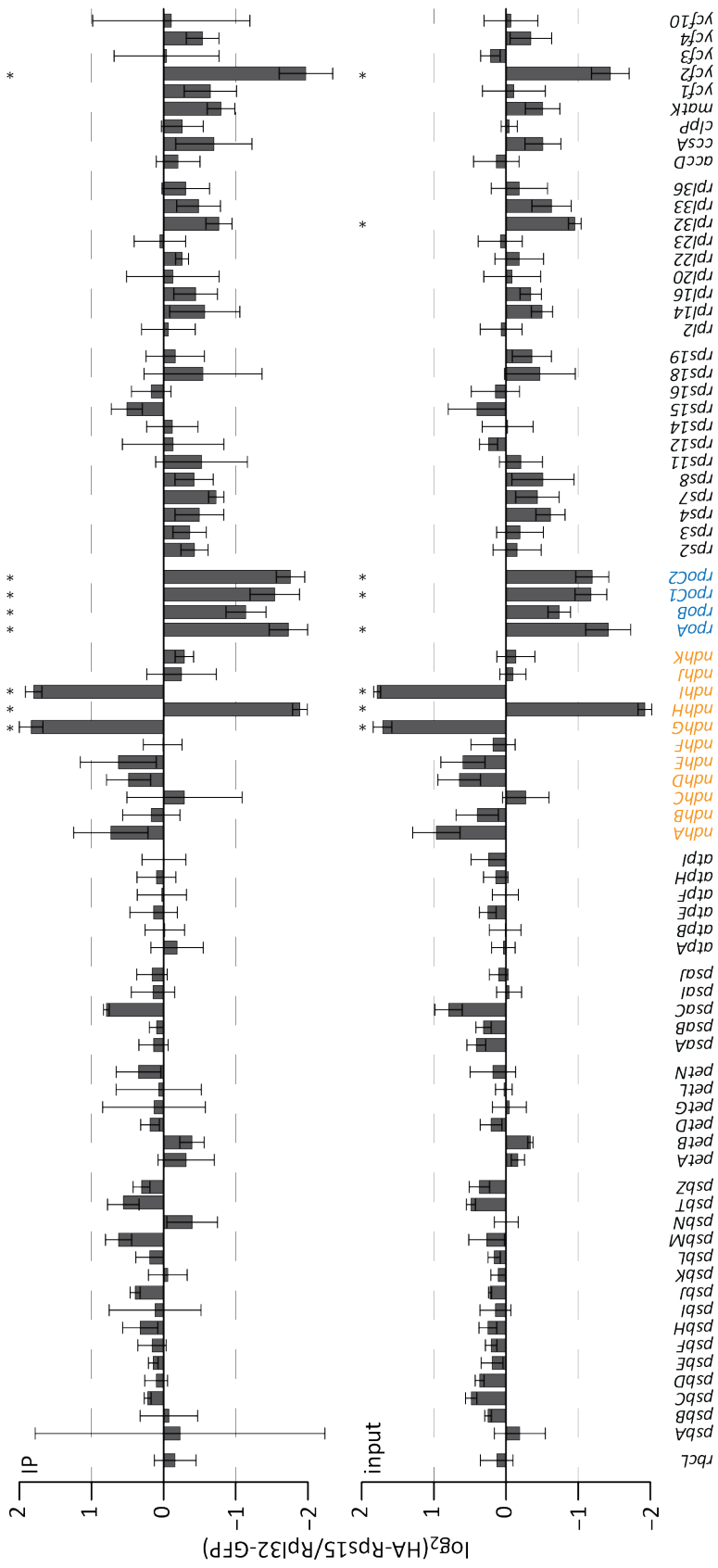

Figure S7: Differential expression of plastid-encoded genes in HA-Rps15 and Rpl32-GFP. Bar plot of $\log_2$-fold change between HA-Rps15 and Rpl32-GFP of plastid-encoded genes in the IP samples (upper panel) and input samples (lower panel). Values represent the average of four biological replicates. Error bars depict the standard deviation. Genes marked with an asterisk (*) were detected significantly enriched by the differential expression analysis in one of the two samples by, at least, twofold (Suppl. Table S2). The threshold of twofold is indicated by the dashed lines. Genes of NDH are highlighted in orange and genes of PEP are highlighted blue.

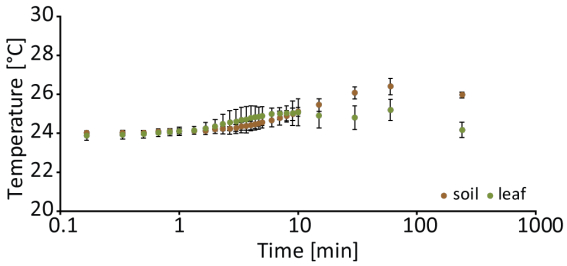

Figure S8: Leaf and soil temperature increased marginally in high light. Tobacco plants were transferred to high light and the leaf and soil temperature were recorded for five hours. Values are mean values of five biological replicates and the error bars depict the SD.

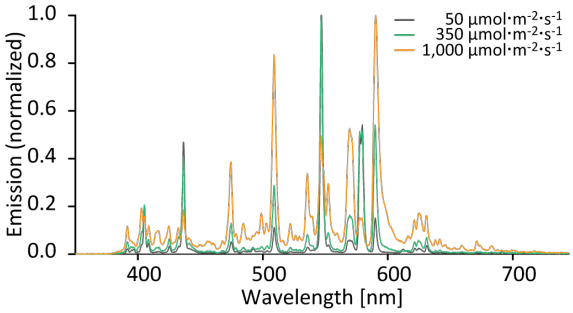

Figure S9: Light spectra of metal-halide bulbs at light intensities used in light shift experiments peaked at same wavelengths. Emission spectra were recorded at 50, 350, and 1,000 μmol·m^{-2}·s^{-1} and normalized to maximal emission. Spectra represent the averages of three independent measurements.

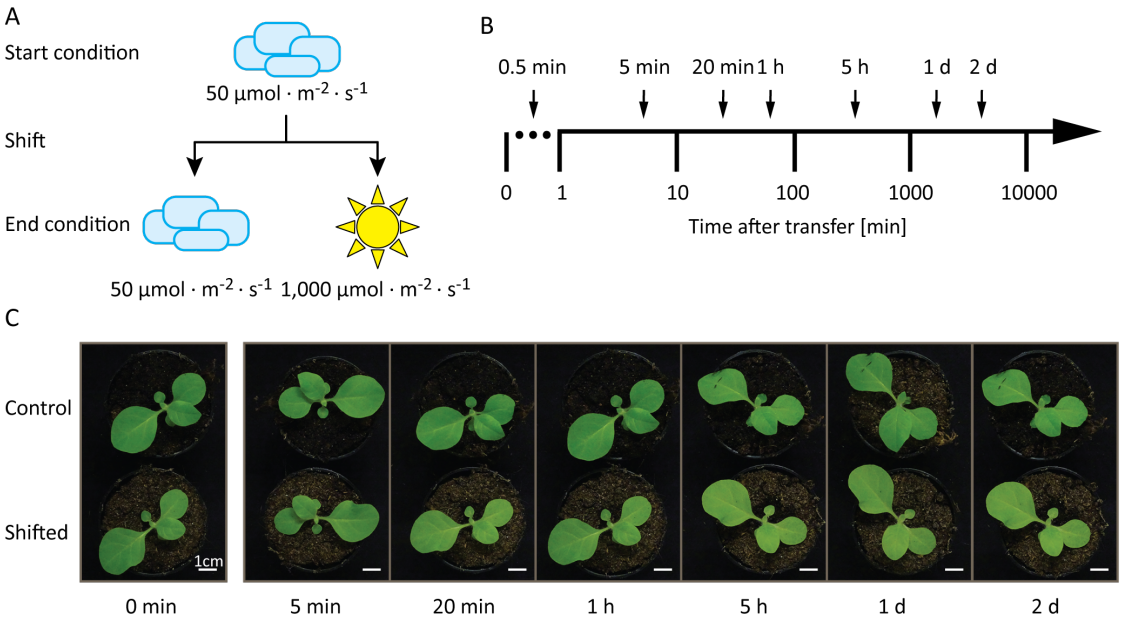

Figure S10: Experimental condition and phenotypes of samples from low-light to high-light shift. Description as in figure 3.11.

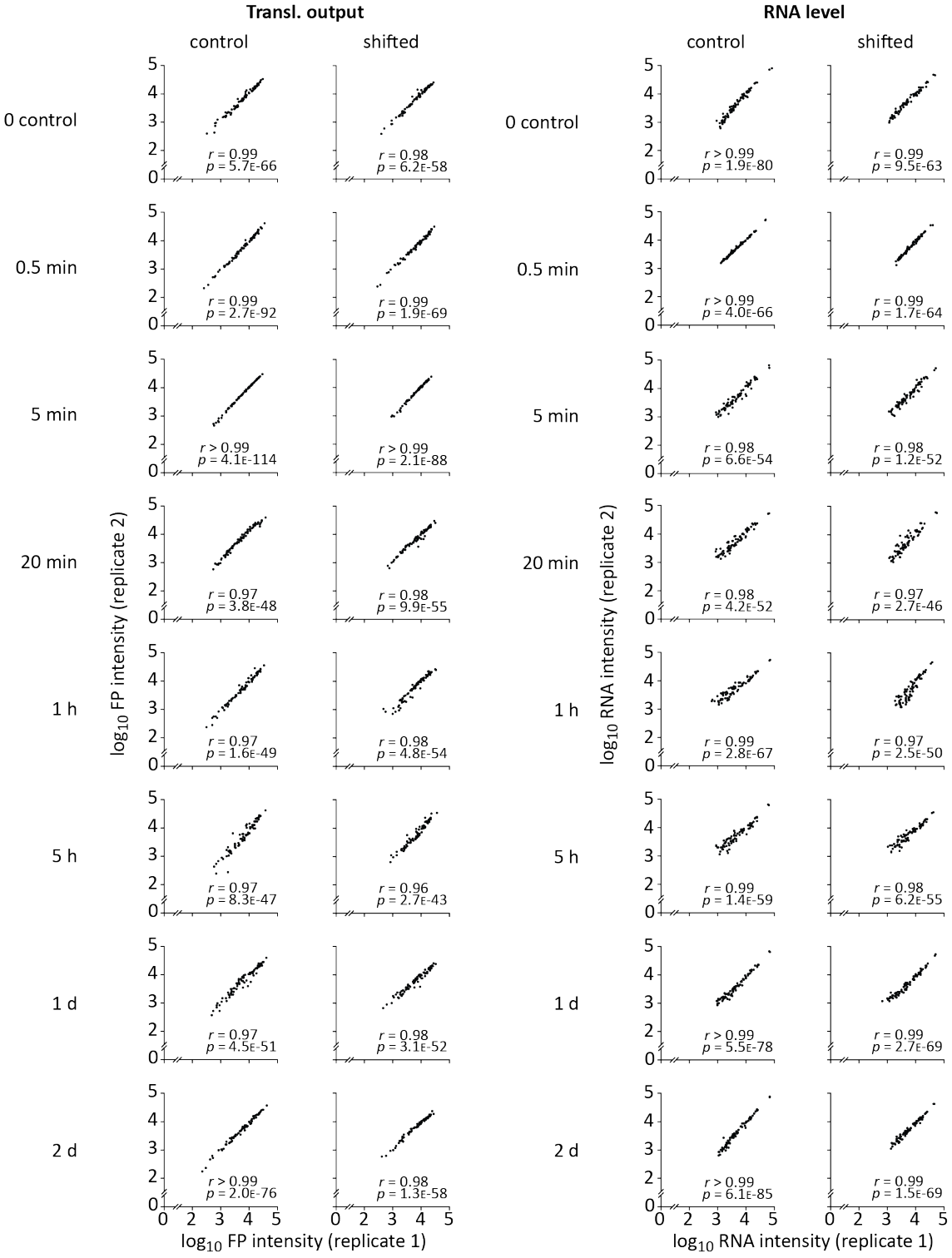

Figure S11: Scatter plots of translational output (Transl. output) and transcript level (RNA level) reproducibility for shifted and control plants for all selected time points. Biological replicate 1 and replicate 2 were representatives of total three replicates.

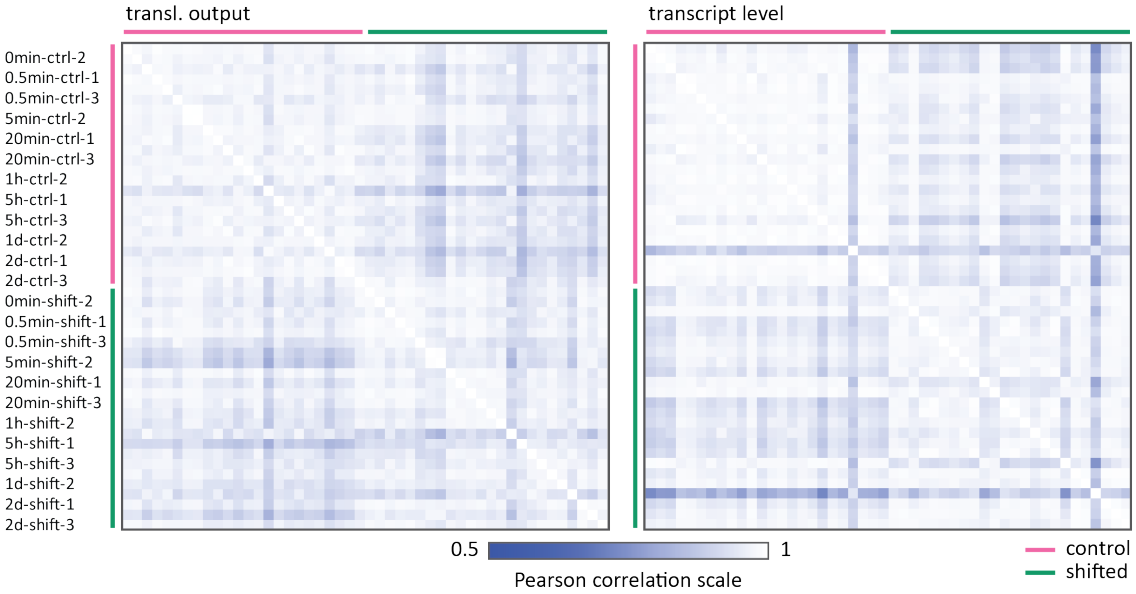

Figure S12: Heatmap of correlation values for all replicates of the light-shift experiment for translational output (left) and transcript level (right). Replicates are sorted first by "control" (magenta) or "shifted" (green) and second by the time point of harvest as indicated on the left side. Correlation scale is from 0.5 to 1 as indicated by the legend on the bottom.

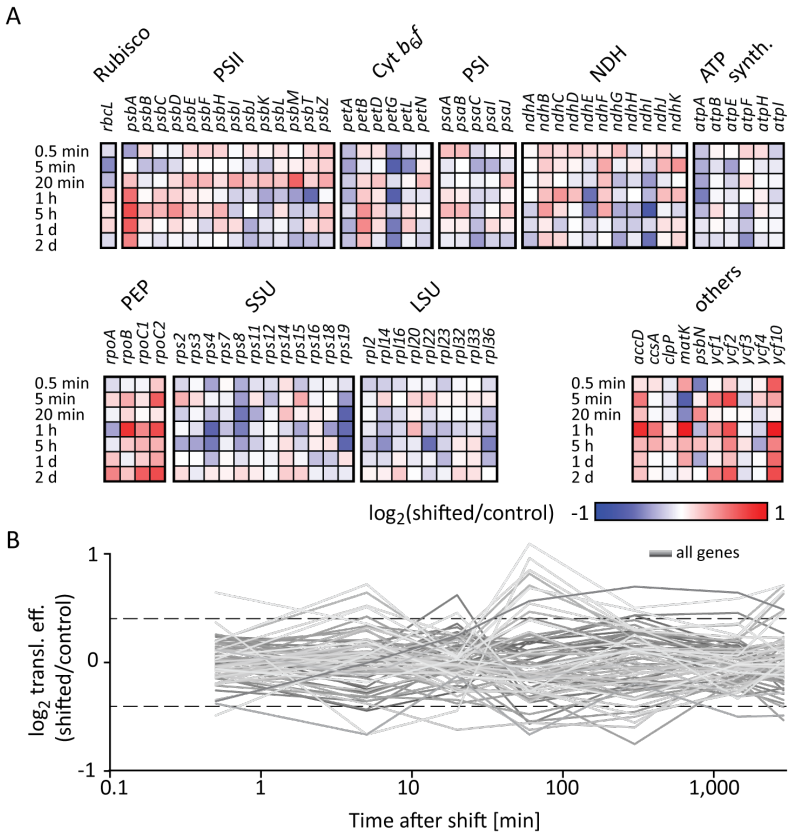

Figure S13: Translational efficiency (transl. eff.) differences between shifted and control plants. Transl. eff. was calculated as translational output normalized to the transcript level. (A) Heatmap of $\log_2$-fold changes of protein-coding genes between shifted and control samples for seven timepoints (represented in the rows). Genes are displayed in the columns and arranged by the complex they belong to. Increased or decreased transl. eff. are colored in red and blue, respectively, as indicated by the scale on the bottom. (B) Line plot representation of $\log_2$-fold changes in transl. eff. between shifted and control samples. The x-axis shows the time in $\log_{10}$-scale. Dashed horizontal lines indicate the $\log_2$-thresholds of -0.4 and 0.4. Transl. eff. is mainly defined by translational output (compare figure 3.14).

A.3 Supplemental tables

Table S1: Enriched nucleus-encoded genes in the Dig:light and Dig:dark samples. Gene identities of enriched nucleus-encoded genes in the Dig:light and Dig:dark sample, respectively, with the length of the gene product in amino acids [AA]. Additionally, the name of the *A. thaliana* orthologue from the TAIR database (Berardini et al., 2015) is given, as well as cellular localization as recorded by UniProt (The UniProt Consortium, 2019). The last two columns give the parameters $\log_2$-fold change ($\log_2$(FC)) and adjusted *p*-value (*p*.adj) from the differential enrichment analysis using DESeq2. Gene products localized in the chloroplast are highlighted in **bold**. Gene without orthologue in *A. thaliana* are given with the species name where an orthologue was found.

gene name	length [AA]	TAIR orthologue	localization	$\log_2$(FC)	*p*.adj
light					
Nitab4.5_0000178g0330.1	387	MAN7	ex. cell.	-1.286	8.76E-03
Nitab4.5_0000200g0190.1	586	GT4 (*F. ananassa*)	membrane	-1.115	1.82E-12
Nitab4.5_0000214g0020.1	510	MIPS3	cytoplasm	-1.882	1.09E-08
Nitab4.5_0000258g0330.1	185	ATPD	**plastid**	-1.112	1.01E-07
Nitab4.5_0000451g0050.1	608	BAM1	**plastid**	-1.404	4.80E-11
Nitab4.5_0000582g0020.1	175	TRXF1	**plastid**	-1.219	1.01E-04
Nitab4.5_0000592g0290.1	330	LHCB1.3	**plastid**	-1.180	2.73E-02
Nitab4.5_0000592g0370.1	284	LHCB1.3	**plastid**	-1.180	2.73E-02
Nitab4.5_0000611g0120.1	147	PSAG	**plastid**	-1.198	5.97E-20
Nitab4.5_0000715g0160.1	517	MIPS2	cytoplasm	-2.646	1.85E-12
Nitab4.5_0000937g0110.1	86	PSAO	**plastid**	-1.184	4.38E-06
Nitab4.5_0000980g0290.1	78	`unknown`		-1.400	3.57E-05
Nitab4.5_0001297g0050.1	270	PIP2A	pl. mem.	-1.948	8.00E-12
Nitab4.5_0001404g0050.1	230	REF/SRPP-like	ER; vacuole; lipid droplet	-1.191	9.32E-03
Nitab4.5_0001448g0030.1	231	LHCA1	**plastid**	-1.060	3.02E-02
Nitab4.5_0001504g0010.1	137	Bet v I allergen (*B. pendula*)	cytoplasm	-1.149	9.00E-04
Nitab4.5_0001617g0070.1	475	MAN7	ex. cell.	-1.459	2.73E-03
Nitab4.5_0001758g0020.1	491	MIPS3	cytoplasm	-1.591	7.66E-10
Nitab4.5_0002589g0060.1	529	SIG5	**plastid**	-1.084	4.86E-03
Nitab4.5_0003068g0060.1	90	PSAO	**plastid**	-1.319	3.70E-02
Nitab4.5_0003368g0030.1	130	PSAK	**plastid**	-1.189	6.24E-04
Nitab4.5_0004599g0080.1	161	EXP14	cell wall; ex. cell.	-1.203	1.76E-05
Nitab4.5_0004821g0050.1	333	FIB	**plastid**	-1.234	7.93E-13
Nitab4.5_0005511g0010.1	265	LHCB2.1	**plastid**	-1.033	3.40E-04
Nitab4.5_0005597g0020.1	460	MIPS3	cytoplasm	-3.799	3.01E-04
Nitab4.5_0006644g0080.1	254	PSBP1	**plastid**	-1.021	1.17E-03
Nitab4.5_0012890g0020.1	246	EXP8	cell wall; ex. cell.	-1.008	2.18E-02
dark					
Nitab4.5_0000033g0360.1	173	UPF0497 membrane protein 17 (*S. tuberosum*)	membrane	-1,386	4,31E-04
Nitab4.5_0000143g0160.1	491	DCP2	cytoplasm; P-body	-1,249	5,54E-03
Nitab4.5_0000335g0090.1	439	CAX3	vac. mem.	-1,010	3,25E-02
Nitab4.5_0000476g0110.1	282	LHCA1	**plastid**	-1,185	4,57E-02
Nitab4.5_0000521g0100.1	331	XTH28	cell wall; apoplast	-1,524	4,37E-02

Enriched nucleus-encoded genes continue ...

gene name	length [AA]	TAIR orthologue	localization	log_2(FC)	*p*.adj
Nitab4.5_0000715g0160.1	517	MIPS2	cytoplasm	-1,483	3,60E-03
Nitab4.5_0000980g0290.1	78	`unknown`		-1,594	3,82E-02
Nitab4.5_0002210g0070.1	267	LHCB1.3	**plastid**	-1,614	3,85E-02
Nitab4.5_0002229g0060.1	267	LHCB1.3	**plastid**	-1,538	3,84E-03
Nitab4.5_0002342g0170.1	267	LHCB1.3	**plastid**	-1,150	1,39E-02
Nitab4.5_0002763g0030.1	296	PIP2-7	pl. mem.	-1,369	3,62E-02
Nitab4.5_0002771g0030.1	173	UPF0497 membrane protein 17 (*S. tuberosum*)	membrane	-1,244	1,07E-02
Nitab4.5_0003155g0010.1	251	TIP1-1	vac. mem.	-1,158	3,84E-03
Nitab4.5_0003328g0020.1	416	FLA1	pl. mem.; apoplast	-1,060	3,82E-02
Nitab4.5_0003449g0030.1	588	NPF6.4	membrane	-1,390	1,45E-02
Nitab4.5_0003828g0030.1	353	EXL5	ex. cell.	-1,344	4,48E-03
Nitab4.5_0003914g0040.1	284	PIP2-7	pl. mem.	-1,109	2,41E-02
Nitab4.5_0006973g0030.1	247	FLA6	pl. mem.	-1,720	2,41E-02
Nitab4.5_0007597g0010.1	292	PIP1E	pl. mem.	-1,611	5,54E-03
Nitab4.5_0009011g0010.1	416	FLA1	pl. mem.; apoplast	-1,115	2,41E-02

Abbr.: ER - endoplasmic reticulum; ex. cell. - extracellular; pl. mem. - plasma membrane, vac. mem. - vacuole membrane

F. ananassa - *Fragaria ananassa* (strawberry); *S. tuberosum* - *Solanum tuberosum* (potato)

B. pendula - *Betula pendula* (silver birch)

Table S2: Results from differential enrichment analysis comparing coverage of plastidial genes between samples from Rpl32-GFP and HA-Rps15. Absolute $\log_2$-fold changes ($|\log_2(FC)| > 1$ are highlighted in **bold** and adjusted p-values ($p.adj$) < 0.05 are highlighted in ***bold-italic***. Values were obtained by differential expression analysis with DESeq2.

	IP		input			IP		input	
gene	$\log_2$(FC)	p.adj	$\log_2$(FC)	p.adj	gene	$\log_2$(FC)	p.adj	$\log_2$(FC)	p.adj
rbcL	0,576	***2,33E-06***	0,3	***1,20E-02***	*rps2*	0,133	3,13E-01	0,017	8,61E-01
psbA	0,085	2,77E-01	0,039	5,87E-01	*rps3*	0,074	6,51E-01	0,095	3,56E-01
psbB	0,184	***2,05E-04***	-0,075	1,59E-01	*rps4*	0,417	***3,99E-04***	0,648	***3,75E-13***
psbC	-0,167	***1,44E-02***	-0,411	***2,20E-16***	*rps7*	0,91	***1,77E-21***	0,824	***5,38E-24***
psbD	-0,022	8,06E-01	-0,251	***1,08E-04***	*rps8*	0,257	***1,92E-02***	0,286	***2,27E-03***
psbE	0,029	8,06E-01	0,074	2,16E-01	*rps11*	0,176	1,56E-01	0,098	3,29E-01
psbF	-0,15	1,36E-01	-0,127	8,95E-02	*rps12*	-0,142	2,13E-01	-0,211	***8,39E-03***
psbH	-0,266	***1,44E-02***	-0,214	***2,37E-03***	*rps14*	-0,013	9,21E-01	-0,14	9,81E-02
psbI	-0,219	***4,60E-02***	-0,159	7,40E-02	*rps15*	-0,858	***6,11E-07***	-0,6	***2,56E-12***
psbJ	-0,263	***1,50E-03***	-0,08	3,18E-01	*rps16*	-0,458	***5,16E-04***	-0,278	***1,51E-02***
psbK	-0,019	8,73E-01	0,025	7,50E-01	*rps18*	0,152	3,30E-01	0,211	5,21E-02
psbL	-0,22	6,79E-02	-0,077	4,00E-01	*rps19*	0,523	***2,42E-03***	0,725	***2,46E-08***
psbM	-0,605	***4,18E-03***	-0,23	1,26E-01	*rpl2*	-0,125	3,17E-01	-0,168	***2,03E-02***
psbT	-0,344	1,04E-01	-0,297	***3,00E-04***	*rpl14*	0,487	***1,16E-05***	0,513	***1,46E-08***
psbZ	-0,295	***1,08E-03***	-0,337	***3,67E-06***	*rpl16*	0,31	***1,04E-02***	0,379	***4,80E-05***
petA	0,327	***2,79E-04***	0,343	***1,22E-08***	*rpl20*	-0,168	2,49E-01	-0,094	3,18E-01
petB	0,412	***4,54E-09***	0,456	***4,21E-15***	*rpl22*	0,022	8,84E-01	0,054	5,38E-01
petD	-0,198	***5,29E-03***	-0,19	***4,61E-03***	*rpl23*	-0,31	***2,08E-02***	-0,185	9,22E-02
petG	-0,041	8,87E-01	0,149	2,00E-01	*rpl32*	0,787	***7,52E-05***	**1,021**	***1,56E-17***
petL	-0,134	6,56E-01	0,079	4,61E-01	*rpl33*	0,409	9,71E-02	0,57	***3,54E-07***
petN	-0,302	3,12E-01	-0,294	***3,70E-03***	*rpl36*	-0,03	8,51E-01	-0,003	9,75E-01
psaA	-0,152	***4,51E-03***	-0,383	***3,53E-12***	*accD*	-0,05	8,06E-01	-0,256	***2,55E-02***
psaB	-0,097	1,37E-01	-0,266	***7,82E-08***	*ccsA*	0,58	***1,40E-03***	0,44	***1,46E-04***
psaC	-0,515	***8,69E-05***	-0,5	***2,29E-16***	*clpP*	0,292	***1,04E-02***	0,213	***1,12E-02***
psaI	-0,313	9,59E-02	0,072	4,95E-01	*matK*	0,681	***6,71E-04***	0,531	***1,46E-04***
psaJ	0,088	7,21E-01	0,121	1,26E-01	*psbN*	0,375	1,04E-01	0,195	8,95E-02
ndhA	-0,518	***5,87E-05***	-0,543	***1,67E-16***	*ycf1*	0,202	3,12E-01	-0,117	2,43E-01
ndhB	-0,456	***4,22E-04***	-0,509	***4,91E-12***	*ycf2*	**1,708**	***4,82E-22***	**1,366**	***2,26E-58***
ndhC	0,15	4,34E-01	0,186	2,00E-01	*ycf3*	-0,158	2,26E-01	-0,157	1,26E-01
ndhD	-0,663	***3,05E-08***	-0,75	***2,54E-29***	*ycf4*	0,342	***1,05E-02***	0,263	***2,47E-02***
ndhE	-0,764	***1,93E-07***	-0,703	***2,01E-18***	*ycf10*	0,439	2,39E-01	0,453	8,95E-02
ndhF	-0,216	1,11E-01	-0,304	***5,24E-05***	*orf105*	NA	NA	NA	NA
ndhG	**-1,835**	***7,23E-35***	**-1,554**	***4,80E-56***	*orf74*	0,014	9,87E-01	0,171	5,01E-01
ndhH	**2,035**	***2,89E-39***	**1,991**	***3,51E-93***	*orf70A*	NA	NA	NA	NA
ndhI	**-1,689**	***3,12E-36***	**-1,633**	***2,17E-96***	*orf99*	NA	NA	NA	NA
ndhJ	0,274	1,11E-01	0,298	***1,83E-02***	*orf103*	NA	NA	NA	NA
ndhK	0,07	7,21E-01	0,082	4,67E-01	*orf79*	NA	NA	NA	NA
atpA	0,089	2,65E-01	-0,04	4,90E-01	*orf131*	NA	NA	NA	NA
atpB	-0,09	6,39E-02	-0,186	***1,08E-04***	*orf70B*	NA	NA	NA	NA
atpE	-0,123	1,12E-01	-0,199	***3,30E-03***	*orf75*	**1,735**	3,13E-01	-0,233	5,33E-01
atpF	-0,154	2,69E-01	-0,023	7,01E-01	*orf350*	NA	NA	NA	NA
atpH	0,04	8,06E-01	-0,147	***1,49E-02***					
atpI	-0,202	***2,24E-02***	-0,312	***2,96E-08***					
rpoA	**1,462**	***1,62E-25***	**1,319**	***1,69E-47***					
rpoB	**1,012**	***2,54E-07***	0,818	***9,00E-09***					
rpoC1	**1,246**	***3,99E-12***	**1,213**	***5,54E-20***					
rpoC2	**1,465**	***1,77E-21***	**1,167**	***7,92E-26***					

Table S3: Results from differential enrichment analysis comparing 5'-UTR coverage of plastidial genes between samples from Rpl32-GFP and HA-Rps15. UTRs are defined as 100 nt upstream and 30 nt downstream of the start codon. $\log_2$-fold changes ($\log_2$(FC)) < -1 were highlighted in **bold** and adjusted *p*-values (*p*.adj) < 0.05 are highlighted in ***bold-italic***. Values were obtained by differential expression analysis with DESeq2.

	IP		input			IP		input	
gene	$\log_2$(FC)	*p*.adj	$\log_2$(FC)	*p*.adj	gene	$\log_2$(FC)	*p*.adj	$\log_2$(FC)	*p*.adj
rbcL	0.229	2.94E-01	0.020	9.36E-01	*rps2*	0.448	6.93E-02	0.365	1.29E-01
psbA	0.360	***2.42E-02***	0.324	***3.50E-02***	*rps3*	0.016	9.44E-01	-0.016	9.36E-01
psbB	-0.718	***1.32E-03***	-0.610	***1.60E-04***	*rps4*	0.850	***1.18E-04***	0.617	***1.70E-02***
psbC	-0.239	2.12E-01	-0.417	***4.13E-03***	*rps7*	0.871	***2.58E-05***	0.393	***2.56E-02***
psbD	-0.455	***2.57E-02***	-0.236	1.18E-01	*rps8*	0.928	***2.58E-05***	1.111	***1.61E-07***
psbE	0.220	4.63E-01	-0.109	6.22E-01	*rps11*	0.523	***3.18E-02***	0.170	4.16E-01
psbF	-0.324	***3.69E-02***	-0.394	***6.77E-03***	*rps12*	0.386	1.38E-01	0.068	7.80E-01
psbH	-0.155	4.33E-01	-0.318	6.85E-02	*rps14*	-0.382	6.01E-02	-0.342	***3.61E-02***
psbI	-0.808	***1.32E-03***	-0.195	4.74E-01	*rps15*	0.237	4.28E-01	0.164	4.74E-01
psbJ	-0.388	***3.59E-02***	-0.384	***5.35E-03***	*rps16*	-0.062	8.37E-01	-0.098	6.49E-01
psbK	-0.220	2.58E-01	-0.390	***2.70E-02***	*rps18*	0.575	***3.18E-02***	0.347	1.64E-01
psbL	-0.363	***9.76E-03***	-0.562	***1.66E-05***	*rps19*	-0.036	8.78E-01	-0.047	7.86E-01
psbM	-0.393	***3.95E-02***	0.006	9.66E-01	*rpl2*	-0.235	2.61E-01	-0.051	7.88E-01
psbT	**-1.084**	***2.11E-05***	-0.809	***1.70E-06***	*rpl14*	0.593	***2.44E-03***	0.695	***1.11E-03***
psbZ	-0.075	6.95E-01	-0.219	9.71E-02	*rpl16*	0.290	8.07E-01	0.517	6.83E-01
petA	0.529	***1.16E-03***	0.572	***1.68E-04***	*rpl20*	0.094	6.61E-01	-0.078	6.83E-01
petB	-0.372	4.00E-01	-0.377	2.35E-01	*rpl22*	0.112	6.51E-01	0.231	1.64E-01
petD	-0.105	7.77E-01	-0.252	2.11E-01	*rpl23*	-0.032	9.28E-01	0.118	6.22E-01
petG	0.149	5.79E-01	0.084	7.02E-01	*rpl32*	0.791	***2.95E-04***	0.971	***2.24E-06***
petL	-0.001	9.96E-01	-0.281	6.73E-02	*rpl33*	0.792	***3.49E-05***	0.547	***2.56E-02***
petN	-0.255	1.56E-01	-0.100	6.10E-01	*rpl36*	0.350	9.74E-02	0.128	4.77E-01
psaA	-0.325	***3.18E-02***	-0.203	1.61E-01	*accD*	**-1.339**	6.06E-01	-0.319	8.81E-01
psaB	-0.258	1.64E-01	-0.620	***3.35E-05***	*ccsA*	0.461	2.73E-01	0.926	***2.16E-02***
psaC	-0.396	8.09E-02	-0.432	***1.00E-03***	*clpP*	0.261	2.74E-01	0.124	7.02E-01
psaI	-0.149	5.79E-01	0.197	3.16E-01	*matK*	0.416	4.63E-01	-0.887	***6.70E-03***
psaJ	-0.211	4.33E-01	-0.248	1.24E-01	*psbN*	-0.060	8.07E-01	0.203	2.75E-01
ndhA	0.436	5.31E-02	0.383	5.13E-02	*ycf1*	n.d.	n.d.	n.d.	n.d.
ndhB	0.271	8.07E-01	-0.542	2.90E-01	*ycf2*	1.514	***2.11E-05***	1.658	***9.33E-05***
ndhC	0.083	8.07E-01	-0.232	4.74E-01	*ycf3*	-0.207	4.30E-01	-0.124	6.05E-01
ndhD	-0.208	5.79E-01	-0.449	***1.15E-02***	*ycf4*	0.325	8.09E-02	-0.026	9.13E-01
ndhE	-0.471	***3.18E-02***	-0.399	***3.48E-02***	*ycf10*	-0.077	9.48E-01	-0.098	9.02E-01
ndhF	0.038	9.29E-01	0.012	9.66E-01	*orf105*	-0.668	9.13E-01	1.681	4.72E-01
ndhG	**-1.803**	***2.60E-14***	**-1.238**	***1.61E-07***	*orf74*	**-1.446**	***2.09E-04***	-0.180	7.17E-01
ndhH	2.485	***1.29E-18***	2.599	***7.54E-14***	*orf70A*	**-1.336**	8.07E-01	n.d.	n.d.
ndhI	**-1.352**	***2.00E-12***	**-1.171**	***1.61E-07***	*orf99*	**-2.025**	5.67E-01	-0.686	6.83E-01
ndhJ	-0.267	3.81E-01	-0.603	***2.88E-02***	*orf103*	1.673	1.64E-01	2.644	1.25E-01
ndhK	0.198	4.63E-01	0.301	6.73E-02	*orf79*	**-2.237**	4.33E-01	-0.101	9.66E-01
atpA	0.022	9.13E-01	0.128	3.39E-01	*orf131*	n.d.	n.d.	n.d.	n.d.
atpB	0.079	7.03E-01	-0.095	6.22E-01	*orf70B*	0.090	9.91E-01	-0.768	7.30E-01
atpE	-0.134	3.84E-01	-0.284	***2.35E-02***	*orf75*	**-1.360**	6.71E-01	1.578	4.84E-01
atpF	0.172	4.33E-01	-0.083	6.49E-01	*orf350*	-0.188	8.04E-01	0.419	6.08E-01
atpH	-0.240	2.12E-01	-0.464	***5.13E-04***					
atpI	-0.250	2.88E-01	-0.469	***1.47E-02***					
rpoA	0.443	***1.03E-02***	0.546	***3.43E-04***					
rpoB	0.529	5.79E-01	0.840	3.39E-01					
rpoC1	1.183	***6.26E-04***	0.619	6.73E-02					
rpoC2	1.128	6.62E-02	2.058	***2.42E-03***					

Bibliography

Y. Abe, T. Shodai, T. Muto, K. Mihara, H. Torii, S.-i. Nishikawa, T. Endo, and D. Kohda. Structural basis of presequence recognition by the mitochondrial protein import receptor Tom20. *Cell*, 100(5):551–560, 2000. ISSN 0092-8674. doi: 10.1016/S0092-8674(00)80691-1.

W. W. Adams, A. M. Watson, K. E. Mueh, V. Amiard, R. Turgeon, V. Ebbert, B. A. Logan, A. F. Combs, and B. Demmig-Adams. Photosynthetic acclimation in the context of structural constraints to carbon export from leaves. *Photosynth. Res.*, 94(2-3):455–466, 2007. ISSN 01668595. doi: 10.1007/s11120-006-9123-3.

R. K. Agrawal, M. R. Sharma, M. C. Kiel, G. Hirokawa, T. M. Booth, C. M. T. Spahn, R. A. Grassucci, A. Kaji, and J. Frank. Visualization of ribosome-recycling factor on the *Escherichia coli* 70S ribosome: Functional implications. *Proc. Natl. Acad. Sci. USA*, 101 (24):8900–8905, 2004. ISSN 00278424. doi: 10.1073/pnas.0401904101.

T. Ahmed, J. Shi, and S. Bhushan. Unique localization of the plastid-specific ribosomal proteins in the chloroplast ribosome small subunit provides mechanistic insights into the chloroplastic translation. *Nucleic Acids Res.*, 45(14):8581–8595, 2017. ISSN 0305-1048. doi: 10.1093/nar/gkx499.

V. Albrecht, A. Ingenfeld, and K. Apel. Characterization of the *Snowy Cotyledon 1* mutant of *Arabidopsis thaliana*: The impact of chloroplast elongation factor G on chloroplast development and plant vitality. *Plant Mol. Biol.*, 60(4):507–518, 2006. ISSN 1573-5028. doi: 10.1007/s11103-005-4921-0.

V. Amiard, K. E. Mueh, B. Demmig-Adams, V. Ebbert, R. Turgeon, and W. W. Adams. Anatomical and photosynthetic acclimation to the light environment in species with differing mechanisms of phloem loading. *Proc. Natl. Acad. Sci. USA*, 102(36):12968–12973, 2005. ISSN 0027-8424. doi: 10.1073/PNAS.0503784102.

P. Amin, D. A. C. Sy, M. L. Pilgrim, D. H. Parry, L. Nussaume, and N. E. Hoffman. Arabidopsis mutants lacking the 43- and 54-kilodalton subunits of the chloroplast signal recognition particle have distinct phenotypes. *Plant Physiol.*, 121(1):61 LP – 70, 1999. doi: 10.1104/pp.121.1.61.

A. Amunts, A. Ben-Shem, and N. Nelson. Solving the structure of plant photosystem I-biochemistry is vital. *Photochem. Photobiol. Sci.*, 4(12):1011–1015, 2005. ISSN 1474-905X. doi: 10.1039/B506132F.

P. R. Anbudurai, T. S. Mor, I. Ohad, S. V. Shestakov, and H. B. Pakrasi. The ctpA gene encodes the C-terminal processing protease for the D1 protein of the photosystem II reaction

center complex. *Proc. Natl. Acad. Sci. USA*, 91(17):8082 LP – 8086, 1994. doi: 10.1073/pnas.91.17.8082.

J. Anderson and W. Chow. Structural and functional dynamics of plant photosystem II. *Philos. Trans. R. Soc. Lond. B. Biol. Sci.*, 357:1421 – 1430, 2002. doi: 10.1098/rstb.2002.1138.

B. Andersson and J. M. Anderson. Lateral heterogeneity in the distribution of chlorophyll-protein complexes of the thylakoid membranes of spinach chloroplasts. *Biochim. Biophys. Acta - Bioenerg.*, 593(2):427–440, 1980. ISSN 0005-2728. doi: https://doi.org/10.1016/0005-2728(80)90078-X.

S. K. Archer, N. E. Shirokikh, T. H. Beilharz, and T. Preiss. Dynamics of ribosome scanning and recycling revealed by translation complex profiling. *Nature*, 535(7613):570–574, 2016. ISSN 14764687. doi: 10.1038/nature18647.

T. Armarego-Marriott, Ł. Kowalewska, A. Burgos, A. Fischer, W. Thiele, A. Erban, D. Strand, S. Kahlau, A. P. Hertle, J. Kopka, D. Walther, Z. Reich, M. A. Schöttler, and R. Bock. Highly resolved systems biology to dissect the etioplast-to-chloroplast transition in tobacco leaves. *Plant Physiol.*, 180(1):654–681, 2019. ISSN 0032-0889. doi: 10.1104/pp.18.01432.

U. K. Aryal, Y. Xiong, Z. McBride, D. Kihara, J. Xie, M. C. Hall, and D. B. Szymanski. A proteomic strategy for global analysis of plant protein complexes. *Plant Cell*, 26(10):3867 LP – 3882, 2014. doi: 10.1105/tpc.114.127563.

A. Ayala, J. Parrado, M. Bougria, and A. Machado. Effect of oxidative stress, produced by cumene hydroperoxide, on the various steps of protein synthesis: Modifications of elongation factor-2. *J. Biol. Chem.*, 271(38):23105–23110, 1996. doi: 10.1074/jbc.271.38.23105.

W. Bae, Y. J. Lee, D. H. Kim, J. Lee, S. Kim, E. J. Sohn, and I. Hwang. AKR2A-mediated import of chloroplast outer membrane proteins is essential for chloroplast biogenesis. *Nat. Cell Biol.*, 10(2):220–227, 2008. ISSN 1476-4679. doi: 10.1038/ncb1683.

B. Bai, S. van der Horst, J. H. G. Cordewener, T. A. H. P. America, J. Hanson, and L. Bentsink. Seed-stored mRNAs that are specifically associated to monosomes are translationally regulated during germination. *Plant Physiol.*, 182(1):378–392, 2020. ISSN 0032-0889. doi: 10.1104/pp.19.00644.

S. Bailey, R. G. Walters, S. Jansson, and P. Horton. Acclimation of *Arabidopsis thaliana* to the light environment: The existence of separate low light and high light responses. *Planta*, 213(5):794–801, 2001. ISSN 1432-2048. doi: 10.1007/s004250100556.

N. R. Baker. Chlorophyll fluorescence: A probe of photosynthesis *in vivo*. *Annu. Rev. Plant Biol.*, 59:89–113, 2008. ISSN 15435008. doi: 10.1146/annurev.arplant.59.032607.092759.

T. Bals, B. Dünschede, S. Funke, and D. Schünemann. Interplay between the cpSRP pathway components, the substrate LHCP and the translocase Alb3: An *in vivo* and *in vitro* study. *FEBS Lett.*, 584(19):4138–4144, 2010. ISSN 0014-5793. doi: https://doi.org/10.1016/j.febslet.2010.08.053.

C. Barat, P. P. Datta, V. S. Raj, M. R. Sharma, H. Kaji, A. Kaji, and R. K. Agrawal. Progression of the ribosome recycling factor through the ribosome dissociates the two ribosomal subunits. *Mol. Cell*, 27(2):250–261, 2007. ISSN 1097-2765. doi: 10.1016/j.molcel.2007.06.005.

A. Barkan. Proteins encoded by a complex chloroplast transcription unit are each translated from both monocistronic and polycistronic mRNAs. *EMBO J.*, 7(9):2637–44, 1988. ISSN 0261-4189.

A. Barkan. Nuclear mutants of maize with defects in chloroplast polysome assembly have altered chloroplast RNA metabolism. *Plant Cell*, 5(4):389–402, 1993. ISSN 1532-298X. doi: 10.1105/tpc.5.4.389.

A. Barkan. Approaches to investigating nuclear genes that function in chloroplast biogenesis in land plants. In L. McIntosh, editor, *Methods in Enzymology*, volume 297, pages 38–57. Academic Press, 1998. ISBN 9780121821982. doi: 10.1016/S0076-6879(98)97006-9.

A. Barkan. Expression of plastid genes: Organelle-specific elaborations on a prokaryotic scaffold. *Plant Physiol.*, 155(4):1520–1532, 2011. ISSN 0032-0889. doi: 10.1104/pp.110.171231.

A. Barkan and I. Small. Pentatricopeptide repeat proteins in plants. *Annu. Rev. Plant Biol.*, 65(1):415–442, 2014. doi: 10.1146/annurev-arplant-050213-040159.

A. Barkan, M. Walker, M. Nolasco, and D. Johnson. A nuclear mutation in maize blocks the processing and translation of several chloroplast mRNAs and provides evidence for the differential translation of alternative mRNA forms. *EMBO J.*, 13(13):3170–3181, 1994. ISSN 0261-4189. doi: 10.1002/j.1460-2075.1994.tb06616.x.

S. A. Barnes, N. K. Nishizawa, R. B. Quaggio, G. C. Whitelam, and N.-H. Chua. Far-red light blocks greening of Arabidopsis seedlings via a phytochrome A-mediated change in plastid development. *Plant Cell*, 8(4):601 – 615, 1996.

J. Bazin, K. Baerenfaller, S. J. Gosai, B. D. Gregory, M. Crespi, and J. Bailey-Serres. Global analysis of ribosome-associated noncoding RNAs unveils new modes of translational regulation. *Proc. Natl. Acad. Sci. USA*, page 201708433, 2017. ISSN 0027-8424. doi: 10.1073/pnas.1708433114.

U. Bechtold, S. Karpiński, and P. M. Mullineaux. The influence of the light environment and photosynthesis on oxidative signalling responses in plant-biotrophic pathogen interactions. *Plant, Cell Environ.*, 28(8):1046–1055, 2005. ISSN 01407791. doi: 10.1111/j.1365-3040.2005.01340.x.

F. E. Belbin, Z. B. Noordally, S. J. Wetherill, K. A. Atkins, K. A. Franklin, and A. N. Dodd. Integration of light and circadian signals that regulate chloroplast transcription by a nuclear-encoded sigma factor. *New Phytol.*, 213(2):727–738, 2017. ISSN 14698137. doi: 10.1111/nph.14176.

M. V. Beligni, K. Yamaguchi, and S. P. Mayfield. Chloroplast elongation factor Ts pro-protein is

an evolutionarily conserved fusion with the S1 domain-containing plastid-specific ribosomal protein-7. *Plant Cell*, 16(12):3357 LP – 3369, 2004. doi: 10.1105/tpc.104.026708.

A. J. Bendich. Why do chloroplasts and mitochondria contain so many copies of their genome? *BioEssays*, 6(6):279–282, 1987. ISSN 0265-9247. doi: 10.1002/bies.950060608.

T. Z. Berardini, L. Reiser, D. Li, Y. Mezheritsky, R. Muller, E. Strait, and E. Huala. The arabidopsis information resource: Making and mining the "gold standard" annotated reference plant genome. *genesis*, 53(8):474–485, 2015. ISSN 1526-954X. doi: 10.1002/dvg.22877.

P. Bieri, M. Leibundgut, M. Saurer, D. Boehringer, and N. Ban. The complete structure of the chloroplast 70S ribosome in complex with translation factor pY. *EMBO J.*, 36(4):475–486, 2017. ISSN 0261-4189. doi: 10.15252/embj.201695959.

G. Blaha, R. E. Stanley, and T. A. Steitz. Formation of the first peptide bond: The structure of EF-P bound to the 70S ribosome. *Science*, 325(5943):966–970, 2009. ISSN 00368075. doi: 10.1126/science.1175800.

R. Bock. Structure, function, and inheritance of plastid genomes. In R. Bock, editor, *Cell and Molecular Biology of Plastids*, pages 29–63. Springer Berlin Heidelberg, Berlin, Heidelberg, 2007. ISBN 978-3-540-75376-6. doi: 10.1007/4735_2007_0223.

H. J. Bohnert, E. J. Crouse, and J. M. Schmitt. Organization and expression of plastid genomes. In B. Parthier and D. Boulter, editors, *Nucleic Acids and Proteins in Plants II*, pages 475–530. Springer Berlin Heidelberg, Berlin, Heidelberg, 1982. ISBN 978-3-642-68347-3. doi: 10.1007/978-3-642-68347-3_14.

P. C. Bonham-Smith and D. P. Bourque. Translation of chloroplast-encoded mRNA: Potential initiation and termination signals. *Nucleic Acids Res.*, 17(5):2057–2080, 1989.

I. V. Boni, D. M. Isaeva, M. L. Musychenko, and N. V. Tzareva. Ribosome-messenger recognition: mRNA target sites for ribosomal protein S1. *Nucleic Acids Res.*, 19(1):155–162, 1991. ISSN 0305-1048. doi: 10.1093/nar/19.1.155.

T. Börner, A. Y. Aleynikova, Y. O. Zubo, and V. V. Kusnetsov. Chloroplast RNA polymerases: Role in chloroplast biogenesis. *Biochim. Biophys. Acta - Bioenerg.*, 1847(9):761–769, 2015. ISSN 00052728. doi: 10.1016/j.bbabio.2015.02.004.

M. A. Borovinskaya, S. Shoji, K. Fredrick, and J. H. D. Cate. Structural basis for hygromycin B inhibition of protein biosynthesis. *RNA*, 14(8):1590–1599, 2008. ISSN 1469-9001. doi: 10.1261/rna.1076908.

M. S. Bretscher. Direct translation of a circular messenger DNA. *Nature*, 220(5172):1088–1091, 1968. ISSN 1476-4687. doi: 10.1038/2201088a0.

J. Brix, K. Dietmeier, and N. Pfanner. Differential recognition of preproteins by the purified cytosolic domains of the mitochondrial import receptors Tom20, Tom22, and Tom70. *J. Biol. Chem.*, 272(33):20730–20735, 1997. doi: 10.1074/jbc.272.33.20730.

D. H. Burkhardt, S. Rouskin, Y. Zhang, G. W. Li, J. S. Weissman, and C. A. Gross. Operon mRNAs are organized into ORF-centric structures that predict translation efficiency. *Elife*, 6:1–23, 2017. ISSN 2050084X. doi: 10.7554/eLife.22037.

B. M. Burmann, K. Schweimer, X. Luo, M. C. Wahl, B. L. Stitt, M. E. Gottesman, and P. Rösch. A NusE:NusG complex links transcription and translation. *Science*, 501:501–505, 2010. doi: 10.1126/science.1184953.

P. A. Burrows, L. A. Sazanov, Z. Svab, P. Maliga, and P. J. Nixon. Identification of a functional respiratory complex in chloroplasts through analysis of tobacco mutants containing disrupted plastid *ndh* genes. *EMBO J.*, 17(4):868–876, 1998. ISSN 0261-4189. doi: 10.1093/emboj/17.4.868.

E. B. Cahoon, J. Shanklin, and J. B. Ohlrogge. Expression of a coriander desaturase results in petroselinic acid production in transgenic tobacco. *Proc. Natl. Acad. Sci. USA*, 89(23): 11184–11188, 1992. ISSN 0027-8424. doi: 10.1073/PNAS.89.23.11184.

S. E. Calvo, D. J. Pagliarini, and V. K. Mootha. Upstream open reading frames cause widespread reduction of protein expression and are polymorphic among humans. *Proc. Natl. Acad. Sci. USA*, 106(18):7507 LP – 7512, 2009. doi: 10.1073/pnas.0810916106.

F. Campos, B. I. García-Gómez, R. M. Solórzano, E. Salazar, J. Estevez, P. León, E. R. Alvarez-Buylla, and A. A. Covarrubias. A cDNA for nuclear-encoded chloroplast translational initiation factor 2 from a higher plant is able to complement an *infB Escherichia coli* null mutant. *J. Biol. Chem.*, 276(30):28388–28394, 2001. doi: 10.1074/jbc.M100605200.

B. Castandet, A. Germain, A. M. Hotto, and D. B. Stern. Systematic sequencing of chloroplast transcript termini from *Arabidopsis thaliana* reveals >200 transcription initiation sites and the extensive imprints of RNA-binding proteins and secondary structures. *Nucleic Acids Res.*, 47(22):11889–11905, 2019. ISSN 0305-1048. doi: 10.1093/nar/gkz1059.

M. Cavaiuolo, R. Kuras, F.-A. Wollman, Y. Choquet, and O. Vallon. Small RNA profiling in *Chlamydomonas*: Insights into chloroplast RNA metabolism. *Nucleic Acids Res.*, 45(18): 10783–10799, 2017. ISSN 13624962. doi: 10.1093/nar/gkx668.

D. D. Chang and D. A. Clayton. A mammalian mitochondrial RNA processing activity contains nucleus-encoded RNA. *Science*, 235(4793):1178 LP – 1184, 1987. doi: 10.1126/science.2434997.

S. S. Chen and J. R. Williamson. Characterization of the ribosome biogenesis landscape in *E. coli* using quantitative mass spectrometry. *J. Mol. Biol.*, 425(4):767–779, 2013. ISSN 1089-8638. doi: 10.1016/j.jmb.2012.11.040.

W. Chi, B. He, J. Mao, J. Jiang, and L. Zhang. Plastid sigma factors: Their individual functions and regulation in transcription. *Biochim. Biophys. Acta - Bioenerg.*, 1847(9): 770–778, 2015. ISSN 0005-2728. doi: 10.1016/J.BBABIO.2015.01.001.

Y. Choquet and F.-A. Wollman. The CES process. In *The Chlamydomonas Sourcebook*, volume 2, pages 1029–1066. 2009. doi: 10.1016/B978-0-12-370873-1.00037-X.

P. Chotewutmontri and A. Barkan. Dynamics of chloroplast translation during chloroplast differentiation in maize. *PLoS Genet.*, 12(7):1–28, 2016. ISSN 15537404. doi: 10.1371/journal.pgen.1006106.

P. Chotewutmontri and A. Barkan. Multilevel effects of light on ribosome dynamics in chloroplasts program genome-wide and *psbA*-specific changes in translation. *PLoS Genet.*, 14(8): 1–26, 2018. doi: 10.1371/journal.pgen.1007555.

P. Chotewutmontri and A. Barkan. Light-induced *psbA* translation in plants is triggered by photosystem II damage via an assembly-linked autoregulatory circuit. *Proc. Natl. Acad. Sci. USA*, 117(35):21775 – 21784, 2020. doi: 10.1073/pnas.2007833117.

P. Chotewutmontri, N. Stiffler, K. P. Watkins, and A. Barkan. *Ribosome profiling in maize*, volume 1676. Springer New York, New York, NY, 2018. ISBN 978-1-4939-7314-9. doi: 10.1007/978-1-4939-7315-6.

P. Chotewutmontri, R. E. Williams-Carrier, and A. Barkan. Exploring the link between photosystem II assembly and translation of the chloroplast *psbA* mRNA. *Plants*, 9(152), 2020. doi: 10.3390/plants9020152.

W. S. Chow and J. M. Anderson. Photosynthetic responses of *Pisum sativum* to an increase in irradiance during growth II. Thylakoid membrane components. *Funct. Plant Biol.*, 14(1): 9, 1987. ISSN 1445-4408. doi: 10.1071/PP9870009.

L. Chun, A. Kawakami, and D. A. Christopher. Phytochrome A mediates blue light and UV-A-dependent chloroplast gene transcription in green leaves. *Plant Physiol.*, 125(4):1957–66, 2001. ISSN 0032-0889. doi: 10.1104/pp.125.4.1957.

B. Y. Chung, T. J. Hardcastle, J. D. Jones, N. Irigoyen, A. E. Firth, D. C. Baulcombe, and I. Brierley. The use of duplex-specific nuclease in ribosome profiling and a user-friendly software package for Ribo-seq data analysis. *RNA*, 21(10):1731–1745, 2015. doi: 10.1261/rna.052548.115.

M. Cole, C. Nolte, and W. Werr. Nuclear import of the transcription factor SHOOT MERISTEMLESS depends on heterodimerization with BLH proteins expressed in discrete subdomains of the shoot apical meristem of *Arabidopsis thaliana*. *Nucleic Acids Res.*, 34(4): 1281–1292, 2006. ISSN 0305-1048. doi: 10.1093/nar/gkl016.

L. Daftuar, Y. Zhu, X. Jacq, and C. Prives. Ribosomal proteins RPL37, RPS15 and RPS20 regulate the Mdm2-p53-MdmX network. *PLoS One*, 8(7), 2013. ISSN 19326203. doi: 10.1371/journal.pone.0068667.

H. Daniell, C.-S. Lin, M. Yu, and W.-J. Chang. Chloroplast genomes: Diversity, evolution, and applications in genetic engineering. *Genome Biol.*, 17(1):134, 2016. ISSN 1474-760X. doi: 10.1186/s13059-016-1004-2.

A. Danon and S. P. Mayfield. Light regulated translational activators: Identification of chloroplast gene specific mRNA binding proteins. *EMBO J.*, 10(13):3993–4001, 1991. ISSN 0261-4189.

A. Danon and S. P. Mayfield. Light-regulated translation of chloroplast messenger RNAs through redox potential. *Science*, 266(5191):1717 LP – 1719, 1994a. doi: 10.1126/science.7992056.

A. Danon and S. P. Mayfield. ADP-dependent phosphorylation regulates RNA-binding *in vitro*: Implications in light-modulated translation. *EMBO J.*, 13(9):2227–2235, 1994b. ISSN 0261-4189. doi: 10.1002/j.1460-2075.1994.tb06500.x.

J. R. DeEll and P. M. A. Toivonen, editors. Springer US, Boston, MA, 2003. ISBN 978-1-4613-5065-1. doi: 10.1007/978-1-4615-0415-3.

J. P. Dekker and E. J. Boekema. Supramolecular organization of thylakoid membrane proteins in green plants. *Biochim. Biophys. Acta - Bioenerg.*, 1706(1-2):12–39, 2005. ISSN 0005-2728. doi: 10.1016/J.BBABIO.2004.09.009.

E. M. del Campo, B. Sabater, and M. Martín. Characterization of the 5'- and 3'-ends of mRNAs of *ndhH*, *ndhA* and *ndhI* genes of the plastid *ndhH-D* operon. *Biochimie*, 88(3-4):347–357, 2006. ISSN 03009084. doi: 10.1016/j.biochi.2005.09.005.

N. Delihas, J. Andersen, H. Sprouse, and B. Dudock. The nucleotide sequence of the chloroplast 5S ribosomal RNA from spinach. *Nucleic Acids Res.*, 9(12):2801–2805, jul 1981. doi: 10.1093/nar/9.12.2801.

E. F. DeLong, G. S. Wickham, and N. R. Pace. Phylogenetic stains: Ribosomal RNA-based probes for the identification of single cells. *Science*, 243(4896):1360 LP – 1363, 1989. doi: 10.1126/science.2466341.

X.-W. Deng and W. Gruissem. Control of plastid gene expression during development: The limited role of transcriptional regulation. *Cell*, 49(3):379–387, 1987. ISSN 0092-8674. doi: https://doi.org/10.1016/0092-8674(87)90290-X.

X.-W. Deng, D. B. Stern, J. C. Tonkyn, and W. Gruissem. Plastid run-on transcription. Application to determine the transcriptional regulation of spinach plastid genes. *J. Biol. Chem.*, 262(20):9641–9648, 1987.

L. F. Dickey, M. Gallo-Meagher, and W. F. Thompson. Light regulatory sequences are located within the 5' portion of the Fed-1 message sequence. *EMBO J.*, 11(6):2311–2317, 1992. ISSN 0261-4189. doi: 10.1002/j.1460-2075.1992.tb05290.x.

C. Dingwall, G. P. Lomonossoff, and R. A. Laskey. High sequence specificity of micrococcal nuclease. *Nucleic Acids Res.*, 9(12):2659 – 2673, 1981.

A. Dobin, C. A. Davis, F. Schlesinger, J. Drenkow, C. Zaleski, S. Jha, P. Batut, M. Chaisson, and T. R. Gingeras. STAR: Ultrafast universal RNA-seq aligner. *Bioinformatics*, 29(1):15–21, 2013. ISSN 1460-2059. doi: 10.1093/bioinformatics/bts635.

M. S. Dobres, R. C. Elliott, J. C. Watson, and W. F. Thompson. A phytochrome regulated pea transcript encodes ferredoxin I. *Plant Mol. Biol.*, 8(1):53–59, 1987. ISSN 1573-5028. doi: 10.1007/BF00016434.

L. K. Doerfel, I. Wohlgemuth, C. Kothe, F. Peske, H. Urlaub, and M. V. Rodnina. EF-P is essential for rapid synthesis of proteins containing consecutive proline residues. *Science*, 339 (6115):85 LP – 88, 2013. doi: 10.1126/science.1229017.

J. J. Doyle and J. L. Doyle. Isolation of plant DNA from fresh tissue. *Focus (Madison).*, 12 (1):13–15, 1990.

D. Drapier, B. Rimbault, O. Vallon, F.-A. Wollman, and Y. Choquet. Intertwined translational regulations set uneven stoichiometry of chloroplast ATP synthase subunits. *EMBO J.*, 26 (15):3581–3591, 2007. ISSN 0261-4189. doi: 10.1038/sj.emboj.7601802.

S. Duncan, T. S. G. Olsson, M. Hartley, C. Dean, and S. Rosa. A method for detecting single mRNA molecules in *Arabidopsis thaliana*. *Plant Methods*, 12(1):13, 2016. ISSN 1746-4811. doi: 10.1186/s13007-016-0114-x.

J. G. Dunn and J. S. Weissman. Plastid: Nucleotide-resolution analysis of next-generation sequencing and genomics data. *BMC Genomics*, 17(1):958, 2016. ISSN 1471-2164. doi: 10.1186/s12864-016-3278-x.

D. Dutta, K. Shatalin, V. Epshtein, M. E. Gottesman, and E. Nudler. Linking RNA polymerase backtracking to genome instability in *E. coli*. *Cell*, 146(4):533–543, 2011. ISSN 00928674. doi: 10.1016/j.cell.2011.07.034.

T. A. Dyer, R. H. Miller, and A. D. Greenwood. Leaf nucleic acids: I. Characteristics and role in the differentiation. *J. Exp. Bot.*, 22(1):125–136, 1971. ISSN 0022-0957. doi: 10.1093/jxb/22.1.125.

I. Edhofer, S. K. Mühlbauer, and L. A. Eichacker. Light regulates the rate of translation elongation of chloroplast reaction center protein D1. *Eur. J. Biochem.*, 257(1):78–84, 1998. ISSN 00142956. doi: 10.1046/j.1432-1327.1998.2570078.x.

K. Edwards and H. Kössel. The rRNA operon from *Zea mays* chloroplasts: Nucleotide sequence of 23S rDNA and its homology with *E.coli* 23S rDNA. *Nucleic Acids Res.*, 9(12):2853–2869, 1981. ISSN 03051048. doi: 10.1093/nar/9.12.2853.

K. D. Edwards, N. Fernandez-Pozo, K. Drake-Stowe, M. E. Humphry, A. D. Evans, A. Bombarely, F. Allen, R. Hurst, B. White, S. P. Kernodle, J. R. Bromley, J. P. Sanchez-Tamburrino, R. S. Lewis, and L. A. Mueller. A reference genome for *Nicotiana tabacum* enables map-based cloning of homeologous loci implicated in nitrogen utilization efficiency. *BMC Genomics*, 18(1):1–14, 2017. ISSN 14712164. doi: 10.1186/s12864-017-3791-6.

A. Eisa, K. Malenica, S. Schwenkert, and B. Bölter. High light acclimation induces chloroplast precursor phosphorylation and reduces import efficiency. *Plants*, 9(24), 2020. doi: 10.3390/plants9010024.

R. C. Elliott, L. F. Dickey, M. J. White, and W. F. Thompson. *cis*-acting elements for light regulation of pea Ferredoxin I gene expression are located within transcribed sequences. *Plant Cell*, 1(7):691 LP – 698, 1989. doi: 10.1105/tpc.1.7.691.

O. Emanuelsson, H. Nielsen, and G. V. Heijne. ChloroP, a neural network-based method for predicting chloroplast transit peptides and their cleavage sites. *Protein Sci.*, 8(5):978–984, 1999. ISSN 0961-8368. doi: 10.1110/ps.8.5.978.

O. Emanuelsson, H. Nielsen, S. Brunak, and G. von Heijne. Predicting subcellular localization of proteins based on their N-terminal amino acid sequence. *J. Mol. Biol.*, 300(4):1005–1016, 2000. ISSN 0022-2836. doi: https://doi.org/10.1006/jmbi.2000.3903.

D. N. Ermolenko and H. F. Noller. mRNA translocation occurs during the second step of ribosomal intersubunit rotation. *Nat. Struct. Mol. Biol.*, 18(4):457–462, 2011. ISSN 1545-9985. doi: 10.1038/nsmb.2011.

J. R. Evans. The relationship between electron transport components and photosynthetic capacity in pea leaves grown at different irradiances. *Funct. Plant Biol.*, 14(2):157, 1987. ISSN 1445-4408. doi: 10.1071/PP9870157.

L. Feng, M. A. Raza, Z. Li, Y. Chen, M. H. B. Khalid, J. Du, W. Liu, X. Wu, C. Song, L. Yu, Z. Zhang, S. Yuan, W. Yang, and F. Yang. The influence of light intensity and leaf movement on photosynthesis characteristics and carbon balance of soybean. *Front. Plant Sci.*, 9:1952, 2019.

N. Fernandez-Pozo, N. Menda, J. D. Edwards, S. Saha, I. Y. Tecle, S. R. Strickler, A. Bombarely, T. Fisher-York, A. Pujar, H. Foerster, A. Yan, and L. A. Mueller. The Sol Genomics Network (SGN) - From genotype to phenotype to breeding. *Nucleic Acids Res.*, 43(D1): D1036–D1041, 2014. ISSN 0305-1048. doi: 10.1093/nar/gku1195.

K. N. Ferreira, T. M. Iverson, K. Maghlaoui, J. Barber, and S. Iwata. Architecture of the photosynthetic oxygen-evolving center. *Science*, 303(5665):1831 LP – 1838, 2004. doi: 10.1126/science.1093087.

M. B. Ferretti, H. Ghalei, E. A. Ward, E. L. Potts, and K. Karbstein. Rps26 directs mRNA-specific translation by recognition of Kozak sequence elements. *Nat. Struct. Mol. Biol.*, 24 (9):700–707, 2017. ISSN 15459985. doi: 10.1038/nsmb.3442.

V. Fey, R. Wagner, K. Bräutigam, M. Wirtz, R. Hell, A. Dietzmann, D. Leister, R. Oelmüller, and T. Pfannschmidt. Retrograde plastid redox signals in the expression of nuclear genes for chloroplast proteins of *Arabidopsis thaliana*. *J. Biol. Chem.*, 280(7):5318–5328, 2005. ISSN 00219258. doi: 10.1074/jbc.M406358200.

C. B. Field, M. J. Behrenfeld, J. T. Randerson, and P. G. Falkowski. Primary production of the biosphere: Integrating terrestrial and oceanic components. *Science*, 281(5374):237 LP – 240, 1998. doi: 10.1126/science.281.5374.237.

S. Finster. *Charakterisierung der Funktion und Lokalisation der plastidären Genexpressionsmaschinerie in Nicotiana tabacum*. PhD thesis, 2014.

L. E. Fish and A. T. Jagendorf. High rates of protein synthesis by isolated chloroplasts. *Plant Physiol.*, 70(4):1107–14, 1982. ISSN 0032-0889.

T. T. Fleischmann, L. B. Scharff, S. Alkatib, S. Hasdorf, M. A. Schöttler, and R. Bock. Nonessential plastid-encoded ribosomal proteins in tobacco: A developmental role for plastid translation and implications for reductive genome evolution. *Plant Cell*, 23(9):3137–3155, 2011. doi: 10.1105/tpc.111.088906.

D. V. Freistroffer, M. Y. Pavlov, J. MacDougall, R. H. Buckingham, and M. Ehrenberg. Release factor RF3 in *E. coli* accelerates the dissociation of release factors RF1 and RF2 from the ribosome in a GTP-dependent manner. *EMBO J.*, 16(13):4126–4133, 1997. ISSN 0261-4189. doi: 10.1093/emboj/16.13.4126.

D. V. Freistroffer, M. Kwiatkowski, R. H. Buckingham, and M. Ehrenberg. The accuracy of codon recognition by polypeptide release factors. *Proc. Natl. Acad. Sci. USA*, 97(5): 2046–2051, 2000. ISSN 0027-8424. doi: 10.1073/pnas.030541097.

A. Friemann and W. Hachtel. Chloroplast messenger RNAs of free and thylakoid-bound polysomes from *Vicia faba* L. *Planta*, 175(1):50–59, 1988. ISSN 0032-0935.

R. Fristedt, A. Willig, P. Granath, M. Crèvecoeur, J.-D. Rochaix, and A. V. Vener. Phosphorylation of photosystem II controls functional macroscopic folding of photosynthetic membranes in *Arabidopsis*. *Plant Cell*, 21(12):3950–3964, 2009. ISSN 10404651. doi: 10.1105/tpc.109.069435.

H. Fromm, M. Devic, R. Fluhr, and M. Edelman. Control of *psbA* gene expression: In mature *Spirodela* chloroplasts light regulation of 32-kd protein synthesis is independent of transcript level. *EMBO J.*, 4(2):291–5, 1985. ISSN 0261-4189.

H.-Y. Fu, R. Ghandour, S. Ruf, R. Zoschke, R. Bock, and M. A. Schöttler. Neither the availability of D2 nor CP43 limits the biogenesis of PSII in tobacco. *bioRxiv*, page 2020.08.31.272526, 2020. doi: 10.1101/2020.08.31.272526.

M. Fujiki and K. Verner. Coupling of cytosolic protein synthesis and mitochondrial protein import in yeast. Evidence for cotranslational import *in vivo*. *J. Biol. Chem.*, 268(3):1914–1920, 1993. ISSN 00219258.

S. Fujimoto, S. S. Sugano, K. Kuwata, K. Osakabe, and S. Matsunaga. Visualization of specific repetitive genomic sequences with fluorescent TALEs in *Arabidopsis thaliana*. *J. Exp. Bot.*, 67(21):6101–6110, 2016. ISSN 0022-0957. doi: 10.1093/jxb/erw371.

M. G. Gagnon, S. V. Seetharaman, D. Bulkley, and T. A. Steitz. Structural basis for the rescue of stalled ribosomes: Structure of YaeJ bound to the ribosome. *Science*, 335(6074):1370 LP – 1372, 2012. doi: 10.1126/science.1217443.

J. G. Gall and M. L. Pardue. Formation and detection of RNA-DNA hybrid molecules in cytological preparations. *Proc. Natl. Acad. Sci. USA*, 63(2):378 LP – 383, 1969. doi: 10.1073/pnas.63.2.378.

J. S. Gantt, S. L. Baldauf, P. J. Calie, N. F. Weeden, and J. D. Palmer. Transfer of *rpl22* to the nucleus greatly preceded its loss from the chloroplast and involved the gain of an intron. *EMBO J.*, 10(10):3073–3078, 1991. ISSN 0261-4189.

X. Gao, F. Zhang, J. Hu, W. Cai, G. Shan, D. Dai, K. Huang, and G. Wang. MicroRNAs modulate adaption to multiple abiotic stresses in Chlamydomonas reinhardtii. *Sci. Rep.*, 6 (May):1–15, 2016. ISSN 20452322. doi: 10.1038/srep38228.

P. Gawroński, P. E. Jensen, S. Karpiński, D. Leister, and L. B. Scharff. Pausing of chloroplast ribosomes is induced by multiple features and is linked to the assembly of photosynthetic complexes. *Plant Physiol.*, 176(3):2557–2569, 2018. ISSN 0032-0889. doi: 10.1104/pp.17.01564.

P. Gawroński, C. Enroth, P. Kindgren, S. Marquardt, and S. Karpiński. Light-dependent translation change of Arabidopsis *psbA* correlates with RNA structure alterations at the translation initiation region. *BioRxiv*, 2020a.

P. Gawroński, A. Pałac, and L. B. Scharff. Secondary structure of chloroplast mRNAs *in vivo* and *in vitro*. *Plants*, 9(3):323, 2020b. ISSN 2223-7747. doi: 10.3390/plants9030323.

R. J. Geider, E. H. Delucia, P. G. Falkowski, A. C. Finzi, J. P. Grime, J. Grace, T. M. Kana, J. La Roche, S. P. Long, B. A. Osborne, T. Platt, I. C. Prentice, J. A. Raven, W. H. Schlesinger, V. Smetacek, V. Stuart, S. Sathyendranath, R. B. Thomas, T. C. Vogelmann, P. Williams, and F. I. Woodward. Primary productivity of planet earth: Biological determinants and physical constraints in terrestrial and aquatic habitats. *Glob. Chang. Biol.*, 7(8):849–882, 2001. ISSN 1354-1013. doi: 10.1046/j.1365-2486.2001.00448.x.

M. A. Godoy Herz, M. G. Kubaczka, G. Brzyżek, L. Servi, M. Krzyszton, C. Simpson, J. Brown, S. Swiezewski, E. Petrillo, and A. R. Kornblihtt. Light regulates plant alternative splicing through the control of transcriptional elongation. *Mol. Cell*, pages 1–9, 2019. ISSN 10972765. doi: 10.1016/j.molcel.2018.12.005.

V. A. M. Gold, P. Chroscicki, P. Bragoszewski, and A. Chacinska. Visualization of cytosolic ribosomes on the surface of mitochondria by electron cryo-tomography. *EMBO Rep.*, 18 (10):1786–1800, 2017. ISSN 1469-221X. doi: https://doi.org/10.15252/embr.201744261.

G. Gómez and V. Pallás. Noncoding RNA mediated traffic of foreign mRNA into chloroplasts reveals a novel signaling mechanism in plants. *PLoS One*, 5(8):e12269, 2010. ISSN 1932-6203. doi: 10.1371/journal.pone.0012269.

M. Graf, S. Arenz, P. Huter, A. Dönhöfer, J. Nováček, and D. N. Wilson. Cryo-EM structure of the spinach chloroplast ribosome reveals the location of plastid-specific ribosomal proteins and extensions. *Nucleic Acids Res.*, 45(5):gkw1272, 2016. ISSN 0305-1048. doi: 10.1093/nar/gkw1272.

S. Grebe. *High light acclimation of the photosynthetic apparatus in plants*. Master, Universität Potsdam, 2015.

S. Greiner, P. Lehwark, and R. Bock. OrganellarGenomeDRAW (OGDRAW) version 1.3.1: Expanded toolkit for the graphical visualization of organellar genomes. *Nucleic Acids Res.*, 47(W1):W59–W64, 2019. ISSN 0305-1048. doi: 10.1093/nar/gkz238.

P. T. J. Hajdukiewicz, L. A. Allison, and P. Maliga. The two RNA polymerases encoded by the

nuclear and the plastid compartments transcribe distinct groups of genes in tobacco plastids. *EMBO J.*, 16(13):4041–4048, 1997. ISSN 0261-4189. doi: 10.1093/emboj/16.13.4041.

M. Hakala, I. Tuominen, M. Keränen, T. Tyystjärvi, and E. Tyystjärvi. Evidence for the role of the oxygen-evolving manganese complex in photoinhibition of photosystem II. *Biochim. Biophys. Acta - Bioenerg.*, 1706(1):68–80, 2005. ISSN 0005-2728. doi: https://doi.org/10.1016/j.bbabio.2004.09.001.

K. Hammani, G. Bonnard, A. Bouchoucha, A. Gobert, F. Pinker, T. Salinas, and P. Giegé. Helical repeats modular proteins are major players for organelle gene expression. *Biochimie*, 100:141–150, 2014. ISSN 0300-9084. doi: https://doi.org/10.1016/j.biochi.2013.08.031.

S. S. Hasan and W. A. Cramer. On rate limitations of electron transfer in the photosynthetic cytochrome b_6f complex. *Phys. Chem. Chem. Phys.*, 14(40):13853–13860, 2012. ISSN 1463-9076. doi: 10.1039/C2CP41386H.

T.-P. Hausner, U. Geigenmüller, and K. H. Nierhaus. The allosteric three-site model for the ribosomal elongation cycle. New insights into the inhibition mechanisms of aminoglycosides, thiostrepton, and viomycin. *J. Biol. Chem.*, 263(26):13103–13111, 1988.

S. Hayashi, M. Watanabe, M. Kobayashi, T. Tohge, T. Hashimoto, and T. Shoji. Genetic manipulation of transcriptional regulators alters nicotine biosynthesis in tobacco. *Plant Cell Physiol.*, 61(6):1041–1053, 2020. ISSN 1471-9053. doi: 10.1093/pcp/pcaa036.

W. R. Hess, A. Prombona, B. Fieder, A. R. Subramanian, and T. Börner. Chloroplast *rps15* and the *rpoB/C1/C2* gene cluster are strongly transcribed in ribosome-deficient plastids: Evidence for a functioning non-chloroplast-encoded RNA polymerase. *EMBO J.*, 12(2): 563–571, 1993. ISSN 02614189. doi: 10.1002/j.1460-2075.1993.tb05688.x.

S. E. Hetherington, J. He, and R. M. Smillie. Photoinhibition at low temperature in chilling-sensitive and -resistant plants. *Plant Physiol.*, 90(4):1609–1615, 1989. ISSN 15322548. doi: 10.1104/pp.90.4.1609.

É. Hideg, P. B. Kós, and U. Schreiber. Imaging of NPQ and ROS formation in tobacco leaves: Heat inactivation of the water-water cycle prevents down-regulation of PSII. *Plant Cell Physiol.*, 49(12):1879–1886, 2008. ISSN 00320781. doi: 10.1093/pcp/pcn170.

T. Higa and M. Wada. Chloroplast avoidance movement is not functional in plants grown under strong sunlight. *Plant. Cell Environ.*, 39(4):871–882, 2016. ISSN 0140-7791. doi: 10.1111/pce.12681.

D. A. Hiller, V. Singh, M. Zhong, and S. A. Strobel. A two-step chemical mechanism for ribosome-catalysed peptide bond formation. *Nature*, 476(7359):236–239, 2011. ISSN 1476-4687. doi: 10.1038/nature10248.

A. G. Hinnebusch. Molecular mechanism of scanning and start codon selection in eukaryotes. *Microbiol. Mol. Biol. Rev.*, 75(3):434 LP – 467, 2011. doi: 10.1128/MMBR.00008-11.

G. Hirokawa, R. M. Nijman, V. S. Raj, H. Kaji, K. Igarashi, and A. Kaji. The role of ribosome

recycling factor in dissociation of 70S ribosomes into subunits. *RNA*, 11(8):1317–1328, 2005. ISSN 1355-8382. doi: 10.1261/rna.2520405.

T. Hirose and M. Sugiura. Cis-acting elements and trans-acting factors for accurate translation of chloroplast *psbA* mRNAs: development of an *in vitro* translation system from tobacco chloroplasts. *EMBO J.*, 15(7):1687–1695, 1996. ISSN 0261-4189. doi: https://doi.org/10.1002/j.1460-2075.1996.tb00514.x.

M. M. Howard, A. Bae, and M. Königer. The importance of chloroplast movement, nonphotochemical quenching, and electron transport rates in light acclimation and tolerance to high light in *Arabidopsis thaliana*. *Am. J. Bot.*, 106(11):1444–1453, 2019. ISSN 0002-9122. doi: 10.1002/ajb2.1378.

P. Y. Hsu, L. Calviello, H.-Y. L. Wu, F.-W. Li, C. J. Rothfels, U. Ohler, and P. N. Benfey. Super-resolution ribosome profiling reveals unannotated translation events in *Arabidopsis*. *Proc. Natl. Acad. Sci. USA*, 113(45):E7126–E7135, 2016. doi: 10.1073/pnas.1614788113.

A. Hulford, L. Hazell, R. M. Mould, and C. Robinson. Two distinct mechanisms for the translocation of proteins across the thylakoid membrane, one requiring the presence of a stromal protein factor and nucleotide triphosphates. *J. Biol. Chem.*, 269(5):3251–6, 1994. ISSN 0021-9258.

J. A. Hussmann, S. Patchett, A. Johnson, S. Sawyer, and W. H. Press. Understanding biases in ribosome profiling experiments reveals signatures of translation dynamics in yeast. *PLOS Genet.*, 11(12):e1005732, 2015.

P. Huter, C. Müller, B. Beckert, S. Arenz, O. Berninghausen, R. Beckmann, and D. N. Wilson. Structural basis for ArfA-RF2-mediated translation termination on mRNAs lacking stop codons. *Nature*, 541(7638):546–549, 2017. ISSN 14764687. doi: 10.1038/nature20821.

N. T. Ingolia, S. Ghaemmaghami, J. R. S. Newman, and J. S. Weissman. Genome-wide analysis *in vivo* of translation with nucleotide resolution using ribosome profiling. *Science*, 324(5924):218–223, 2009. ISSN 0036-8075. doi: 10.1126/science.1168978.

N. T. Ingolia, L. F. Lareau, and J. S. Weissman. Ribosome profiling of mouse embryonic stem cells reveals the complexity and dynamics of mammalian proteomes. *Cell*, 147(4):789–802, 2011. ISSN 0092-8674. doi: 10.1016/j.cell.2011.10.002.

N. T. Ingolia, G. A. Brar, S. Rouskin, A. M. McGeachy, and J. S. Weissman. The ribosome profiling strategy for monitoring translation *in vivo* by deep sequencing of ribosome-protected mRNA fragments. *Nat. Protoc.*, 7(8):1534–1550, 2012. ISSN 1754-2189. doi: 10.1038/nprot.2012.086.

Y. Ivanova, M. D. Smith, K. Chen, and D. J. Schnell. Members of the Toc159 import receptor family represent distinct pathways for protein targeting to plastids. *Mol. Biol. Cell*, 15(7):3379–3392, 2004. ISSN 1059-1524. doi: 10.1091/mbc.e03-12-0923.

C. H. Jan, C. C. Williams, and J. S. Weissman. Principles of ER cotranslational translocation

revealed by proximity-specific ribosome profiling. *Science*, 346(6210):1257521–1257521, 2014. ISSN 0036-8075. doi: 10.1126/science.1257521.

R. P. Jarvis. Targeting of nucleus-encoded proteins to chloroplasts in plants. *New Phytol.*, 179 (2):257–285, 2008. ISSN 0028646X. doi: 10.1111/j.1469-8137.2008.02452.x.

M. P. Johnson and A. V. Ruban. Photoprotective energy dissipation in higher plants involves alteration of the excited state energy of the emitting chlorophyll(s) in the light harvesting antenna II (LHCII). *J. Biol. Chem.*, 284(35):23592–23601, 2009. doi: 10.1074/jbc.M109.013557.

M. P. Johnson, C. Vasilev, J. D. Olsen, and C. N. Hunter. Nanodomains of cytochrome b_6f and photosystem II complexes in spinach grana thylakoid membranes. *Plant Cell*, 26(7): 3051 LP – 3061, 2014. doi: 10.1105/tpc.114.127233.

W. Junge, O. Pänke, D. A. Cherepanov, K. Gumbiowski, M. Müller, and S. Engelbrecht. Inter-subunit rotation and elastic power transmission in F_0F_1-ATPase. *FEBS Lett.*, 504(3): 152–160, 2001. ISSN 00145793. doi: 10.1016/S0014-5793(01)02745-4.

P. Juntawong and J. Bailey-Serres. Dynamic light regulation of translation status in *Arabidopsis thaliana*. *Front. Plant Sci.*, 3:66, 2012. ISSN 1664-462X. doi: 10.3389/fpls.2012.00066.

P. Juntawong, T. Girke, J. Bazin, and J. Bailey-Serres. Translational dynamics revealed by genome-wide profiling of ribosome footprints in *Arabidopsis*. *Proc. Natl. Acad. Sci. USA*, 111(1):E203–E212, 2014. ISSN 0027-8424. doi: 10.1073/pnas.1317811111.

S. Kahlau and R. Bock. Plastid transcriptomics and translatomics of tomato fruit development and chloroplast-to-chromoplast differentiation: Chromoplast gene expression largely serves the production of a single protein. *Plant Cell*, 20(4):856–874, 2008. ISSN 1040-4651. doi: 10.1105/tpc.107.055202.

E. Kaiser, A. Morales, and J. Harbinson. Fluctuating light takes crop photosynthesis on a rollercoaster ride. *Plant Physiol.*, 176(2):977–989, 2018. ISSN 0032-0889. doi: 10.1104/pp.17.01250.

E. Kapri-Pardes, L. Naveh, and Z. Adam. The thylakoid lumen protease Deg1 is involved in the repair of photosystem II from photoinhibition in *Arabidopsis*. *Plant Cell*, 19(3):1039 LP – 1047, 2007. doi: 10.1105/tpc.106.046573.

S. Karpiński, H. Gabrys, A. Mateo, B. Karpińska, and P. M. Mullineaux. Light perception in plant disease defence signalling. *Curr. Opin. Plant Biol.*, 6(4):390–396, 2003. ISSN 13695266. doi: 10.1016/S1369-5266(03)00061-X.

M. Kasahara, T. Kagawa, K. Oikawa, N. Suetsugu, M. Miyao, and M. Wada. Chloroplast avoidance movement reduces photodamage in plants. *Nature*, 420(6917):829–832, 2002. ISSN 1476-4687. doi: 10.1038/nature01213.

L. S. Kaufman, W. R. Briggs, and W. F. Thompson. Phytochrome control of specific mRNA

levels in developing pea buds. *Plant Physiol.*, 78(2):388 LP – 393, 1985. doi: 10.1104/pp.78.2.388.

R. Kawaguchi, T. Girke, E. A. Bray, and J. Bailey-Serres. Differential mRNA translation contributes to gene regulation under non-stress and dehydration stress conditions in *Arabidopsis thaliana*. *Plant J.*, 38(5):823–839, 2004. ISSN 0960-7412. doi: 10.1111/j.1365-313X.2004.02090.x.

T. Kawashima, C. Berthet-Colominas, M. Wulff, S. Cusack, and R. Leberman. The structure of the *Escherichia coli* EF-Tu•EF-Ts complex at 2.5 Å resolution. *Nature*, 379(6565):511–518, 1996. ISSN 1476-4687. doi: 10.1038/379511a0.

R. E. Kellems and R. A. Butow. Cytoplasmic type 80 S ribosomes associated with yeast mitochondria: I. Evidence for ribosome binding sites on yeast mitochondria. *J. Biol. Chem.*, 247(24):8043–8050, 1972.

R. E. Kellems, V. F. Allison, and R. A. Butow. Cytoplasmic type 80 S ribosomes associated with yeast mitochondria: II. Evidence for the association of cytoplasmic ribosomes with the outer mitochondrial membrane *in situ*. *J. Biol. Chem.*, 249(10):3297–3303, 1974.

R. E. Kellems, V. F. Allison, and R. A. Butow. Cytoplasmic type 80S ribosomes associated with yeast mitochondria. IV. Attachment of ribosomes to the outer membrane of isolated mitochondria. *J. Cell Biol.*, 65(1):1–14, 1975. ISSN 0021-9525. doi: 10.1083/jcb.65.1.1.

N. Keren, H. Gong, and I. Ohad. Oscillations of reaction center II-D1 protein degradation *in vivo* induced by repetitive light flashes: Correlation between the level of RCII-Q_B and protein degradation in low light. *J. Biol. Chem.*, 270(2):806–814, 1995. doi: 10.1074/jbc.270.2.806.

A. Khandelwal, T. Elvitigala, B. Ghosh, and R. S. Quatrano. Arabidopsis transcriptome reveals control circuits regulating redox homeostasis and the role of an AP2 transcription factor. *Plant Physiol.*, 148(4):2050 LP – 2058, 2008. doi: 10.1104/pp.108.128488.

J. Kim, P. G. Klein, and J. E. Mullet. Ribosomes pause at specific sites during synthesis of membrane-bound chloroplast reaction center protein D1. *J. Biol. Chem.*, 266(23):14931–14938, 1991.

J. Kim, L. A. Eichacker, W. Rudiger, and J. E. Mullet. Chlorophyll regulates accumulation of the plastid-encoded chlorophyll proteins P700 and D1 by increasing apoprotein stability. *Plant Physiol.*, 104(3):907–916, 1994a.

J. Kim, P. G. Klein, and J. E. Mullet. Synthesis and turnover of photosystem II reaction center protein D1. *J. Biol. Chem.*, 269(27):17918–17923, 1994b. ISSN 00219258.

J. H. Kim, R. E. Glick, and A. Melis. Dynamics of photosystem stoichiometry adjustment by light quality in chloroplasts. *Plant Physiol.*, 102(1):181 LP – 190, 1993a. doi: 10.1104/pp.102.1.181.

M. Kim, D. A. Christopher, and J. E. Mullet. Direct evidence for selective modulation of *psbA*,

rpoA, *rbcL* and 16S RNA stability during barley chloroplast development. *Plant Mol. Biol.*, 22(3):447–463, 1993b. ISSN 1573-5028. doi: 10.1007/BF00015975.

S. J. Kim, C. Robinson, and A. Mant. Sec/SRP-independent insertion of two thylakoid membrane proteins bearing cleavable signal peptides. *FEBS Lett.*, 424(1):105–108, 1998. ISSN 0014-5793. doi: https://doi.org/10.1016/S0014-5793(98)00148-3.

M. Kimura, Y. Y. Yamamoto, M. Seki, T. Sakurai, M. Sato, T. Abe, S. Yoshida, K. Manabe, K. Shinozaki, and M. Matsui. Identification of *Arabidopsis* genes regulated by high light-stress using cDNA microarray. *Photochem. Photobiol.*, 77(2):226–233, 2003. ISSN 00318655. doi: 10.1562/0031-8655(2003)0770226IOAGRB2.0.CO2.

K. Kitahara and K. Miyazaki. Specific inhibition of bacterial RNase T2 by helix 41 of 16S ribosomal RNA. *Nat. Commun.*, 2(1):549, 2011. ISSN 2041-1723. doi: 10.1038/ncomms1553.

K. Kitajima and K. P. Hogan. Increases of chlorophyll *a/b* ratios during acclimation of tropical woody seedlings to nitrogen limitation and high light. *Plant. Cell Environ.*, 26(6):857–865, 2003. ISSN 0140-7791. doi: 10.1046/j.1365-3040.2003.01017.x.

P. Klaff and W. Gruissem. Changes in chloroplast mRNA stability during leaf development. *Plant Cell*, 3(5):517–529, 1991. ISSN 10404651. doi: 10.2307/3869357.

P. Klaff and W. Gruissem. A 43 kD light-regulated chloroplast RNA-binding protein interacts with the *psbA* 5' non-translated leader RNA. *Photosynth. Res.*, 46(1):235–248, 1995. ISSN 1573-5079. doi: 10.1007/BF00020436.

R. R. Klein and J. E. Mullet. Regulation of chloroplast-encoded chlorophyll-binding protein translation during higher plant chloroplast biogenesis. *J. Biol. Chem.*, 261(24):11138–45, 1986. ISSN 0021-9258.

R. R. Klein, H. S. Mason, and J. E. Mullet. Light-regulated translation of chloroplast proteins. I. Transcripts of PsaA-PsaB, PsbA, and RbcL are associated with polysomes in dark-grown and illuminated barley seedlings. *J. Cell Biol.*, 106(2):289–301, 1988. ISSN 00219525. doi: 10.1083/jcb.106.2.289.

W. Kofer, H.-U. Koop, G. Wanner, and K. Steinmüller. Mutagenesis of the genes encoding subunits A, C, H, I, J and K of the plastid NAD(P)H-plastoquinone-oxidoreductase in tobacco by polyethylene glycol-mediated plastome transformation. *Mol. Gen. Genet. MGG*, 258(1):166–173, 1998. ISSN 1432-1874. doi: 10.1007/s004380050719.

K. Kojima, M. Oshita, Y. Nanjo, K. Kasai, Y. Tozawa, H. Hayashi, and Y. Nishiyama. Oxidation of elongation factor G inhibits the synthesis of the D1 protein of photosystem II. *Mol. Microbiol.*, 65(4):936–947, 2007. ISSN 0950-382X. doi: 10.1111/j.1365-2958.2007.05836.x.

K. Kojima, K. Motohashi, T. Morota, M. Oshita, T. Hisabori, H. Hayashi, and Y. Nishiyama. Regulation of translation by the redox state of elongation factor G in the cyanobacterium *Synechocystis* sp. PCC 6803. *J. Biol. Chem.*, 284(28):18685–18691, 2009. doi: 10.1074/jbc.M109.015131.

J. Komenda, R. Sobotka, and P. J. Nixon. Assembling and maintaining the photosystem II complex in chloroplasts and cyanobacteria. *Curr. Opin. Plant Biol.*, 15(3):245–251, 2012. ISSN 1369-5266. doi: https://doi.org/10.1016/j.pbi.2012.01.017.

N. Komissarova and M. Kashlev. Transcriptional arrest: *Escherichia coli* RNA polymerase translocates backward, leaving the 3' end of the RNA intact and extruded. *Proc. Natl. Acad. Sci. USA*, 94(5):1755–1760, 1997. ISSN 00278424. doi: 10.1073/pnas.94.5.1755.

K. S. Koutmou, M. E. McDonald, J. L. Brunelle, and R. Green. RF3:GTP promotes rapid dissociation of the class 1 termination factor. *RNA*, 20(5):609–620, 2014. ISSN 1469-9001. doi: 10.1261/rna.042523.113.

M. Kozak. How do eucaryotic ribosomes select initiation regions in messenger RNA? *Cell*, 15 (4):1109–1123, 1978. ISSN 0092-8674. doi: 10.1016/0092-8674(78)90039-9.

M. Kozak. Inability of circular mRNA to attach to eukaryotic ribosomes. *Nature*, 280(5717): 82–85, 1979. ISSN 1476-4687. doi: 10.1038/280082a0.

M. Kozak. An analysis of 5'-noncoding sequences from 699 vertebrate messenger RNAs. *Nucleic Acids Res.*, 15(20):8125–8148, 1987. ISSN 0305-1048. doi: 10.1093/nar/15.20.8125.

M. Kozak. Adherence to the first-AUG rule when a second AUG codon follows closely upon the first. *Proc. Natl. Acad. Sci. USA*, 92(7):2662–2666, 1995. ISSN 00278424. doi: 10.1073/pnas.92.7.2662.

D. M. Kramer, C. A. Sacksteder, and J. A. Cruz. How acidic is the lumen? *Photosynth. Res.*, 60(2-3):151–163, 1999. ISSN 01668595. doi: 10.1023/a:1006212014787.

K. Krech, S. Ruf, F. F. Masduki, W. Thiele, D. Bednarczyk, C. A. Albus, N. Tiller, C. Hasse, M. A. Schöttler, and R. Bock. The plastid genome-encoded Ycf4 protein functions as a nonessential assembly factor for photosystem I in higher plants. *Plant Physiol.*, 159:579–591, 2012. doi: 10.1104/pp.112.196642.

A. Krieger, A. W. Rutherford, I. Vass, and É. Hideg. Relationship between activity, D1 loss, and Mn binding in photoinhibition of photosystem II. *Biochemistry*, 37(46):16262–16269, 1998. ISSN 0006-2960. doi: 10.1021/bi981243v.

A. Kubicki, E. Funk, P. Westhoff, and K. Steinmüller. Differential expression of plastome-encoded ndh genes in mesophyll and bundle-sheath chloroplasts of the C4 plant *Sorghum bicolor* indicates that the complex I-homologous NAD(P)H-plastoquinone oxidoreductase is involved in cyclic electron transport. *Planta*, 199(2):276–281, 1996. ISSN 0032-0935. doi: 10.1007/BF00196569.

L. Lancaster, M. C. Kiel, A. Kaji, and H. F. Noller. Orientation of ribosome recycling factor in the ribosome from directed hydroxyl radical probing. *Cell*, 111(1):129–140, 2002. ISSN 0092-8674. doi: 10.1016/S0092-8674(02)00938-8.

H. Latif, R. Szubin, J. Tan, E. Brunk, A. Lechner, K. Zengler, and B. O. Palsson. A streamlined

ribosome profiling protocol for the characterization of microorganisms. *Biotechniques*, 58 (6):329–332, 2015. ISSN 0736-6205. doi: 10.2144/000114302.

M. Laurberg, H. Asahara, A. Korostelev, J. Zhu, S. Trakhanov, and H. F. Noller. Structural basis for translation termination on the 70S ribosome. *Nature*, 454(7206):852–857, 2008. ISSN 1476-4687. doi: 10.1038/nature07115.

J. Legen, S. Kemp, K. Krause, B. Profanter, R. G. Herrmann, and R. M. Maier. Comparative analysis of plastid transcription profiles of entire plastid chromosomes from tobacco attributed to wild-type and PEP-deficient transcription machineries. *Plant J.*, 31(2):171–188, 2002. ISSN 09607412. doi: 10.1046/j.1365-313X.2002.01349.x.

L. Lei, J. Shi, J. Chen, M. Zhang, S. Sun, S. Xie, X. Li, B. Zeng, L. Peng, A. Hauck, H. Zhao, W. Song, Z. Fan, and J. Lai. Ribosome profiling reveals dynamic translational landscape in maize seedlings under drought stress. *Plant J.*, 84(6):1206–1218, 2015. doi: 10.1111/tpj.13073.

D. Leister, I. Romani, L. Mittermayr, F. Paieri, E. Fenino, and T. Kleine. Identification of target genes and transcription factors implicated in translation-dependent retrograde signaling in *Arabidopsis*. *Mol. Plant*, 7(7):1228–1247, 2014. ISSN 17529867. doi: 10.1093/mp/ssu066.

I. J. Leitch, L. Hanson, K. Y. Lim, A. Kovarik, M. W. Chase, J. J. Clarkson, and A. R. Leitch. The ups and downs of genome size evolution in polyploid species of *Nicotiana* (Solanaceae). *Ann. Bot.*, 101(6):805–814, 2008. ISSN 0305-7364. doi: 10.1093/aob/mcm326.

S. Lerbs-Mache. The 110-kDa polypeptide of spinach plastid DNA-dependent RNA polymerase: Single-subunit enzyme or catalytic core of multimeric enzyme complexes? *Proc. Natl. Acad. Sci. USA*, 90(12):5509 LP – 5513, 1993. doi: 10.1073/pnas.90.12.5509.

C. Lesnik, Y. Cohen, A. Atir-Lande, M. Schuldiner, and Y. Arava. OM14 is a mitochondrial receptor for cytosolic ribosomes that supports co-translational import into mitochondria. *Nat. Commun.*, 5:5711, 2014. ISSN 2041-1723. doi: 10.1038/ncomms6711.

R. A. Lewin, editor. *Origins of plastids*. Springer US, Boston, MA, 1993. ISBN 978-1-4613-6218-0. doi: 10.1007/978-1-4615-2818-0.

G.-W. Li, E. Oh, and J. S. Weissman. The anti-Shine-Dalgarno sequence drives translational pausing and codon choice in bacteria. *Nature*, 484(7395):538–541, 2012. ISSN 1476-4687. doi: 10.1038/nature10965.

G.-W. Li, D. Burkhardt, C. Gross, and J. S. Weissman. Quantifying absolute protein synthesis rates reveals principles underlying allocation of cellular resources. *Cell*, 157(3):624–635, 2014. ISSN 0092-8674. doi: 10.1016/j.cell.2014.02.033.

H. Li, B. Handsaker, A. Wysoker, T. Fennell, J. Ruan, N. Homer, G. Marth, G. Abecasis, and R. Durbin. The sequence alignment/map format and SAMtools. *Bioinformatics*, 25(16): 2078–2079, 2009. ISSN 1367-4803. doi: 10.1093/bioinformatics/btp352.

H.-m. Li and C.-C. Chiu. Protein transport into chloroplasts. *Annu. Rev. Plant Biol.*, 61(1): 157–180, 2010. ISSN 1543-5008. doi: 10.1146/annurev-arplant-042809-112222.

L. Li, C. J. Nelson, J. Trösch, I. R. Castleden, S. Huang, and A. H. Millar. Protein degradation rate in *Arabidopsis thaliana* leaf growth and development. *Plant Cell*, 29(2):207–228, 2017. ISSN 1040-4651. doi: 10.1105/tpc.16.00768.

X.-P. Li, A. M. Gilmore, S. Caffarri, R. Bassi, T. Golan, D. M. Kramer, and K. K. Niyogi. Regulation of photosynthetic light harvesting involves intrathylakoid lumen pH sensing by the PsbS protein. *J. Biol. Chem.*, 279(22):22866–22874, 2004. ISSN 0021-9258. doi: 10.1074/jbc.M402461200.

H. K. Lichtenthaler, C. Buschmann, M. Döll, H.-J. Fietz, T. Bach, U. Kozel, D. Meier, and U. Rahmsdorf. Photosynthetic activity, chloroplast ultrastructure, and leaf characteristics of high-light and low-light plants and of sun and shade leaves. *Photosynth. Res.*, 2(2):115–141, 1981. ISSN 1573-5079. doi: 10.1007/BF00028752.

K. Liere, A. Weihe, and T. Börner. The transcription machineries of plant mitochondria and chloroplasts: Composition, function, and regulation. *J. Plant Physiol.*, 168(12):1345–1360, 2011. ISSN 01761617. doi: 10.1016/j.jplph.2011.01.005.

M. Lindahl, C. Spetea, T. Hundal, A. B. Oppenheim, Z. Adam, and B. Andersson. The thylakoid FtsH protease plays a role in the light-induced turnover of the photosystem II D1 protein. *Plant Cell*, 12(3):419 LP – 431, 2000. doi: 10.1105/tpc.12.3.419.

G. Link. Phytochrome control of plastid mRNA in mustard (*Sinapis alba* L.). *Planta*, 154(1): 81–86, 1982. ISSN 00320935, 14322048.

S. Link, K. Engelmann, K. Meierhoff, and P. Westhoff. The atypical short-chain dehydrogenases HCF173 and HCF244 are jointly involved in translational initiation of the *psbA* mRNA of Arabidopsis. *Plant Physiol.*, 160(4):2202 LP – 2218, 2012. doi: 10.1104/pp.112.205104.

Z. Liu, H. Yan, K. Wang, T. Kuang, J. Zhang, L. Gui, X. An, and W. Chang. Crystal structure of spinach major light-harvesting complex at 2.72 Å resolution. *Nature*, 428(6980):287–292, 2004. ISSN 1476-4687. doi: 10.1038/nature02373.

M. Lohse, O. Drechsel, S. Kahlau, and R. Bock. OrganellarGenomeDRAW–A suite of tools for generating physical maps of plastid and mitochondrial genomes and visualizing expression data sets. *Nucleic Acids Res.*, 41(Web Server issue):575–581, 2013. ISSN 13624962. doi: 10.1093/nar/gkt289.

M. I. Love, W. Huber, and S. Anders. Moderated estimation of fold change and dispersion for RNA-seq data with DESeq2. *Genome Biol.*, 15(12):1–21, 2014. ISSN 1474760X. doi: 10.1186/s13059-014-0550-8.

A. B. Loveland, G. Demo, and A. A. Korostelev. Cryo-EM of elongating ribosome with EF-Tu GTP elucidates tRNA proofreading. *Nature*, 584(7822):640–645, 2020. ISSN 1476-4687. doi: 10.1038/s41586-020-2447-x.

R. Lukoszek, P. Feist, and Z. Ignatova. Insights into the adaptive response of *Arabidopsis thaliana* to prolonged thermal stress by ribosomal profiling and RNA-Seq. *BMC Plant Biol.*, 16(1):1–13, 2016. ISSN 14712229. doi: 10.1186/s12870-016-0915-0.

H. Lyu and D. Lazár. Modeling the light-induced electric potential difference ($\Delta\Psi$), the pH difference (ΔpH) and the proton motive force across the thylakoid membrane in C3 leaves. *J. Theor. Biol.*, 413:11–23, 2017. ISSN 10958541. doi: 10.1016/j.jtbi.2016.10.017.

C. Ma, D. Kurita, N. Li, Y. Chen, H. Himeno, and N. Gao. Mechanistic insights into the alternative translation termination by ArfA and RF2. *Nature*, 541(7638):550–553, 2017. ISSN 14764687. doi: 10.1038/nature20822.

U. G. Maier, A. Bozarth, H. T. Funk, S. Zauner, S. A. Rensing, C. Schmitz-Linneweber, T. Börner, and M. Tillich. Complex chloroplast RNA metabolism: Just debugging the genetic programme? *BMC Biol.*, 6(1):36, 2008. ISSN 1741-7007. doi: 10.1186/1741-7007-6-36.

W. Majeran, G. Friso, Y. Asakura, X. Qu, M. Huang, L. Ponnala, K. P. Watkins, A. Barkan, and K. J. van Wijk. Nucleoid-enriched proteomes in developing plastids and chloroplasts from maize leaves: A new conceptual framework for nucleoid functions. *Plant Physiol.*, 158 (1):156–189, 2012. ISSN 00320889. doi: 10.1104/pp.111.188474.

P. Maliga and R. Bock. Plastid biotechnology: Food, fuel, and medicine for the 21st century. *Plant Physiol.*, 155(4):1501 LP – 1510, 2011. doi: 10.1104/pp.110.170969.

A. Mant, V. S. Nielsen, T. G. Knott, B. L. Møller, and C. Robinson. Multiple mechanisms for the targeting of photosystem I subunits F, H, K, L, and N into and across the thylakoid membrane. *J. Biol. Chem.*, 269(44):27303–27309, 1994.

P. Marc, A. Margeot, F. Devaux, C. Blugeon, M. Corral-Debrinski, and C. Jacq. Genome-wide analysis of mRNAs targeted to yeast mitochondria. *EMBO Rep.*, 3(2):159–164, 2002. ISSN 1469-221X. doi: 10.1093/embo-reports/kvf025.

J. Marks, K. Kannan, E. J. Roncase, D. Klepacki, A. Kefi, and C. Orelle. Context-specific inhibition of translation by ribosomal antibiotics targeting the peptidyl transferase center. *Proc. Natl. Acad. Sci. USA*, 113(43):12150 – 12155, 2016. doi: 10.1073/pnas.1613055113.

F. Martin, J. F. Ménétret, A. Simonetti, A. G. Myasnikov, Q. Vicens, L. Prongidi-Fix, S. K. Natchiar, B. P. Klaholz, and G. Eriani. Ribosomal 18S rRNA base pairs with mRNA during eukaryotic translation initiation. *Nat. Commun.*, 7:1–7, 2016. ISSN 20411723. doi: 10.1038/ncomms12622.

M. Martin. Cutadapt removes adapter sequences from high-throughput sequencing reads. *EMBnet.journal*, 17(1):1–3, 2013.

M. Martín and B. Sabater. Plastid *ndh* genes in plant evolution. *Plant Physiol. Biochem.*, 48 (8):636–645, 2010. ISSN 0981-9428. doi: https://doi.org/10.1016/j.plaphy.2010.04.009.

M. Martín, L. M. Casano, J. M. Zapata, A. Guéra, E. M. del Campo, C. Schmitz-Linneweber, R. M. Maier, and B. Sabater. Role of thylakoid Ndh complex and peroxidase in the protection

against photo-oxidative stress: Fluorescence and enzyme activities in wild-type and *ndhF*-deficient tobacco. *Physiol. Plant.*, 122(4):443–452, 2004. ISSN 0031-9317. doi: 10.1111/j.1399-3054.2004.00417.x.

A. Mateo, P. Mühlenbock, C. Rustérucci, C. C. C. Chang, Z. Miszalski, B. Karpińska, J. E. Parker, P. M. Mullineaux, and S. Karpiński. LESION SIMULATING DISEASE 1 is required for acclimation to conditions that promote excess excitation energy. *Plant Physiol.*, 136(1): 2818–2830, 2004. ISSN 00320889. doi: 10.1104/pp.104.043646.

P. Matt, U. Schurr, D. Klein, A. Krapp, and M. Stitt. Growth of tobacco in short-day conditions leads to high starch, low sugars, altered diurnal changes in the *Nia* transcript and low nitrate reductase activity, and inhibition of amino acid synthesis. *Planta*, 207(1):27–41, 1998. ISSN 00320935. doi: 10.1007/s004250050452.

S. P. Mayfield, A. Cohen, A. Danon, and C. B. Yohn. Translation of the *psbA* mRNA of *Chlamydomonas reinhardtii* requires a structured RNA element contained within the 5' untranslated region. *J. Cell Biol.*, 127(6):1537 – 1545, 1994. doi: 10.1083/jcb.127.6.1537.

G. Menschaert, W. Van Criekinge, T. Notelaers, A. Koch, J. Crappé, K. Gevaert, and P. Van Damme. Deep proteome coverage based on ribosome profiling aids mass spectrometry-based protein and peptide discovery and provides evidence of alternative translation products and near-cognate translation initiation events. *Mol. Cell. Proteomics*, 12(7):1780 LP – 1790, 2013. doi: 10.1074/mcp.M113.027540.

J. Meurer, L. Lezhneva, K. Amann, M. Gödel, S. Bezhani, I. Sherameti, and R. Oelmüller. A peptide chain release factor 2 affects the stability of UGA-containing transcripts in Arabidopsis chloroplasts. *Plant Cell*, 14(12):3255–3269, 2002. ISSN 10404651. doi: 10.1105/tpc.006809.

K. R. Miller. A chloroplast membrane lacking photosystem I. Changes in unstacked membrane regions. *Biochim. Biophys. Acta - Bioenerg.*, 592(1):143–152, 1980. ISSN 0005-2728. doi: https://doi.org/10.1016/0005-2728(80)90121-8.

O. L. Miller Jr, B. A. Hamkalo, and C. A. Thomas Jr. Visualization of bacterial genes in action. *Science*, 169(3943):392–395, 1970. ISSN 00368075. doi: 10.1126/science.169.3943.392.

P. Milon, A. L. Konevega, C. O. Gualerzi, and M. V. Rodnina. Kinetic checkpoint at a late step in translation initiation. *Mol. Cell*, 30(6):712–720, 2008. ISSN 1097-2765. doi: 10.1016/j.molcel.2008.04.014.

L. Minai, K. Wostrikoff, F.-A. Wollman, and Y. Choquet. Chloroplast biogenesis of photosystem II cores involves a series of assembly-controlled steps that regulate translation. *Plant Cell*, 18(1):159–175, 2006. doi: 10.1105/tpc.105.037705.precomplex.

E.-I. Minami and A. Watanabe. Thylakoid membranes: The translational site of chloroplast DNA-regulated thylakoid polypeptides. *Arch. Biochem. Biophys.*, 235(2):562–570, 1984. ISSN 0003-9861. doi: https://doi.org/10.1016/0003-9861(84)90230-3.

E.-i. Minami, K. Shinohara, N. Kawakami, and A. Watanabe. Localization and properties of

transcripts of *psbA* and *rbcL* genes in the stroma of spinach chloroplast. *Plant Cell Physiol.*, 29(8):1303–1309, 1988. ISSN 0032-0781. doi: 10.1093/oxfordjournals.pcp.a077639.

S. Miras, D. Salvi, L. Piette, D. Seigneurin-Berny, D. Grunwald, C. Reinbothe, J. Joyard, S. Reinbothe, and N. Rolland. Toc159- and Toc75-independent import of a transit sequence-less precursor into the inner envelope of chloroplasts. *J. Biol. Chem.*, 282(40):29482–29492, 2007. ISSN 00219258. doi: 10.1074/jbc.M611112200.

C. Miyake, S. Horiguchi, A. Makino, Y. Shinzaki, H. Yamamoto, and K. I. Tomizawa. Effects of light intensity on cyclic electron flow around PSI and its relationship to non-photochemical quenching of Chl fluorescence in tobacco leaves. *Plant Cell Physiol.*, 46(11):1819–1830, 2005. ISSN 00320781. doi: 10.1093/pcp/pci197.

D. Moazed and H. F. Noller. Intermediate states in the movement of transfer RNA in the ribosome. *Nature*, 342(6246):142–148, 1989. ISSN 1476-4687. doi: 10.1038/342142a0.

F. Mohammad, C. J. Woolstenhulme, R. Green, and A. R. Buskirk. Clarifying the translational pausing landscape in bacteria by ribosome profiling. *Cell Rep.*, 14(4):686–694, 2016. ISSN 2211-1247. doi: 10.1016/j.celrep.2015.12.073.

F. Mohammad, R. Green, and A. R. Buskirk. A systematically-revised ribosome profiling method for bacteria reveals pauses at single-codon resolution. *Elife*, 8:e42591, 2019. ISSN 2050-084X. doi: 10.7554/eLife.42591.

I. Moll, G. Hirokawa, M. C. Kiel, A. Kaji, and U. Bläsi. Translation initiation with 70S ribosomes: An alternative pathway for leaderless mRNAs. *Nucleic Acids Res.*, 32(11):3354–3363, 2004. ISSN 1362-4962. doi: 10.1093/nar/gkh663.

R.-A. Monde, F. Zito, J. Olive, F.-A. Wollman, and D. B. Stern. Post-transcriptional defects in tobacco chloroplast mutants lacking the cytochrome b_6/f complex. *Plant J.*, 21(1):61–72, 2000. ISSN 09607412. doi: 10.1046/j.1365-313X.2000.00653.x.

R. Motohashi, T. Yamazaki, F. Myouga, T. Ito, K. Ito, M. Satou, M. Kobayashi, N. Nagata, S. Yoshida, A. Nagashima, K. Tanaka, S. Takahashi, and K. Shinozaki. Chloroplast ribosome release factor 1 (AtcpRF1) is essential for chloroplast development. *Plant Mol. Biol.*, 64(5):481–497, 2007. ISSN 1573-5028. doi: 10.1007/s11103-007-9166-7.

S. K. Mühlbauer and L. A. Eichacker. Light-dependent formation of the photosynthetic proton gradient regulates translation elongation in chloroplasts. *J. Biol. Chem.*, 273(33):20935–20940, 1998. ISSN 0021-9258. doi: 10.1074/jbc.273.33.20935.

E. H. Murchie and P. Horton. Acclimation of photosynthesis to irradiance and spectral quality in British plant species: Chlorophyll content, photosynthetic capacity and habitat preference. *Plant, Cell Environ.*, 20(4):438–448, 1997. ISSN 01407791. doi: 10.1046/j.1365-3040.1997.d01-95.x.

L. Mustárdy, K. Buttle, G. Steinbach, and G. Garab. The three-dimensional network of the thylakoid membranes in plants: Quasihelical model of the granum-stroma assembly. *Plant Cell*, 20(10):2552–2557, 2008. ISSN 1040-4651. doi: 10.1105/tpc.108.059147.

A. Nada and J. Soll. Inner envelope protein 32 is imported into chloroplasts by a novel pathway. *J. Cell Sci.*, 117(17):3975–3982, 2004. ISSN 00219533. doi: 10.1242/jcs.01265.

M. Nagao, F. Tsuchiya, R. Motohashi, and T. Abo. Ribosome rescue activity of an *Arabidopsis thaliana* ArfB homolog. *Genes Genet. Syst.*, pages 119–131, 2020. ISSN 1880-5779. doi: 10.1266/ggs.20-00007.

A. Nagashima, M. Hanaoka, T. Shikanai, M. Fujiwara, K. Kanamaru, H. Takahashi, and K. Tanaka. The multiple-stress responsive plastid sigma factor, SIG5, directs activation of the *psbD* Blue Light-Responsive Promoter (BLRP) in *Arabidopsis thaliana*. *Plant Cell Physiol.*, 45(4):357–368, 2004. ISSN 00320781. doi: 10.1093/pcp/pch050.

Y. Nanjo, H. Oka, N. Ikarashi, K. Kaneko, A. Kitajima, T. Mitsui, F. J. Muñoz, M. Rodríguez-López, E. Baroja-Fernández, and J. Pozueta-Romero. Rice plastidial N-glycosylated nucleotide pyrophosphatase/phosphodiesterase is transported from the ER-Golgi to the chloroplast through the secretory pathway. *Plant Cell*, 18(10):2582 LP – 2592, 2006. doi: 10.1105/tpc.105.039891.

J. Nickelsen and B. Rengstl. Photosystem II assembly: From cyanobacteria to plants. *Annu. Rev. Plant Biol.*, 64(1):609–635, 2013. ISSN 1543-5008. doi: 10.1146/annurev-arplant-050312-120124.

M. Nicolaï, A. Duprat, R. Sormani, C. Rodriguez, M.-A. Roncato, N. Rolland, and C. Robaglia. Higher plant chloroplasts import the mRNA coding for the eucaryotic translation initiation factor 4E. *FEBS Lett.*, 581(21):3921–3926, 2007. ISSN 0014-5793. doi: https://doi.org/10.1016/j.febslet.2007.07.017.

K. H. Nierhaus and M. Pech. Problems with the analyses of the ribosomal allosteric three-site model. *J. Biol. Chem.*, 287(32):27049, 2012. ISSN 1083-351X. doi: 10.1074/jbc.L112.381848.

R. Nilsson, J. Brunner, N. E. Hoffman, and K. J. van Wijk. Interactions of ribosome nascent chain complexes of the chloroplast-encoded D1 thylakoid membrane protein with cpSRP54. *EMBO J.*, 18(3):733–742, 1999. ISSN 0261-4189. doi: 10.1093/emboj/18.3.733.

Y. Nishiyama and N. Murata. Revised scheme for the mechanism of photoinhibition and its application to enhance the abiotic stress tolerance of the photosynthetic machinery. *Appl. Microbiol. Biotechnol.*, 98(21):8777–8796, 2014. ISSN 1432-0614. doi: 10.1007/s00253-014-6020-0.

G. Noctor, D. Rees, A. Young, and P. Horton. The relationship between zeaxanthin, energy-dependent quenching of chlorophyll fluorescence, and trans-thylakoid pH gradient in isolated chloroplasts. *Biochim. Biophys. Acta - Bioenerg.*, 1057(3):320–330, 1991. ISSN 0005-2728. doi: https://doi.org/10.1016/S0005-2728(05)80143-4.

H. F. Noller, L. Lancaster, J. Zhou, and S. Mohan. The ribosome moves: RNA mechanics and translocation. *Nat. Struct. Mol. Biol.*, 24(12):1021–1027, 2017. ISSN 15459985. doi: 10.1038/nsmb.3505.

Z. B. Noordally, K. Ishii, K. A. Atkins, S. J. Wetherill, J. Kusakina, E. J. Walton, M. Kato, M. Azuma, K. Tanaka, M. Hanaoka, and A. N. Dodd. Circadian control of chloroplast transcription by a nuclear-encoded timing signal. *Science*, 339(6125):1316–1319, 2013. ISSN 0036-8075. doi: 10.1126/science.1230397.

E. Nudler, A. Mustaev, E. Lukhtanov, and A. Goldfarb. The RNA-DNA hybrid maintains the register of transcription by preventing backtracking of RNA polymerase. *Cell*, 89(1):33–41, 1997. ISSN 00928674. doi: 10.1016/s0092-8674(00)80180-4.

E. Oh, A. H. Becker, A. Sandikci, D. Huber, R. Chaba, F. Gloge, R. J. Nichols, A. Typas, C. A. Gross, J. S. Weissman, and B. Bukau. Selective ribosome profiling reveals the cotranslational chaperone action of trigger factor *in vivo*. *Cell*, 147(6):1295–1308, 2011. doi: 10.1016/j.cell.2011.10.044.

S. Oh and B. L. Montgomery. Phytochrome-induced SIG2 expression contributes to photoregulation of phytochrome signalling and photomorphogenesis in *Arabidopsis thaliana*. *J. Exp. Bot.*, 64(18):5457–5472, 2013. ISSN 0022-0957. doi: 10.1093/jxb/ert308.

I. Ohad, A. Berg, S. M. Berkowicz, A. Kaplan, and N. Keren. Photoinactivation of photosystem II: Is there more than one way to skin a cat? *Physiol. Plant.*, 142(1):79–86, 2011. ISSN 0031-9317. doi: 10.1111/j.1399-3054.2011.01466.x.

C. Orelle, S. Carlson, B. Kaushal, M. M. Almutairi, H. Liu, A. Ochabowicz, S. Quan, V. C. Pham, C. L. Squires, B. T. Murphy, and A. S. Mankin. Tools for characterizing bacterial protein synthesis inhibitors. *Antimicrob. Agents Chemother.*, 57(12):5994 LP – 6004, 2013. doi: 10.1128/AAC.01673-13.

F. Ossenbühl, M. Inaba-Sulpice, J. Meurer, J. Soll, and L. A. Eichacker. The *Synechocystis* sp PCC 6803 Oxa1 homolog is essential for membrane integration of reaction center precursor protein pD1. *Plant Cell*, 18(9):2236 LP – 2246, 2006. doi: 10.1105/tpc.106.043646.

S. K. Pal, M. Liput, M. Piques, H. Ishihara, T. Obata, M. C. M. Martins, R. Sulpice, J. T. van Dongen, A. R. Fernie, U. P. Yadav, J. E. Lunn, B. Usadel, and M. Stitt. Diurnal changes of polysome loading track sucrose content in the rosette of wild-type Arabidopsis and the starchless *pgm* mutant. *Plant Physiol.*, 162(3):1246–1265, 2013. ISSN 0032-0889. doi: 10.1104/pp.112.212258.

O. O. Panasenko, S. P. Somasekharan, Z. Villanyi, M. Zagatti, F. Bezrukov, R. Rashpa, J. Cornut, J. Iqbal, M. Longis, S. H. Carl, C. Peña, V. G. Panse, and M. A. Collart. Co-translational assembly of proteasome subunits in NOT1-containing assemblysomes. *Nat. Struct. Mol. Biol.*, 26(2):110–120, 2019. ISSN 1545-9985. doi: 10.1038/s41594-018-0179-5.

Y.-I. Park, J. M. Anderson, and W. S. Chow. Photoinactivation of functional photosystem II and D1-protein synthesis *in vivo* are independent of the modulation of the photosynthetic apparatus by growth irradiance. *Planta*, 198(2):300–309, 1996. ISSN 1432-2048. doi: 10.1007/BF00206257.

M. Pech and K. H. Nierhaus. The thorny way to the mechanism of ribosomal peptide-bond

formation. *ChemBioChem*, 13(2):189–192, 2012. ISSN 1439-4227. doi: 10.1002/cbic.201100660.

S. Pechmann, J. W. Chartron, and J. Frydman. Local slowdown of translation by nonoptimal codons promotes nascent-chain recognition by SRP *in vivo*. *Nat. Struct. Mol. Biol.*, 21(12): 1100–1105, 2014. ISSN 1545-9993. doi: 10.1038/nsmb.2919.

A. Perez Boerema, S. Aibara, B. Paul, V. Tobiasson, D. Kimanius, B. O. Forsberg, K. Wallden, E. Lindahl, and A. Amunts. Structure of the chloroplast ribosome with chl-RRF and hibernation-promoting factor. *Nat. Plants*, 4(4):212–217, 2018. ISSN 2055-0278. doi: 10.1038/s41477-018-0129-6.

F. Peske, S. Kuhlenkoetter, M. V. Rodnina, and W. Wintermeyer. Timing of GTP binding and hydrolysis by translation termination factor RF3. *Nucleic Acids Res.*, 42(3):1812–1820, 2014. ISSN 1362-4962. doi: 10.1093/nar/gkt1095.

M. E. Petracek, L. F. Dickey, T.-T. Nguyen, C. Gatz, D. A. Sowinski, G. C. Allen, and W. F. Thompson. Ferredoxin-1 mRNA is destabilized by changes in photosynthetic electron transport. *Proc. Natl. Acad. Sci. USA*, 95(15):9009–9013, 1998. ISSN 0027-8424. doi: 10.1073/pnas.95.15.9009.

A. D. Petropoulos and R. Green. Further *in vitro* exploration fails to support the allosteric three-site model. *J. Biol. Chem.*, 287(15):11642–11648, 2012. doi: 10.1074/jbc.C111.330068.

J. Pfalz, K. Liere, A. Kandlbinder, K.-J. Dietz, and R. Oelmüller. pTAC2, -6, and -12 are components of the transcriptionally active plastid chromosome that are required for plastid gene expression. *Plant Cell*, 18(1):176–197, 2006. ISSN 10404651. doi: 10.1105/tpc.105.036392.

J. Pfalz, O. A. Bayraktar, J. Prikryl, and A. Barkan. Site-specific binding of a PPR protein defines and stabilizes 5' and 3' mRNA termini in chloroplasts. *EMBO J.*, 28(14):2042–2052, 2009. ISSN 02614189. doi: 10.1038/emboj.2009.121.

T. Pfannschmidt, K. Schütze, M. Brost, and R. Oelmüller. A novel mechanism of nuclear photosynthesis gene regulation by redox signals from the chloroplast during photosystem stoichiometry adjustment. *J. Biol. Chem.*, 276(39):36125–36130, 2001. doi: 10.1074/jbc.M105701200.

M. Piques, W. X. Schulze, M. Höhne, B. Usadel, Y. Gibon, J. Rohwer, and M. Stitt. Ribosome and transcript copy numbers, polysome occupancy and enzyme dynamics in *Arabidopsis*. *Mol. Syst. Biol.*, 5(314), 2009. ISSN 17444292. doi: 10.1038/msb.2009.68.

W. Plader and M. Sugiura. The Shine-Dalgarno-like sequence is a negative regulatory element for translation of tobacco chloroplast *rps2* mRNA: An additional mechanism for translational control in chloroplasts. *Plant J.*, 34(3):377–382, 2003.

N. Planchard, P. Bertin, M. Quadrado, C. Dargel-Graffin, I. Hatin, O. Namy, and H. Mireau. The translational landscape of *Arabidopsis* mitochondria. *Nucleic Acids Res.*, 46(12):6218–6228, 2018. ISSN 13624962. doi: 10.1093/nar/gky489.

R. J. Porra, W. A. Thompson, and P. E. Kriedemann. Determination of accurate extinction coefficients and simultaneous equations for assaying chlorophylls *a* and *b* extracted with four different solvents: Verification of the concentration of chlorophyll standards by atomic absorption spectroscopy. *BBA - Bioenerg.*, 975(3):384–394, 1989. ISSN 00052728. doi: 10.1016/S0005-2728(89)80347-0.

E. Pötter and K. Kloppstech. Effect of light stress on the expresion of early light-induced proteins in barley. *Eur. J. Biochem.*, 214(1993):779–786, 1993.

S. Proshkin, A. R. Rahmouni, A. Mironov, and E. Nudler. Cooperation between translating ribosomes and RNA polymerase in transcription elongation. *Science*, 328:504–509, 2010.

K. A. Pyke. Plastid biogenesis and differentiation. In R. Bock, editor, *Cell and Molecular Biology of Plastids*, pages 1–28. Springer Berlin Heidelberg, Berlin, Heidelberg, 2007. ISBN 978-3-540-75376-6. doi: 10.1007/4735_2007_0226.

S. Qbadou, T. Becker, O. Mirus, I. Tews, J. Soll, and E. Schleiff. The molecular chaperone Hsp90 delivers precursor proteins to the chloroplast import receptor Toc64. *EMBO J.*, 25 (9):1836–1847, 2006. ISSN 0261-4189. doi: 10.1038/sj.emboj.7601091.

A. R. Quinlan and I. M. Hall. BEDTools: A flexible suite of utilities for comparing genomic features. *Bioinformatics*, 26(6):841–842, 2010. ISSN 1367-4803. doi: 10.1093/bioinformatics/btq033.

R Core Team. R: A language and environment for statistical computing., 2019.

R. N. Radhamony and S. M. Theg. Evidence for an ER to Golgi to chloroplast protein transport pathway. *Trends Cell Biol.*, 16(8):385–387, 2006. ISSN 09628924. doi: 10.1016/j.tcb.2006.06.003.

J. C. Rapp, B. J. Baumgartner, and J. E. Mullet. Quantitative analysis of transcription and RNA levels of 15 barley chloroplast genes. *J. Biol. Chem.*, 267(25):21404–21411, 1992.

A. H. Ratje, J. Loerke, A. Mikolajka, M. Brünner, P. W. Hildebrand, A. L. Starosta, A. Dönhöfer, S. R. Connell, P. Fucini, T. Mielke, P. C. Whitford, J. N. Onuchic, Y. Yu, K. Y. Sanbonmatsu, R. K. Hartmann, P. A. Penczek, D. N. Wilson, and C. M. T. Spahn. Head swivel on the ribosome facilitates translocation by means of intra-subunit tRNA hybrid sites. *Nature*, 468(7324):713–716, 2010. ISSN 1476-4687. doi: 10.1038/nature09547.

D. Rees, G. Noctor, A. V. Ruban, J. Crofts, A. Young, and P. Horton. pH dependent chlorophyll fluorescence quenching in spinach thylakoids from light treated or dark adapted leaves. *Photosynth. Res.*, 31(1):11–19, 1992. ISSN 1573-5079. doi: 10.1007/BF00049532.

D. W. Reid, S. Shenolikar, and C. V. Nicchitta. Simple and inexpensive ribosome profiling analysis of mRNA translation. *Methods*, 91:69–74, 2015. ISSN 1046-2023. doi: https://doi.org/10.1016/j.ymeth.2015.07.003.

J. S. Reuter and D. H. Mathews. RNAstructure: software for RNA secondary structure

prediction and analysis. *BMC Bioinformatics*, 11(1):129, 2010. ISSN 1471-2105. doi: 10.1186/1471-2105-11-129.

A. Riba, N. Di Nanni, N. Mittal, E. Arhné, A. Schmidt, and M. Zavolan. Protein synthesis rates and ribosome occupancies reveal determinants of translation elongation rates. *Proc. Natl. Acad. Sci. USA*, 116(30):15023 LP – 15032, 2019. doi: 10.1073/pnas.1817299116.

E. Richly and D. Leister. An improved prediction of chloroplast proteins reveals diversities and commonalities in the chloroplast proteomes of *Arabidopsis* and rice. *Gene*, 329(1-2):11–16, 2004. ISSN 03781119. doi: 10.1016/j.gene.2004.01.008.

A. Rivadossi, G. Zucchelli, F. M. Gariaschi, and R. C. Jennigns. Light absorption by the chlorophyll *a-b* complexes of photosystem II in a leaf with special reference to LHCII. *Photochem. Photobiol.*, 80(3):492–498, 2004. ISSN 0031-8655. doi: 10.1111/j.1751-1097.2004.tb00120.x.

C. Robinson, D. Cai, A. Hulford, I. W. Brock, D. Michl, L. Hazell, I. Schmidt, R. G. Herrmann, and R. B. Klösgen. The presequence of a chimeric construct dictates which of two mechanisms are utilized for translocation across the thylakoid membrane: Evidence for the existence of two distinct translocation systems. *EMBO J.*, 13(2):279–285, 1994. ISSN 0261-4189. doi: 10.1002/j.1460-2075.1994.tb06260.x.

D. Robinson, I. Karnauchov, R. G. Herrmann, R. B. Klösgen, and C. Robinson. Protease-sensitive thylakoidal import machinery for the Sec-, ΔpH- and signal recognition particle-dependent protein targeting pathways, but not for CF_oII integration. *Plant J.*, 10(1):149–155, 1996. ISSN 0960-7412. doi: 10.1046/j.1365-313X.1996.10010149.x.

J. T. Robinson, H. Thorvaldsdóttir, W. Winckler, M. Guttman, E. S. Lander, G. Getz, and J. P. Mesirov. Integrative genomics viewer. *Nat. Biotechnol.*, 29(1):24–26, 2011. ISSN 1546-1696. doi: 10.1038/nbt.1754.

A. Rokka, E.-M. Aro, R. G. Herrmann, B. Andersson, and A. V. Vener. Dephosphorylation of photosystem II reaction center proteins in plant photosynthetic membranes as an immediate response to abrupt elevation of temperature. *Plant Physiol.*, 123(4):1525 LP – 1536, 2000. doi: 10.1104/pp.123.4.1525.

N. Rolland, L. Janosi, M. A. Block, M. Shuda, E. Teyssier, C. Miège, C. Chéniclet, J.-P. Carde, A. Kaji, and J. Joyard. Plant ribosome recycling factor homologue is a chloroplastic protein and is bactericidal in *Escherichia coli* carrying temperature-sensitive ribosome recycling factor. *Proc. Natl. Acad. Sci. USA*, 96(10):5464 LP – 5469, 1999. doi: 10.1073/pnas.96.10.5464.

D. A. Romero, A. H. Hasan, Y.-F. Lin, L. Kime, O. Ruiz-Larrabeiti, M. Urem, G. Bucca, L. Mamanova, E. E. Laing, G. P. van Wezel, C. P. Smith, V. R. Kaberdin, and K. J. McDowall. A comparison of key aspects of gene regulation in *Streptomyces coelicolor* and *Escherichia coli* using nucleotide-resolution transcription maps produced in parallel by global and differential RNA sequencing. *Mol. Microbiol.*, 94(5):963–987, 2014. ISSN 1365-2958. doi: 10.1111/mmi.12810.

K. Rooijers, F. Loayza-Puch, L. G. Nijtmans, and R. Agami. Ribosome profiling reveals features of normal and disease-associated mitochondrial translation. *Nat. Commun.*, 4(1): 2886, 2013. ISSN 2041-1723. doi: 10.1038/ncomms3886.

R. J. Rose and A. G. C. Lindbeck. Morphological studies on the transcription of spinach chloroplast DNA. *Zeitschrift für Pflanzenphysiologie*, 106(2):129–137, 1982. ISSN 0044328X. doi: 10.1016/s0044-328x(82)80075-5.

J. B. Rossel, I. W. Wilson, and B. J. Pogson. Global changes in gene expression in response to high light in Arabidopsis. *Plant Physiol.*, 130(3):1109–1120, 2002. ISSN 00320889. doi: 10.1104/pp.005595.

M. Rott, N. F. Martins, W. Thiele, W. Lein, R. Bock, D. M. Kramer, and M. A. Schöttler. ATP synthase repression in tobacco restricts photosynthetic electron transport, CO_2 assimilation, and plant growth by overacidification of the thylakoid lumen. *Plant Cell*, 23(1):304–321, 2011. ISSN 1040-4651. doi: 10.1105/tpc.110.079111.

L. M. Roy and A. Barkan. A SecY homologue is required for the elaboration of the chloroplast thylakoid membrane and for normal chloroplast gene expression. *J. Cell Biol.*, 141(2):385–395, 1998. ISSN 0021-9525. doi: 10.1083/jcb.141.2.385.

P. R. Rozak, R. M. Seiser, W. F. Wacholtz, and R. A. Wise. Rapid, reversible alterations in spinach thylakoid appression upon changes in light intensity. *Plant, Cell Environ.*, 25 (3) (2):421–429., 2002.

D. L. Rudler, L. A. Hughes, K. L. Perks, T. R. Richman, I. Kuznetsova, J. A. Ermer, L. N. Abudulai, A.-M. J. Shearwood, H. M. Viola, L. C. Hool, S. J. Siira, O. Rackham, and A. Filipovska. Fidelity of translation initiation is required for coordinated respiratory complex assembly. *Sci. Adv.*, 5(12):1–15, 2019. ISSN 23752548. doi: 10.1126/sciadv.aay2118.

M. Ruf and H. Kössel. Occurrence and spacing of ribosome recognition sites in mRNAs of chloroplasts from higher plants. *FEBS Lett.*, 240(1-2):41–44, 1988. ISSN 00145793. doi: 10.1016/0014-5793(88)80336-3.

S. Ruf, D. Karcher, and R. Bock. Determining the transgene containment level provided by chloroplast transformation. *Proc. Natl. Acad. Sci. USA*, 104(17):6998–7002, 2007. ISSN 0027-8424. doi: 10.1073/PNAS.0700008104.

S. Ruf, J. Forner, C. Hasse, X. Kroop, S. Seeger, L. Schollbach, A. Schadach, and R. Bock. High-efficiency generation of fertile transplastomic *Arabidopsis* plants. *Nat. Plants*, 5(3): 282–289, 2019. ISSN 20550278. doi: 10.1038/s41477-019-0359-2.

N. J. Ruppel and R. P. Hangarter. Mutations in a plastid-localized elongation factor G alter early stages of plastid development in *Arabidopsis thaliana*. *BMC Plant Biol.*, 7:37, 2007. ISSN 1471-2229. doi: 10.1186/1471-2229-7-37.

S. Saeedi and G. Roblin. Effects of respiration inhibitors and uncouplers on dark- and light-induced leaflet movements of *Cassia fasciculata*. *Plant Physiol.*, 82(1):270–273, 1986. ISSN 0032-0889. doi: 10.1104/pp.82.1.270.

W. Sakamoto, X. Chen, K. L. Kindle, and D. B. Stern. Function of the *Chlamydomonas reinhardtii petD* 5' untranslated region in regulating the accumulation of subunit IV of the cytochrome b_6/f complex. *Plant J.*, 6(4):503–512, 1994.

S. Santabarbara, I. Cazzalini, A. Rivadossi, F. M. Garlaschi, G. Zucchelli, and R. C. Jennings. Photoinhibition *in vivo* and *in vitro* involves weakly coupled chlorophyll-protein complexes. *Photochem. Photobiol.*, 75(6):613–618, 2002. ISSN 0031-8655. doi: 10.1562/0031-8655(2002)0750613PIVAIV2.0.CO2.

D. Sapkota, A. M. Lake, W. Yang, C. Yang, H. Wesseling, A. Guise, C. Uncu, J. S. Dalal, A. W. Kraft, J.-M. Lee, M. S. Sands, J. A. Steen, and J. D. Dougherty. Cell-type-specific profiling of alternative translation identifies regulated protein isoform variation in the mouse brain. *Cell Rep.*, 26(3):594–607.e7, 2019. ISSN 22111247. doi: 10.1016/j.celrep.2018.12.077.

N. Sato. Origin and evolution of plastids: Genomic view on the unification and diversity of plastids. In R. R. Wise and J. K. Hoober, editors, *The Structure and Function of Plastids*, pages 75–102. Kluwer Academic Publishers, Dordrecht, 2006. ISBN 9781402065705. doi: 10.1007/1-4020-4061-X_4.

S. Sato, Y. Nakamura, T. Kaneko, E. Asamizu, and S. Tabata. Complete structure of the chloroplast genome of *Arabidopsis thaliana*. *DNA Res.*, 290(6):283–290, 1999.

J. Schachtsiek and F. Stehle. Nicotine-free, nontransgenic tobacco (*Nicotiana tabacum* L.) edited by CRISPR-Cas9. *Plant Biotechnol. J.*, 17(12):2228–2230, 2019. ISSN 1467-7644. doi: 10.1111/pbi.13193.

L. B. Scharff, L. Childs, D. Walther, and R. Bock. Local absence of secondary structure permits translation of mRNAs that lack ribosome-binding sites. *PLoS Genet.*, 7(6):e1002155, 2011. doi: 10.1371/journal.pgen.1002155.

L. B. Scharff, M. Ehrnthaler, M. Janowski, L. H. Childs, C. Hasse, J. Gremmels, S. Ruf, R. Zoschke, and R. Bock. Shine-Dalgarno sequences play an essential role in the translation of plastid mRNAs in tobacco. *Plant Cell*, 29(12):3085–3101, 2017. ISSN 1040-4651. doi: 10.1105/tpc.17.00524.

M. A. Schöttler and S. Z. Tóth. Photosynthetic complex stoichiometry dynamics in higher plants: Environmental acclimation and photosynthetic flux control. *Front. Plant Sci.*, 5: 1–15, 2014. ISSN 1664462X. doi: 10.3389/fpls.2014.00188.

M. A. Schöttler, W. Thiele, K. Belkius, S. V. Bergner, C. Flügel, G. Wittenberg, S. Agrawal, S. Stegemann, S. Ruf, and R. Bock. The plastid-encoded PsaI subunit stabilizes photosystem I during leaf senescence in tobacco. *J. Exp. Bot.*, 68(5):1137–1155, 2017. ISSN 0022-0957. doi: 10.1093/jxb/erx009.

K. Schult, K. Meierhoff, S. Paradies, T. Töller, P. Wolff, and P. Westhoff. The nuclear-encoded factor HCF173 is involved in the initiation of translation of the *psbA* mRNA in *Arabidopsis thaliana*. *Plant Cell*, 19(4):1329–1346, 2007. doi: 10.1105/tpc.106.042895.

D. Schünemann, S. Gupta, F. Persello-Cartieaux, V. I. Klimyuk, J. D. G. Jones, L. Nussaume,

and N. E. Hoffman. A novel signal recognition particle targets light-harvesting proteins to the thylakoid membranes. *Proc. Natl. Acad. Sci. USA*, 95(17):10312 LP – 10316, 1998. doi: 10.1073/pnas.95.17.10312.

M. Schuster, Y. Gao, M. A. Schöttler, R. Bock, and R. Zoschke. Limited responsiveness of chloroplast gene expression during acclimation to high light in tobacco. *Plant Physiol.*, 182 (1):424–435, 2020. ISSN 0032-0889. doi: 10.1104/pp.19.00953.

R. Schwacke, A. Schneider, E. van der Graaff, K. Fischer, E. Catoni, M. Desimone, W. B. Frommer, U.-I. Flügge, and R. Kunze. ARAMEMNON, a novel database for Arabidopsis integral membrane proteins. *Plant Physiol.*, 131(1):16 LP – 26, 2003. doi: 10.1104/pp.011577.

Z. Schwarz and H. Kössel. The primary structure of 16S rDNA from *Zea mays* chloroplast is homologous to *E. coli* 16S rRNA. *Nature*, 283(1):1–12, 1980.

J. Schweer, H. Türkeri, A. Kolpack, and G. Link. Role and regulation of plastid sigma factors and their functional interactors during chloroplast transcription - Recent lessons from *Arabidopsis thaliana*. *Eur. J. Cell Biol.*, 89(12):940–946, 2010. ISSN 0171-9335. doi: 10.1016/J.EJCB.2010.06.016.

S. Schwenkert, J. Legen, T. Takami, T. Shikanai, R. G. Herrmann, and J. Meurer. Role of the low-molecular-weight subunits PetL, PetG, and PetN in assembly, stability, and dimerization of the cytochrome b_6f complex in tobacco. *Plant Physiol.*, 144(4):1924–1935, 2007. ISSN 00320889. doi: 10.1104/pp.107.100131.

H. Seelert, A. Poetsch, N. A. Dencher, A. Engel, H. Stahlberg, and D. J. Müller. Proton-powered turbine of a plant motor. *Nature*, 405(6785):418–419, 2000. ISSN 00280836. doi: 10.1038/35013148.

M. Selmer, S. Al-Karadaghi, G. Hirokawa, A. Kaji, and A. Liljas. Crystal structure of *Thermotoga maritima* ribosome recycling factor: A tRNA mimic. *Science*, 286(5448):2349–2352, 1999. ISSN 00368075. doi: 10.1126/science.286.5448.2349.

J. Semer, M. Štroch, V. Špunda, and M. Navrátil. Partitioning of absorbed light energy within photosystem II in barley can be affected by chloroplast movement. *J. Photochem. Photobiol. B Biol.*, 186:98–106, 2018. ISSN 1011-1344. doi: 10.1016/J.JPHOTOBIOL.2018.06.019.

P. Shah, Y. Ding, M. Niemczyk, G. Kudla, and J. B. Plotkin. Rate-limiting steps in yeast protein translation. *Cell*, 153(7):1589–1601, 2013. ISSN 0092-8674. doi: 10.1016/j.cell.2013.05.049.

M. Shapira, A. Lers, P. B. Heifetz, V. Irihimovitz, C. B. Osmond, N. W. Gillham, and J. E. Boynton. Differential regulation of chloroplast gene expression in *Chlamydomonas reinhardtii* during photoacclimation: Light stress transiently suppresses synthesis of the Rubisco LSU protein while enhancing synthesis of the PS II D1 protein. *Plant Mol. Biol.*, 33:1001–1011, 1997.

M. R. Sharma, A. Dönhöfer, C. Barat, V. Marquez, P. P. Datta, P. Fucini, D. N. Wilson, and

R. K. Agrawal. PSRP1 is not a ribosomal protein, but a ribosome-binding factor that is recycled by the ribosome-recycling factor (RRF) and elongation factor G (EF-G). *J. Biol. Chem.*, 285(6):4006–4014, 2010. ISSN 00219258. doi: 10.1074/jbc.M109.062299.

L.-X. Shi and S. M. Theg. The chloroplast protein import system: From algae to trees. *Biochim. Biophys. Acta - Mol. Cell Res.*, 1833(2):314–331, 2013. ISSN 01674889. doi: 10.1016/j.bbamcr.2012.10.002.

Z. Shi, K. Fujii, K. M. Kovary, N. R. Genuth, H. L. Röst, M. N. Teruel, and M. Barna. Heterogeneous ribosomes preferentially translate distinct subpools of mRNAs genome-wide. *Mol. Cell*, 67(1):71–83.e7, 2017. ISSN 10974164. doi: 10.1016/j.molcel.2017.05.021.

A. Shiber, U. Friedrich, K. Klann, D. Merker, M. Zedan, F. Tippmann, and B. Bukau. Co-translational assembly of protein complexes in eukaryotes revealed by ribosome profiling. *Nature*, 2018. doi: 10.1038/s41586-018-0462-y.

T. Shikanai. Central role of cyclic electron transport around photosystem I in the regulation of photosynthesis. *Curr. Opin. Biotechnol.*, 26:25–30, 2014. ISSN 0958-1669. doi: https://doi.org/10.1016/j.copbio.2013.08.012.

T. Shikanai, T. Endo, T. Hashimoto, Y. Yamada, K. Asada, and A. Yokota. Directed disruption of the tobacco *ndhB* gene impairs cyclic electron flow around photosystem I. *Proc. Natl. Acad. Sci. USA*, 95(16):9705 LP – 9709, 1998. doi: 10.1073/pnas.95.16.9705.

O. Shimomura, F. H. Johnson, and Y. Saiga. Extraction, purification and properties of Aequorin, a bioluminescent protein from the luminous hydromedusan, *Aequorea*. *J. Cell. Comp. Physiol.*, 59(3):223–239, 1962. ISSN 0095-9898. doi: 10.1002/jcp.1030590302.

E. Shimoni, O. Rav-Hon, I. Ohad, V. Brumfeld, and Z. Reich. Three-dimensional organization of higher-plant chloroplast thylakoid membranes revealed by electron tomography. *Plant Cell*, 17(9):2580 LP – 2586, 2005. doi: 10.1105/tpc.105.035030.

J. Shine and L. Dalgarno. The 3'-terminal sequence of *Escherichia coli* 16S ribosomal RNA: Complementarity to nonsense triplets and ribosome binding sites. *Proc. Natl. Acad. Sci. USA*, 71(4):1342–1346, 1974. ISSN 0027-8424. doi: 10.1073/pnas.71.4.1342.

K. Shinozaki, M. Ohme, M. Tanaka, T. Wakasugi, N. Hayashida, T. Matsubayashi, N. Zaita, J. Chunwongse, J. Obokata, K. Yamaguchi-Shinozaki, C. Ohto, K. Torazawa, B. Y. Meng, M. Sugita, H. Deno, T. Kamogashira, K. Yamada, J. Kusuda, F. Takaiwa, A. Kato, N. Tohdoh, H. Shimada, and M. Sugiura. The complete nucleotide sequence of the tobacco chloroplast genome: Its gene organization and expression. *EMBO J.*, 5(9):2043–2049, 1986. ISSN 02614189. doi: 10.1002/j.1460-2075.1986.tb04464.x.

N. E. Shirokikh, S. K. Archer, T. H. Beilharz, D. Powell, and T. Preiss. Translation complex profile sequencing to study the *in vivo* dynamics of mRNA-ribosome interactions during translation initiation, elongation and termination. *Nat. Protoc.*, 12(4):697–731, 2017. ISSN 1754-2189. doi: 10.1038/nprot.2016.189.

A. Shteiman-Kotler and G. Schuster. RNA-binding characteristics of the chloroplast S1-like

ribosomal protein CS1. *Nucleic Acids Res.*, 28(17):3310–3315, 2000. ISSN 0305-1048. doi: 10.1093/nar/28.17.3310.

N. Sierro, J. N. D. Battey, S. Ouadi, L. Bovet, S. Goepfert, N. Bakaher, M. C. Peitsch, and N. V. Ivanov. Reference genomes and transcriptomes of *Nicotiana sylvestris* and *Nicotiana tomentosiformis*. *Genome Biol.*, 14(6), 2013. ISSN 1474760X. doi: 10.1186/gb-2013-14-6-r60.

G. Sijben-Müller, R. B. Hallick, J. Alt, P. Westhoff, and R. G. Herrmann. Spinach plastid genes coding for initiation factor IF-1, ribosomal protein S11 and RNA polymerase α -subunit. *Nucleic Acids Res.*, 14(2):1029–1044, 1986. ISSN 0305-1048. doi: 10.1093/nar/14.2.1029.

B. N. Singh, R. N. Mishra, P. K. Agarwal, M. Goswami, S. Nair, S. K. Sopory, and M. K. Reddy. A pea chloroplast translation elongation factor that is regulated by abiotic factors. *Biochem. Biophys. Res. Commun.*, 320(2):523–530, 2004. ISSN 0006-291X. doi: https://doi.org/10.1016/j.bbrc.2004.05.192.

B. L. Slinger, H. Newman, Y. Lee, S. Pei, and M. M. Meyer. Co-evolution of bacterial ribosomal protein S15 with diverse mRNA regulatory structures. *PLoS Genet.*, 11(12):1–21, 2015. ISSN 15537404. doi: 10.1371/journal.pgen.1005720.

C. Smaczniak, N. Li, S. Boeren, T. America, W. van Dongen, S. S. Goerdayal, S. de Vries, G. C. Angenent, and K. Kaufmann. Proteomics-based identification of low-abundance signaling and regulatory protein complexes in native plant tissues. *Nat. Protoc.*, 7(12):2144–2158, 2012. ISSN 1750-2799. doi: 10.1038/nprot.2012.129.

I. Small, L. Maréchal-Drouard, J. Masson, G. Pelletier, A. Cosset, J.-H. Weil, and A. Dietrich. *In vivo* import of a normal or mutagenized heterologous transfer RNA into the mitochondria of transgenic plants: Towards novel ways of influencing mitochondrial gene expression? *EMBO J.*, 11(4):1291–1296, 1992. ISSN 0261-4189.

M. D. Smith, C. M. Rounds, F. Wang, K. Chen, M. Afitlhile, and D. J. Schnell. atToc159 is a selective transit peptide receptor for the import of nucleus-encoded chloroplast proteins . *J. Cell Biol.*, 165(3):323–334, 2004. ISSN 0021-9525. doi: 10.1083/jcb.200311074.

T. S. Smith, A. Heger, and I. Sudbery. UMI-tools: Modelling sequencing errors in Unique Molecular Identifiers to improve quantification accuracy. *Genome Res.*, 2017. doi: 10.1101/gr.209601.116.

D. B. Stern and W. Gruissem. Control of plastid gene expression: 3' inverted repeats act as mRNA processing and stabilizing elements, but do not terminate transcription. *Cell*, 51(6):1145–1157, 1987. ISSN 0092-8674. doi: 10.1016/0092-8674(87)90600-3.

J. J. Stewart, S. K. Polutchko, W. W. Adams, and B. Demmig-Adams. Acclimation of Swedish and Italian ecotypes of *Arabidopsis thaliana* to light intensity. *Photosynth. Res.*, 134(2):215–229, 2017. ISSN 15735079. doi: 10.1007/s11120-017-0436-1.

M. Stitt and H.-W. Heldt. Physiological rates of starch breakdown in isolated intact spinach chloroplasts. *Plant Physiol.*, 68(3):755 LP – 761, 1981. doi: 10.1104/pp.68.3.755.

R. Stoppel, L. Lezhneva, S. Schwenkert, S. Torabi, S. Felder, K. Meierhoff, P. Westhoff, and J. Meurer. Recruitment of a ribosomal release factor for light-and stress-dependent regulation of *petB* transcript stability in *Arabidopsis* chloroplasts. *Plant Cell*, 23(7):2680–2695, 2011. ISSN 10404651. doi: 10.1105/tpc.111.085324.

D. Strenkert, S. Schmollinger, S. D. Gallaher, P. A. Salomé, S. O. Purvine, C. D. Nicora, T. Mettler-Altmann, E. Soubeyrand, A. P. M. Weber, M. S. Lipton, G. J. Basset, and S. S. Merchant. Multiomics resolution of molecular events during a day in the life of Chlamydomonas. *Proc. Natl. Acad. Sci. USA*, 116(6):2374–2383, 2019. ISSN 0027-8424. doi: 10.1073/PNAS.1815238116.

S. Sullivan, C. E. Thomson, D. J. Lamont, M. A. Jones, and J. M. Christie. *In vivo* phosphorylation site mapping and functional characterization of Arabidopsis phototropin 1. *Mol. Plant*, 1(1):178–194, 2008. ISSN 1674-2052. doi: 10.1093/MP/SSM017.

Q. Sun, O. Emanuelsson, and K. J. Van Wijk. Analysis of curated and predicted plastid subproteomes of Arabidopsis. Subcellular compartmentalization leads to distinctive proteome properties. *Plant Physiol.*, 135(2):723–734, 2004. ISSN 00320889. doi: 10.1104/pp.104.040717.

X. Sun, L. Peng, J. Guo, W. Chi, J. Ma, C. Lu, and L. Zhang. Formation of DEG5 and DEG8 complexes and their involvement in the degradation of photodamaged photosystem II reaction center D1 protein in *Arabidopsis*. *Plant Cell*, 19(4):1347 LP – 1361, 2007. doi: 10.1105/tpc.106.049510.

X. Sun, T. Fu, N. Chen, J. Guo, J. Ma, M. Zou, C. Lu, and L. Zhang. The stromal chloroplast Deg7 protease participates in the repair of photosystem II after photoinhibition in Arabidopsis. *Plant Physiol.*, 152(3):1263 LP – 1273, 2010. doi: 10.1104/pp.109.150722.

C. Sundby, S. McCaffery, and J. M. Anderson. Turnover of the photosystem II D1 protein in higher plants under photoinhibitory and nonphotoinhibitory irradiance. *J. Biol. Chem.*, 268 (34):25476–25482, 1993.

N. Suzuki, A. R. Devireddy, M. A. Inupakutika, A. Baxter, G. Miller, L. Song, E. Shulaev, R. K. Azad, V. Shulaev, and R. Mittler. Ultra-fast alterations in mRNA levels uncover multiple players in light stress acclimation in plants. *Plant J.*, 84(4):760–772, 2015. ISSN 1365313X. doi: 10.1111/tpj.13039.

Z. Svab, P. T. J. Hajdukiewicz, and P. Maliga. Stable transformation of plastids in higher plants. *Proc. Natl. Acad. Sci. USA*, 87(21):8526–8530, 1990. ISSN 0027-8424. doi: 10.1073/pnas.87.21.8526.

M. Swiatecka-Hagenbruch, K. Liere, and T. Börner. High diversity of plastidial promoters in *Arabidopsis thaliana*. *Mol. Genet. Genomics*, 277(6):725–734, 2007. ISSN 16174615. doi: 10.1007/s00438-007-0222-4.

L. Tadini, P. Pesaresi, T. Kleine, F. Rossi, A. Guljamow, F. Sommer, T. Mühlhaus, M. Schroda, S. Masiero, M. Pribil, M. Rothbart, B. Hedtke, B. Grimm, and D. Leister. GUN1 controls accumulation of the plastid ribosomal protein S1 at the protein level and interacts with

proteins involved in plastid protein homeostasis. *Plant Physiol.*, 170(3):1817–1830, 2016. ISSN 0032-0889. doi: 10.1104/pp.15.02033.

J. C. Taggart and G.-w. Li. Production of protein-complex components is stoichiometric and lacks general feedback regulation in eukaryotes. *Cell Syst.*, 7(6):580–589.e4, 2018. ISSN 2405-4712. doi: 10.1016/j.cels.2018.11.003.

K. Takizawa, J. A. Cruz, A. Kanazawa, and D. M. Kramer. The thylakoid proton motive force *in vivo*. Quantitative, non-invasive probes, energetics, and regulatory consequences of light-induced *pmf*. *Biochim. Biophys. Acta - Bioenerg.*, 1767(10):1233–1244, 2007. ISSN 0005-2728. doi: 10.1016/J.BBABIO.2007.07.006.

J. Tamarit, E. Cabiscol, and J. Ros. Identification of the major oxidatively damaged proteins in *Escherichia coli* cells exposed to oxidative stress. *J. Biol. Chem.*, 273(5):3027–3032, 1998. doi: 10.1074/jbc.273.5.3027.

M. Tanaka, J. Obokata, J. Chunwongse, K. Shinozaki, and M. Sugiura. Rapid splicing and stepwise processing of a transcript from the *psbB* operon in tobacco chloroplasts: Determination of the intron sites in *petB* and *petD*. *Mol. Gen. Genet. MGG*, 209(3):427–431, 1987. ISSN 1432-1874. doi: 10.1007/BF00331145.

I. A. Tarassov and N. S. Entelis. Mitochondrially-imported cytoplasmic $tRNA^{Lys}$ (CUU) of *Saccharomyces cerevisiae*: *In vivo* and *in vitro* targeting systems . *Nucleic Acids Res.*, 20 (6):1277–1281, 1992. ISSN 0305-1048. doi: 10.1093/nar/20.6.1277.

The UniProt Consortium. UniProt: A worldwide hub of protein knowledge. *Nucleic Acids Res.*, 47(D1):D506–D515, 2019. ISSN 0305-1048. doi: 10.1093/nar/gky1049.

J. Theis and M. Schroda. Revisiting the photosystem II repair cycle. *Plant Signal. Behav.*, 11 (9):e1218587, 2016. doi: 10.1080/15592324.2016.1218587.

U. Theissen and W. Martin. The difference between organelles and endosymbionts. *Curr. Biol.*, 16(24):R1016–R1017, 2006. ISSN 09609822. doi: 10.1016/j.cub.2006.11.020.

W. F. Thompson, M. Everett, N. O. Polans, R. A. Jorgensen, and J. D. Palmer. Phytochrome control of RNA levels in developing pea and mung-bean leaves. *Planta*, 158(6):487–500, 1983. ISSN 1432-2048. doi: 10.1007/BF00397240.

M. Tikkanen, M. Nurmi, S. Kangasjärvi, and E.-m. Aro. Core protein phosphorylation facilitates the repair of photodamaged photosystem II at high light. *BBA - Bioenerg.*, 1777(11):1432–1437, 2008. ISSN 0005-2728. doi: 10.1016/j.bbabio.2008.08.004.

N. Tiller and R. Bock. The translational apparatus of plastids and its role in plant development. *Mol. Plant*, 7(7):1105–20, 2014. ISSN 1752-9867. doi: 10.1093/mp/ssu022.

T. Trebitsh and A. Danon. Translation of chloroplast *psbA* mRNA is regulated by signals initiated by both photosystems II and I. *Proc. Natl. Acad. Sci. USA*, 98(21):12289–12294, 2001. ISSN 00278424. doi: 10.1073/pnas.211440698.

T. Trebitsh, A. Levitan, A. Sofer, and A. Danon. Translation of chloroplast *psbA* mRNA is modulated in the light by counteracting oxidizing and reducing activities. *Mol. Cell. Biol.*, 20(4):1116–23, 2000. ISSN 0270-7306. doi: 10.1128/MCB.20.4.1116-1123.2000.

R. Trösch, R. Barahimipour, Y. Gao, J. A. Badillo-Corona, V. L. Gotsmann, D. Zimmer, T. Mühlhaus, R. Zoschke, and F. Willmund. Commonalities and differences of chloroplast translation in a green alga and land plants. *Nat. Plants*, 4(8):564–575, 2018. ISSN 20550278. doi: 10.1038/s41477-018-0211-0.

E. Tyystjärvi and E. M. Aro. The rate constant of photoinhibition, measured in lincomycin-treated leaves, is directly proportional to light intensity. *Proc. Natl. Acad. Sci. USA*, 93(5): 2213–2218, 1996. ISSN 0027-8424. doi: 10.1073/pnas.93.5.2213.

N. V. Tzareva, V. I. Makhno, and I. V. Boni. Ribosome-messenger recognition in the absence of the Shine-Dalgarno interactions. *FEBS Lett.*, 337(2):189–194, 1994. ISSN 0014-5793. doi: 10.1016/0014-5793(94)80271-8.

T. Tzvetkova-Chevolleau, C. Hutin, L. D. Noël, R. Goforth, J.-P. Carde, S. Caffarri, I. Sinning, M. Groves, J.-M. Teulon, N. E. Hoffman, R. Henry, M. Havaux, and L. Nussaume. Canonical signal recognition particle components can be bypassed for posttranslational protein targeting in chloroplasts. *Plant Cell*, 19(5):1635 LP – 1648, 2007. doi: 10.1105/tpc.106.048959.

T. Udagawa, Y. Shimizu, and T. Ueda. Evidence for the translation initiation of leaderless mRNAs by the intact 70 S ribosome without its dissociation into subunits in eubacteria. *J. Biol. Chem.*, 279(10):8539–8546, 2004. doi: 10.1074/jbc.M308784200.

S. Ude, J. Lassak, A. L. Starosta, T. Kraxenberger, D. N. Wilson, and K. Jung. Translation elongation factor EF-P alleviates ribosome stalling at polyproline stretches. *Science*, 339 (6115):82 LP – 85, 2013. doi: 10.1126/science.1228985.

J. Uniacke and W. Zerges. Chloroplast protein targeting involves localized translation in *Chlamydomonas*. *Proc. Natl. Acad. Sci. USA*, 106(5):1439–1444, 2009.

J. J. S. van Rensen, W. J. Vredenberg, and G. C. Rodrigues. Time sequence of the damage to the acceptor and donor sides of photosystem II by UV-B radiation as evaluated by chlorophyll *a* fluorescence. *Photosynth. Res.*, 94:291–297, 2007. doi: 10.1007/s11120-007-9177-x.

K. J. van Wijk. Plastid proteomics. *Plant Physiol. Biochem.*, 42(12):963–977, 2004. ISSN 09819428. doi: 10.1016/j.plaphy.2004.10.015.

I. Vass. Role of charge recombination processes in photodamage and photoprotection of the photosystem II complex. *Physiol. Plant.*, 142(1):6–16, 2011. ISSN 0031-9317. doi: 10.1111/j.1399-3054.2011.01454.x.

I. Vass, S. Styring, T. Hundal, A. Koivuniemi, E.-M. Aro, and B. Andersson. Reversible and irreversible intermediates during photoinhibition of photosystem II: Stable reduced Q_A species promote chlorophyll triplet formation. *Proc. Natl. Acad. Sci. USA*, 89(4):1408–1412, 1992. ISSN 0027-8424. doi: 10.1073/pnas.89.4.1408.

O. Vesper, S. Amitai, M. Belitsky, K. Byrgazov, A. C. Kaberdina, H. Engelberg-Kulka, and I. Moll. Selective translation of leaderless mRNAs by specialized ribosomes generated by MazF in *Escherichia coli*. *Cell*, 147(1):147–157, 2011. ISSN 0092-8674. doi: 10.1016/j.cell.2011.07.047.

T. Vincent, A. Vingadassalon, E. Ubrig, K. Azeredo, O. Srour, V. Cognat, S. Graindorge, T. Salinas, L. Maréchal-Drouard, and A.-M. Duchêne. A genome-scale analysis of mRNAs targeting to plant mitochondria: Upstream AUGs in 5' untranslated regions reduce mitochondrial association. *Plant J.*, 92(6):1132–1142, 2017. ISSN 09607412. doi: 10.1111/tpj.13749.

A. G. von Arnim, Q. Jia, and J. N. Vaughn. Regulation of plant translation by upstream open reading frames. *Plant Sci.*, 214:1–12, 2014. ISSN 0168-9452. doi: https://doi.org/10.1016/j.plantsci.2013.09.006.

G. von Heijne, T. Hirai, R.-B. Klösgen, J. Steppuhn, B. Bruce, K. Keegstra, and R. Herrmann. CHLPEP-A database of chloroplast transit peptides. *Plant Mol. Biol. Report.*, 9(2):104–126, 1991. ISSN 1572-9818. doi: 10.1007/BF02669204.

S. Wagner, A. Herrmannová, V. Hronová, S. Gunišová, N. D. Sen, R. D. Hannan, A. G. Hinnebusch, N. E. Shirokikh, T. Preiss, and L. S. Valášek. Selective translation complex profiling reveals staged initiation and co-translational assembly of initiation factor complexes. *Mol. Cell*, 79(4):546–560.e7, 2020. ISSN 10972765. doi: 10.1016/j.molcel.2020.06.004.

T. Wakasugi, M. Sugita, T. Tsudzuki, and M. Sugiura. Updated gene map of tobacco chloroplast DNA. *Plant Mol. Biol. Report.*, 16(3):231–241, 1998. ISSN 07359640. doi: 10.1023/A:1007564209282.

B. Walter, A. Hristou, M. M. Nowaczyk, and D. Schünemann. *In vitro* reconstitution of co-translational D1 insertion reveals a role of the cpSec-Alb3 translocase and Vipp1 in photosystem II biogenesis. *Biochem. J.*, 468(2):315–324, 2015. ISSN 0264-6021. doi: 10.1042/BJ20141425.

F. Waltz, T.-T. Nguyen, M. Arrivé, A. Bochler, J. Chicher, P. Hammann, L. Kuhn, M. Quadrado, H. Mireau, Y. Hashem, and P. Giegé. Small is big in *Arabidopsis* mitochondrial ribosome. *Nat. Plants*, 5(1):106–117, 2019. ISSN 20550278. doi: 10.1038/s41477-018-0339-y.

M. A. Ware, E. Belgio, and A. V. Ruban. Photoprotective capacity of non-photochemical quenching in plants acclimated to different light intensities. *Photosynth. Res.*, 126(2-3):261–274, 2015. ISSN 15735079. doi: 10.1007/s11120-015-0102-4.

B. L. Weis, E. Schleiff, and W. Zerges. Protein targeting to subcellular organelles via mRNA localization. *Biochim. Biophys. Acta - Mol. Cell Res.*, 1833(2):260–273, 2013. ISSN 0167-4889. doi: 10.1016/J.BBAMCR.2012.04.004.

A. Weixlbaumer, S. Petry, C. M. Dunham, M. Selmer, A. C. Kelley, and V. Ramakrishnan. Crystal structure of the ribosome recycling factor bound to the ribosome. *Nat. Struct. Mol. Biol.*, 14(8):733–737, 2007. ISSN 1545-9985. doi: 10.1038/nsmb1282.

D. Wessel and U.-I. Flügge. A method for the quantitative recovery of protein in dilute solution in the presence of detergents and lipids. *Anal. Biochem.*, 138(1):141–143, 1984. ISSN 00032697. doi: 10.1016/0003-2697(84)90782-6.

P. Westhoff and R. G. Herrmann. Complex RNA maturation in chloroplasts. *Eur. J. Biochem.*, 171(3):551–564, 1988.

C. C. Williams, C. H. Jan, and J. S. Weissman. Targeting and plasticity of mitochondrial proteins revealed by proximity-specific ribosome profiling. *Science*, 346(6210):748–751, 2014. ISSN 0036-8075. doi: 10.1126/science.1257522.

R. R. Wise and J. K. Hooper, editors. *The structure and function of plastids*. Springer Netherlands, 2006. ISBN 978-1-4020-4060-3.

W. H. J. Wood, C. MacGregor-Chatwin, S. F. H. Barnett, G. E. Mayneord, X. Huang, J. K. Hobbs, C. N. Hunter, and M. P. Johnson. Dynamic thylakoid stacking regulates the balance between linear and cyclic photosynthetic electron transfer. *Nat. Plants*, 4(February):1, 2018. ISSN 20550278. doi: 10.1038/s41477-018-0163-4.

K. Wostrikoff and D. B. Stern. Rubisco large-subunit translation is autoregulated in response to its assembly state in tobacco chloroplasts. *Proc. Natl. Acad. Sci. USA*, 104(15):6466 LP – 6471, 2007. doi: 10.1073/pnas.0610586104.

K. Wostrikoff, J. Girard-Bascou, F.-A. Wollman, and Y. Choquet. Biogenesis of PSI involves a cascade of translational autoregulation in the chloroplast of *Chlamydomonas*. *EMBO J.*, 23(13):2696–2705, 2004. ISSN 0261-4189. doi: 10.1038/sj.emboj.7600266.

C. C.-C. Wu, B. Zinshteyn, K. A. Wehner, and R. Green. High-resolution ribosome profiling defines discrete ribosome elongation states and translational regulation during cellular stress. *Mol. Cell*, 73(5):959–970.e5, 2019a. ISSN 1097-2765. doi: https://doi.org/10.1016/j.molcel.2018.12.009.

H.-Y. L. Wu, G. Song, J. W. Walley, and P. Y. Hsu. The tomato translational landscape revealed by transcriptome assembly and ribosome profiling. *Plant Physiol.*, 181(1):367–380, 2019b. ISSN 0032-0889. doi: 10.1104/pp.19.00541.

M. S. Yagura. The complete nucleotide sequence and multipartite organization of the tobacco mitochondrial genome: Comparative analysis of mitochondrial genomes in higher plants. *Mol. Genet. Genomics*, pages 603–615, 2005. doi: 10.1007/s00438-004-1075-8.

K. Yamaguchi and A. R. Subramanian. The plastid ribosomal proteins: Identification of all the proteins in the 50 S subunit of an organelle ribosome (chloroplast). *J. Biol. Chem.*, 275 (37):28466–28482, 2000. ISSN 0021-9258. doi: 10.1074/jbc.M005012200.

K. Yamaguchi and A. R. Subramanian. Proteomic identification of all plastid-specific ribosomal proteins in higher plant chloroplast 30S ribosomal subunit. *Eur. J. Biochem.*, 270(2):190–205, 2003. ISSN 0014-2956. doi: 10.1046/j.1432-1033.2003.03359.x.

K. Yamaguchi, K. von Knoblauch, and A. R. Subramanian. The plastid ribosomal proteins:

Identification of all the proteins in the 30 S subunit of an organelle ribosome (chloroplast). *J. Biol. Chem.*, 275(37):28455–28465, 2000. ISSN 0021-9258. doi: 10.1074/jbc.M004350200.

H. Yamamoto, D. Wittek, R. Gupta, B. Qin, T. Ueda, R. Krause, K. Yamamoto, R. Albrecht, M. Pech, and K. H. Nierhaus. 70S-scanning initiation is a novel and frequent initiation mode of ribosomal translation in bacteria. *Proc. Natl. Acad. Sci. USA*, 113(9):E1180–E1189, 2016. ISSN 10916490. doi: 10.1073/pnas.1524554113.

F. Yang, S. Huang, R. Gao, W. Liu, T. Yong, X. Wang, X. Wu, and W. Yang. Growth of soybean seedlings in relay strip intercropping systems in relation to light quantity and red:far-red ratio. *F. Crop. Res.*, 155:245–253, 2014. ISSN 0378-4290. doi: https://doi.org/10.1016/j.fcr.2013.08.011.

E. Yángüez, A. B. Castro-Sanz, N. Fernández-Bautista, J. C. Oliveros, and M. M. Castellano. Analysis of genome-wide changes in the translatome of Arabidopsis seedlings subjected to heat stress. *PLoS One*, 8(8):e71425, 2013.

C. B. Yohn, A. Cohen, C. Rosch, M. R. Kuchka, and S. P. Mayfield. Translation of the chloroplast *psbA* mRNA requires the nuclear-encoded poly(A)-binding protein, RB47. *J. Cell Biol.*, 142(2):435–442, 1998. ISSN 0021-9525. doi: 10.1083/jcb.142.2.435.

Q. Yu, L. M. LaManna, M. E. Kelly, K. A. Lutz, and P. Maliga. New tools for engineering the Arabidopsis plastid genome. *Plant Physiol.*, 181(2):394–398, 2019. ISSN 15322548. doi: 10.1104/pp.19.00761.

J. Yuan, A. Kight, R. L. Goforth, M. Moore, E. C. Peterson, J. Sakon, and R. Henry. ATP stimulates signal recognitionparticle (SRP)/FtsY-supported protein integration in chloroplasts. *J. Biol. Chem.*, 277(35):32400–32404, 2002. doi: 10.1074/jbc.M206192200.

M. Yukawa, T. Tsudzuki, and M. Sugiura. The 2005 version of the chloroplast DNA sequence from tobacco (*Nicotiana tabacum*). *Plant Mol. Biol. Report.*, 23(4):359–365, 2005. ISSN 1572-9818. doi: 10.1007/BF02788884.

M. Yukawa, T. Tsudzuki, and M. Sugiura. The chloroplast genome of *Nicotiana sylvestris* and *Nicotiana tomentosiformis*: Complete sequencing confirms that the *Nicotiana sylvestris* progenitor is the maternal genome donor of *Nicotiana tabacum*. *Mol. Genet. Genomics*, 275 (4):367–373, 2006. ISSN 1617-4623. doi: 10.1007/s00438-005-0092-6.

M. E. Zanetti, I.-F. Chang, F. Gong, D. W. Galbraith, and J. Bailey-Serres. Immunopurification of polyribosomal complexes of Arabidopsis for global analysis of gene expression. *Plant Physiol.*, 138(2):624–635, 2005. ISSN 0032-0889. doi: 10.1104/pp.105.059477.

A. V. Zavialov, R. H. Buckingham, and M. Ehrenberg. A posttermination ribosomal complex is the guanine nucleotide exchange factor for peptide release factor RF3. *Cell*, 107(1):115–124, 2001. ISSN 0092-8674. doi: 10.1016/S0092-8674(01)00508-6.

A. V. Zavialov, L. Mora, R. H. Buckingham, and M. Ehrenberg. Release of peptide promoted by the GGQ motif of class 1 release factors regulates the GTPase activity of RF3. *Mol. Cell*, 10(4):789–798, 2002. ISSN 1097-2765. doi: 10.1016/S1097-2765(02)00691-3.

F. Zeng, Y. Chen, J. Remis, M. Shekhar, J. C. Phillips, E. Tajkhorshid, and H. Jin. Structural basis of co-translational quality control by ArfA and RF2 bound to ribosome. *Nature*, 541 (7638):554–557, 2017. ISSN 14764687. doi: 10.1038/nature21053.

L. Zhang, V. Paakkarinen, K. J. van Wijk, and E.-M. Aro. Co-translational assembly of the D1 protein into photosystem II. *J. Biol. Chem.*, 274(23):16062–16067, 1999. doi: 10.1074/jbc.274.23.16062.

L. Zhang, V. Paakkarinen, M. Suorsa, and E.-M. Aro. A SecY homologue is involved in chloroplast-encoded D1 protein biogenesis. *J. Biol. Chem.*, 276(41):37809–37814, 2001. ISSN 00219258. doi: 10.1074/jbc.M105522200.

P. Zhelyazkova, C. M. Sharma, K. U. Forstner, K. Liere, J. Vogel, and T. Börner. The primary transcriptome of barley chloroplasts: Numerous noncoding RNAs and the dominating role of the plastid-encoded RNA polymerase. *Plant Cell*, 24(1):123–136, 2012. ISSN 1040-4651. doi: 10.1105/tpc.111.089441.

M. Zheng, X. Liu, S. Liang, S. Fu, Y. Qi, J. Zhao, J. Shao, L. An, and F. Yu. Chloroplast translation initiation factors regulate leaf variegation and development. *Plant Physiol.*, 172 (2):1117–1130, 2016. ISSN 15322548. doi: 10.1104/pp.15.02040.

X. G. Zhu, Govindjee, N. R. Baker, E. DeSturler, D. R. Ort, and S. P. Long. Chlorophyll *a* fluorescence induction kinetics in leaves predicted from a model describing each discrete step of excitation energy and electron transfer associated with photosystem II. *Planta*, 223 (1):114–133, 2005. ISSN 00320935. doi: 10.1007/s00425-005-0064-4.

D. Ziehe, B. Dünschede, and D. Schünemann. Molecular mechanism of SRP-dependent light-harvesting protein transport to the thylakoid membrane in plants. *Photosynth. Res.*, 138 (3):303–313, 2018. ISSN 1573-5079. doi: 10.1007/s11120-018-0544-6.

R. Zoschke and A. Barkan. Genome-wide analysis of thylakoid-bound ribosomes in maize reveals principles of cotranslational targeting to the thylakoid membrane. *Proc. Natl. Acad. Sci. USA*, 112(13):E1678–E1687, 2015. ISSN 10916490. doi: 10.1073/pnas.1424655112.

R. Zoschke, K. P. Watkins, and A. Barkan. A rapid ribosome profiling method elucidates chloroplast ribosome behavior *in vivo*. *Plant Cell*, 25(6):2265–2275, 2013. doi: 10.1105/tpc.113.111567.

R. Zoschke, P. Chotewutmontri, and A. Barkan. Translation and co-translational membrane engagement of plastid-encoded chlorophyll-binding proteins are not influenced by chlorophyll availability in maize. *Front. Plant Sci.*, 8, 2017. ISSN 1664-462X. doi: 10.3389/fpls.2017.00385.

B. Zybailov, H. Rutschow, G. Friso, A. Rudella, O. Emanuelsson, Q. Sun, and K. J. van Wijk. Sorting signals, N-terminal modifications and abundance of the chloroplast proteome. *PLoS One*, 3(4):e1994, 2008. ISSN 1932-6203. doi: 10.1371/journal.pone.0001994.

Acknowledgement

This thesis was not only based on my own work, but many people contributed actively or passively to the successful course of experiments, the evaluation of results, and the preparation of this document. To all those people I commit my sincerest thanks.

Reimo Zoschke and Ralph Bock gave me the chance to grow scientifically and personally by accepting me as PhD student.
Reimo was always helpful with suggestions, answers, and discussion. He gave me the freedom to develop my projects, even he refused to let me stop the light acclimation project until it was published.
Ralph gave always useful input during the department and progress seminars. Additionally, he provided us with access to facilities and instruments as well as the unpublished plant line Rpl32-GFP for the TRAP experiment.

A special thank goes to the group "Translational Regulation in Plants". All members made the days great, and I loved to come to work just by knowing to be with them. They are the reason I never dropped.
Ines Gerlach was immensely helpful in the light acclimation project by helping with the isolation of footprints and the fragmentation of RNA. Also, she was a real help for harvesting plant tissue in dark and light for the translatome project.
Yang Gao introduced the ribosome profiling method to me and was always willing to share her experience and results of the shift experiment. Additionally, she provided the data of the "zero control" for the shift experiment.
My two student helpers, Darya Malko and Md Ahsan Habib Maruf, were also extremely helpful in the light acclimation project. Darya was highly active to make the immuno blots reproducible and representative but gave also helping hands by preprocessing the array data and isolating footprints. Maruf did a good job by determining the chlorophyll content and the leaf absorption of shifted and control plants.
Darya, talented and handy, produced also the polysome profiles for the tagged ribosomal protein plant lines and verified the presence of the proteins in the polysome fractions by immuno blots.
Mike Ting helped me a lot with the deduplication of sequencing reads by providing his script for UMI processing.

Many thanks also for AG Bock, especially to all technicians and Stephanie Ruf for providing always help and a well-organized department which I appreciated a lot.
Mark Aurel Schöttler and its student helper Anita Henze helped immensely by determining the chlorophyll-*a* fluorescence and thereby photosynthetic parameters of shifted and control plants.

I am incredibly grateful that I could do the PhD in this institute as part of the Max Planck Society.
Many thanks go to the Bioinformatics group. Axel Fischer who had no time to spare, could

still manage to explain programs to me and find explanation for my error messages. Jürgen Gremmels who gave me access to `vector` and told me some bash tricks. And last but not least, Dirk Walther, who discussed normalization and analysis strategies with me.
The Green Team was a real treasure for me. They sowed and transplanted all my plants and took care of their wellbeing. Britta Hausmann and Florian Hundert were always helpful, also in short term notice. Karin Köhl taught me a lot of plants and their maintenance. Dirk Zerning introduced me to the handling of tractors. It may be helpful later but was fun in any way.
There was no problem the IT crowd could not manage. Small and big issues were solved by them in a virtuous way. A special thank goes to Sven Borngräber who managed to recover my thesis when I broke my Nextcloud file system, to show me nice and helpful programs, and to discuss with me the topics of the world.
André Gehrmann and Andreas Grüneberg did great jobs by adjusting the growth chamber for the light shift experiment. The Haustechnik Team were real "Heinzelmännchen". Thank you.
I also thank all the other groups and people who took care of the smooth flow in the institute, i.e., HR and purchasing, the store, the media kitchen, and the cleaning team.

For scientific guidance and suggestions, as well as career development I want to thank Dirk Walther, Dirk Hincha, and Kristina Kühn (Martin-Luther-Universität, Halle-Wittenberg). I really enjoyed the annual meetings and learned a lot from them.
Further, I want to thank all members of the TRR175 (2016-2020) for nice discussion, useful suggestions, and funny moments during the annual meetings and workshops. Particularly, Christian Schmitz-Linneweber (Humboldt University, Berlin) supported me by providing the unpublished plant line HA-Rps15. Dermot Harnett (Max Delbrück Center, Berlin) was always helpful to discuss bioinformatic-related questions of ribosome profiling.

Joachim Selbig was and is allways supportive and willing to share his expertise, experience, and help. Furthermore, he was so kind to review the first draft of this document. I am very thankful to have him as a mentor and friend.

I want to thank all my family and friends who supported me during my whole life and career. Tino, who loves and cherishes me, took me into a hug any time I needed. My parents, sister, and her family, I thank for free food, financial support during my bachelor and master studies and supportive words ("Get the stuff done!" ☺). My friends, who could choose the acquaintance with me, were always by my side. Antje and Natalie for their support the last 15 years with laughing and crying, cookies and wine. Stephie, Rini, Nicole, and Sabrina for our shared time during the Bachelor, the ongoing friendship during Master and PhD studies. Thank you so much.
Additionally, many thanks to Andelé for correcting all the errors in the manuscript and to Sabrina-Eagle Eye for identifying the small and big inconsistencies in the writing.
Finally, I am much obliged to Manuel Kühnert for providing his awesome LaTeXthesis template (`www.bedienhaptik.de/latex-template/`) to lazy students like me. His template shortened the writing time by many months.

Selbstständigkeitserklärung

Ich erkläre hiermit, dass ich die vorliegende Arbeit selbständig und ohne Benutzung anderer als der angegebenen Hilfsmittel angefertigt habe; die aus fremden Werken wörtlich oder sinngemäß übernommenen Gedanken sind als solche und unter Angabe der Quellen gekennzeichnet.

Berlin, December 2020